

Development of variable and robust brain wiring patterns in the fly visual system

Inaugural-Dissertation

To obtain the academic degree

Doctor rerum naturalium (Dr. rer. nat.)

Submitted to the Department of Biology, Chemistry, Pharmacy
of Freie Universität Berlin

by

Suchetana B. Dutta

Born in Kolkata, India

2022

I hereby declare that all experiments and writing contained within this thesis were conducted by myself, all references used are cited accordingly and any personal assistance has been acknowledged by name. I also declare that I have not submitted the dissertation in this or any other form to any other institution as a dissertation.

All experiments for this dissertation were conducted from August 2016 to August 2022 at the Division of Neurobiology of Institute of Biology of Freie Universität Berlin under the supervision of Prof. Dr. P. Robin Hiesinger and Prof. Dr. Bassem Hassan.

1st reviewer: Prof. Dr. Bassem Hassan

ICM Paris

2nd reviewer: Prof. Dr. P. Robin Hiesinger

Division of Neurobiology, Freie Universität Berlin

Prof. Dr. Bassem Hassan

Date of defence: 11th November 2022

1. Summary	1
2. Zusammenfassung	3
3. General Introduction.....	5
3.1 The brain wiring problem.....	6
3.2 The chemoaffinity hypothesis and instructive molecules.....	6
3.3 Algorithmic brain growth; from simple developmental rules to a complex brain	8
3.4 From random developmental processes to precise synapse formation.....	11
3.5 The synaptotropic hypothesis.....	13
3.6 Dynamic processes of axonal branching:	14
3.7 Synaptic homeostasis.....	16
3.8 Endo-membrane degradation pathways in synapse maintenance and brain wiring.....	17
3.9 Molecular coupling of axon branching and synapse formation.....	19
3.10 Receptor tyrosine kinase and phosphatases in neuronal wiring.....	20
3.11 Environmental effects on neuronal wiring.....	21
3.12 The Drosophila visual system; A model to study axon branching and synaptogenesis .	23
4. Aim	27
5. Manuscript 1	28
Contribution	28
Article.....	29
Supplemental information:	56
6. Manuscript 2	70
Contribution.....	70
Article.....	72
Supplemental information	96
7. Manuscript 3	110
Contribution.....	110
Parts of Article.....	Error! Bookmark not defined.
8. Manuscript 4	115
Contribution.....	115
Article.....	116
Supplemental information:	127
9. General Discussion	130
9.1 Spatial and temporal regulation of signaling receptor molecules in synaptogenesis and axon branching.....	131
9.2 Suppression of local synaptic protein degradation via autophagy as a homeostatic mechanism for proper neuronal assembly:	133

9.3 Brain wiring as a functional output of time.....	135
10. Outlook and future directions.....	137
11. References.....	140
12. Appendix	152
12.1 Dedication & Acknowledgement	152
12.2 List of publications from the doctoral work.....	153

1. Summary

Development of robust brain wiring through stochastic developmental processes

Precise generation of synapse-specific neuronal connections are crucial for establishing a robust and functional brain. Neuronal wiring patterns emerge from proper spatiotemporal regulation of axon branching and synapse formation during development. Several neuropsychiatric and neurodevelopmental disorders exhibit defects in neuronal wiring owing to synapse loss and/or dys-regulated axon branching. Despite decades of research, how the two inter-dependent cellular processes: axon branching and synaptogenesis are coupled locally in the presynaptic arborizations is still unclear.

In my doctoral work, I investigated the possible role of EGF receptor (EGFR) activity in coregulating axon branching and synapse formation in a spatiotemporally restricted fashion, locally in the medulla innervating Dorsal Cluster Neuron (M-DCN)/LC14 axon terminals. In this work I have explored how genetically encoded EGFR randomly recycles in the axon branch terminals, thus creating an asymmetric, non-deterministic distribution pattern. Asymmetric EGFR activity in the branches acts as a permissive signal for axon branch pruning. I observed that the M-DCN branches which stochastically becomes EGFR '+' during development are synaptogenic, which means they can recruit synaptic machineries like Syd1 and Bruchpilot (Brp). My work showed that EGFR activity has a dual role in establishing proper M-DCN wiring; first in regulating primary branch consolidation possibly via actin regulation prior to synaptogenesis. Later in maintaining/protecting the levels of late Active Zone (AZ) protein Brp in the presynaptic branches by suppressing basal autophagy level during synaptogenesis. When M-DCNs lack optimal EGFR activity, the basal autophagy level increases resulting in loss of Brp marked synapses which is causal to increased exploratory branches and post-synaptic target loss. Lack of EGFR activity affects the M-DCN wiring pattern that makes adult flies more active and behave like obsessive compulsive in object fixation assay. In the second part of my doctoral work, I have asked how non-genetic factors like developmental temperature affects adult brain wiring. To test that, I increased or decreased rearing temperature which is known to inversely affect pupal developmental rate. We asked

if all the noisy cellular processes of neuronal assembly: filopodial dynamics, axon branching, synapse formation and postsynaptic connections scale up or down accordingly. I observed that indeed all the cellular processes slow down at lower developmental temperature and vice versa, which changes the DCN wiring pattern accordingly. Interestingly, behavior of flies adapts to their developmental temperature, performing best at the temperature they have been raised at. This shows that optimal brain function is an adaptation of robust brain wiring patterns which are specified by noisy developmental processes.

In conclusion, my doctoral work helps us better understand the developmental regulation of axon branching and synapse formation for establishing precise brain wiring pattern. We need all the cell intrinsic developmental processes to be highly regulated in space and time. It is infact a combinatorial effect of such stochastic processes and external factors that contribute to the final outcome, a functional and robust adult brain.

2. Zusammenfassung

Entwicklung einer robusten Hirnverdrahtung durch stochastische Entwicklungsprozesse

Die präzise Erzeugung von synapsenspezifischen neuronalen Verbindungen ist entscheidend für den Aufbau eines robusten und leistungsfähigen Gehirns. Neuronale Verdrahtungsmuster entstehen aus der Entwicklungsregulation der Axonverzweigung und Synapsenbildung in Raum und Zeit. Mehrere neuropsychiatrische und neurologische Entwicklungsstörungen weisen Defekte in der neuronalen Verdrahtung auf, die durch Synapsenverlust und dysregulierte Axonverzweigung entstehen. Trotz jahrzehntelanger Forschung ist es noch immer unklar, wie die beiden voneinander abhängigen zellulären Prozesse Axonverzweigung und Synaptogenese in präsynaptischen Arborisationen lokal gekoppelt sind.

In dieser Doktorarbeit untersuchte ich in Axonterminalien die spezifische Rolle der EGF-Rezeptoraktivität (EGFR) in Raum und Zeit bei der Axonverzweigung und Synapsenbildung in den Medulla-spezifischen dorsalen Clusterneuronen (M-DCN) / LC14-Axonterminals. In dieser Arbeit haben wir untersucht, wie genetisch kodiertes EGFR zufällig in den Axonterminals recycelt wird, wodurch ein asymmetrisches, nicht-deterministisches Verteilungsmuster entsteht. Dies wirkt als permissives Signal für die Beschneidung der Verzweigungen des Axons. Es war zu beobachten, dass alle M-DCN-Verzweigungen, die stochastisch in der Entwicklung EGFR '+' werden, synaptogen sind, was bedeutet, dass sie synaptische Materialien wie Syd1 und Bruchpilot (Brp) rekrutieren können. Ich habe gezeigt, dass die EGFR-Aktivität eine Doppelrolle bei einer normalen M-DCN-Entwicklung spielt. Erstens, bei der Regulierung der Konsolidierung von primären Axon Verzweigungen, möglicherweise durch die Regulation von Aktin vor der Synaptogenese, gefolgt von der Aufrechterhaltung der Brp-Level in den ehemals stabilisierten Axonverzweigungen durch Unterdrückung der Autophagie. Bei Fehlen einer optimalen EGFR-Aktivität steigt der basale Autophagie-Level an, was zu einem Verlust von Brp-markierten Synapsen führt, was ursächlich für erhöhte explorative Axonverzweigungen und Verluste von postsynaptischen Zielen ist. Der Mangel an EGFR-Aktivität verändert

das M-DCN-Verdrahtungsmuster, das erwachsene Fliegen aktiver macht und sie dazu bringt, sich bei einem Objektfixierungsassay zwanghaft-fixiert zu verhalten. Im zweiten Teil meiner Doktorarbeit habe ich gefragt, wie extrinsische Faktoren wie die Umgebungstemperatur während der Entwicklung die Verdrahtung des Gehirns bei Erwachsenen beeinflussen. Ich habe eine erhöhte oder verringerte Aufzuchttemperatur verwendet, von der bekannt ist, dass sie die Entwicklungsgeschwindigkeit der Puppen beeinflusst. Die Frage war, ob alle zellulären Prozesse der neuronalen Assemblierung wie filopodiale Dynamik, Axonverzweigung, Synapsenbildung und postsynaptische Verbindungen, entsprechend nach oben oder unten skaliert werden. Es war zu beobachten, dass sich tatsächlich alle neuronalen Prozesse bei niedrigerer Entwicklungstemperatur verlangsamen und bei höherer beschleunigen, das DCN-Verdrahtungsmuster verändert sich entsprechend. Interessanterweise passt sich das Verhalten von Fliegen an ihre Entwicklungstemperatur an und die Tiere bewegen sich am meisten bei der Temperatur, in der sie aufgewachsen sind. Das zeigt, dass eine optimale Gehirnfunktion eine Anpassung an robuste Verdrahtungsmuster des Gehirns ist, die durch verlässliche Entwicklungsprozesse spezifiziert werden.

Zusammenfassend hilft uns meine Doktorarbeit, die Entwicklungsregulation der Axonverzweigung und Synapsenbildung für den Aufbau einer präzisen Gehirnverdrahtung besser zu verstehen. Wir benötigen alle zellulären Prozesse, die die Entwicklung in Raum und Zeit regulieren. Es ist eine kombinatorische Wirkung zwischen intrinsischen stochastischen Prozessen und externen Faktoren, die zum Endergebnis beitragen: einem funktionellen und robusten erwachsenem Gehirn.

3. General Introduction

“Nothing exists for itself alone, but only in relation to other forms of life”- Charles Darwin.

Natural selection, the key mechanism of evolution, has played important roles in speciation. Particularly in the evolution of *Homo sapiens*, in advancing us emotionally, intellectually, and socially. Still the mysterious question remains- What makes us as humans different from other creatures? Philosophers of the 18th century have discussed this existential question for over several years and have reached certain conclusions after debating about “personhood”. First viewpoint called “Empirical functionalism” defines personhood as “a set of functions or abilities” which includes self-awareness, higher brain function or social behavior. Whereas, a second school of thought, called “Ontological Personalism” states that all human beings are human persons, irrespective of what they can or can’t do.

Even in 2022, we are still trying to understand how our brain can perform higher order cognitive and behavioral functions. A debate through the ages, which started way before Aristotle, famously known as “mind-body dualism” or “Cartesian dualism”. Descartes believed that the mind and body are separate entities, they can exist without each other and that human beings are the only dualistic creature. While his ideology was partially driven by religious motifs to coax irreligious people into believing in afterlife and the existence of the Supreme. This was refuted in Darwin’s theory of “Monism” where nothing exists apart from physical matter, like the brain. Darwin’s theory strongly suggests that all living beings are a product of evolution and human species are higher order animals because our brain has undergone positive natural selection compared to other apes over the last 5–6 millions of years to gain the present structural complexity. The fact that our mind/thought is not separate from our brain/body but rather it is a result of our brain function/activity, poses several challenging questions. Where does the information to build a brain come from? How do we build a robust brain which shows functional flexibilities? How much of the information comes from nature (genes), nurture (experience), or random developmental processes? When, where and how is that information turned into synapse-specific wiring to form functional neuronal circuits?

3.1 The brain wiring problem

Human brain size has quadrupled in size since *Homo* has last shared a common ancestor with chimpanzees, containing 100 billion neurons, more than 100,000 km of inter-connections and an estimated storage capacity of 1.25×10^{25} bytes information (Hofman, 2014). First neurons are born at distinct brain regions by temporally regulated expression of sets of transcription factors (Holguera & Desplan, 2018; Shirasaki & Pfaff, 2002). Following neurogenesis, neurons develop spatially segregated and functionally distinct neuronal compartments; dendrites and axons which interact with each other to form a neural circuit. Neuronal polarity is achieved by expressing specific sets of membrane proteins, ion channels, cell-surface receptors, adhesion molecules or microtubule polarity itself (Baas et al., 1988; Cheng & Poo, 2012; Horton & Ehlers, 2003). Filopodias facilitate neuronal growth cones located in axon terminals to navigate through brain space and intermediate choice points to reach the final target by following guidance cue gradients (Chédotal, 2019; Donato et al., 2019; Gallo & Letourneau, 2004; Zheng et al., 1996). During pathfinding, they undergo a transition from a stochastic exploratory phase to a stable phase once they form limited numbers of synapses with their canonical post-synaptic partners amongst numerous possible targets (M Neset Özel et al., 2019; Mehmet Neset Özel et al., 2015; Wit & Hiesinger, 2022). After decades of research, the biggest unanswered question remains: how can our genome encode synapse specific information for every neuron? If so, how do genes instruct when, where and how to target to form precise neuronal connections? Or is it genetically encoded intrinsic developmental processes which are inherently noisy/stochastic, allowing variable brain wiring outcomes to develop a robust and functional brain.

3.2 The chemoaffinity hypothesis and instructive molecules

Roger Sperry summarized in his chemoaffinity theory back in 1963: “[...] *the growing fibres are extremely particular when it comes to establishing synaptic connections, each axon linking only with certain neurons to which it becomes selectively attached by specific chemical affinities*” (Sperry, 1963). Are these “chemical affinities”

instructive molecules to wire a brain? If these were to be true, selective loss of such “instructive molecules” or “Sperry molecules” from the target region would result in miswiring of neurons. One such “Sperry molecule”, Netrin, has long been considered as a long-range, diffusible guidance cue in developing vertebrate nervous system (Serafini et al., 1996). Interestingly, loss of Netrin from the target region had very little effect on axon targeting, whereas loss from the growing region showed pathfinding defect. This simply reveals that there cannot be specific instructive molecules throughout development, rather their roles are more context-dependent and non-binary (composite instruction). Later, Sperry included additional features to his chemo-affinity hypothesis such as morphogen gradients to explain topographic projections of axons.

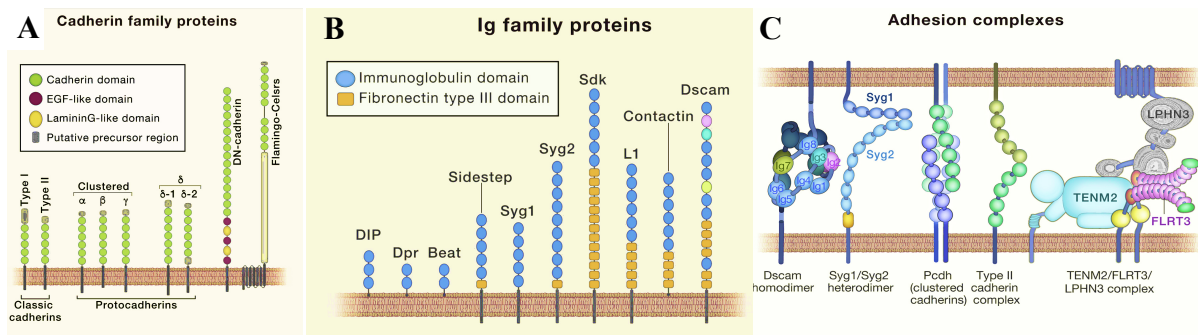


Figure 1: Different classes of recognition molecules implicated to have role in synaptic specificity. A) Different subclasses of Cadherin family proteins. B) Domain structures of Immunoglobulin (Ig) family proteins. Pink, turquoise and yellow Ig domains represent variable domains in invertebrate Dscam1 proteins present (or not) in different isoforms. C) Structure of adhesion proteins and binding partners located on pre- and postsynaptic membranes. Adapted from (Sanes & Zipursky, 2020)

Given we have approximately 20,000 protein coding genes in humans, stoichiometrically there might not be enough distinct chemical tags to account for all the neuronal connections and inter-neuron networks. This urged the possible combinations of short-range (contact mediated) and long-range (diffusible) cues/molecules that have been described as attractants/repellants to act as instructive cues. Slit, robo, semaphorins, ephrins has emerged as guidance molecules and receptors for proper neuronal targeting(Boyle et al., 2006; Fiederling

et al., 2017; Kidd et al., 1999; Y. Luo et al., 1993; Raper Jonathan A, 2000). Dscam, protocadherin (Pcdhs), neurexin-neuroligin, Dpr-DIPs interactions has been shown to be promising cell-recognition molecules for forming specific synaptic contacts in both vertebrates and invertebrates (Figure 1). But gene mutation studies of these “cell-recognition molecules” have shown them to work more as a composite instruction which are context- dependent rather than a single instructive cue. For example, Dscam-Dscam interaction mediates cell-avoidance in one compartment whereas dynamic exploratory behavior of sister axonal branches in another compartment in a context dependent manner. This describes Dscam to act more like a permissive cue (He et al., 2014; J. H. Kim et al., 2013). Another such example is DIP-gamma/Dpr-11 interaction which has been suggested to be the instructive cue for molecular matchmaking of R7 photoreceptors in *Drosophila* with its predominant post-synaptic partner Dm8 neurons (Courgeon & Desplan, 2019; Menon et al., 2019). How do two different subtypes of R7 find their reciprocal Dm8 partners during development? As per Sperry’s rules, Dm8 must express proper molecular tags (Dpr11 in this case) to contact specific R7 via DIP-Dpr interaction. Biology presents beautiful ways of creating patterns, where Dm8 is initially produced in excess and the ones that meet the correct R7 owing to these molecular tags survive, whereas others die (Courgeon & Desplan, 2019). Here, Dpr11-DIP-gamma interaction serves a part of the composite cue along with stochastic distribution of Dm8.

3.3 Algorithmic brain growth; from simple developmental rules to a complex brain

How can a limited amount of information in our genome encode the complex brain wiring explicitly? The pattern must arise from rather simpler genetically encoded developmental programs which can tolerate intrinsic stochasticity to achieve robustness in the outcome. The concept of building a complex structure/pattern from simple and iterative sets of rules is hugely influenced by Cellular automaton, first established by Stanislaw Ulam and John Neumann back in the 1940s. It is simply a collection of cells arranged in a grid of distinct shapes (1D,2D or 3D) where each cell state is a function of time, and the defined set of rules are driven by the states of neighboring cells. Later in 1970, John Horton Conway publicized this theory in the

form of a simulation game called “Game of Life” which is a zero-player game. This means the output/result is determined by the initial seeding state which is guided by four simple deterministic rules iterating in every step of the game where succeeding step is a function of the previous step (Hiesinger, 2021).

If we look carefully at nature or the brain, we do find similar examples of complex patterns which seems quite robust between individuals but has high variabilities within their own projections. For example, no two apple trees from the same mother plant are identical to each other. Just like no two neuronal projections from the same neuronal progenitor are. One famous example is the spatial patterning of the famous Purkinjee cells which has a stereotypical elaborate tree like dendritic morphology, but no two branches have the same lengths, angles or positions (Hassan & Hiesinger, 2015).

How is it possible for our genome to encode complex neuronal structure even at branch level? Similar to “Game of life”, brain wiring patterns can emerge from simple developmental rules that determine the endpoint structure, but the noise of the developmental processes can incorporate some random variations which makes our brain robust. Here the concept of genetically determined molecular matchmaking for ending up with correct partner has been challenged, as it does not consider the early stochastic developmental events starting from neurogenesis, axon pathfinding, branching of dendrites and axons, differential filopodial dynamics that leads to synapse specific brain wiring.

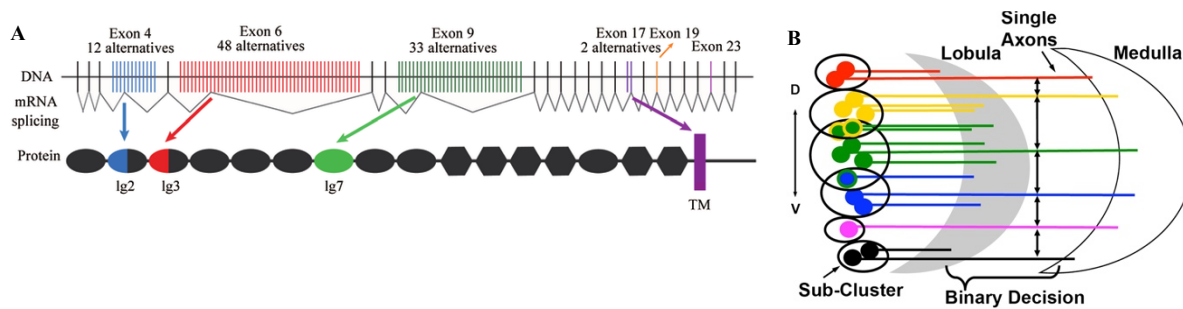


Figure 2: Stochastic developmental processes that result in phenotypic variabilities . A) Generation of diverse isoforms of Dscam by random alternative splicing of exons. Adapted from (Zhu et.al., 2011) **B)** Schematic representation of an equally spaced DCN projection pattern with neighboring cell bodies being subdivided into several sub-clusters, where a single neuron belonging to each sub-cluster can potentially target to medulla depending on Notch based symmetry breaking amongst the cell bodies in a particular sub-cluster. Adapted from (Langen et al., 2013; K. Zhu et al., 2011).

How do “genetically encoded” neurons give rise to variable patterns? One way is to incorporate noise or random inaccuracies of the system into the developmental program. Some examples being the invertebrate Dscams and vertebrate Protocadherins which has thousands of unique splice variants due to “random” mRNA splicing which are crucial for wiring specificity (Figure.2A)(Tasic et al., 2002; Wojtowicz et al., 2004). Another example of genetically encoded stochastic process that gives rise to deterministic pattern is Notch signaling executing symmetry breaking between competing neurons in the dorsal cluster neurons of fly visual system, resulting in a probabilistic selection of the winner axons (1/3) to target the distal optic neuropil (Figure.2B)(Langen et al., 2013). This does not undermine the role of genetically encoded “molecules” like cell adhesion molecules, cell surface receptors, guidance cues, signaling molecules etc. in brain wiring, but includes them as an integral part of the stochastic gene expression program. But how exactly does noisy axonal or dendritic growth processes turn into specific synaptic contacts?

3.4 From random developmental processes to precise synapse formation

There are different strategies to give rise to a precise neuronal wiring pattern. As per “promiscuous synapse formation hypothesis”, any two neurons which happen to be in spatial proximity to each other can form synapses. The other extreme will be no promiscuity at all, where synapses are formed only between correct partners by key and lock mechanism (Figure 3A). There are several examples of synaptic promiscuity where neurons form synapses with non-canonical partners in the absence of the correct ones. For example, when R7 in *Drosophila* visual system were redirected to incorrect target layer, they could still form synapses or when the canonical post-synaptic partner of R7 is missing, they end up forming synaptic connections with wrong or non-canonical partners in the same target region (Berger-Müller et al., 2013; Kulkarni et al., 2016). A single neuron in primary culture even forms autapses which are even capable of neurotransmission (Gomperts et al., 1998). Detailed investigation will reveal us the tendency/propensity of every neuron to form promiscuous synapses. Other cellular processes during brain development like neuronal birth order, cell body position, axon-axon interaction, branching pattern in target region may contribute to specific brain wiring, although none of these developmental processes itself dictate synaptic specificity (Figure.3B,C,D) (Agi et al., 2020). For example, in vertebrate visual systems early born neurons extend their axon over larger area compared to the late born (Osterhout et al., 2014). In the *Drosophila* visual system, a specific type of commissural interneurons projects their dendritic and axonal arbors in relation to the cell body position; dorsally positioned cell bodies (the late born) project their neurites in the dorsal side compared to the ventrally positioned ones (the early born) (Srahna et al., 2006).

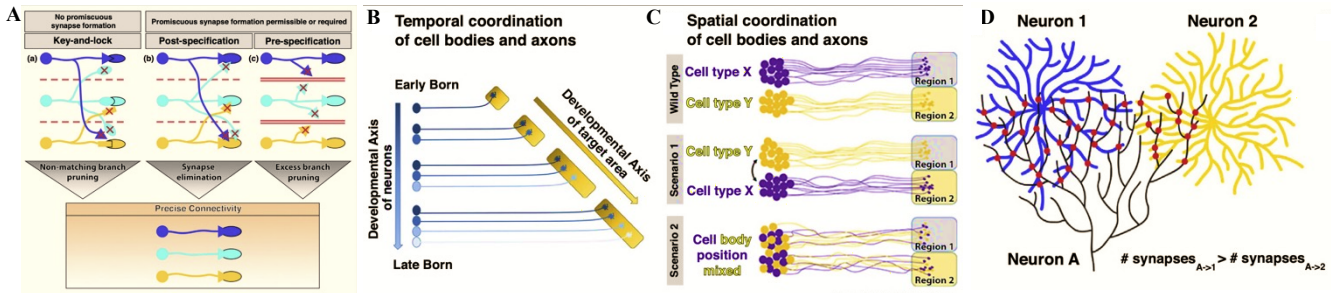


Figure 3: Neuronal strategies for meeting the right partner during brain development. **A)** Key-lock mechanism of molecular matchmaking precludes any promiscuous synapse formation, post-specification allows initial formation of exuberant promiscuous synapses whereas in pre-specification, neurons have capacity to form synapses with neurons they encounter in time and space thus requiring synaptic promiscuity for neuronal patterning. **B)** Temporal coordination of cell body and axonal positioning where birth order of cell bodies decides their neuronal target areas. **C)** Relative positioning of cell bodies decides their target area. For example, in scenario 1 and 2, while swapping or mixing the cell body positions, neurons need to form promiscuous synapses to form connections in improper target regions. **D)** Positional properties of axo-dendritic contacts restrict synapse formation. For example, as per Peter’s rule, overlap between dendrite and axonal arborizations influence synapse formation. Adapted from (Agi et al., 2020).

Theoretically, simple “no contact” rules can give rise to column and layer specific synaptic contacts and in turn complex brain wiring, given promiscuous synapses are allowed. Developmental noise is not an enemy of precision but a way of inducing variabilities in an otherwise stereotypical outcome. For example, if the splicing machinery for producing Dscam variants becomes non-noisy, then there will be acute wiring defect as many neurons will express similar types of Dscam, hence won’t separate self vs non-self. Promiscuous synapse formation can still lead to precise outcomes, but also ensures flexibility and robustness of development. For example, in *Drosophila* photoreceptors lack of autophagy changes the filopodial kinetics and hence affecting the rate/speed at which PRs see their partners in time and space, thus forming promiscuous synapses with non-canonical partners (Kiral et al., 2020). Owing to this developmental algorithm, we can build functionally robust brain wiring patterns.

3.5 The synaptotropic hypothesis

Back in the 1960s, D.K. Morest studied the development of calyces of Held in cats, rats and rabbits by Golgi staining and first suggested that the growth and branch patterning of dendritic filopodia has some synaptic engagement (Kent, 1960). In 1974, J.E. Vaughn states “[...] that presynaptic boutons initially make contacts with dendritic filopodia and growth cones, and that, as these synapses are formed, the dendritic growth regions move farther distally into the marginal zone leaving behind the synapses that have already been made.” He further states that “[...] as synaptically contacted filopodium expands into a new growth cone, the former growth cone develops the characteristic of a dendrite” (Vaughn et al., 1974). Following this hypothesis in 1976, Berry and Bradley working on Purkinjee cells came up with “synaptogenic filopodial theory” which predicted that “[...]that growth will be directed into areas of neuropil where ongoing synaptogenesis is most active; and that the magnitudes of the order of branching (dichotomy, trichotomy, etc.), and of segment lengths, will be correlated with fluctuations in prevailing synaptogenic activity during ontogeny” (Dailey & Smith, 1996). Finally in 1988 the term “synaptic tropism” was coined by Vaughn which reiterates the preferential dendritic growth in synaptic fields after studying electron microscopic analysis of the dendritic growth of motor neurons.

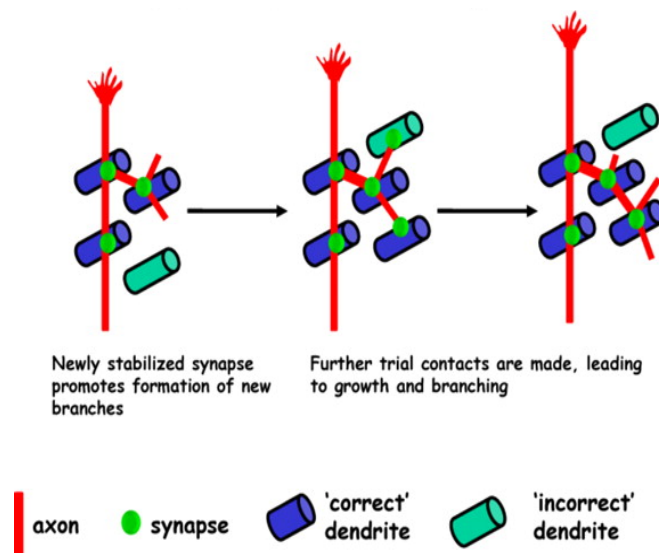


Figure 4: Synaptotropic hypothesis: feedback between axon branching and synapse formation. A) Schematic illustration showing axonal branches develops

from sites of synapses which in turn forms more synapses. These de novo synaptic sites act as branch initiation points. Axonal branches that can form synapses are stabilized, whereas failure to do so makes them prune back. Adapted from (Meyer & Smith, 2006)

Since then, the advancement of live imaging in vertebrate brains has revealed dynamic axonal and dendritic growth where the localization of synaptic machineries/molecules highly correlate to branch stabilization (Constance et al., 2018). Whereas the outcome of axonal branching and synapse formation is spatially and temporally highly stereotypical, the developmental process itself relies heavily on probabilistic local events like filopodial growth and retraction, local protein recycling and degradation, self-avoidance of exploratory filopodia through stochastic expression of cell adhesion molecules, cytoskeletal polymerization and depolymerization, mitochondrial fusion and fission, and stochastic synaptic seeding (Chia et al., 2014; Lewis et al., 2018; M Neset Özel et al., 2019; Mehmet Neset Özel et al., 2015; Rajgor et al., 2021). Synaptotropic growth is an ideal example of implying a re-iterative simple set of rules by local autonomous agents which makes context-dependent decisions (Figure. 4). This process leads to stereotypical branching patterns with the possibility to have local variabilities, like every snowflake is different from each other. But a major gap in knowledge is the limiting factor that ends this developmental phase. It can either be restricted by growth duration or by the limit of synaptic input. One other way might be temporal coupling of these positive feedback processes by local regulators like signaling molecules in the branches.

3.6 Dynamic processes of axonal branching:

Development of neural circuit connections rely on the proper regulation of axon branching, a developmental process that allows a neuron to connect with multiple targets across vertebrates and invertebrates. There are examples of different forms of branching patterns observed in nature that are tailored for optimum neuronal function. Axons of Retinal ganglion cells sensory neurons follow arborization pattern, central sensory projections follow bifurcation while descending projections from the cortex have collateral branches (Gibson & Ma, 2011). Irrespective of the

branching pattern, axonal branching is a multi-step process starting with specification of axon branch location. Most axonal branches are formed at terminals which might be induced by target derived factors like NGF which promotes terminal branching of the sensory axons in peripheral tissue. They can also be locally induced by guidance molecules like netrin1 which stimulates branch formation in cultured hamster cortical neurons. The initiation, growth, and guidance of axon branches in response to extra-cellular or cell intrinsic cues require the regulation of cytoskeletal dynamics(Dent et al., 2004; Ketschek et al., 2015). Dynamic filopodial protrusions which serve as the branch precursors are actin rich meshwork, followed by microtubule invasion and stabilization of nascent branches into stable ones. Dynamic interaction of actin and microtubule is necessary for proper branch formation which if ablated results in inhibition of neurite initiation(Dent & Kalil, 2001).

Two models of branching morphogenesis have emerged from studying different branched organs. First is deterministic where the branching pattern is stereotypical for example as described in mouse lung or *Drosophila* tracheal system(Christos Samakovlis†, 1996). Second model is probabilistic, where an exuberant number of branches are formed initially followed by elimination of some branches to give rise to the final adult pattern. Classical example of axon branch pruning is the layer-five projection neuron of the motor and visual mammalian cortex(O'leary & Koester, 1993). There can be activity-dependent, small scale, stochastic terminal arbor pruning as observed in NMJs, in the peripheral nervous system or climbing fiber inputs to the cerebellum in mouse CNS(Berke et al., 2013; Budnik et al., 1990; Kawamura et al., 2013). Another possibility is large scale, stereotypical axon branch pruning where an axon projects its collateral branches to both appropriate and inappropriate targets followed by predictable removal from the wrong target. This kind of pruning was first shown in the remodeling of cortical callosal axon branches in cats(G.M.Innocenti, 1981), later there is evidence in CA1 neurons in the hippocampo-septal pruning (Bagri et al., 2003) or retinotopic connections of RGC axons(L. Luo & O'Leary, 2005). Both intrinsic factors like ubiquitin-proteasome system, cytoskeletal dynamics, transcription factors, synaptogenesis etc. and extrinsic factors like hormones, trophic factors, axon repulsion molecules influence axon branch pruning.

3.7 Synaptic homeostasis

During brain wiring, axons and dendrites project to their respective target environment to form synaptic connections during development, which ideally needs to be maintained throughout the lifetime of the neuron. Since neurons are largely non-replenishable, there is a fixed pool of neurons except for certain brain regions capable of adult neurogenesis, which also decreases with age (Braun & Jessberger, 2014; Kase et al., 2020; Ming & Song, 2011). To keep the brain functional, neurons must employ robust cellular mechanisms for maintaining synaptic homeostasis over a long time starting at development. Failure to do so results in synapse loss, followed by neuronal degeneration and ultimately leading to circuit malformations, which underlies several neurodegenerative, psychiatric, and neurodevelopmental defects (Powchik et al., 1998; Shah et al., 2017; Taoufik et al., 2018). There is some evidence suggesting that the actin cytoskeleton, adhesion receptors and scaffolding proteins provide structural support for synapse maintenance (Berger-Müller et al., 2013; Gentile et al., 2022; MacGillavry et al., 2013).

Synapses are systematic accumulation of several proteins with finite lifetimes. Consequently, maintaining a functional synapse involves continued removal and degradation of aged or damaged proteins and subsequent replacement with newly synthesized ones. For further efficacy, it can be done locally at synaptic sites or at bulk in the cell body (Alvarez-Castelao & Schuman, 2015). “Synapse turnover” must be active during development while neural circuits are formed and later in adulthood which is important for acquiring synaptic specificity (Ruffolo et al., 1978; Soykan et al., 2021). For example, neurons generated in the retina of chick embryo form transient synapses, whereas spinal cord neurons form long-lived synapses with striatal muscle (Thompson et al., 1983). This suggests that synapse turnover; synapse formation and termination rates are regulated, and that the specificity of synaptic connections can be increased by selective termination of synapses. Another such example is memory formation where 50% of the synapse population are altered over a time course of weeks in response to altered experience-dependent inputs (Faust et al., 2021).

3.8 Endo-membrane degradation pathways in synapse maintenance and brain wiring

Back in the 1980s, Feinberg and others suggested that unproportioned synaptic elimination could lead to altered circuits, which are seen in neurodevelopmental and neuropsychiatric disorders like Schizophrenia (Feinberg, 1982). In general, infants are born with 15% more neurons than adults which are pruned by neural activity during the critical period of development (Sakai, 2020; Spear, 2013). For proper brain functioning, elimination of synapses is a critical cellular process which functions as a quality control mechanism for proper development, functionality, and survival (Faust et al., 2021; Paolicelli et al., 2011; Scholl et al., 2021; Shatz & Kirkwood, 1984). However, neurons usually being polarized cells with clear spatial segregation of axons and dendrites challenges the homeostatic regulation of protein turnover locally. The distance between cell body, dendrites and axon terminals raises the question about spatial regulation for protein sorting and degradation. The existence of local protein synthetic machinery and mRNAs at developing axon growth cones suggest local ability of growth cones to react to changing internal and external states during development (Steward & Worley, 2002). Local protein synthesis at the axon terminals is important for synaptic plasticity, on the flip side protein degradation (either locally or at bulk) is important for functional synapse (Deglincerti et al., 2015; Eberwine et al., 2001; Glock et al., 2017; Gumy et al., 2010; Hobson et al., 2022).

Many synaptic proteins are degraded by the canonical ubiquitin proteasome system (UPS), where the protein to be degraded are being ubiquitinated and then targeted to degradation via proteasomes (Bingol & Schuman, 2005; Ciechanover & Schwartz, 1998; Hakim et al., 2016). Suppression of the system pharmacologically affects synaptic proteins (Hakim et al., 2016). Although this degradation system has received most attention, an alternative catabolic route which is receiving increasing attention is the endo-membrane degradation pathway. Endo-lysosomal degradation and macro-autophagy (autophagy) are the major endo-membrane degradation pathways which intersect and interconnect in amphisome (autophagosome + late endosome) formation followed by lysosome mediated degradation of the engulfed proteins (Boecker & Holzbaur, 2019). The hallmark of maturation process from early endosomes to lysosomes is progressive increase of luminal pH, which is required for

initiation of degradation (Bright et al., 2016). Rab GTPases, which are the molecular coordinators of membrane trafficking, have been shown to be both ubiquitous and neuron specific (Chan et al., 2011). There are ample examples suggesting local degradation of both cytoplasmic and membrane proteins in dendritic spines and/or axon terminals (Frampton et al., 2012; Goo et al., 2017; Jin et al., 2018). In axons of cultured neurons, autophagosomes form at the distal ends containing cargoes from synapses. Following autophagosome formation at axon terminals, they are transported back to the cell bodies where they fuse with lysosome (Figure. 5).

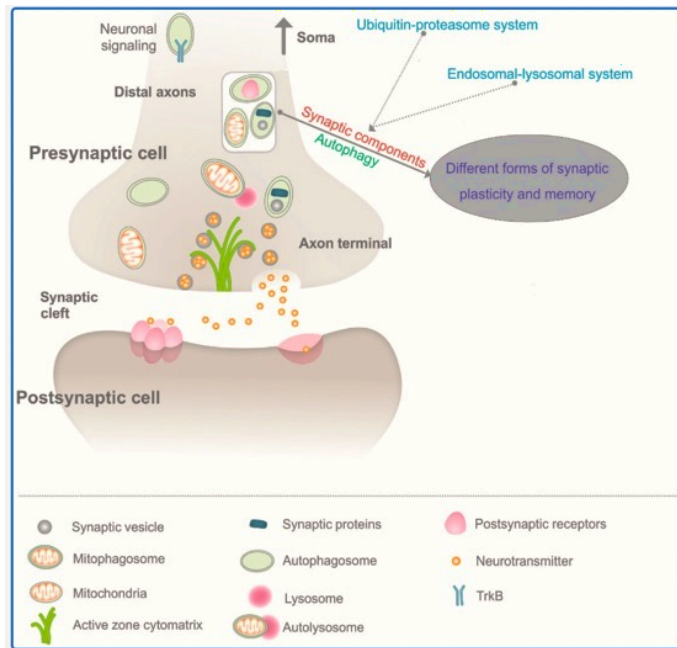


Figure 5: Synaptic autophagy (Syntophagy) in maintaining presynaptic proteostasis. Emerging concepts and functions of how autophagy might regulate synaptic components and synaptic plasticity. Synaptic components (in red, outlined in the white rectangle within the presynapse) including synaptic proteins (PSD-95, PICK1 and SHANK3), synaptic vesicles, postsynaptic receptors (GABAA receptors and AMPA receptors following endocytic removal from the plasma membrane) and mitochondria are known to be degraded (straight line) by autophagy (in green), thereby potentially contributing to different forms synaptic plasticity (in purple, outlined in an oval-shaped frame) such as long-term potentiation (LTP), long-term depression (LTD) and memory formation. Ubiquitin-proteasome system (in blue) and endosomal-lysosomal system (in blue) also degrade (dotted lines) certain

synaptic components and, thus contribute to synaptic plasticity and memory. Adapted from (Liang, 2019)

Basal level of autophagy has been shown to be required for neuronal maintenance in healthy neurons and low level of increased autophagy has neuroprotective effects(Cherra Iii & Chu, 2008; Ray, 2020; Stavoe & Holzbaur, 2019). Although autophagy is a major degradative pathway for removal and recycling of cytosolic proteins, over the last decade neuroscientists are focusing more on the role of autophagy in synapses with less known role in neurodevelopment. Although we can get a functional brain in loss of autophagy; in specific neurons in worms and flies, autophagy loss results in reduced synapse development and aberrant dendritic arborization(Clark et al., 2018; H. J. Kim et al., 2017). Whereas induction or basal level of autophagy suppresses neurotransmitter release and affects presynaptic structure in dopaminergic neurons of mice(Hernandez et al., 2012). In the human model for neurodevelopmental disorders, imbalance in autophagy causes synaptic deficits(Linda et al., 2022). In *Drosophila* photoreceptors, loss of autophagy affects filopodial dynamics and changes the kinetics of synapse formation and specificity which in turn changes post-synaptic partner choice(Kiral et al., 2020). This shows that a basal level of autophagy is required for maintaining proper synaptic homeostasis which in turn affects the neuronal partner choice.

3.9 Molecular coupling of axon branching and synapse formation

Animal behavior is a function of an intricate network of connections formed between neurons via synapses. Axons form elaborate branching patterns to target multiple target areas where they form synaptic connections. Although we know various examples of correlated synaptogenesis and neurite branching supporting the synaptotropic hypothesis(Fiala et al., 1998; Vaughn et al., 1988), very little is known about the regulation of the two cellular processes. Actin assembly initiates filopodia formation followed by microtubule invasion which marks a matured branch(Pacheco & Gallo, 2016). In *Drosophila* photoreceptors and visual system interneurons, filopodial dynamics predict the rate of synapse formation; faster dynamics results in less synapse formation(Kiral et al., 2021). F-actin has been shown to interact with presynaptic active zone components and affect their recruitment in the synapse;

pre-synaptic proteins also regulate F-actin organization at synapses (Chia et al., 2014a). For example, in vertebrates active zone protein Piccolo interacts with actin-regulator Profilin (Waites et al., 2011). In *Drosophila*, F-actin regulator Wasp binds to a perisynaptic adaptor protein Nervous Wreck to control synapse morphology (Coyle et al., 2004). WRC, activator of Arp2/3 complex, regulates both axon branching and presynaptic assembly in *C.elegans* (Chia et al., 2014a). Other regulators are the neurotrophins which were originally identified to promote neuronal survival and differentiation (Cohen-Cory & Fraser, 1995), BDNF which regulates branch morphology of axons and dendrites along with promoting synapse number and modulating synaptic maturation in developing brain. (Granseth et al., 2013; Lom & Cohen-Cory, 1999). Drp1 receptor mitochondrial fission factor (MFF) controls neurotransmitter release and axon branching in mouse cortical neurons (Lewis et al., 2018).

3.10 Receptor tyrosine kinase and phosphatases in neuronal wiring

The human genome encodes 90 types of Receptor tyrosine kinases (RTKs) and 107 receptor protein tyrosine phosphatases (PTPs) (M. Kim et al., 2017). They are involved in many cellular processes like axon growth/guidance, axon branching, dendrite growth/guidance and synaptic growth and function (Cornejo et al., 2021; Holland et al., 1998; Neben et al., 2019; Zschätzsch et al., 2014). For example, Ephrin is involved in the patterning of fly visual system and guides axonal branches in mushroom body neurons (Boyle et al., 2006; Malin & Desplan, 2021). Whereas Ryks are involved in axon guidance in both vertebrates and invertebrates and in organization of olfactory maps during fly development (Keeble et al., 2006; Liu et al., 2005; Schmitt et al., 2006; Yao et al., 2007). Similarly, LKB1-NUAK1 has been shown to control cortical axon branching and critical for establishment of neural circuits in vertebrates (Courchet et al., 2013). Similarly, EGFR which has important roles in cell-proliferation, differentiation and cancer, is also crucial for axon guidance in the adult ocellar sensory system (OSS) of *Drosophila* (Fraguas et al., 2011; García-Alonso et al., 2000). Lack of EGFR activity partially affects OP axons while fully affects BM axonal growth/guidance towards reaching the target region. EGFR signaling has also been shown to affect presynaptic branch pruning in Dorsal Cluster Neurons, a type of commissural interneurons of the fly visual system (Zschätzsch et al., 2014). Insulin

receptor which is involved in cell-metabolism is also required for *Drosophila* photoreceptor targeting mediated by adaptor protein Dock(J. Song et al., 2003). LARs are a type of PTPs which are shown to be involved in axon targeting and synaptogenesis in *Drosophila* photoreceptors and NMJ respectively(Choe et al., 2006; McNeill et al., 2020). LAR mutants exhibit abnormal synapse morphology and synaptic function. Like LARs, Ptp69D participates in diverse aspects of neuronal development(J. K. Song et al., 2008). In Ptp69D mutants, R1-R6 photoreceptors in *Drosophila* show abnormal medulla outgrowth and inhibition of synaptic growth in the giant fiber system (GFS)(L. T. H. Lee & Godenschwege, 2015). Homeostatic activity/signaling of protein kinases and protein phosphatases at synapses are important for maintaining proper balance in LTP/LTD, thus regulating synaptic plasticity and memory formation(Khan et al., 2021; H. K. Lee, 2006). Dys-regulation of it results in brain's cognitive impairment, which has links to several neurologic diseases (Braithwaite et al., 2012; Ramos et al., 2003).

3.11 Environmental effects on neuronal wiring

The nature vs nurture debate has been going on since Hippocrates. Nature refers to the genetic makeup of an individual passed on through heredity. Whereas nurture is the environmental effect one has been raised in, which can positively or negatively influence one's genetic constitution. Forty years ago, brain development was believed to be strongly deterministic; we are born with specific sets of hardwired neurons and brain function is a direct effect of it. Recent advances in neurobiological techniques have revealed that brain development is a robust process which considers both genetic and environmental input to perform behavioral function. In 1998, Fred "Rusty" Gage showed in mice that adult animals can produce new neurons. Later it has been demonstrated that neurons can form new connections and change their connectivity strength and pattern in response to external cue (Arnsten et al., 2010; Dahmen et al., 2022). On top of genes and extrinsic factors, in 2021, an intrinsic source of brain wiring regulation has been described that results in variable neuronal projections in *Drosophila* visual system which is causal to behavioral individuality (Linneweber et al., 2020). Although the role of environmental factors in establishing a functional brain is undeniable, most of the studies are done in postnatal cases when experience plays a major role in brain

wiring and plasticity. Even lack of proper nutrition in late prenatal and early postnatal development has been linked to arrested brain growth leading to aberrant neurodevelopment (Georgieff et al., 2018; Keunen et al., 2015). This strongly suggests further need for studying the potential role of environmental factors on brain development and function.

Temperature is another such factor that plays an important role in various biological processes like sex determination in some reptiles, body size and pigmentation regulation in ectothermic animals (Figure. 6B) or growth rate of embryonic, larval and pupal development in (Figure. 6A) (Angilletta et al., 2004; Ludwig & Cable, 1933; Phillips & Heath, 1995; Powsner, 1935). Endothermic animals like humans, have sophisticated thermoregulatory mechanisms to maintain stability of internal organs. This makes it hard to study the direct effect of minor temperature change on brain development. Human cognitive function is known to decline in extreme temperatures. Heat stroke is one such example when the internal body temperature rises leading to convulsion, coma etc. (Koh, 2018; Wang et al., 2008). In another animal study, temperature can alter the frequency of pauses during nesting behaviour by changing the developmental rate of offspring (Abram et al., 2017). To what extent such behavioral changes stem from differences in brain wiring at different developmental temperatures is intriguing and largely unknown.

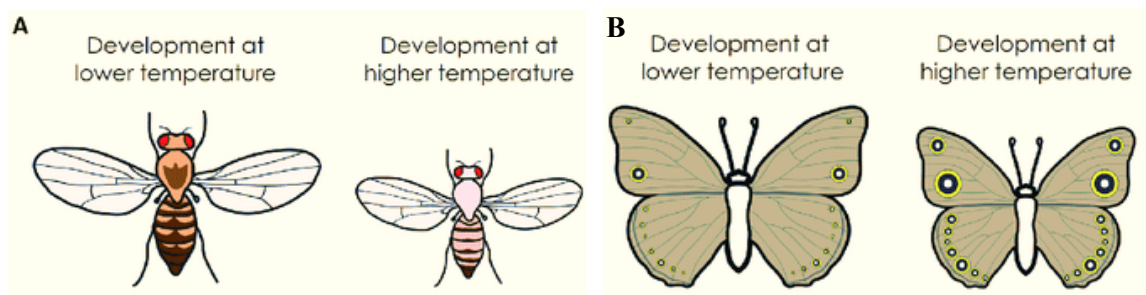


Figure 6: Effect of environmental temperature on phenotype expression. Examples of developmental plasticity; temperature induced change in body size and pigmentation in *D.melanogaster* flies and *B.anynana* butterflies. Adapted from (Lafuente & Beldade et.al., 2019).

3.12 The *Drosophila* visual system; A model to study axon branching and synaptogenesis

Human brain is one of the most complex systems to study even with the recent biotechnological tools available. One essential way to investigate how an adult human brain works is to trace back the early developmental events, like solving a puzzle. Scientists conduct causal studies on simpler model organisms with manageable number of traceable neurons. Ethical considerations restrict study of human brain development ex-vivo and unavailability of post-mortem brains exacerbates this. *Drosophila melanogaster*, also known as fruit fly, has become a popular system for genetic studies largely due to the simplicity and malleability of the fly genome. *Drosophila* has 60% homology to humans, less redundant, and 75% of genes responsible for human diseases have homologs in the fly genome which makes it even more significant to model and study human diseases in flies (Mirzoyan et al., 2019). Fruit fly genome was sequenced back in 2000 and has been extensively annotated. They have one sex chromosome and three autosomal chromosomes with advanced genetic tools to manipulate, track and stabilize various genetic alterations over multiple generations (Jeibmann & Paulus, 2009; Reiter et al., 2001; Tolwinski, 2017).

The *Drosophila* visual system consists of four main neuropils in each optic lobes: lamina, medulla, lobula plate, lobula which contains approximately 150,000 neurons and glial cell types with over 70 neuronal subtypes (functional, molecular, and spatial). Two major types of neurons can be identified within the *Drosophila* optic lobes: “interneurons” which project in the optic lobe and “projection neurons” which connect the optic lobe to the central brain, similar to vertebrate systems where the former projects to the targets in vicinity and later millimeters away (Chédotal & Richards, 2010; Fischbach & Dittrich, 1989). Like other vertebrate and invertebrate brain structures, *Drosophila* axons and dendrites are spatially segregated and arranged in sub-type specific layers and columns in the neuropils (Fischbach & Dittrich, 1989; Morante & Desplan, 2008). This allows the study of biological rules of pattern formation and assembly of neurons into circuits. Over the years, *Drosophila* photoreceptors have been the model of choice for studying visual systems and understanding the principles of neuronal connectivity (Tolwinski, 2017).

Photoreceptors extract information from the external world, such as shape, motion, color, e-vector orientation of polarized light etc. and transmit it to the central brain via interneurons and projection neurons. The medulla neuropil receives direct input from the photoreceptors and contains about 40,000 interneurons which consists of the major neuronal sub-population in the optic lobe (Schnaitmann et al., 2018; Y. Zhu, 2013).

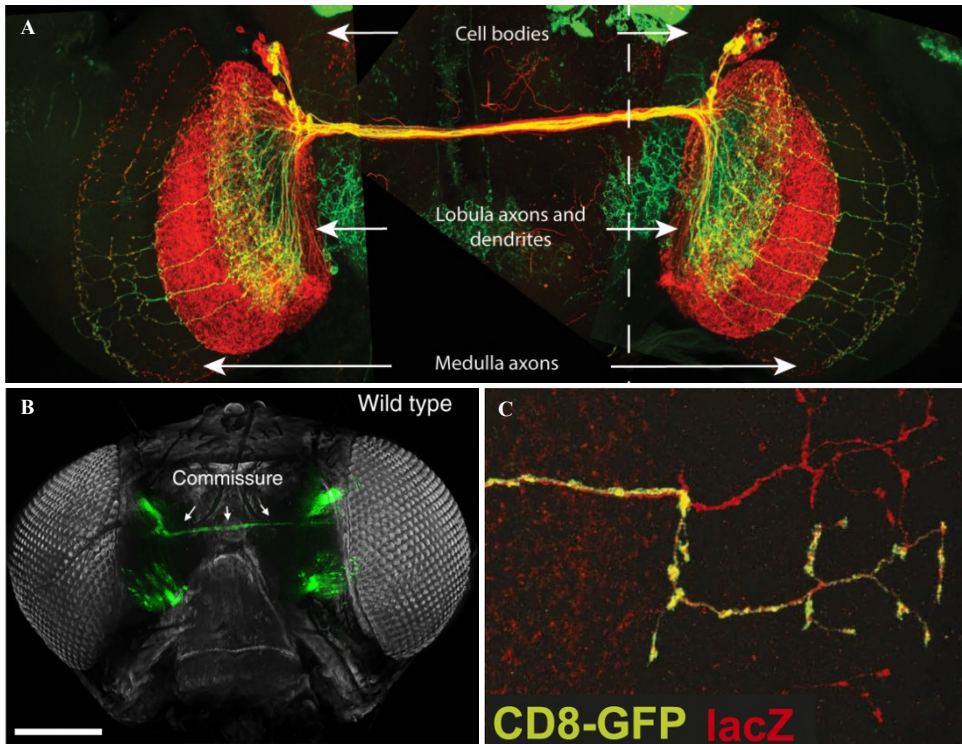


Figure 7: Commissural interneuron of adult *Drosophila* visual system. A-B) The Dorsal Cluster Neurons (DCNs) are the commissural interneurons of the fly visual system. They have dorsally located cell bodies and send out ipsilateral dendrites and contralateral axons which innervate either the lobula or the medulla where they form ladder-like branching patterns. **C)** Medulla innervating DCNs form stereotypical presynaptic branches; 1st level in the lobula plate-medulla junction, 2nd level between M7-M8 and 3rd level between M1-M3 layers of medulla. Adapted from (Linneweber et al., 2020; Pende et al., 2018; Zschätzsch et al., 2014)

Dorsal cluster neurons (DCNs), also known as LC14, are a class of commissural, cholinergic interneurons of the fly visual system with variable number of cell bodies (22 to 68) between the two optic lobes in an individual fly brain. DCNs show

stereotypical projection patterns in the optic lobe; dendrite projects to the ipsilateral (ipsi) lobula, whereas axons project either to the lobula or the medulla of the contralateral (contra) optic lobe. The axons and dendrites retain the positional information of their respective cell bodies while projecting to their target regions: dorsally located cells will project their neurites to the dorsal side of the ipsi and contra optic lobes and vice versa (Hassan Bassem A., 2000; Langen et al., 2013; Linneweber et al., 2020; Srahna et al., 2006; Zschätzsch et al., 2014). DCNs serve as a nice model system to study integration of positional information into cellular memory for making stereotypical projections. DCNs are post-mitotic neurons which extend their axons into the optic lobe during metamorphosis, between larvae and adult, which makes it an interesting model to study development of adult-specific axon guidance and branching in-vivo. Initially it was shown that Jnk signaling is required for DCN axon extension followed by axon retraction regulated by FGF signaling, finally leading to neuronal patterning during development. Later it was discovered that DCN cell bodies participate in Notch based cellular competition to form variable axonal projection patterns in the medulla. (Langen et al., 2013; Srahna et al., 2006). During development Notch signaling facilitates stochastic projection of ~6-23 (one third) of the axons to the distal neuropil, medulla (M-DCNs). There they form stereotypical fan-shaped branching patterns whereas the remaining ~11-55 axons project to the proximal neuropil, lobula (L-DCNs) (Langen et al., 2013; Linneweber et al., 2020; Zschätzsch et al., 2014). This variable projection pattern of DCNs (L/M-DCN ratio) in an individual is required for visual attention behavior in adult flies as loss of DCNs resulted in no stripe fixation in Buridan's paradigm assay. Although these flies behave robustly in a population level, individual flies from the same genetic background behaved variably when tested separately, suggesting unique DCN projection pattern underlies individual object fixation behavior. Also, higher the variability in DCN projection pattern, more fixated those flies are between two stripes in Buridan's assay, showing input asymmetry is important for visual attention (Linneweber et al., 2020).

Following the projection of axons in the lobula or medulla, DCNs form pre-synaptic arbors in a stereotypical manner. While the L-DCN axons form bushy arborization patterns, M-DCN axon form branches at the lobula-lobula plate intersection, M7-M8 layer and M1-M3 layer, with some occasional branches in between (Zschätzsch et

al., 2014). Although the branching positions are robust, the number, length or angle of branches formed by each axon at specific layers are variable. Due to easier visualization of M-DCN branches and lack of a proper driver for L-DCNs, the branch development of the former has been studied in detail. M-DCNs start forming collateral branches around 42% APF followed by pruning between 55% APF to 72% APF to give rise to the adult branching pattern. Optimum level of EGFR activity has been shown to be crucial for the branch pruning process. Both lack or constitutive activation of EGFR affects actin polymerization in the DCN axons which results in less pruning and more branches in adults. Interestingly, lack of EGFR activity increases the variability of adult M-DCN branch number (Zschätzsch et al., 2014). Hence, understanding the developmental regulation of asymmetric M-DCN wiring pattern, especially at synaptic level is interesting. If or how dys-regulated EGFR activity affects synapse formation is not known. Hence, M-DCNs pose as a good model system to study co-regulation of axon branching and synapse formation possibly via EGFR signaling to shape the adult DCN circuitry.

4. Aim

How the adult brain circuitry develops with precision and robustness poses one of the major riddles in the field of neurobiology. Both deterministic and noisy/stochastic processes can lead to robust outcomes. It is important to understand when noise is not an antagonist of precision, but a mechanism to integrate variability in the system. For example, axon branching and synaptogenesis are two inter-dependent cellular processes crucial for adult wiring pattern formation. Both the processes are independently guided by stochastic developmental events like filopodial dynamics, branch pruning, recruitment of synaptic machineries and synapse stabilization to form precise wiring patterns. The positive feedback between axon branching and synapse formation (synaptotropic growth) has been studied intensively, with some neurons showing synaptotropic growth. Still, it is not clear how, when and where these events are regulated during the development of adult brain circuitry.

The goal of my doctoral work is to understand the mechanism of molecular links or regulators of axon branching and synaptogenesis during *Drosophila* pupal brain development which gives rise to stereotypical yet variable M-DCN circuitry in adult brains. The second part of my work focuses on how environmental factors like developmental temperature affect synaptic choice thus influencing adult brain wiring. My doctoral work addresses the following questions: Is axon branching a function of synaptogenesis? Is axon branching and synapse formation spatio-temporally regulated? If so, how might the two processes be co-regulated in space and time? How does it affect the adult brain wiring and behavior? Finally, to what extent neuronal strategies to find right synaptic partners are affected by environmental factors such as temperature experienced during synaptogenesis? In this context, I have investigated the role of EGFR signaling in regulating M-DCN axon branch consolidation and synapse formation during development and how it ultimately affects synaptic partner choice and behavior in adults. I have also investigated the possible effects of different developmental temperatures on synapse formation and partner choice in M-DCNs.

5. Manuscript 1

A critical developmental interval of coupling axon branching to synaptic degradation during neural circuit formation

Suchetana B. Dutta, Gerit Arne Linneweber, Maheva Andriatsilavo, Peter Robin Hiesinger, Bassem Hassan

Submitted in Current Biology (under revision)

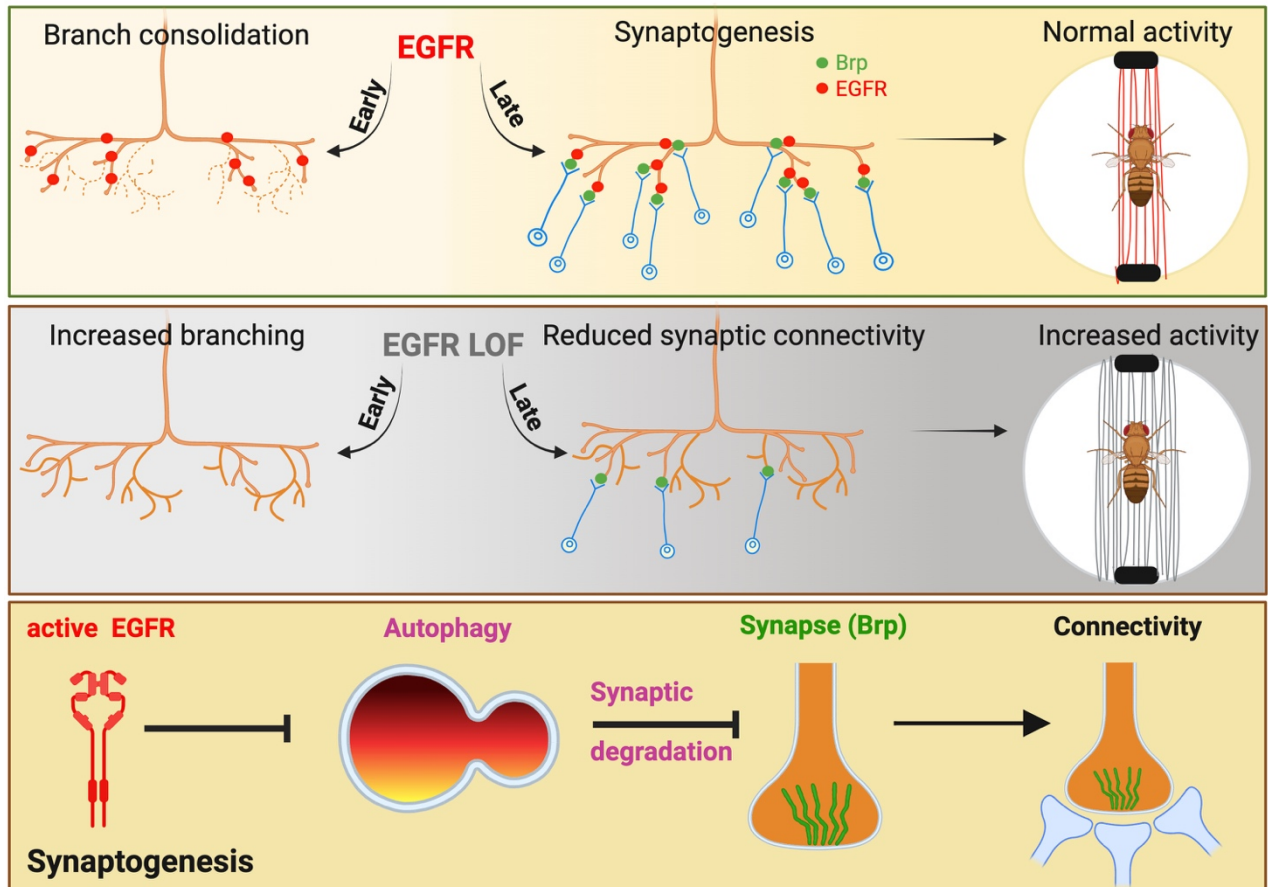
Contribution

I designed, performed and analyzed all experiments in this manuscript under the supervision of Prof. Dr. Bassem Hassan and Prof. Dr. P. Robin Hiesinger except the Buridan's paradigm. Buridan's paradigm experiments were designed, carried out, and analyzed by Gerit Arne Linneweber. The paper was written by myself, Prof. Dr. Bassem A. Hassan and Prof. Dr. P. Robin Hiesinger. The original article including the supplemental information is included on the following pages and available online at:

<https://www.biorxiv.org/content/10.1101/2022.04.06.486606v1.full>

Article

A critical developmental interval of coupling axon branching to synaptic degradation during neural circuit formation



Graphical abstract

Authors

Suchetana B. Dutta^{1,2,3}, Gerit Arne Linneweber², Maheva Andriatsilavo^{1,2,3}, Peter Robin Hiesinger^{2*}, Bassem A Hassan^{1,2,3*}

¹Institut du Cerveau-Paris Brain Institute (ICM), Sorbonne Université, Inserm, CNRS, Hôpital Pitié-Salpêtrière, Paris, France.

²Division of Neurobiology, Free University of Berlin, Berlin, Germany.

³Einstein-BIH, Charité Universitätsmedizin, Berlin, Germany.

*Corresponding authors: PRH prh@zedat.fu-berlin.de and B.A.H. bassem.hassan@icm-institute.org

Keywords

Neuronal circuit, Wiring specificity, Axon branching, Synaptogenesis, Synaptic autophagy, *Drosophila*

Title

A critical developmental interval of coupling axon branching to synaptic degradation during neural circuit formation

ABSTRACT

The emergence of neuronal wiring specificity requires stabilization of dynamic axonal branches at sites of selective synapse formation. Models that explain how axonal branching is coupled to synaptogenesis postulate molecular regulators acting in a spatiotemporally restricted fashion. We report that Epidermal Growth Factor Receptor (EGFR) activity is required in presynaptic axonal branches during two distinct temporal intervals to regulate circuit wiring in the developing *Drosophila* visual system. EGFR is required early to regulate primary axonal branching and independently again later to prevent autophagic degradation of the synaptic active zone protein Bruchpilot (Brp). The protection of synaptic material during this later interval of wiring ensures the stabilization of terminal branches, circuit connectivity and appropriate visual behavior. Phenotypes of EGFR inactivation were rescued by increasing Brp levels or downregulating autophagic genes. We identify a temporally restricted molecular mechanism required for coupling axonal branching and synaptic stabilization that contributes to the emergence of neuronal wiring specificity.

INTRODUCTION

Stereotypy and robustness of neuronal circuit wiring is thought to be critical for normal brain function, and malformations of neuronal circuits are associated with a spectrum of neurodevelopmental and neuropsychiatric diseases like Autism Spectrum Disorder and Schizophrenia (Powchik *et al.*, 1998; Doll and Broadie, 2014; Moyer, Shelton and Sweet, 2015). Whereas the outcome of axonal branching and synapse formation is spatially and temporally highly stereotyped, the developmental process itself relies heavily on probabilistic local events like filopodial growth and retraction, local protein recycling and degradation, self-avoidance of exploratory filopodia through non-deterministic expression of cell adhesion molecules, cytoskeletal polymerization and depolymerization, mitochondrial fusion and fission, and stochastic synaptic seeding (Chen *et al.*, 2006; Zschätzsch *et al.*, 2014; Winkle *et al.*, 2016; Simmons *et al.*, 2017; Constance *et al.*, 2018; Lewis *et al.*, 2018; M. Neset Özel *et al.*, 2019; Urwyler *et al.*, 2019). This raises the question of how such events are orchestrated in space and time to reproduce stereotyped circuit wiring diagrams. The formation of functional neuronal circuits relies on neurons branching their axons during development in an orderly spatial and temporal manner to connect with a specific

set of post-synaptic neurons (Rico *et al.*, 2004; Colón-Ramos, 2009; Kalil and Dent, 2014; Batool *et al.*, 2019; Agi, Kulkarni and Hiesinger, 2020) but how individual axons and their branches locally pattern their connectivity to their post-synaptic targets is not well understood. Evidence from various systems shows that during late stages of neuronal circuit formation, after an initial phase of exploratory axonal branching, interdependence between synapse formation and branching dynamics plays a key role in the selection of future synaptic partners (Meyer and Smith, 2006; Ruthazer, Li and Cline, 2006; Chia *et al.*, 2014; Kalil and Dent, 2014; Xu and Quinn, 2016; Constance *et al.*, 2018). This ‘synaptotropic’ iterative interaction between branching and synapse formation ensures reproducibility of circuit wiring patterns (Rico *et al.*, 2004; Chia *et al.*, 2014) and might itself act as a limiting factor during development to prevent excessive branch growth resulting in a stable adult pattern (Niell, 2006). These findings necessitate the existence of local molecular mechanisms that act in a temporally specific manner to couple axonal branching dynamics to synapse formation. The identity and mode of action of such temporal molecular coupling events are poorly understood.

The formation of a stable synaptic contact is a function of the equilibrium between synaptic seeding and synaptic degradation as shown by developmental pruning of up to 40%-50% of synapses (Bourgeois and Rakic, 1993). Synapse elimination is an important cellular phenomenon which fine tunes neural circuitry (Hua and Smith, 2004) especially during the widely studied postnatal experience dependent plasticity known the as “critical period” (Cisneros-Franco *et al.*, 2020). Interestingly, there is evidence for what has been referred to as “precritical period” plasticity in the visual cortex (Feller and Scanziani, 2005), suggesting that genetically encoded developmental events may define critical developmental intervals of synaptic consolidation and elimination prior to the onset of experience dependent plasticity. The timing, role and molecular regulation of such developmental events are unknown.

Autophagy is a key cellular homeostasis mechanism, the dysregulation of which is thought to contribute to several neurodegenerative and neurodevelopmental diseases (Poultney *et al.*, 2013; Huber *et al.*, 2015; Kim *et al.*, 2016; Menzies *et al.*, 2017; Vijayan and Verstreken, 2017; Stavoe and Holzbaur, 2019). Recent work has established that autophagy also plays a role in brain development. Loss of autophagy results in morphological and functional presynaptic organization defects in wide-range of systems, including the mouse cochlear ribbon synapse (Xiong *et al.*, 2020) and the *Drosophila* mushroom body and photoreceptor neurons, for example (Bhukel *et al.*, 2019; Fleming and Rubinsztein, 2020; Kiral *et al.*, 2020). At the *Drosophila* neuromuscular junction, disruption of autophagy reduces its size whereas induction of autophagy increases synaptic boutons and neuronal branches (Shen and Ganetzky, 2009). Autophagy deficiency also causes dendritic spine pruning defects and Autism-like social behaviors in a mouse model (Tang *et al.*, 2014). Pre-synaptic sites are zones of autophagosome biogenesis that have been linked to synaptic plasticity (Azarnia Tehran, Kuijpers and Haucke, 2018; Wang *et al.*, 2019). Local autophagy may also play a role in positioning axonal branches (Adnan *et al.*, 2020). How axonal branch growth and refinement are molecularly coupled to synapse formation and pruning in space and time during neuronal circuit wiring is not well understood.

We have previously identified a role for local activation and recycling of the Epidermal Growth Factor Receptor (EGFR) in regulating dynamics and final patterning of axonal branches (Zschätzsch *et al.*, 2014) in higher order object response neurons (Linneweber *et al.*, 2020) in the fly visual system. Dorsal Cluster Neurons (DCN) are a bilateral cluster of 22-68 commissural interneurons in the *Drosophila* brain with their cell bodies in the dorso-lateral portion of the central brain and axons crossing the central brain to project onto contralateral optic lobes. A subset of DCNs, referred to as M-DCNs, project their axons to a distal visual neuropil called the Medulla where they form a stereotypical fan shaped branching pattern (Srahna *et al.*, 2006; Langen *et al.*, 2013). M-DCN wiring patterns determine visual object orientation behavior in flies. Local asymmetric localization and recycling of EGFR in M-DCN axonal filopodia during development has been linked with actin

polymerization and filopodial dynamics underlying the patterning of presynaptic M-DCN branches. This offers a convenient model system and a molecular entry point to dissect the mechanisms that link axonal branching to synapse formation during neuronal circuit development resulting in specific wiring patterns underlying behavior.

We investigated whether and how M-DCN axonal branching is molecularly coupled to synapse formation and what the consequences to circuit wiring and behavior might be if this link is disrupted. We found that EGFR activity is required at two distinct temporal intervals: an early actin-dependent interval to establish primary axonal branches where presynaptic material accumulates, and a later interval to prevent autophagic degradation of the presynaptic active zone scaffold protein Bruchpilot (Brp) and allow stabilization of the synaptic contacts. Therefore, a temporal sequence of local molecular interactions coordinated by EGFR signaling ensures the coupling between progressive axonal branch refinement and stabilization of the presynaptic active zone leading to the emergence of axon-specific connectivity.

RESULTS

Spatio-temporal correlation of the molecular mechanisms of branching and synapse formation during development

To investigate the relationship between terminal axon branching and synapse formation at high spatio-temporal resolution, we used the medulla innervating Dorsal Cluster Neurons (M-DCNs) as a model. M-DCN axons form stable, terminal primary (orange arrowhead) and secondary (blue arrowhead) presynaptic branches in several posterior medulla layers with their dendrites projecting to the ipsilateral lobula (Zschätzsch *et al.*, 2014) (Fig.1A,A'). Each M-DCN axon forms an average of 4.5 primary branches/axon and an average of 0.25 secondary branches/primary branch (Fig.S1G). These terminal branches contain the presynaptic sites of M-DCNs as marked by several presynaptic and active zone markers such as Syt, Syd1 and Brp (Fig.1A,A'-C,C')(green-orange/green-blue arrowheads for respective branches). We have previously shown that the number of M-DCN axonal presynaptic branches is regulated by local EGFR activity (Zschätzsch *et al.*, 2014) between 48 and 72 hours of pupal development (P48-P72) at 25 degrees.

To investigate the spatio-temporal pattern of synapse formation in the context of axonal branching, we quantified the order of appearance of EGFR (EGFR-GFP), Syd1 (Syd1-GFP) and Brp (BrpD3-GFP) in M-DCN branches between P48 and P72 using well-established reporters of the localization of the endogenous proteins that show no known overexpression phenotypes (Fouquet *et al.*, 2009; Oswald *et al.*, 2010; Zschätzsch *et al.*, 2014). At P48, ~60% of the branches contain Syd1-GFP (Fig.S1A, A',D), ~30% contain EGFR-GFP, but less than 10% contain BrpD3 (Fig.1D,D',G,G',J). Between P55 and P65 almost all branches contain Syd1-GFP (Fig.S1B,B',D), ~90% contain EGFR-GFP and BrpD3 increases from ~50% at P55 to ~75% at P65 (Fig.1E,E',H,H',D). By P72, all three proteins have reached their stable adult levels (Fig.1F,F',I,I',J; Fig.S1C-D). In conclusion, Syd1 enters DCN axons much earlier than EGFR prior to branch formation at around P40 (Fig.S1E,E'-F,F'), followed by Brp entry. To reveal the dynamics of this process, we live imaged and quantified the trafficking of discrete clusters (henceforth "puncta") of BrpD3-GFP, Syd-1-GFP and EGFR GFP in *ex vivo* cultures at P55 when all three proteins are present in branches *in vivo* and EGFR is known to regulate branch growth and pruning (Zschätzsch *et al.*, 2014). We defined any branch as stable that was present during the entire imaging session (~8hours), and as unstable any branch that retracted without re-growing during the same time. Whereas Syd1 entered all branches regardless of stability (Fig.S1H,H'-J,J',K, Supplemental Video S1), EGFR accumulated preferentially, but not exclusively, in stable branches (arrow) compared to unstable branches (arrowhead) (Fig.1K,K'-M,M',N, Supplemental Video S1). Brp exclusively accumulated in stable branches (arrow), despite being present throughout the entire axon shaft (asterisks). None of the branches which failed to accumulate BrpD3 puncta during development stabilized, suggesting active zone maturation is a prerequisite for branch stabilization (Fig.1O,O'-Q,Q', R, Supplemental Video S1). Taken together, our spatial and temporal analyses of *in vivo* and live imaging data suggest that almost all branches are synapse competent (contain Syd1 early), but only the fraction that accumulates both EGFR and Brp is stabilized to contain future synaptic active zones.

Synapse formation is required for branch patterning

To investigate the molecular interdependence of axon branching and synapse formation, we inactivated EGFR, Syd1 or Brp and examined the development of the branches *in vivo* starting at P48. In controls, M-DCN axon branch numbers increased gradually over time between P48 and P65 and then began to decline, reaching near adult branch numbers at P72 (Fig.2A-A5, C). This gradual branch refinement between P65 and P72, follows Brp entry into stable branches (Fig.1J, R), suggesting a link between final branch pruning and stabilization under wild type conditions. As previously shown, we found that inactivating EGFR using a well-established dominant negative

transgene (EGFR-DN) (Buff *et al.*, 1998) resulted in an increase in the total number of branches in adult (Fig.2C). Surprisingly however, loss of EGFR function changed the temporal pattern of branch pruning from a gradual increase followed by a gradual decrease, into a bi-phasic growth and pruning (Fig.2B-B5,C) mode affecting both primary and secondary axon branches (Fig.2D-E). We had previously shown that loss of EGFR function causes primary branch pruning defects between P48 and P55 through an actin-dependent mechanism (Zschätzsch *et al.*, 2014); whereas our data suggests a surge in secondary branch outgrowth between P65-P72 as the possible reason behind second branching peak during late development (Fig.S2G, Supplemental Video S2.1). We therefore asked whether both the primary and secondary branching phenotypes of EGFR inactivation at two distinct phases can be explained by changes to actin dynamics. We found that RNAi knockdown of several cytoskeletal regulators resulted in an increase in in primary branches, but not in secondary branches (Fig.S2A-F). Together, these data suggest that EGFR is required at two distinct temporal phases for DCN branch dynamics. The second phase, which starts at P65, appears to be mechanistically distinct from the first, and coincides with Brp recruitment into stable branches. We therefore asked whether loss of synaptic proteins influences axonal branching specifically during the second phase of branch outgrowth. We knocked down Syd-1 and Brp specifically in DCNs (using ato-Gal4) throughout development using Syd1 RNAi and Brp RNAi (line B3,C8;Wagh *et al.*, 2006). Like EGFR inactivation, knockdown of both Syd1 and especially Brp, resulted in an increase in the numbers of primary and secondary branches in adults (Fig.2C,F-K). However, the branch pruning defects caused by loss of Syd1 and Brp only overlapped with the second phase of EGFR requirement between P65 and P72 (Fig.2C) with similar increased secondary branching during late development starting P65 in Brp KD (Fig.S2G, Supplemental Video S2.1). Finally, downregulation of Brp resulted in continued exploratory growth and retraction even in adult brains (Supplemental Video S2.2). These observations suggest a temporally restricted link between EGFR activity, branching dynamics and synapse formation during a late developmental interval of neural circuit wiring.

EGFR is required for Brp stabilization and synaptic connectivity

To cross-regulation between EGFR activity and synapse formation, we asked whether and how Syd1, EGFR, and Brp interact genetically to establish the pattern of M-DCN connectivity. Syd1 is known to recruit Brp (Spinner, Walla and Herman, 2018) to future presynaptic sites (Owald *et al.*, 2010). However, knockdown of Syd1 had no effect on the distribution or levels of EGFR, neither did knockdown of Brp (Fig.S3A,A'-C,C',D). Conversely, inactivation of EGFR did not affect Syd1 levels or distribution (Fig.3A,A'-B,B', E). This suggests that EGFR and Syd1 act in parallel during synapse formation. In contrast, loss of EGFR activity resulted in a significant decrease of BrpD3-GFP puncta – which colocalize with endogenous Brp (Fig.S3E,E'-F,F') – in terminal branches from 0.22 puncta per μm to 0.1per μm . This corresponds to a 2.5-fold decrease in the total number of BrpD3 puncta from ~ 15 per axon to ~ 6.5 per axon and was accompanied by a redistribution from numerous small puncta at presynaptic sites into a few large BrpD3 aggregates (arrow) (Fig.3C,C'-D,D',F,G), an indicator of loss of endogenous active zones in DCNs (Kiral *et al.*, 2021).

Given that EGFR and Brp enter branches with different temporal dynamics (EGFR before Brp), we asked when EGFR is required for the presence of Brp in branches by examining the recruitment and accumulation of BrpD3 GFP in M-DCN axons and branches over time. Inactivation of EGFR did not interfere with the initial recruitment of BrpD3 at P55 or at P65 where the increase in the number of branches caused by EGFR inactivation also caused an increase in the number of BrpD3 puncta. In contrast, we observed a significant decrease of BrpD3 levels starting at P72 and continuing into adults (Fig.3H,H'-M,M',N). To examine the temporal dynamics of the gradual loss of BrpD after initial recruitment, we performed live imaging and calculated the stability of BrpD3 GFP puncta in branches during synaptogenesis. We tracked the stability of Brp puncta for 2 hours in our *ex-vivo* cultures at P65 and P72 and classified puncta as stable if they were present throughout tracking, or

as unstable if they disappeared at any point during the tracking. Between P65 and P67, in control DCNs, 82% of Brp puncta were stable, compared to 57% in EGFR-DN DCNs. Between P72 and P74, 93% of Brp puncta became stable in controls compared to 76% in EGFR DN expressing DCNs (Fig.S3G, Supplemental Video S3). Because Brp acts as a scaffold protein for active zone formation (Huang *et al.*, 2020), these observations suggest that lack of EGFR activity reduces the stability of active zones during late brain development.

Altogether, the data above show that while EGFR inactivation causes an increase in primary and secondary axon branches, it causes a sharp decrease in the presynaptic active zone protein Brp. What is the impact of these seemingly opposing changes on DCN postsynaptic connectivity and circuit wiring? To test this, we first needed to determine the connectome of DCNs in the medulla. We used the anterograde trans-synaptic method for target tracing approach “Trans-Tango”, which labels all the post-synaptic targets in an unbiased manner without required prior knowledge of cell types (Talay *et al.*, 2017). We used stringent conditions (see methods) to optimize sparse labelling of postsynaptic targets (Fig.S4A-D). We found that M-DCNs connect to a large variety of medulla projecting neurons along with some lobula and lobula plate targeting neurons (Fig.S4F1-F21). Their most frequent partners are lamina wide field cells (Lawf1/2) (Fig.S4F18,G), followed distantly by trans medulla neurons (Tm2/21/Y8/9) (Fig.S4F2,F3,F7,F8,G) (Fischbach and Dittrich, 1989). We further validated Lawf1 and Tm2 subtypes using activity dependent GRASP which confirmed them as DCN postsynaptic targets (Fig.S4H-H’,I-I’). Next, we tested the effects of loss of EGFR activity on DCN circuit wiring. We observed a drastic reduction in overall connectivity (Fig.3O-Q, Fig.S4C-E), with a significant reduction in the most frequent partners, Lawf1/2, Tm2/21, and a complete loss of less frequent partners (Fig.S4G,G’). Therefore, the stabilization of Brp by EGFR is required for the specific pattern of M-DCN connectivity.

Thus far we have found that knock-down of Brp causes an increase in secondary branching and that loss of EGFR activity results in a late loss of Brp puncta as well as a similar increase in secondary branching (Fig.S2G, Supplemental Video 2.1). We therefore asked if reduction of Brp might explain the secondary branching phenotype of EGFR inactivation. To test this idea, we introduced an extra genomic copy of the *brp* gene in a DCN EGFR-DN background. Remarkably, increasing Brp levels with one genomic copy rescues the loss of BrpD3-GFP puncta showing specificity of the phenotype (Fig.3R-T,U). The extra copy of *brp* also rescued the secondary branching phenotype (Fig.3R-T,W) but did not rescue the primary branching phenotype associated with the early role of EGFR (Fig.3R-T,V). Together these data show that inactivation of EGFR causes loss of Brp which in turn destabilizes terminal axon branches leading to an increase in their numbers. We conclude that the quantity of stable Brp is a determinant of terminal branch stability.

Temporally specific requirement for EGFR activity in synapse formation and terminal branching dynamics

We have previously shown that early DCN branch pruning is regulated by EGFR via the control of actin dynamics. In this study, we have observed that EGFR is also required during a second phase to maintain Brp and synaptic connectivity. We asked whether these two effects reflect different temporal requirements of EGFR, or whether the late phenotype is an indirect consequence of the early effect of EGFR on primary branching. To distinguish between these two possibilities, we used temperature sensitive inactivation of EGFR, by inducing the EGFR-DN transgene at different times during development using the Gal4 temperature-sensitive repressor Gal80^{ts}. We ascertained that the transgene is active and prevents GFP expression at 22°C (Fig.S5A) and calibrated the temporal progression of branch development at 22°C with respect to control at 25°C (Fig.S5B-F). Gal80^{ts} prevents EGFR-DN expression (and thus allows EGFR activity) at 22°C (green bar). At 29 degrees Gal80^{ts} is inactivated, thus allowing EGFR-DN to be expressed, which in turn will inhibit EGFR activity (magenta bar). Thus, at 22°C EGFR is active, while at 29°C EGFR is inactive. As expected,

continuously inactivating EGFR starting at P48 till adult results in a significant increase in primary and secondary branches (asterisks) and a significant decrease in Brp (Fig.4A-E). Inactivating EGFR only early between P42 and P57 increases primary branches but has no effect on secondary branches (asterisks) or Brp (Fig.4F-J). In contrast, inactivating EGFR starting either at P55 (Fig.4K-O) or at P65 (Fig.4P-T) has no effect on primary branch number, but significantly increases secondary branches (asterisks) and significantly decreases Brp. This role of EGFR in synapse formation appears strictly developmental as inactivating EGFR specifically in adults does not result in any defects in branching or Brp levels and distribution (Fig.S5G-K). Therefore, mechanistic regulation of EGFR at pre-synaptic branches defines a developmental critical interval for terminal branch consolidation and synapse stabilization required for neuronal circuit wiring in adults.

EGFR activity is required to prevent Brp degradation during synaptogenesis

We have previously shown that autophagy can regulate synapse formation by restricting filopodial kinetics (Kiral *et al.*, 2020) and EGFR has been shown to regulate autophagy in *Drosophila* testis (Sênos Demarco and Jones, 2020) and in many tumorigenic contexts (Wu and Zhang, 2020). We asked whether loss of EGFR activity results in increased Brp degradation. To this end, we first used a general degradation reporter (myr-mCherry-pHluorin) (Jin *et al.*, 2018) and observed a significant increase in localization of this probe in acidic compartments (Fig.S6A-C). Next, we examined the proportion of BrpD3-GFP puncta in acidic late endosomal/autophagosomal compartments in control and EGFR-DN M-DCNs using endogenous Rab7, DCN expressed Rab7-RFP and DCN-expressed pH sensitive BrpD3-mCherry-pHluorin, as independent markers of such compartments. We observed a progressive increase in the colocalization of BrpD3-GFP with endogenous Rab7 in axon branches upon EGFR inactivation starting at P65 and continuing into adults (Fig.5A-F,G). We obtained similar results using the Rab7-RFP reporter expressed specifically in DCNs (Fig.S6D-G). Importantly, this colocalization was not observed for Syd1 (Fig.S6H-J), whose levels and distribution were not affected by EGFR inactivation (Fig.3B,B',E). Finally, the BrpD3-mCherry-pHluorin probe showed increased localization into acidic compartments upon EGFR inactivation as detected by increased mcherry to pHluorin signal intensity starting at P72 and into adults (Fig.5H-M,N).

These data suggest that EGFR is not required for increasing the levels of Brp import into the synaptic terminal, but instead for maintaining Brp pools already present in presynaptic branches by preventing their degradation. If Brp degradation is already fully suppressed by wild type levels of EGFR activity, then increasing EGFR activity further should not lead to an increase in Brp levels. We tested this idea by examining Brp upon expression of a constitutively activated EGFR (EGFR-CA) in DCNs. We found no effect on BrpD3 density or distribution, nor on the degree of colocalization with Rab7-RFP (Fig.S6K-N).

EGFR signals through autophagy to maintain DCN presynaptic active zone, circuit connectivity, and behavior

To investigate the potential causal role of increased degradation for the loss of Brp and synaptic connectivity, we performed knockdown of the autophagic regulators Rab7 and Atg6 upon inhibition of EGFR activity and assayed terminal branching, BrpD3 distribution, and M-DCN postsynaptic connectivity. Knockdown of either Rab7 or Atg6 alone did not cause a significant change in the number of terminal secondary branches or level of BrpD3 (Fig.6A,A'-C,C',M,N). In contrast, knockdown of either Rab7 or Atg6 upon EGFR inactivation completely suppressed the increase in secondary branches and restored Brp at M-DCN synaptic terminals back to control levels (Fig.6D,D'-F,F',M,N), demonstrating that autophagy is required for the synaptic loss caused by EGFR inactivation.

Next, we asked whether this cell-autonomous rescue of presynaptic terminals suffices to restore M-DCN postsynaptic connectivity. Downregulation of either Rab7 or Atg6 alone resulted in a ~50% decrease in the number of trans-tango labelled M-DCN postsynaptic cells, while EGFR inactivation caused an almost complete loss of connectivity (Fig.6G-J,O). Importantly however, knockdown of either Rab7 or Atg6 in the EGFR-DN background rescued the connectivity to postsynaptic cells back to the levels observed upon knockdown of Rab7 or Atg6 alone (Fig.6J-L,O) showing that the effect of EGFR inactivation requires autophagy.

We have previously shown that the M-DCNs regulates behavioral responses in the multiparametric single fly visual response assay called Buridan's paradigm (Linneweber *et al.*, 2020). In this assay, single flies walk freely between two identical visual cues (Fig.7A) and reduction of synapses causes increased fly activity when flies were tested at the same temperature at which they developed (Kiral *et al.*, 2021). Consistent with this, we find that inactivation of EGFR specifically in DCNs results in flies walking longer distances, staying active for a longer time, and increasing the number of walks between the two cues (Fig.7B-H; Table S1). Specifically, we observed ~1.12-fold increased distance travelled (total path length between the 2-stripes (Fig.7F), ~1.14 fold increased activity time (total time the flies were moving) (Fig.7G) and ~1.2 fold more number of walks (Fig.7H). Remarkably, DCN-specific knockdown of Rab7 in in the EGFR-DN background completely rescued all these phenotypes back to control levels (Fig.7D,F-H), suggesting that even partial rescue of DCN synaptic connectivity (Fig.6O), is sufficient to support normal behavioral activity at the level assayed here.

Discussion

The complexity of neuronal circuit wiring patterns, driven to a significant extent by the degree of axonal branching during development (Hoerstring and Schmucker, 2021), is thought to be key to the emergence of complex behaviors and cognitive capacities. In the mammalian motor cortex for example, axon branch complexity can allow a single neuron to innervate very distant ipsi- and contra-lateral cortical and sub-cortical targets (Economo *et al.*, 2016). Some genetic risk factors for human neuropsychiatric disorders such as Schizophrenia appear to be associated with alterations in terminal axonal branches (Shao *et al.*, 2019). In insects, the relative conservation of axonal projections patterns is thought to underlie species-specific innate behavioral patterns while permitting individual variation in these behaviors. For instance, the unique branching pattern of L-fibers supports the nocturnal lifestyle of *M.genalis* (Grueber *et al.*, 2005), while intrinsic variation in M-DCN connectivity underlies individual variation in *Drosophila* visual response behavior (Linneweber *et al.*, 2020). While it is critical to dissect the specific phenomena of axonal branching and synaptogenesis during circuit wiring, it is equally critical to understand the spatial, temporal, and mechanistic coordination of these processes during development to arrive at a more complete description of the emergence of both the conserved patterns and the individual variation of neuronal circuit diagrams.

Here we asked if, when and how molecular factors that play key roles in regulating axon branching, synapse formation and membrane degradation interact to produce specific presynaptic patterns, neuronal circuit connectivity and behavior using the developing *Drosophila* visual system as a model. This diverse list of cellular processes is tied together by their collaborative effects during the development of synaptic connectivity. Axo-dendritic branching and synapses formation have long been known to depend on each other during synaptotropic growth of branches based on synapse stabilization (Vaughn, Barber and Sims, 1988). The developmental interactions of axonal and dendritic processes are a major contributor, and can sometimes predict, the adult synaptic connectivity (Agi, Kulkarni and Hiesinger, 2020). By contrast, cell biological processes like cytoskeletal dynamics or membrane degradation have long been described as a 'permissive' basis for more 'instructive' molecular mechanisms of synaptic specification. However, to the extent that such cell biological mechanisms directly contribute to branching and synapse formation, they become parts of a composite instruction that cannot be pinned on a single molecular mechanism but require the consideration of several collaborating factors to understand a neuron's choice to branch and form a synapse (Hiesinger, 2021). Hence, an integrative analysis of molecular recognition, signaling and cell biological machinery is necessary to mechanistically understand how branching contributes to adult synaptic connectivity.

Numerous molecular and cellular mechanism have been implicated in the spatiotemporal control of how synaptic partners are brought together for synapse formation (Agi, Kulkarni and Hiesinger, 2020). Over the last 25 years, investigating the role of EGFR in nervous systems has demonstrated its roles in neural stem cell maintenance (Aguirre, Rubio and Gallo, 2010), astrocyte and oligodendrocyte maturation (Galvez-Contreras, Quiñones-Hinojosa and Gonzalez-Perez, 2013), axon regeneration (Koprivica *et al.*, 2005) and more recently in neurite outgrowth and branching (Goldshmit *et al.*, 2004). In addition, we have recently demonstrated roles for the cell biological regulation of filopodial dynamics and autophagic degradation in establishing specific synaptic connectivity (M Neset Özel *et al.*, 2019; Kiral *et al.*, 2020). How such basic cellular processes are coupled to the process of patterning axonal branches and how the three processes – branching, synaptogenesis and autophagy – are coordinated in time to establish circuit-specific wiring diagrams has remained unclear. We find that that these processes are indeed coupled but only during a very specific temporal interval through the activity of the Epidermal Growth Factor Receptor (EGFR) preventing the autophagic degradation of the synaptic active zone protein Bruchpilot (Brp). Inactivation of EGFR during this specific critical interval in late development, but not before or after, causes Brp degradation, changes to circuit wiring and altered visually driven behaviors.

An interesting observation are the differences in dynamics upon inactivation of EGFR and knockdown of Brp. While both result in increased secondary branches, loss of Brp leads to a more dynamic state of these branches even in the adult brain. In contrast, loss of EGFR causes these secondary branches to be largely static, even though EGFR inactivation also causes Brp loss. This is likely because EGFR loss also impairs actin dynamics which are required for filopodial dynamics, while Brp loss does not affect EGFR activity and thus does not impair actin dynamics. These observations underline the critical importance of live imaging for discovering and interpreting otherwise seemingly similar phenotypes. These observations are also consistent with the genetic hierarchy we observed whereby EGFR regulates BrpD3 levels, but Brp does not appear to regulate EGFR levels. Again, live imaging combined with temporally restricted inactivation of EGFR allowed us to dissect the temporal logic of this genetic hierarchy and discover the role of EGFR activity as coupling mechanism between branching dynamics, local degradation, and synapse formation.

Our observations show that the coupling between branching, autophagy and synaptogenesis is only required during a very specific temporal interval which, perhaps not surprisingly, coincides with active synaptogenesis in the developing fly brain [REF]. Our analysis of the temporal sequence of

trafficking of various molecules indicates that this developmental critical interval is opened by the spatial and temporal coincidence of EGFR and BrpD3 in exploratory branches. Similarly, it is likely that the critical interval ends once synaptic contacts between DCNs and their postsynaptic cells have been established. What remains to be explored is how exactly synapse formation ends the interactive feedback between branch dynamics and synapse degradation. One possibility is that postsynaptic dendrites provide molecular signals to presynaptic axonal branches to limit active zone degradation. Another possibility is that the initiation of spontaneous activity alters local endolysosomal recycling (Tagliatti *et al.*, 2016) to reduce degradation and favor maintenance, for example through the activity-dependent regulation of local translation of resident mRNAs (Rajgor, Welle and Smith, 2021). A third possibility is the late arrival of presynaptic proteins that protect the active zone, reduce autophagy or alter EGFR function. Clearly, none of these mechanisms are mutually exclusive and we speculate that a combination of such feedback mechanisms would be the best way to ensure a robust closing of the developmental critical interval we discovered here. Flies, like vertebrates, undergo a critical period of postnatal experience-dependent synaptic pruning with unknown molecular mechanism. It would be interesting to explore whether the mechanism we uncovered here also plays a role in synaptic regulation and neural circuit plasticity during that critical period. It is possible that similar molecular modules are used re-iteratively to regulate synaptic homeostasis and pre-synaptic branching in experience-independent and dependent brain development.

We have previously shown that an increase in local autophagy also led to a decrease of adult synapses in R7 photoreceptor neurons (Kiral *et al.*, 2020), albeit by a different mechanism. In R7 photoreceptors, local autophagosome formation at the tips of synaptogenic filopodia is accompanied by engulfment of synaptic seeding factors but not Brp, followed by filopodial collapse and thus less filopodial availability to form synapses. In DCNs, axonally localized autophagosome formation is accompanied by engulfment of Brp but not synaptic seeding factors, leading to a destabilization and reduction of mature synapses. Hence, the spatiotemporal specific roles of autophagy in different types of axon terminals during synapse formation are highly context-specific, involve different substrates, and yet lead to similar outcomes. An obvious contextual difference between R7s and DCNs is that only the latter form branched axons and employ synaptotropic-like branch stabilization through mature synapses.

Increasing evidence supports the important roles that stochastic and/or noisy molecular processes play in the early phases of establishing wiring specificity prior to the final step of spatially and temporally restricted local synaptic matching (Hassan and Hiesinger, 2015). While neuronal circuit wiring patterns across the animal kingdom are highly robust, they, almost without exception, show at least some degree of intrinsic variation within and between individuals. Noise in the genetically encoded program can ensure robustness of highly reproducible wiring patterns, for example when stochastic exploration ensures partner finding (Hiesinger and Hassan, 2018). Correspondingly, axon branch initiation in DCNs is noisy and exploratory, while the final axonal pattern is robustly stereotypic. The evidence presented in this work demonstrates the importance of intrinsic local control of the feedback between axonal branching and synapse formation to ensure the robust outcome. Such local feedback regulation ensures that genetically encoded noisy molecular and cellular processes such as filopodial growth and retraction and synaptic seeding are coordinated in time and space to produce conserved, robust, yet individually variable, non-random neuronal circuit diagrams.

ACKNOWLEDGMENTS

This work was supported by the Einstein-BIH program and DFG Research Unit 5289 RobustCircuit project P2 (to B.A.H and P.R.H), DFG Research Unit Syntophagy RP7 (Hi 1886/8), funding from the European Research Council (ERC) under the European Union's Horizon 2020 research and

innovation programme (grant agreement No. 101019191 (to P.R.H), the Investissements d’Avenir program (ANR-10-IAIHU-06), Paris Brain Institute-ICM core funding, the Paul G. Allen Frontiers Group Allen Distinguished Investigator grant, the Roger De Spoelberch Prize and an NIH Brain Initiative RO1 grant (1R01NS121874-01) (to B.A.H.). M.A. is funded by the Fondation de la Recherche Medical (FRM) postdoctoral fellowship (ARF202005011913). We thank the BioSupraMol Optical Microscopy facility for STED microscopy, members of the Hassan and Hiesinger labs for helpful discussions and Drs. Stephan Sigrist and Dietmar Schmucker for comments on the manuscript.

AUTHOR CONTRIBUTIONS

S.D., B.A.H. and P.R.H. conceived the study, designed the experiments, and wrote the manuscript. S.D., G.A.L. and M.A. conducted all experiments and data analysis.

DECLARATION OF INTEREST

The authors declare no conflict of interest.

Materials and Methods:

Experimental model and subject details:

Flies were reared at 25°C on standard cornmeal/yeast diet for all crosses and at 21°C and 29°C for Gal80ts experiments. For developmental analyses, white pre-pupae (P+0%) were collected and incubated at 25°C to pupal stages as stated on figures. The following *Drosophila* strains were either obtained from Bloomington *Drosophila* Stock Center (BDSC), Vienna *Drosophila* Resource Center (VDRC) or other groups: *ato*-Gal4-14a (Hassan Bassem A. et al., 2000), MDCN-Gal4 (Linneweber et al., 2020), *ato*-LexA (Langen et al., 2013), *Lawf1*-Gal4 (Konstantinides et al., 2018); *Tm2*-Gal4 (Ting et al., 2011), *nsyb*-GRASP flies (BDSC), UAS-Denmark (BDSC), UAS-CD4 tdGFP(BDSC), UAS-CD4 tdTomato(BDSC), UAS-CD8 GFP(BDSC), UAS-BrpD3 GFP (Schmid et al., 2008), UAS-BrpD3 mCherry (Schmid et al., 2008), UAS-Syd1 GFP (Owald et al., 2010), UAS-EGFR DN (Zschätzsch et al., 2014), UAS-Rab7 RFP(BDSC), UAS-lacZ(BDSC), UAS-BrpD3-mCherryPhourin (gift from R. Hiesinger), UAS-myr-mCherryPhourin (Jin et al., 2018), UAS-EGFR GFP (Zschätzsch et al., 2014), UAS-Brp B3.C8 RNAi (Knapek, Sigrist and Tanimoto, 2011), UAS-Syd1 RNAi(BDSC), UAS-Rab7 RNAi (VDRC), UAS-Atg6 RNAi (VDRC), UAS-Trans Tango (Talay et al., 2017), UAS-EGFR CA (Zschätzsch et al., 2014), UAS-tubulin Gal80^{ts}(BDSC), Pacman Brp (Huang et al., 2020), UAS-Wasp RNAi(VDRC), UAS-Ensconsin RNAi(VDRC), UAS-Act42A RNAi(VDRC). Additional fly stocks used are w1118, valium 20, valium 10, canton-S as genetic controls (BDSC).

Immunohistochemistry and Fixed Imaging:

Pupal and adult brains were dissected in cold Schneider’s *Drosophila* medium and fixed in 4% paraformaldehyde (PFA) in PBS for ~20 minutes. Tissues were then washed in PBST (1% Triton-X) on a shaker for 3x15mins followed by overnight incubation with primary antibodies at 4°C shaker. The primary antibodies used in this study were used with the following dilutions: chicken anti-GFP(1:250)(abcam), mouse anti-GFP (1:500)(Life Technology), goat anti-GFP (1:500)(abcam), goat anti-mCherry (1:500)(Sicgen), rabbit anti-Dsred (1:200)(Takara), mouse anti-LacZ (1:200)(Promega), rabbit anti-CD4 (1:250)(Invitrogen), rabbit anti-Rab7 (1:1000)(gift from Patrick Dolph). Next, the brains were washed again with 1% PBST on a shaker for 3x15mins. The brains were incubated with appropriate secondary antibodies (Alexa 488, 554, 647, 405, 594) at a concentration of 1:500 from Jackson ImmunoResearch Laboratories for 5-6hours at room temperature, followed by final wash with 1% PBST for 3x15mins. Tissues were mounted on taped

cover slides using vector shield. Images were obtained with a Leica TCS SP8-X white laser confocal microscope with a 63x glycerol objective (NA=1.3)(Jin *et al.*, 2018; Kiral *et al.*, 2021).

STED imaging:

Adult brains were dissected in cold Schneider's *Drosophila* medium and fixed in 4% paraformaldehyde (PFA) in PBS for ~20 minutes. Tissues were then in PBST (1% Triton-X) on a shaker for 3x15mins followed by overnight incubation with primary antibodies at 4°C shaker. The primary antibodies used in this study with given dilutions were as follows: chicken anti-GFP (1:500) (abcam), mouse anti-Nc82 (1:10) (DSHB), rabbit anti-CD4(1:200) (Invitrogen). Next, the brains were washed again with 1% PBST on a shaker for 3x15mins. The brains were incubated in secondary antibodies: anti-ck STAR RED (1:250) (Abberior dyes), anti-mouse Alexa594 (1:100) (Thermofischer Scientific), anti-rabbit Alexa 488(1:100) (Thermofischer Scientific) for 5-6hours, followed by final wash with 1% PBST for 3x15mins. Then they were mounted on taped cover slides using Prolong Gold (Invitrogen) and kept 24hours at RT in dark. The slides were then stored at 4°C for 48hours before imaged. Images were obtained with a STED Expert Line Microscope from Abberior Instruments with a 100x oil objective (NA=1.4)(Pooryasin *et al.*, 2021).

Pupal brain culture and Live-Imaging:

For all ex-vivo live imaging experiments, pupal or adult brain was carefully dissected out of the pupal case or the surrounding exoskeleton respectively. The resultant eye-brain complexes were mounted in 0.4% dialyzed low-melting agarose in a modified culture medium as described before (Özel *et al.*, 2015). We used double sided tapes cut into 1inch x 1inch small squares as coverslips. Since all our developmental imaging were done after P48, we used Hydroxyecdysone free culture media. To fully expose DCN branch projection patterns, the pupae were mounted posterior side up. Live imaging was performed at room temperature using a Leica TCS SP8 X confocal microscope with a resonant scanner, using 63X water objective (NA=1.2), and optimized settings of minimal white laser excitation and crosstalk avoiding SP detector emission windows. White laser excitation was set to 488 nm for GFP, 554 nm for tdTomato signal acquisitions.

Trans-tango and activity-dependent GRASP:

Trans-tango was performed with DCN-specific ato-Gal4-14a (Hassan Bassem A., 2000)and M-DCN specific Gal4 (Linneweber *et al.*, 2020)whereas GRASP experiment was performed with DCN-specific ato-LexA(Langen *et al.*, 2013) . Trans-tango flies were raised both at 18°C and 25°C to optimize the dissection conditions. 7 days old flies raised at 25°C showed dense connectivity pattern. The number of postsynaptic neurons was counted manually from their cell bodies using the “surface” tool in IMARIS, including all cell bodies with weak or strong labelling to reveal all potential connections. Since postsynaptic partner labeling by Trans-tango is age-dependent, 3-days old flies reared at 25°C were dissected for sparse labeling to reveal the identity of post-synaptic cell types connected to M-DCNs.

For activity-dependent GRASP experiments, to activate DCNs, freshly eclosed flies were transferred to 25°C incubator with 12-12hours light-dark cycle for 5 days. Brains were dissected and stained with a polyclonal anti-GFP antibody to label DCN pre-synaptic sites, monoclonal anti-GFP antibody to label GRASP signal, and polyclonal anti-CD4 antibody to label postsynaptic neurons(Kiral *et al.*, 2021).

Buridan's paradigm assay

Fly navigation behavior was tested in a Buridan's paradigm arena (Linneweber *et al.*, 2020) using flies grown in a 12/12 hours light–dark cycle at 50% relative humidity. The arena consists of a round platform of 117 mm in diameter, surrounded by a water-filled moat and placed inside a uniformly illuminated white cylinder. The light was produced by four circular fluorescent tubes (Osram, L 40w, 640 C circular cool white) powered by an Osram Quicktronic QT-M 1 × 26–42. The fluorescent tubes were located outside of a diffuser (DeBanier, Belgium, 2090051, Kalk transparent, 180 g, white) positioned 147.5 mm away from the arena center. The temperature on the platform was kept

constant at 25 °C. 30 mm-wide stripes of black cardboard were placed on opposing sides inside of the diffuser and served as visual targets. The retinal size of the visual object depends on the position of the fly on the platform. In this arena it ranges from 8.4° to 19.6° in width (11.7° in the center of the platform). Fly tracks were analyzed using CeTrAn (coulomb) and custom-written python code (Linneweber *et al.*, 2020). 25 partially overlapping behavioral parameters were evaluated. Significant differences between experiment and controls and the rescue experiment were only found for parameters affecting motility.

The three selected activity related behavioral parameters are the following:

1. **Distance traveled (mm/min):** Total distance travelled in mm per minute
2. **Activity time (s):** Time active per minute in seconds
3. **Number of walks:** The number a fly walks from one stripe to the other. The fly needs to be on both ends near the edge closer than 80% of the platform radius for a walk to count.

Quantification and statistical analysis:

Branch number and length analysis:

All imaging data were analyzed and presented with Imaris 9.0.1 (Bitplane). Branch numbers were detected automatically with the filament module using identical parameters for all experimental conditions (largest dendrite diameter: 3.0 μm, thinnest dendrite diameter: 0.2 μm). The resultant branch numbers were then recorded directly from the statistics tab of filament module and normalized it to the total number of axons per optic lobe. Any inconsistencies in automatic detection of branches were checked and corrected manually. Branch lengths were calculated manually using the "automatic placement" version of the filament module to calculate the 3D length of all branches. Intersection of axon shaft-primary branch were considered as the starting node and a filament was drawn till the respective branch tip. The resultant values of branch lengths were taken and recorded directly from the statistics tab of the filament module. Graph generation and statistical analyses were done using GraphPad Prism 8.2.0

Synapse number analysis:

All imaging data were analyzed and presented with Imaris 9.0.1 (Bitplane). For synapse number analysis, CD4-tomato channel was used to generate surfaces for DCN axonal branches. Brp-positive puncta inside the surface were filtered using the masking function and were detected manually for individual branches. To obtain synapse distribution, we normalized the number of Brp-positive puncta inside individual DCN branch to the respective branch length which was calculated using the filament module as discussed above. Graph generation and statistical analyses were done using GraphPad Prism 8.2.0

Live tracing of molecules in branches:

All imaging data were analyzed and presented with Imaris 9.0.1 (Bitplane) and the background noise was corrected with the threshold > background subtraction with a filter width of 60um in Imaris. GFP '+' ve puncta were then tracked individually and manually for all the branches marked in CD4 channel over time and recorded. To obtain a distribution, we normalized the number of GFP-positive puncta inside individual DCN branch to the respective branch length which was calculated using the filament module. Graph generation and statistical analyses were done using GraphPad Prism 8.2.0

mCherry/pHluorin intensity analysis:

Intensity analysis was performed using the surface module of Imaris 9.0.1 (Bitplane). All mCherry positive BrpD3 puncta were used to generate surface using the same threshold parameters (Diameter of largest spere which fits into the object=0.700 um; surface detail=0.481um) for experiments and controls. Mean intensity of the individual red channel (mCherry) to green channel (pHluorin) within

each surface were recorded. Graph generation and statistical analyses were done using GraphPad Prism 8.2.0.

Colocalization analysis:

All imaging data were analyzed and presented with Imaris 9.0.1 (Bitplane). For colocalization analysis, CD4-tomato channel was used to generate surfaces for DCN axonal branches. Brp-positive puncta (green channel) and the Rab7 puncta (red channel) inside the surface were filtered using the “masking” tool of surface module. All co-localization events were quantified manually on slice-by-slice basis for the entire z-stack in 2D. Only discernible individual compartments were counted. Partial or full correlation were given a score of 1 (“yes” colocalization) whereas 0 (“no” colocalization) if not. To obtain the fraction of colocalized events, the total number of colocalized Brp-Rab7 puncta were divided by the total BrpD3 puncta per axon. Graph generation and statistical analyses were done using GraphPad Prism 8.2.0.

Statistical Analysis

Statistical comparison of two groups was performed with non-parametric Mann-Whitney test (T-test). Statistical comparison of more than two groups was performed with non-parametric Kruskal-Wallis test and corrected for multiple comparisons with Dunn’s as a post-hoc test. All significance values are denoted on the graphs and in their respective legends. Graph generation and statistical analyses were done using GraphPad Prism 8.2.0.

Figures:

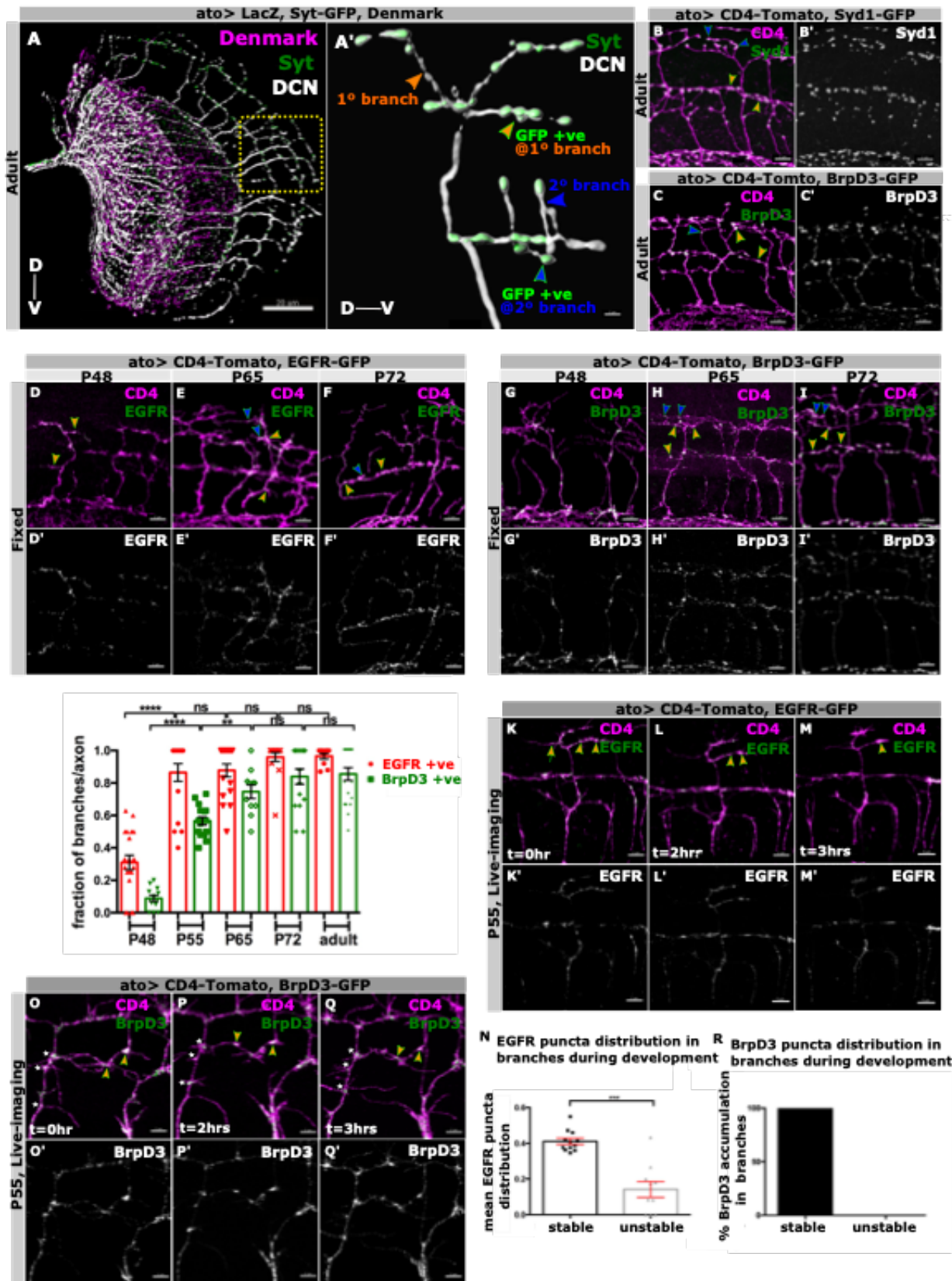


Fig.1**Spatio-temporal correlation of the molecular mechanisms of branching and synapse formation during development:**

(A-A') Adult stereotypic projection pattern of DCNs driven by *atoGal4-14a* labelled with LacZ (white), dendritic arborizations marked by Denmark (magenta) and pre-synaptic sites marked by Syt-GFP (green). *atoGal4-14a* is used in all the following experiments unless otherwise stated. Yellow box represents region of interest where DCN axons forms ladder-like branches as shown in (A') higher resolution with primary (asterisks) and secondary branches (arrowheads) harboring Syt-GFP (green) puncta. (B/B'-C/C') Adult DCN branches (magenta) are associated with clusters of early synaptic seeding factor; marked with Syd1 GFP (green) (B/B') and late Active zone (AZ) protein Brp, marked with BrpD3 GFP (green) (C/C'). (D-I) Temporal order of recruitment of EGFR GFP (green) and BrpD3 GFP (green) in the DCN branches (magenta) during development; P48 (D/D',G/G'), P65 (E/E',H/H') and P72 (F/F',I/I') showing EGFR enters the branches before Brp. (J) Quantification showing the fraction of branches recruiting EGFR GFP (red datapoints) and BrpD3 GFP (green datapoints) during development. N=20 axons at P48 (EGFR), N=17 axons for at P48 (BrpD3), N=17 axons at P55 (EGFR), N=17 axons at P55(BrpD3), N=17 axons at P65 (EGFR), N=14 axons at P65 (BrpD3), N=15 axons at P72 (EGFR), N=16 axons at P72 (BrpD3), N=10 axons in adult (EGFR) and N=20 axons in adult (BrpD3). Mann Whitney test; **** $p < 0.0001$, ^{ns} $p = 0.8124$, ^{ns} $p = 0.7934$, ^{ns} $p = 0.4932$. Ex-vivo imaging of EGFR GFP (K/K'-M/M') and BrpD3 GFP (O/O'-Q/Q') in the DCN branches (magenta) during development shows EGFR GFP (green) asymmetrically localizes in the DCN branches; stable branches with higher proportion of EGFR punctas (arrow) compared to unstable branches (arrowhead)(K/K'-M/M'). Whereas late AZs marked by BrpD3 GFP (green) accumulates only in stable branches (arrow), while being excluded from unstable branches (arrowhead) (O/O'-Q/Q'). (N) Quantification of mean EGFR GFP puncta normalized to branch length in stable (black bar) vs unstable branches (gray bar) in ex-vivo cultures during development. N=12 for stable branches and N=10 for unstable branches, Mann Whitney test, *** $p = 0.0003$. (R) Quantification of percentage of BrpD3 GFP puncta accumulation in stable (black bar) vs unstable branches during development. N=10 for stable branches and N=15 for unstable branches. Error bars denote mean \pm SEM, scalebar represents 5 μ m except (A) which is 20 μ m.

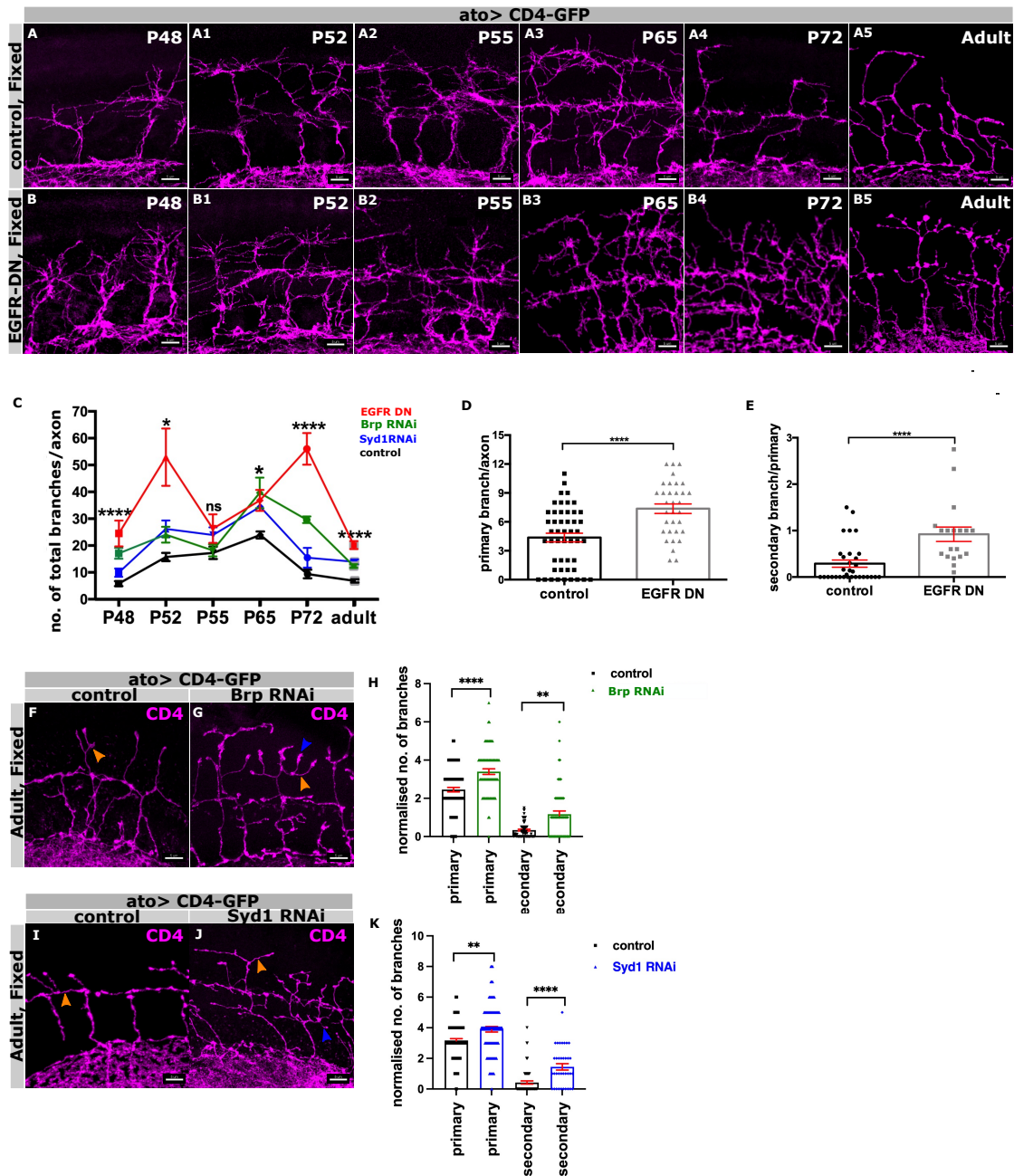
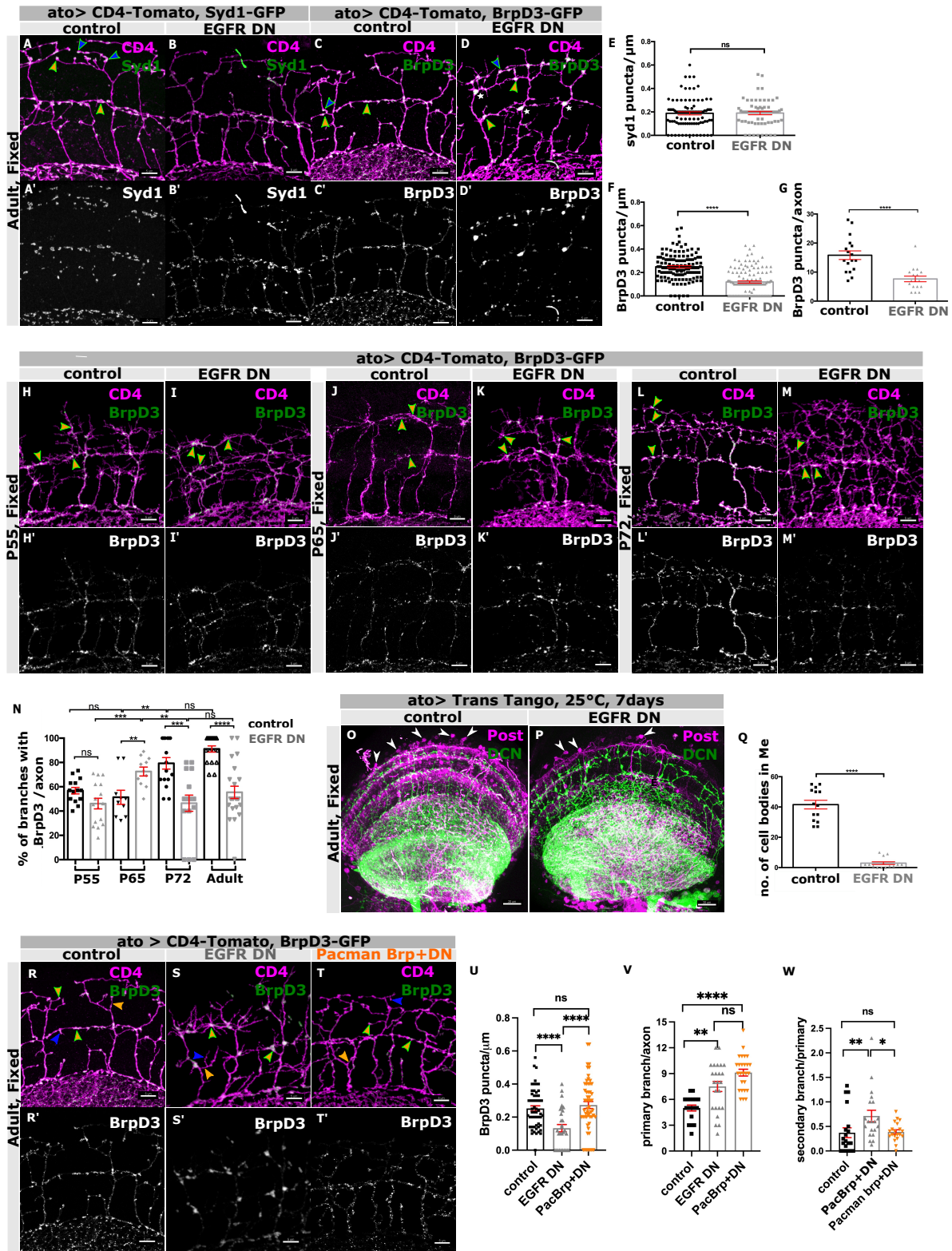


Fig.2

Synapse formation is required for terminal branch patterning:

(A-A5) DCN axonal branch progression (magenta) during development in control brains reveals an increase in branching complexity from early to mid-pupal stage; P48 (A), P52 (A1), P55 (A2), P65 (A3). Branch refinement occurs from mid to late-pupal development; P65 (A3), P72 (A4), adult (A5). (B-B5) Surprisingly, EGFR DN expressing DCNs show dys-regulation of branch refinement process with branching peaks at two phases of development: first from P48 to P55 (B-B2) and later from P65 to adult (B3-B5). (C) Quantification showing overall branch refinement progression (mean of the total number of branches per axon) during development in EGFR DN (red), Brp RNAi (green), Syd1 RNAi (blue) compared to control (black). N=8 lobes for control, N=10 lobes for EGFR DN, N=7 lobes for Syd1 RNAi and N=6 lobes for Brp RNAi. Kruskal–Wallis and Dunn’s as post-hoc test; ** $p=0.0015$ (P48), ** $p=0.0033$ (P52), ns $p=0.2135$ (P55), ** $p=0.0024$ (P65),

*** $p=0.0002$ (P72) and *** $p=0.0004$ (adult). **(D)** Quantification showing more normalized primary branch number in EGFR DN (gray) expressing DCNs compared to genetic control (black) in adults. N=49 axons for control, N=33 axons for EGFR DN; T-test, **** $p < 0.0001$. **(E)** Quantification showing more normalized secondary branch number in EGFR DN (gray) expressing DCNs compared to control (black) in adults. N=32 primary branches for control, N=19 primary branches for EGFR DN; T-test, **** $p < 0.0001$. Error bars denote mean \pm SEM. **(F-G, J-K)** Adult axonal branch pattern (magenta) upon knocking down Brp **(F-G)** and Syd1 **(J-K)** specifically in DCNs compared to their genetic controls. **(H-I)** Adult quantification showing normalized primary **(H)** and secondary **(I)** branch number increases in Brp B3,C8 RNAi (green) compared to control (black). N=49 axons for control, N=38 axons for Brp B3,C8-RNAi for primary branch quantification **(H)**, N=54 branches in control, N=60 branches for secondary branch quantification in Brp B3,C8 RNAi **(I)**. Mann Whitney test, **** $p < 0.0001$, ** $p = 0.0011$. **(L-M)** Adult quantification showing similar increase in normalized primary **(L)** and secondary **(M)** branch number of adult DCNs in Syd1 RNAi (blue) compared to control (black). N=92 axons for control, N=90 axons for Syd1-RNAi **(L)**, N=66 branches in control, N=36 branches in Syd1-RNAi **(M)**. Mann Whitney test, ** $p = 0.0011$, **** $p < 0.0001$. Error bars denote mean \pm SEM, scalebar represents 5 μ m.



Quantification showing unaffected distribution of Syd1-GFP puncta normalized to axon branch length in control (black) vs EGFR DN (gray) in adults. N=93 branches for control and N=66 branches for EGFR DN. T-test, $p=0.6688$. **(F)** Quantification showing the reduced distribution of BrpD3-GFP puncta normalized to axon branch length in control (black) vs EGFR^{DN} (gray) in adults. N=124 branches for control and N=124 branches for EGFR DN, T-test, **** $p < 0.0001$. **(G)** Adult quantification of the total number of BrpD3-GFP puncta per axon in control (black) vs EGFR DN (gray). N=17 axons for control and N=17 for EGFR DN. Mann Whitney test; **** $p < 0.0001$. **(H/H'-M/M')** Recruitment of BrpD3-GFP puncta (green) in developing DCN branches labeled by CD4-tomato (magenta) in fixed samples during different stages of pupal development in control vs EGFR DN; P55 **(H/H'-I/I')**, P65 **(J/J'-K/K')** and P72 **(L/L'-M/M')**. **(N)** Quantification showing percentage of BrpD3-GFP positive DCN branches per axon during development in control (black) vs EGFR DN (gray). N=14 for control branches; P55, N=16 for EGFR DN branches; P55, N=14 for control branches; P65, N=11 for EGFR DN branches; P65, N=16 for control branches; P72, N=18 for EGFR DN branches, N=18 branches for control branches; adult, N=22 branches for EGFR DN branches; adult. Kruskal–Wallis and Dunn's as post-hoc test; **** $p < 0.0001$. **(O-P)** Labelling of post-synaptic partners (magenta) of adult DCNs (green) using Trans-Tango at 25°C for 7 days showing reduced connectivity in EGFR DN **(P)** compared to control **(O)**. **(Q)** Quantification showing reduced post-synaptic cell body number in medulla in control (black) vs EGFR DN (gray) in adult DCNs at 25°C for 7 days old adults. N=14 optic lobes for control and N=14 optic lobes for EGFR DN; **** $p < 0.0001$, Mann Whitney test. **(R/R'-T/T')** Rescue of BrpD3 GFP (green) puncta and secondary branches in adult DCNs labeled by uas-CD4 tomato (magenta) with increased gene copy number of Brp (Pacman Brp) in EGFR DN background **(T/T')** back to control level **(R/R')** compared to EGFR DN alone **(S/S')** in adults. **(U)** Adult quantification showing the rescue of BrpD3 GFP puncta normalized to individual axon branch length in Pacman Brp + EGFR^{DN} (orange) back to control (black) level compared to EGFR DN (gray). N=58 primary branches for control, N=30 primary branches for EGFR DN and N=56 primary branches for Pacman Brp+ EGFR DN. Kruskal–Wallis and Dunn's as post-hoc test; **** $p < 0.0001$. **(V)** Quantification showing no rescue of adult primary branch number per axon in Pacman Brp + EGFR DN (orange) back compared to EGFR DN (gray). N=18 axons for control, N=24 axons for EGFR DN and N=26 axons for Pacman Brp+ EGFR DN. Kruskal–Wallis and Dunn's as post-hoc test; **** $p < 0.0001$. **(W)** Quantification showing rescue of adult secondary branch number per primary branch in Pacman Brp + EGFR DN (orange) back to control (black) level compared to EGFR DN (gray). N=20 primary branches for control, EGFR DN and Pacman Brp + EGFR DN. Kruskal–Wallis and Dunn's as post-hoc test; ** $p = 0.0007$. Error bars denote mean±SEM, scalebar represents 5µm except **(O,P)** where it represents 20µm.

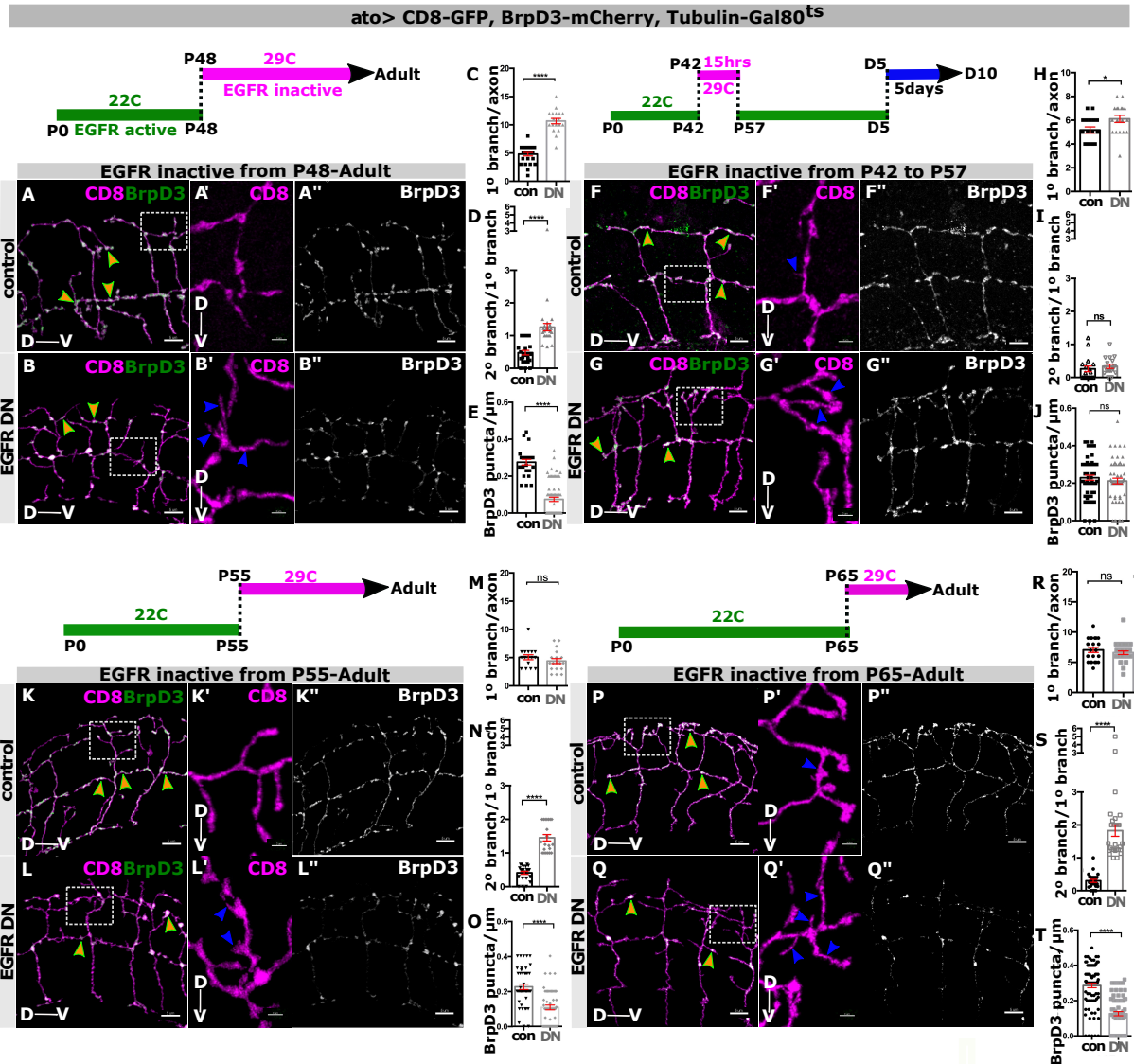


Fig.4

Temporally specific requirement for EGFR activity in synapse formation and primary branch consolidation:

Adult DCN branch morphology labeled by *uas-CD8 GFP* (green) and AZs marked by *uas-BrpD3-mCherry* (red). EGFR is active when shifted to 22°C (green bar) whereas inactive when shifted to 29°C (magenta bar). We inactivated EGFR temporally by shifting the Gal80^{ts} construct to 29°C during different developmental time intervals and analyzed young adults unless otherwise stated. White squares represent regions of higher magnification. (A/A''-B/B'') Lack of EGFR activity from P48 throughout development results in more primary and secondary branching (asterisks) with reduced BrpD3-mCherry puncta in adult DCNs compared to control. (C) Quantification showing increased primary branch number per axon in control (black) vs EGFR DN (gray). N=25 axons for control, N=26 axons for EGFR DN. Mann Whitney test; *****p* = 0.0001. (D) Quantification showing increased secondary branches per primary branch in control (black) vs EGFR DN (gray). N=25 primary branches for control and N=22 primary branches for EGFR DN. Mann-Whitney test; *****p* < 0.0001. (E) Quantification showing decreased BrpD3-mCherry puncta per unit branch length in control (black) vs EGFR DN (gray). N=25 branches for control and N=66 branches for EGFR DN. Mann Whitney test; *****p* = 0.0001. (F/F''-G/G'') Lack of EGFR activity only between

P42 to P57 during development results in more primary branching with no effect on secondary branching (asterisks) or BrpD3-mCherry puncta localisation in adult DCNs compared to control. The young adults were shifted to 25°C for 5 days after eclosion for transgene expression prior to analyses. **(H)** Quantification showing increased primary branch number per axon in control (black) vs EGFR DN (gray). N=17 axons for control and N=18 axons for EGFR DN. Mann-Whitney test; * $p=0.0139$. **(I)** Quantification showing unaffected secondary branch number per primary branch in control (black) vs EGFR DN (gray). N=17 primary branches for control and EGFR DN. Mann-Whitney test; ^{ns} $p=0.1462$. **(J)** Quantification showing comparable BrpD3 mCherry puncta per unit branch length in control (black) vs EGFR DN (gray). N=59 primary branches for control and N=56 primary branches for EGFR DN. Mann-Whitney test; ^{ns} $p=0.36$. EGFR activity blocked only late; either from P55 (**K/K**"-L/L") or from P65 (**P/P**"-Q/Q") throughout development leads to decreased BrpD3-mCherry puncta and increased secondary branches (asterisks) with no significant change in primary branches in adult DCNs. **(M,R)** Quantification showing unaffected primary branches per axon in control (black) vs EGFR DN (gray). **(M)** N=38 axons for control, N=43 axons for EGFR DN. Mann Whitney test; ^{ns} $p=0.538$. **(R)** N=36 axons for control, N=26 axons for EGFR DN. Mann Whitney test; ^{ns} $p=0.7204$ **(N,S)** Quantification showing increased secondary branches per primary branch in control (black) vs EGFR DN (gray). **(N)** N=22 primary branches for control and N=21 primary branches for EGFR DN. Mann-Whitney test; **** $p < 0.0001$. **(S)** N=25 primary branches for control and n=26 primary branches for EGFR DN. Mann-Whitney test; **** $p < 0.0001$. **(O,T)** Quantification showing decreased BrpD3-mCherry puncta per unit branch length in control (black) vs EGFR DN (gray). **(O)** N=47 primary branches for control and N=53 primary branches for EGFR DN. Mann Whitney test; **** $p < 0.0001$. **(T)** N=87 primary branches for control and N=94 primary branches for EGFR DN. Mann Whitney test; **** $p < 0.0001$. Error bars denote mean±SEM, scalebar represents 5µm.

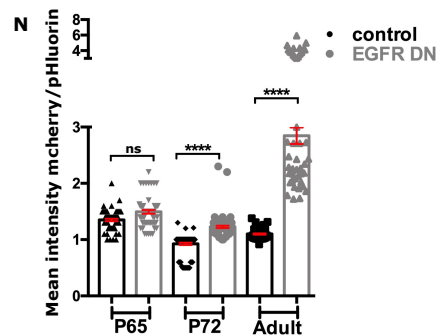
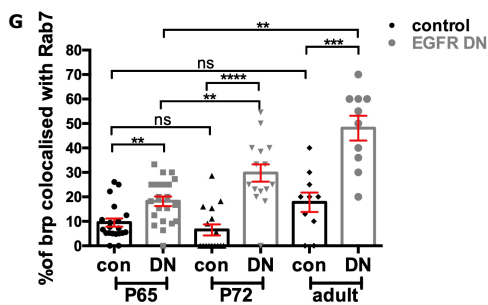
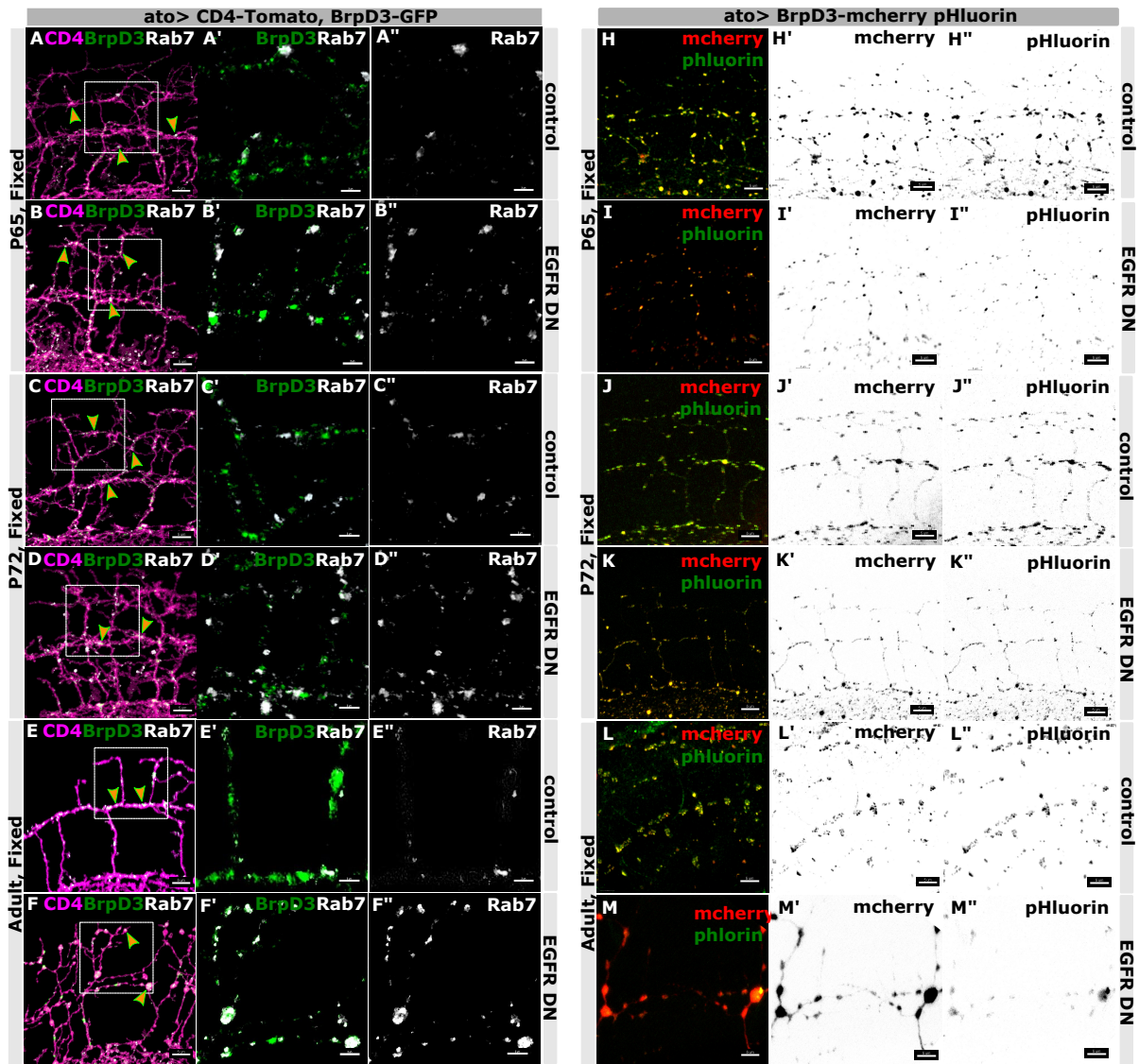


Fig.5

EGFR activity is required to prevent Brp degradation during synaptogenesis:

(A/A''-F/F'') Progressively increased colocalization of endogenous Rab7 (white) with BrpD3-GFP puncta (green) in DCN axon terminals labeled with CD4-tomato (magenta) in control vs EGFR DN during late development; P65 (A/A''-B/B''), P72 (C/C''-D/D'') and adult (E/E''-F/F''). White squares represent regions of higher magnification showing Rab7-BrpD3 colocalization in (A'/A''-

F/F''). (G) Quantification showing increased percentage of BrpD3-GFP puncta colocalized with endogenous Rab7 per axon at P65, P72 and adults in control (black) vs EGFR^{DN} (gray). N=20 axons for control vs N=21 axons for EGFR DN at P65; N=16 axons for control vs N=15 axons for EGFR DN at P72, N=10 axons for control vs N=10 axons for EGFR DN at adults. **** $p < 0.0001$, Kruskal Wallis and Dunn's as post-hoc test. **(H/H''-M/M'')** Simultaneous increase in mCherry signal (red) intensity compared to pHluorin (green) intensity when expressing the degradation probe uas-BrpD3-mCherry-pHluorin in DCN branches in EGFR DN compared to control during late development: P65 **(H'/H''-I/I'')**, P72 **(J/J''-K/K'')** and adult **(L/L''-M/M'')**. **(N)** Quantification showing increased mean intensity of mCherry channel to pHluorin channel across several BrpD3-DF puncta per axon during P65, P72 and adults in control (black) vs EGFR DN (gray). N=65 BrpD3-DF punctum for control vs N=65 BrpD3-DF punctum for EGFR DN at P65, N=82 BrpD3-DF punctum for control vs N=83 BrpD3-DF punctum for EGFR DN at P72; N=68 BrpD3-DF puncta for control vs N=47 BrpD3-DF puncta for EGFR DN at adults. **** $p < 0.0001$; Kruskal Wallis and Dunn's as post-hoc test; Error bars denote mean \pm SEM, scalebar represents 5 μ m; apart from **(A'/A'', B'/B'', C'/C'', D'/D'', E'/E'', F',F'')** which represents 3 μ m.

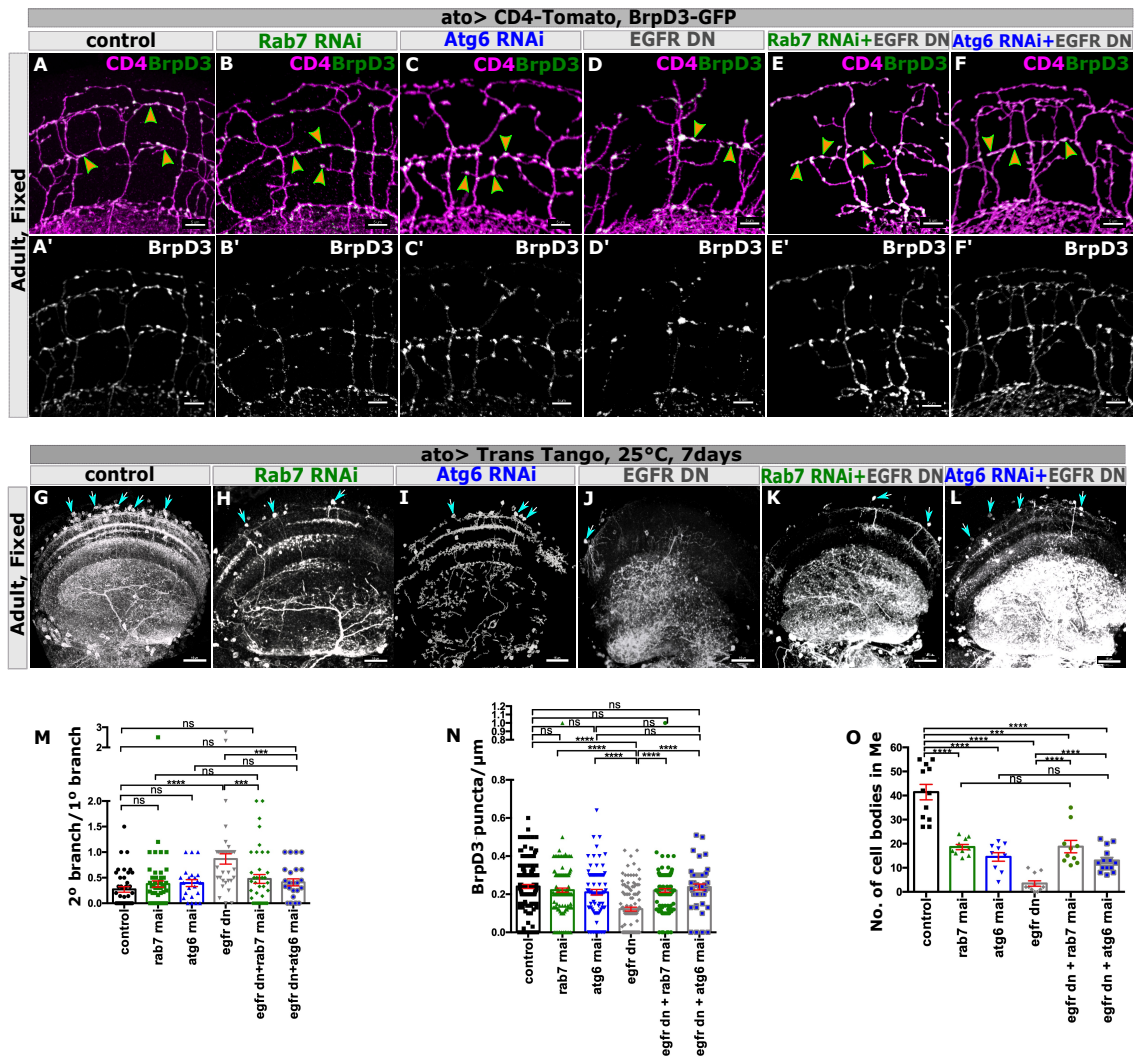


Fig.6

EGFR signals through autophagy to maintain DCN presynaptic active zone and circuit connectivity:

(A/A'-F/F') Rescuing loss of adult DCN terminal axon branch (magenta) number and BrpD3-GFP puncta (green) distribution in Rab7 RNAi + EGFR DN (E/E') and Atg6 RNAi + EGFR DN (F/F') back to the level of control (A/A'), Rab7-RNAi (B/B') or Atg6-RNAi (C/C') as compared to EGFR DN (D/D'). (G-L) Corresponding rescue of post-synaptic partner (white) loss in DCNs using TransTango at 25°C for 7 days old adults in EGFR DN (H) by expressing Rab7 RNAi + EGFR DN (K) or Atg6 RNAi + EGFR DN (L) back to the level of Rab7-RNAi (H) or Atg6-RNAi (I) respectively but only partial rescue compared to control (G). (M) Quantification showing rescue of secondary branch number per primary in Rab7 RNAi + EGFR DN (green+gray) and Atg6 RNAi + EGFR DN (blue+gray) back to the level of control (black), Rab7 RNAi (green), Atg6 RNAi (blue) as compared to EGFR DN (gray). N=41 branches for control, N=50 branches for Rab7 RNAi, N=22 branches for Atg6 RNAi, N=35 branches for EGFR DN, N=41 branches for Rab7 RNAi + EGFR DN, N= 25 branches for Atg6 RNAi + EGFR DN. Kruskal–Wallis and Dunn's as post-hoc test; **** $p < 0.0001$. (N) Quantification showing similar rescue of BrpD3-GFP puncta per unit branch length in Rab7 RNAi + EGFR DN and Atg6 RNAi + EGFR DN back to the level of control, Rab7 RNAi, Atg6

RNAi as compared to EGFR DN. N=153 branches for control, N=138 branches for Rab7 RNAi, N=84 branches for Atg6 RNAi, N=124 branches for EGFR DN, N=122 branches for Rab7 RNAi + EGFR DN, N=50 for Atg6 RNAi + EGFR DN; Kruskal–Wallis and Dunn’s as post-hoc test; **** $p < 0.0001$. **(O)** Quantification for rescuing post-synaptic cell body number in medulla per optic lobe in Rab7 RNAi + EGFR DN and Atg6 RNAi + EGFR DN back to the level of control, Rab7 RNAi, Atg6 RNAi as compared to EGFR DN. N=12 optic lobes in control, N=11 optic lobes in Rab7 RNAi, N=10 optic lobes in Atg6 RNAi, N=13 optic lobes in EGFR DN, N=12 optic lobes in Rab7 RNAi + EGFR DN and N=14 optic lobes in Atg6 RNAi + EGFR DN. Kruskal–Wallis and Dunn’s as post-hoc test; **** $p < 0.0001$. Error bars denote mean \pm SEM, scalebar represents 5 μ m except **(G-L)** where it is 15 μ m.

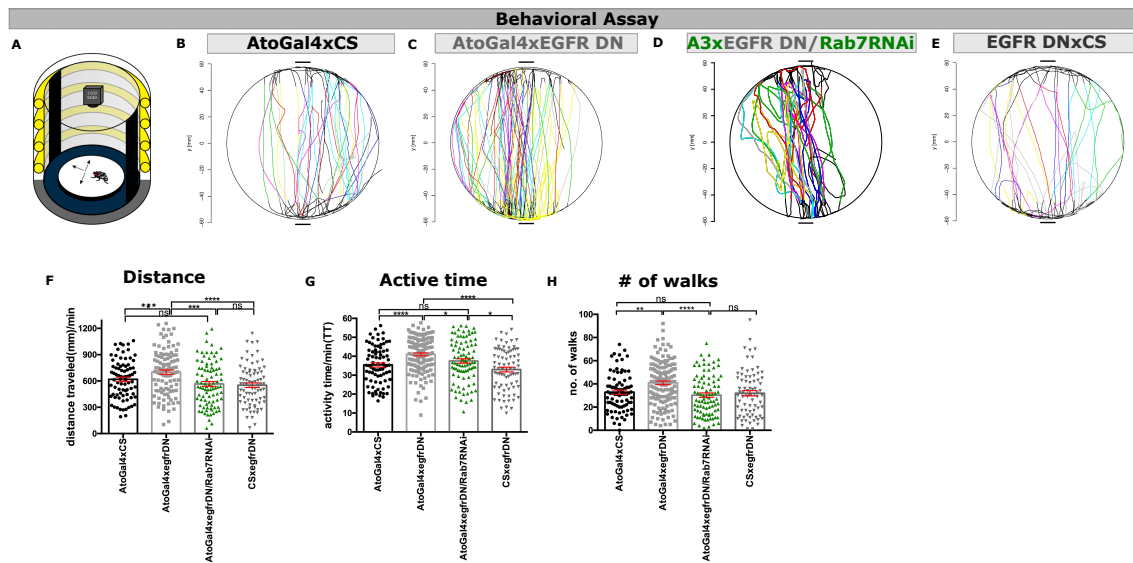
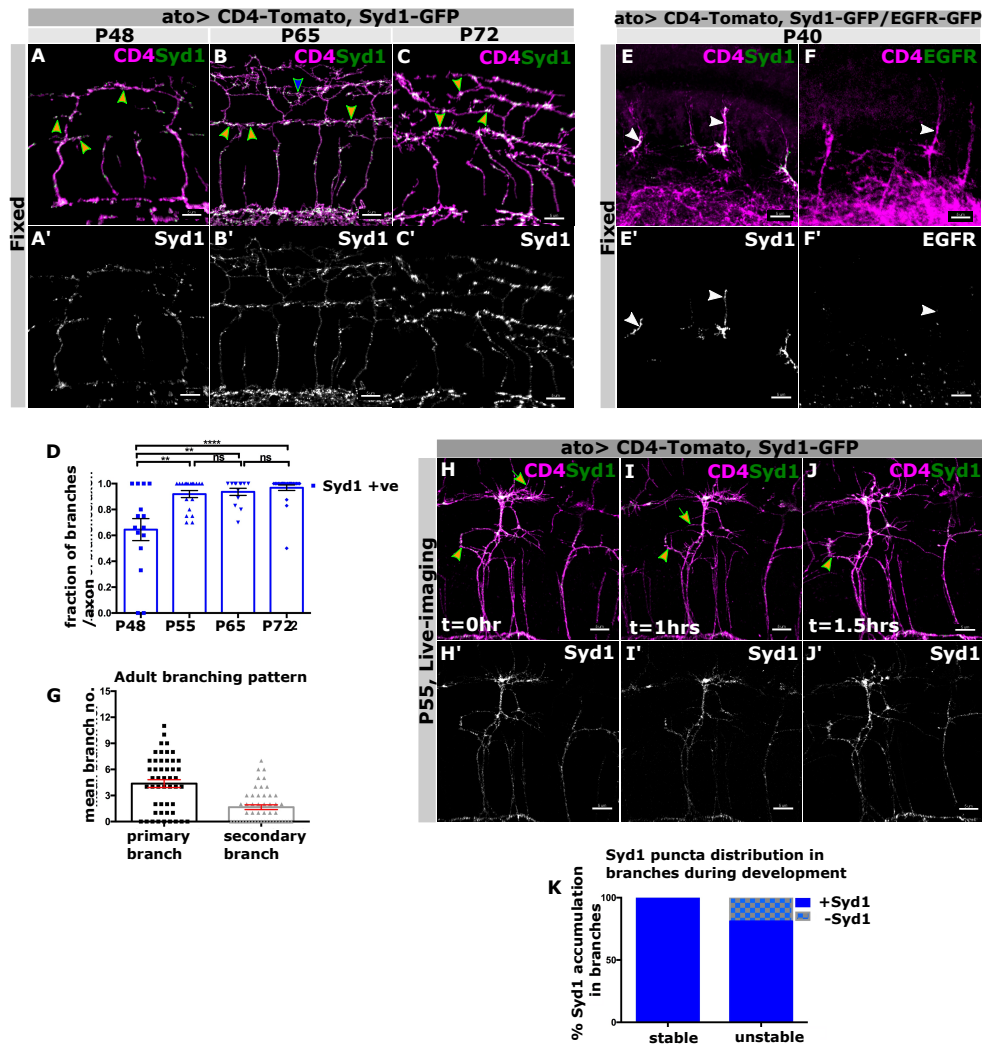


Fig.7 EGFR signals through autophagy to maintain proper behavioral activity:

(A) Schematic illustration of the adult fly behavior assay; Buridan’s paradigm. **(B-E)** Individual fly walking tracks between 2 black stripes in AtoGal4-14a(A3)xCS**(B)**, Atogal4-14a(A3)/EGFR DN **(C)** Atogal4-14a(A3)/ EGFR DN+ Rab7 RNAi **(D)** EGFR DNxCS **(E)**. **(F-H)** Quantification of fly activity behavior using 3 parameters: distance traveled **(F)**, activity time **(G)** and number of walks **(H)** showing rescue in behavioral phenotype in Atogal4-14a/ EGFR DN+ Rab7 RNAi (gray+green) back to the level of AtoGal4-14axCS (black) or EGFR DNxCS (dark gray) compared to Atogal4-14a(A3)/EGFR DN (gray). Each dot represents individual flies. N=80 individuals for AtoGal4xCS, N=106 individuals for AtoGal4x EGFR DN, N=89 individuals for AtoGal4x EGFR DN/Rab7 RNAi, N=79 individuals for CSxEGFR DN. Kruskal–Wallis and Dunn’s as post-hoc test; *** $p = 0.0002$ **(F)**, *** $p = 0.0005$ **(G)**, **** $p < 0.0001$ **(H)**. Error bars denote mean \pm SEM.

Supplemental information:



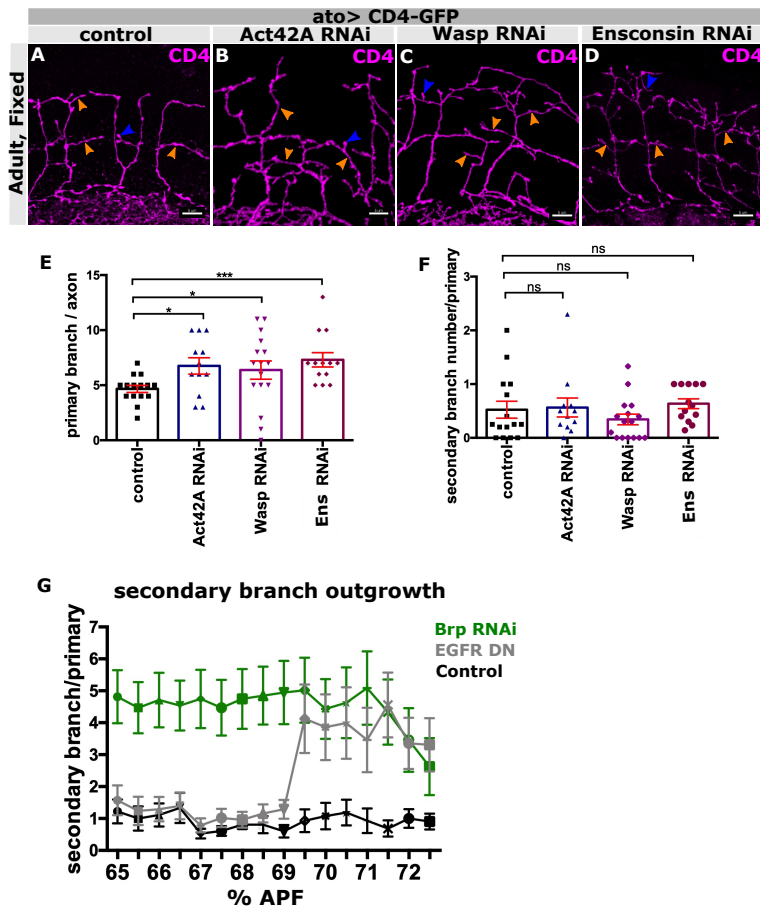
Supplementary 1

Spatio-temporal trafficking of Syd1 in the DCN branches during pupal development:

(A/A'-C/C') Temporal order of recruitment of Syd1 GFP (green) in the DCN branches (magenta) during development; P48 (A/A'), P65 (B/B') and P72 (C/C'). (D) Quantification showing the fraction of DCN branches containing Syd1 puncta per axon during development. N=15 axons at P48, N=19 axons at P55, N=13 axons at P65 and N=25 axons at P72; **** $p < 0.0001$, Mann Whitney test. (E/E'-F/F') Syd1 GFP (green)(arrowhead) puncta (E/E') gets trafficked prior to EGFR GFP (green)(arrowhead)(F/F') in DCN axonal shafts (magenta) at P40. (G/G'-I/I') Spatial distribution pattern of Syd1 GFP (green) in DCN branches (magenta) during development in ex-vivo pupal brain cultures between P55-P57. Z-stack projection of ex-vivo time-lapse imaging of control axons showing Syd1 GFP (green) localize in both stable (arrow) and unstable branches (arrowhead). (J) Quantification showing percentage of stable (blue) and unstable (checkered blue) branches containing Syd1 puncta during development. N=25 stable branches and N=36 unstable branches. Error bars denote mean \pm SEM, scalebar represents 5 μ m.

Supplementary Video 1

Live trafficking of Syd1, EGFR and BrpD3 in the DCN branches during pupal development:
 Live-imaging of EGFR GFP, BrpD3 GFP and Syd1 GFP in DCN branches labeled by membrane marker CD4 Tomato driven by atoGal4-14a starting P55.



Supplementary 2

Effect of knocking down cytoskeletal proteins on axon branching; temporal outgrowth of secondary branches:

(A-D) Adult DCN branch morphology (magenta) upon knocking down several cytoskeletal regulators like Act42A (B), Wasp (C), Ensconsin(Ens) (D) compared to genetic control (A). (E) Adult quantification showing increased number of primary branches per axon in uas-Act42A RNAi (blue), uas-Wasp RNAi (pink), uas-Ens RNAi (purple) compared to control (black). N=15 axons for control, N=12 axons for Act42A RNAi, N=16 axons for Wasp RNAi and N=13 axons for Ens RNAi; * $p=0.0231$, * $p=0.0294$, *** $p=0.0003$, Mann Whitney test. (F) Adult quantification showing unaffected secondary branches normalized to primary branch number in uas-Act42A RNAi (blue), uas-Wasp RNAi (pink), uas-Ens RNAi (purple) compared to control (black). N=15 axons for control, N=12 axons for Act42A RNAi, N=16 axons for Wasp RNAi and N=13 axons for Ens RNAi; $^{ns}p=0.5059$, $^{ns}p=0.6402$, $^{ns}p=0.1545$, Mann Whitney test. (G) Quantification of the temporal outgrowth of secondary branches (secondary branch number normalized to primary branches) in every 30mins interval between P65-P72 ex-vivo cultures in Brp B3,C8 RNAi (green) or EGFR DN (gray) compared to control (black). N=29 branches for Brp B3,C8 RNAi (green); N=20 branches for EGFR DN (gray) and N=18 branches for control (black). $^{ns}p=0.6867$ for control, $^{ns}p=0.9441$ for

Brp B3,C8 RNAi and **** $p < 0.0001$ for EGFR DN. Error bars denote mean \pm SEM, scalebar represents 5 μ m.

Supplementary Video 2.1

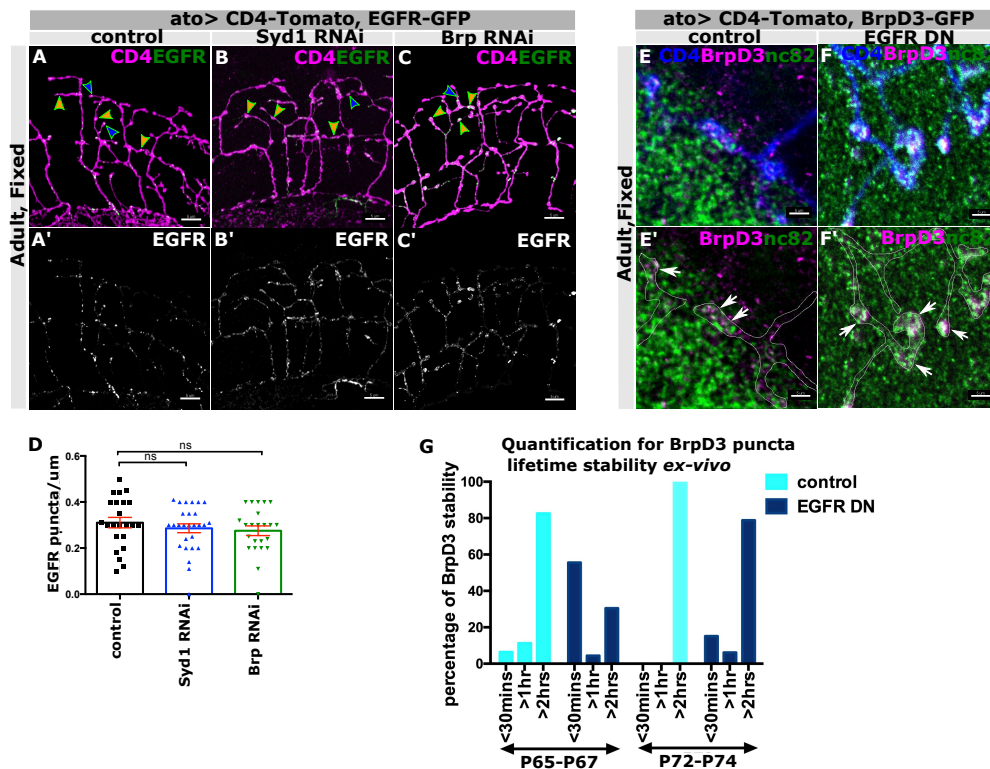
Ext./retr. dynamics of adult DCN branches in control vs Brp KD:

Live-imaging of adult (~5-7 days old) DCN branches labeled by atoGal4-14a driving membrane marker uas-CD4 GFP in control vs Brp B3,C8 RNAi.

Supplementary Video 2.2

Secondary branch outgrowth in DCN branches in control vs Brp KD and EGFR DN:

Live-imaging of DCN branches labeled by atoGal4-14a driven membrane marker uas-CD4 GFP in control vs Brp B3,C8 RNAi and EGFR DN post P65.



Supplementary 3

Genetic hierarchy of EGFR, Syd1 and BrpD3; co-localization of endogenous Brp with uas-BrpD3 GFP; temporal stability of BrpD3 GFP punctum in control vs EGFR DN

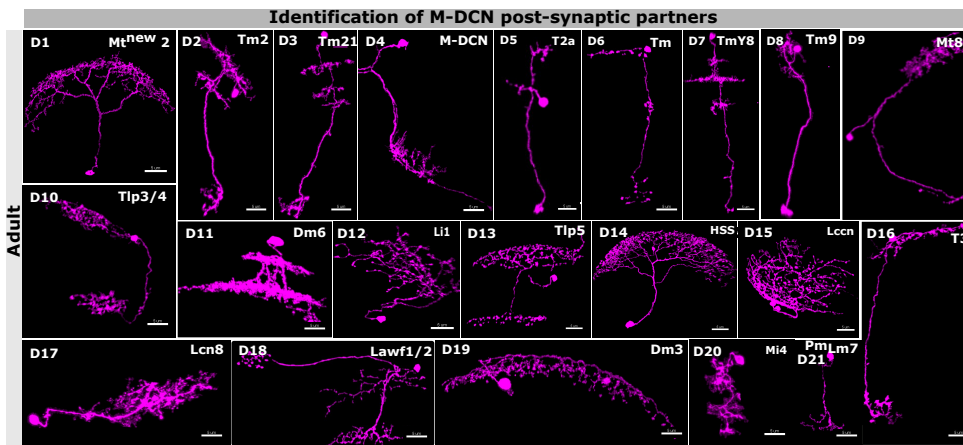
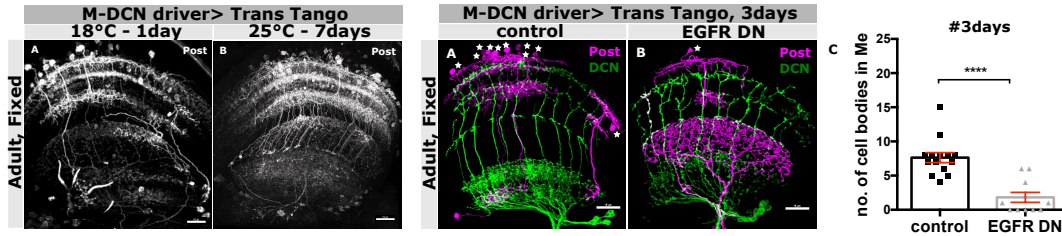
(A/A'-C/C') EGFR-GFP (green) localization in adult DCN branches (magenta) upon knocking down Syd1 (B), Brp (C) compared to control (A). (D) Quantification showing unaffected distribution of EGFR GFP puncta per unit branch length in Syd1 RNAi (blue), Brp B3,C8 RNAi (green) compared to control (black) in adults. N=23 branches for control, N=27 branches for Syd1 RNAi and N=23 branches for Brp RNAi; $^{ns}p=0.4714$, $^{ns}p=0.2612$. Mann Whitney test. (E/E'-F/F') STED co-localization analysis of endogenous Brp marked by Nc82 staining (green) and BrpD3 GFP (magenta) in DCN axon branches (red) in control (E/E') vs EGFR DN (F/F'). (G) Quantification of percentage of BrpD3-GFP puncta lifetime (<30mins, <1hour, >2hours) in individual DCN branches tracked for 2hours from P65 and P72 in control (black) vs EGFR DN (gray). N=20 punctum for

control and 23 punctum, for EGFR DN in P65-P67 ex-vivo culture. N=28 punctum for control and 33 punctum for EGFR DN in P72-P74 ex-vivo culture. Error bars denote mean±SEM, scalebar represents 5µm.

Supplementary Video 3

Temporal stability of BrpD3 GFP punctum in control vs EGFR DN:

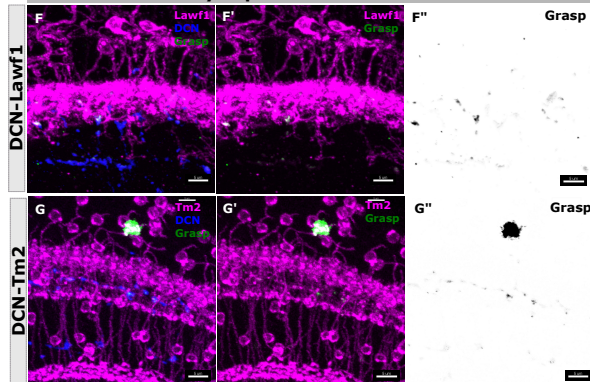
Live-imaging of *atoGal4-14a* driven BrpD3 GFP in DCN branches marked by *uas-CD4 Tomato* starting P65 and P72 of pupal development in control vs EGFR DN.



E M-DCN Gal4 > Trans Tango, 25°C-3days

	control	EGFR DN
Lawf1/2	2,125±0,23	1,739±0,32
Tm2/21	0,821±0,14	0,26±0,16
Li1	0,678±0,18	0,391±0,16
M-DCN	0,536±0,11	0,478±0,16
Dm3/6	0,428±0,08	0,13±0,07
PmLM7	0,304±0,08	0,043±0,04
HSS	0,286±0,06	
Li4	0,286±0,06	
T3	0,143±0,05	
Mi4	0,107±0,06	
Lcn8	0,107±0,05	
Lpi	0,089±0,04	
Li2	0,089±0,04	
Lccn1	0,071±0,03	
Lp-CB	0,054±0,03	
Lccn2	0,018±0,02	
Mt	0,018±0,02	
Tip5	0,018±0,02	

activity dependent GRASP with DCNs

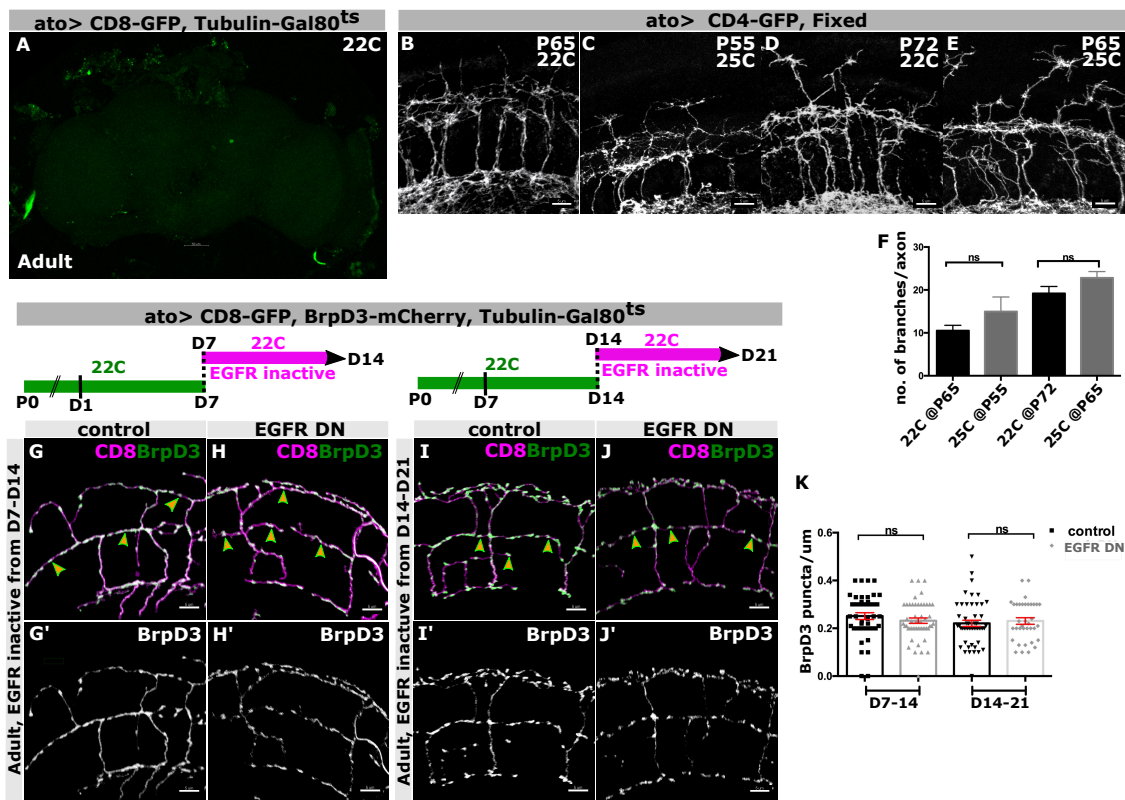


Supplementary 4

Loss of EGFR activity causes a reduction in M-DCN circuit connectivity:

(A-B) Optimization for labeling of post-synaptic partners of adult M-DCNs driven by a M-DCN specific Gal4 using Trans-Tango at 18°C for 1day old adults (A) and 25°C for 7days old adults (B). (C-D) Sparse labeling of post-synaptic partners (magenta) of adult M-DCNs (green) driven by a M-DCN specific Gal4 using Trans-Tango at 25°C for 3 days old adults in control (C) vs EGFR DN

(D). (E) Quantification showing reduced number of post-synaptic cell bodies in medulla per optic lobe in control (black) vs EGFR DN (gray) in adult DCNs at 25°C for 3 days. N=14 optic lobes for control, N=11 optic lobes for EGFR DN. Kruskal–Wallis and Dunn’s as post-hoc test; **** $p < 0.0001$. **(F1-F21)** Identification of post-synaptic partners (magenta) of adult DCNs using Trans-Tango at 25°C for 3 days using a M-DCN specific neuronal driver. We characterized and identified several post-synaptic targets like Mt^{new2} **(F1)**, Tm2 **(F2)**, Tm21**(F3)**, M-DCN **(F4)**, T2a **(F5)**, Tm**(F6)**, TmY8 **(F7)**, Tm9 **(F8)**, Mt8 **(F9)**, Tlp3/4 **(F10)**, Dm6 **(F11)**, Li1 **(F12)**, Tlp5 **(F13)**, HSS **(F14)**, Lccn **(F15)**, T3 **(F16)**, Lcn8 **(F17)**, Lawf1/2**(F18)**, Dm3 **(F29)**, Mi4 **(F20)**, Pm_{LM7} **(F21)**. Table of Post-synaptic partner distribution of M-DCN in control **(G)** vs EGFR DN **(G’)**. **(H/H’-I/I’)** Grasp signal (green) confirming synaptic connection between adult DCN pre-synaptic sites (blue) with Lawf1 (magenta) **(H-H’)** and Tm2 (magenta) **(I-I’)**. Ato-LexA is used to drive adult DCNs for this experiment. N= 50 optic lobes for control, N= 50 optic lobes for EGFR DN. Error bars denote mean±SEM, scalebar represents 20µm in **(A-B)**, 15 µm in **(C-D)** and 5µm in **(F1-21, H/H’-I/I’)** except **(F18)** which represents 10µm.

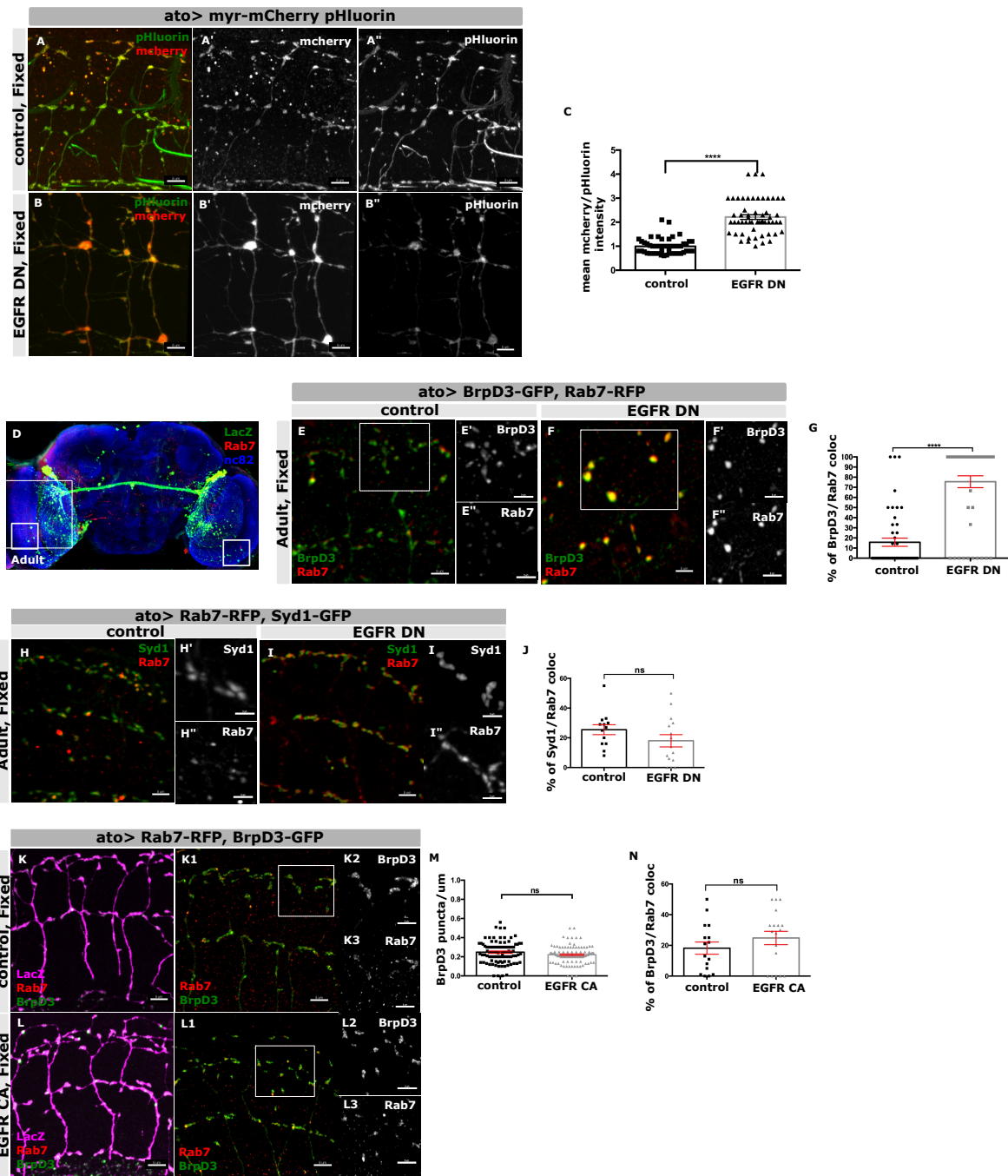


Supplementary 5

Experimental set up control and DCN developmental calibration of 22°C vs 25°C; adult specific requirement of EGFR activity for proper branch consolidation and synaptogenesis:

(A) Control experiment for checking Gal80^{ts} efficiency in repressing *atoGal4-14a* driven uas-CD8 GFP expression when the fly was raised at 22°C throughout development. **(B-E)** Calibration of DCN axon branch progression at 22°C vs 25°C during development. In-vivo progression of DCN branch morphology (white) at 65hours APF at 22°C **(B)** vs 55hours APF at 25°C **(C)**, and 72hours APF at 22°C **(D)** vs 65hours APF at 25°C **(E)**. **(F)** Quantification showing branch number per axon of

65hours APF and 72hours APF at 22°C (black) corresponds to 55hours APF and 65hours APF at 25°C (gray) respectively. N=5 lobes for P65 at 22°C, N=7 lobes for P55 at 25°C, N=5 lobes for P72 at 22°C and N=7 lobes for P65 at 22°C; $^{ns}p = 0.4476$, $^{ns}p = 0.2476$, Mann Whitney test. **(G/G'-J/J')** Inactivating EGFR activity in adult DCN branches (green) only between D7-D14 **(G/G'-H/H')** or between D14-D21 **(I/I'-J/J')** did not affect BrpD3-mCherry (red) puncta localization in the branches. **(K)** Quantification showing unaltered number of BrpD3 GFP puncta per unit branch length in control (black) vs EGFR DN (gray) expressed during D7-D17 and D14-D21. N=44 branches for control D7-14, N=51 branches for EGFR DN D7-14, N=51 branches for control D14-21 and N=36 branches for EGFR DN D14-21; $^{ns}p = 0.1344$ and $^{ns}p = 0.5053$, Mann Whitney test. Error bars denote mean \pm SEM, scalebar represents 5 μ m whereas in **(A)** represents 50 μ m.



Supplementary 6

Lack of EGFR activity in adult DCNs causes degradation of general plasma membrane cargoes; Adult co-localization of Active Zones (AZ) with uas-Rab7 RFP in lack of EGFR activity; Syd1 GFP does not colocalize with late endosomes in lack of EGFR activity; DCNs expressing EGFR CA shows no AZs loss in branches with no increased co-localization with late endosomes:

(A/A''-B/B'') Increase in mCherry signal (red) intensity compared to pFluorin (green) intensity when expressing the general membrane degradation probe uas-myr-mCherry-pFluorin in adult DCN branches in EGFR DN (B-B'') compared to control (A-A''). (C) Quantification showing increased mean intensity of mCherry channel to pFluorin channel across several myr-DF regions per axon in

adults. N=50 axons in control and 56 axons in EGFR DN. Mann Whitney test; **** $p < 0.0001$. **(D)** Representative adult fly brain with neuropils marked by Nc82 (blue), DCNs labeled by LacZ (green) and late endosomes marked by Rab7 RFP (red) localized in the branches in medulla (white box). **(E/E''-F/F'')** Adult localization of BrpD3 GFP (green) and Rab7 RFP (red) in control **(E-E'')** vs EGFR DN **(F-F'')** in DCN branches. White box represents region shown in higher magnification **(E'/E''-F'/F'')**. **(G)** Quantification showing increased percentage of BrpD3 GFP puncta colocalized with Rab7 RFP puncta in the adult branches per axon in control (black) vs EGFR DN (gray). N=49 punctum for control, N=49 punctum for EGFR DN. Mann Whitney test; **** $p < 0.0001$. **(H/H''-I/I'')** Adult localization of Syd1 GFP (green) and Rab7 RFP in control **(H-H'')** vs EGFR DN **(I-I'')** in DCN branches. **(J)** Adult quantification showing unaffected percentage of Syd1 GFP puncta colocalized with Rab7 RFP puncta in DCN branches per axon in control (black) vs EGFR DN (gray). N=13 axons for control and N=15 branches for EGFR DN; $^{ns}p=0.1386$, Mann Whitney test. **(K/K3-L/L3)** Adult DCN branches (magenta) exhibits BrpD3 GFP (green) and Rab7 RFP (red) puncta in control **(K)** vs EGFR CA **(L)**. **(M)** Adult quantification showing unaffected number of BrpD3 GFP puncta per unit branch in control (black) vs EGFR CA (gray). N=90 branches for control and N=114 branches for EGFR CA; $^{ns}p=0.0590$, Mann Whitney test. **(N)** Quantification showing unaltered percentage of BrpD3 GFP puncta colocalized with Rab7 RFP puncta per axon in control (black) vs EGFR CA (gray) adults. Individual dots represent single axons. N=16 branches in control and N=18 branches in EGFR CA; $^{ns}p=0.3750$, Mann Whitney test. Error bars denote mean \pm SEM, scalebar in **(D)** represents 50 μ m, **(A-A'', B-B'', E, F, H, I, K, L)** represents 5 μ m and **(E'/E'', F'/F'', H'/H'', I'/I'', K2/K3, L2/L3)** represents 3 μ m.

	value if sig to exp	given if sig to one c	if sig to exp	if sig to exp
	A3xCS	A3xEGFR	A3xEGFR_RAB7 KD	CSxEGFR
Walking activity	2,19	2,73	2,01	2,13
Pause duration	1,94	1,57	n.s.	n.s.
Distance traveled	618,82	686,55	562,26	551,96
Relative time moving	0,52	0,6	0,53	0,47
Activity time	36,14	41,62	37,75	33,64
Speed	20,72	19,63	17,92	n.s.
Number of pauses	n.s.	n.s.	n.s.	n.s.
Activity bouts	n.s.	8,9	6,92	6,65
Turning angle	n.s.	6,46	7,14	n.s.
Meandering	n.s.	0,33	0,15	0,13
Centrophobism while moving	n.s.	0,51	0,4	n.s.
Center deviation while moving	n.s.	83,07	79,64	n.s.
Centrophobism while stationary	n.s.	n.s.	n.s.	n.s.
Center deviation while stationary	n.s.	n.s.	n.s.	n.s.
Absolute stripe Deviation while stationary	n.s.	n.s.	n.s.	n.s.
Absolute stripe Deviation while moving	n.s.	n.s.	n.s.	n.s.
Absolute angle Deviation	n.s.	n.s.	n.s.	n.s.
Absolute horizon deviation while stationary	n.s.	n.s.	n.s.	n.s.
Absolute horizon deviation while moving	58,03	59,56	56,86	n.s.
Stripe deviation while stationary	n.s.	n.s.	n.s.	n.s.
Stripe deviation while moving	n.s.	n.s.	n.s.	n.s.
Angle deviation while stationary	n.s.	n.s.	n.s.	n.s.
Horizon deviation while stationary	n.s.	n.s.	n.s.	n.s.
Angle deviation while moving	n.s.	n.s.	n.s.	n.s.
Horizon deviation while moving	n.s.	n.s.	n.s.	n.s.
overall activity				
movement angles or location independent of visual cue				
movement angles or location relative to visual cue				

Supplementary 7

Table of parameters measured for individual flies in Buridan's paradigm.

References:

- Adnan, G. *et al.* (2020) ‘The GTPase Arl8B plays a principle role in the positioning of interstitial axon branches by spatially controlling autophagosome and lysosome location’, *Journal of Neuroscience*, 40(42), pp. 8103–8118. doi: 10.1523/JNEUROSCI.1759-19.2020.
- Agi, E., Kulkarni, A. and Hiesinger, P. R. (2020) ‘Neuronal strategies for meeting the right partner during brain wiring’, *Current Opinion in Neurobiology*. Elsevier Ltd, pp. 1–8. doi: 10.1016/j.conb.2020.01.002.
- Aguirre, A., Rubio, M. E. and Gallo, V. (2010) ‘Notch and EGFR pathway interaction regulates neural stem cell number and self-renewal’, *Nature*, 467(7313). doi: 10.1038/nature09347.
- Azarnia Tehran, D., Kuijpers, M. and Haucke, V. (2018) ‘Presynaptic endocytic factors in autophagy and neurodegeneration’, *Current Opinion in Neurobiology*. doi: 10.1016/j.conb.2017.12.018.
- Batool, S. *et al.* (2019) ‘Synapse formation: From cellular and molecular mechanisms to neurodevelopmental and neurodegenerative disorders’, *Journal of Neurophysiology*, 121(4). doi: 10.1152/jn.00833.2018.
- Bhukel, A. *et al.* (2019) ‘Autophagy within the mushroom body protects from synapse aging in a non-cell autonomous manner’, *Nature Communications*, 10(1). doi: 10.1038/s41467-019-09262-2.
- Bourgeois, J. P. and Rakic, P. (1993) ‘Changes of synaptic density in the primary visual cortex of the macaque monkey from fetal to adult stage’, *Journal of Neuroscience*, 13(7). doi: 10.1523/jneurosci.13-07-02801.1993.
- Buff, E. *et al.* (1998) ‘Signalling by the Drosophila epidermal growth factor receptor is required for the specification and diversification of embryonic muscle progenitors’, *Development*, 125, pp. 2075–2086. Available at: https://cob.silverchair-cdn.com/cob/content_public/journal/dev/125/11/10.1242_dev.125.11.2075/1/2075.pdf?Expires=1643013366&Signature=Awz9f59jhGNfKXWb6R~a8TKyq4bTBpNcpY9fGb0gLNkmi2SOB0wJJeIRDS6btIz3IYH5AhSBe98nZguOHYAhY-1uI9q2waRfU0qfbiQxb7pCJFqdIaYz0SVxL.
- Chen, B. E. *et al.* (2006) ‘The Molecular Diversity of Dscam Is Functionally Required for Neuronal Wiring Specificity in Drosophila’, *Cell*, 125(3). doi: 10.1016/j.cell.2006.03.034.
- Chia, P. H. *et al.* (2014) ‘Local F-actin network links synapse formation and axon branching’, *Cell*, 156(1–2). doi: 10.1016/j.cell.2013.12.009.
- Cisneros-Franco, J. M. *et al.* (2020) ‘Critical periods of brain development’, in *Handbook of Clinical Neurology*. Elsevier B.V., pp. 75–88. doi: 10.1016/B978-0-444-64150-2.00009-5.
- Colón-Ramos, D. A. (2009) ‘Chapter 2 Synapse Formation in Developing Neural Circuits’, *Current Topics in Developmental Biology*. doi: 10.1016/S0070-2153(09)01202-2.
- Constance, W. D. *et al.* (2018) ‘Neurexin and neuroligin-based adhesion complexes drive axonal arborisation growth independent of synaptic activity’, *eLife*, 7. doi: 10.7554/eLife.31659.
- Doll, C. A. and Brodie, K. (2014) ‘Impaired activity-dependent neural circuit assembly and refinement in autism spectrum disorder genetic models’, *Frontiers in Cellular*

Neuroscience, 8(FEB). doi: 10.3389/fncel.2014.00030.

Economo, M. N. *et al.* (2016) ‘A platform for brain-wide imaging and reconstruction of individual neurons’, *eLife*, 5(JANUARY2016). doi: 10.7554/eLife.10566.

Feller, M. B. and Scanziani, M. (2005) ‘A precritical period for plasticity in visual cortex’, *Current Opinion in Neurobiology*, 15(1), pp. 94–100. doi: 10.1016/J.CONB.2005.01.012.

Fischbach, K. F. and Dittrich, A. P. M. (1989) ‘The optic lobe of *Drosophila melanogaster*. I. A Golgi analysis of wild-type structure’, *Cell and Tissue Research*, 258(3), pp. 441–475. doi: 10.1007/BF00218858.

Fleming, A. and Rubinsztein, D. C. (2020) ‘Autophagy in Neuronal Development and Plasticity’, *Trends in Neurosciences*. doi: 10.1016/j.tins.2020.07.003.

Fouquet, W. *et al.* (2009) ‘Maturation of active zone assembly by *Drosophila* Bruchpilot’, *Journal of Cell Biology*, 186(1), pp. 129–145. doi: 10.1083/jcb.200812150.

Galvez-Contreras, A. Y., Quiñones-Hinojosa, A. and Gonzalez-Perez, O. (2013) ‘The role of EGFR and ErbB family related proteins in the oligodendrocyte specification in germinal niches of the adult mammalian brain’, *Frontiers in Cellular Neuroscience*, 7(DEC). doi: 10.3389/fncel.2013.00258.

Goldshmit, Y. *et al.* (2004) ‘SOCS2 Induces Neurite Outgrowth by Regulation of Epidermal Growth Factor Receptor Activation’, *Journal of Biological Chemistry*, 279(16). doi: 10.1074/jbc.M312873200.

Grueber, W. B. *et al.* (2005) ‘The development of neuronal morphology in insects’, *Current Biology*. doi: 10.1016/j.cub.2005.08.023.

Hassan, B. A. and Hiesinger, P. R. (2015) ‘Beyond Molecular Codes: Simple Rules to Wire Complex Brains’, *Cell*, 163(2). doi: 10.1016/j.cell.2015.09.031.

Hassan Bassem A. (2000) *atonal Regulates Neurite Arborization but Does Not Act as a Proneural Gene in the Drosophila Brain*.

Hiesinger, P. R. (2021) ‘Brain wiring with composite instructions’, *BioEssays*, 43(1). doi: 10.1002/BIES.202000166.

Hiesinger, P. R. and Hassan, B. A. (2018) ‘The Evolution of Variability and Robustness in Neural Development’, *Trends in Neurosciences*, 41(9), pp. 577–586. doi: 10.1016/j.tins.2018.05.007.

Hoerstring, A. K. and Schmucker, D. (2021) ‘Axonal branch patterning and neuronal shape diversity: roles in developmental circuit assembly: Axonal branch patterning and neuronal shape diversity in developmental circuit assembly’, *Current Opinion in Neurobiology*. Elsevier Ltd, pp. 158–165. doi: 10.1016/j.conb.2020.10.019.

Hua, J. Y. and Smith, S. J. (2004) ‘Neural activity and the dynamics of central nervous system development’, *Nature Neuroscience*. doi: 10.1038/nn1218.

Huang, S. *et al.* (2020) ‘Presynaptic Active Zone Plasticity Encodes Sleep Need in *Drosophila*’, *Current Biology*, 30(6), pp. 1077–1091.e5. doi: 10.1016/j.cub.2020.01.019.

Huber, K. M. *et al.* (2015) ‘Dysregulation of mammalian target of rapamycin signaling in mouse models of autism’, *Journal of Neuroscience*, 35(41), p. 13836. doi: 10.1523/JNEUROSCI.2656-15.2015.

Jin, E. J. *et al.* (2018) ‘Live Observation of Two Parallel Membrane Degradation Pathways at Axon Terminals’, *Current Biology*, 28(7), pp. 1027–1038.e4. doi: 10.1016/j.cub.2018.02.032.

Kalil, K. and Dent, E. W. (2014) ‘Branch management: Mechanisms of axon branching in

the developing vertebrate CNS', *Nature Reviews Neuroscience*. doi: 10.1038/nrn3650.

Kim, M. *et al.* (2016) 'Mutation in ATG5 reduces autophagy and leads to ataxia with developmental delay', *eLife*, 5(JANUARY2016). doi: 10.7554/eLife.12245.001.

Kiral, F. R. *et al.* (2020) 'Autophagy-dependent filopodial kinetics restrict synaptic partner choice during *Drosophila* brain wiring', *Nature Communications*, 11(1). doi: 10.1038/s41467-020-14781-4.

Kiral, F. R. *et al.* (2021) 'Brain connectivity inversely scales with developmental temperature in *Drosophila*', *Cell Reports*, 37(12), p. 110145. doi: 10.1016/j.celrep.2021.110145.

Knappek, S., Sigrist, S. and Tanimoto, H. (2011) 'Bruchpilot, A synaptic active zone protein for anesthesia-resistant memory', *Journal of Neuroscience*, 31(9), pp. 3453–3458. doi: 10.1523/JNEUROSCI.2585-10.2011.

Konstantinides, N. *et al.* (2018) 'Phenotypic Convergence: Distinct Transcription Factors Regulate Common Terminal Features', *Cell*, 174(3), pp. 622-635.e13. doi: 10.1016/j.cell.2018.05.021.

Koprivica, V. *et al.* (2005) 'Neuroscience: EGFR activation mediates inhibition of axon regeneration by myelin and chondroitin sulfate proteoglycans', *Science*, 310(5745). doi: 10.1126/science.1115462.

Langen, M. *et al.* (2013) 'Mutual inhibition among postmitotic neurons regulates robustness of brain wiring in *Drosophila*', *eLife*, 2013(2). doi: 10.7554/eLife.00337.

Lewis, T. L. *et al.* (2018) 'MFF-dependent mitochondrial fission regulates presynaptic release and axon branching by limiting axonal mitochondria size', *Nature Communications*, 9(1). doi: 10.1038/s41467-018-07416-2.

Linneweber, G. A. *et al.* (2020) 'A neurodevelopmental origin of behavioral individuality in the *Drosophila* visual system', *Science*, 367(6482). doi: 10.1126/science.aaz4547.

Menzies, F. M. *et al.* (2017) 'Autophagy and Neurodegeneration: Pathogenic Mechanisms and Therapeutic Opportunities', *Neuron*. doi: 10.1016/j.neuron.2017.01.022.

Meyer, M. P. and Smith, S. J. (2006) 'Evidence from in vivo imaging that synaptogenesis guides the growth and branching of axonal arbors by two distinct mechanisms', *Journal of Neuroscience*, 26(13). doi: 10.1523/JNEUROSCI.0223-06.2006.

Moyer, C. E., Shelton, M. A. and Sweet, R. A. (2015) 'Dendritic spine alterations in schizophrenia', *Neuroscience Letters*. doi: 10.1016/j.neulet.2014.11.042.

Niell, C. M. (2006) 'Theoretical analysis of a synaptotropic dendrite growth mechanism', *Journal of Theoretical Biology*, 241(1), pp. 39–48. doi: 10.1016/j.jtbi.2005.11.014.

Owald, D. *et al.* (2010) 'A Syd-1 homologue regulates pre- and postsynaptic maturation in *Drosophila*', *Journal of Cell Biology*, 188(4), pp. 565–579. doi: 10.1083/jcb.200908055.

Özel, M. N. *et al.* (2015) 'Filopodial dynamics and growth cone stabilization in *Drosophila* visual circuit development', *eLife*, 4(OCTOBER2015). doi: 10.7554/eLife.10721.

Özel, M. Neset *et al.* (2019) 'Serial Synapse Formation through Filopodial Competition for Synaptic Seeding Factors', *Developmental Cell*, 50(4), pp. 447-461.e8. doi: 10.1016/j.devcel.2019.06.014.

Özel, M Neset *et al.* (2019) 'Serial Synapse Formation through Filopodial Competition for Synaptic Seeding Factors', *Developmental Cell*, 50(4), pp. 447-461.e8. doi: 10.1016/j.devcel.2019.06.014.

Pooryasin, A. *et al.* (2021) 'Unc13A and Unc13B contribute to the decoding of distinct

- sensory information in *Drosophila*’, *Nature Communications*, 12(1). doi: 10.1038/s41467-021-22180-6.
- Poultney, C. S. *et al.* (2013) ‘Identification of small exonic CNV from whole-exome sequence data and application to autism spectrum disorder’, *American Journal of Human Genetics*, 93(4), pp. 607–619. doi: 10.1016/j.ajhg.2013.09.001.
- Powchik, P. *et al.* (1998) ‘Postmortem studies in schizophrenia’, *Schizophrenia Bulletin*, 24(3). doi: 10.1093/oxfordjournals.schbul.a033330.
- Rajgor, D., Welle, T. M. and Smith, K. R. (2021) ‘The Coordination of Local Translation, Membranous Organelle Trafficking, and Synaptic Plasticity in Neurons’, *Frontiers in Cell and Developmental Biology*. Frontiers Media S.A. doi: 10.3389/fcell.2021.711446.
- Rico, B. *et al.* (2004) ‘Control of axonal branching and synapse formation by focal adhesion kinase’, *Nature Neuroscience*, 7(10). doi: 10.1038/nn1317.
- Ruthazer, E. S., Li, J. and Cline, H. T. (2006) ‘Stabilization of axon branch dynamics by synaptic maturation’, *Journal of Neuroscience*, 26(13). doi: 10.1523/JNEUROSCI.0069-06.2006.
- Schmid, A. *et al.* (2008) ‘Activity-dependent site-specific changes of glutamate receptor composition in vivo’, *Nature Neuroscience*, 11(6), pp. 659–666. doi: 10.1038/nn.2122.
- Sênos Demarco, R. and Jones, D. L. (2020) ‘EGFR signaling promotes basal autophagy for lipid homeostasis and somatic stem cell maintenance in the *Drosophila* testis’, *Autophagy*, 16(6), pp. 1145–1147. doi: 10.1080/15548627.2020.1739450.
- Shao, Z. *et al.* (2019) ‘Dysregulated protocadherin-pathway activity as an intrinsic defect in induced pluripotent stem cell-derived cortical interneurons from subjects with schizophrenia’, *Nature Neuroscience*, 22(2), pp. 229–242. doi: 10.1038/s41593-018-0313-Z.
- Shen, W. and Ganetzky, B. (2009) ‘Autophagy promotes synapse development in *Drosophila*’, *Journal of Cell Biology*, 187(1). doi: 10.1083/jcb.200907109.
- Simmons, A. B. *et al.* (2017) ‘DSCAM-mediated control of dendritic and axonal arbor outgrowth enforces tiling and inhibits synaptic plasticity’, *Proceedings of the National Academy of Sciences of the United States of America*, 114(47). doi: 10.1073/pnas.1713548114.
- Spinner, M. A., Walla, D. A. and Herman, T. G. (2018) ‘*Drosophila* syd-1 has rhogap activity that is required for presynaptic clustering of bruchpilot/elks but not neurexin-1’, *Genetics*, 208(2), pp. 705–716. doi: 10.1534/genetics.117.300538.
- Srahna, M. *et al.* (2006) ‘A signaling network for patterning of neuronal connectivity in the *Drosophila* brain’, *PLoS Biology*, 4(11). doi: 10.1371/journal.pbio.0040348.
- Stavoe, A. K. H. and Holzbaur, E. L. F. (2019) ‘Autophagy in neurons’, *Annual Review of Cell and Developmental Biology*. doi: 10.1146/annurev-cellbio-100818-125242.
- Tagliatti, E. *et al.* (2016) ‘Arf6 regulates the cycling and the readily releasable pool of synaptic vesicles at hippocampal synapse’, *eLife*, 5. doi: 10.7554/eLife.10116.
- Talay, M. *et al.* (2017) ‘Transsynaptic Mapping of Second-Order Taste Neurons in Flies by trans-Tango’, *Neuron*, 96(4), pp. 783–795.e4. doi: 10.1016/j.neuron.2017.10.011.
- Tang, G. *et al.* (2014) ‘Loss of mTOR-Dependent Macroautophagy Causes Autistic-like Synaptic Pruning Deficits’, *Neuron*, 83(5), pp. 1131–1143. doi: 10.1016/j.neuron.2014.07.040.
- Ting, C. Y. *et al.* (2011) ‘Focusing transgene expression in *drosophila* by Coupling Gal4

with a Novel Split-Lex A Expression System’, *Genetics*, pp. 229–233. doi: 10.1534/genetics.110.126193.

Urwyler, O. *et al.* (2019) ‘Branch-restricted localization of phosphatase Prl-1 specifies axonal synaptogenesis domains’, *Science*, 364(6439). doi: 10.1126/science.aau9952.

Vaughn, J. E., Barber, R. P. and Sims, T. J. (1988) ‘Dendritic development and preferential growth into synaptogenic fields: A quantitative study of Golgi-impregnated spinal motor neurons’, *Synapse*, 2(1). doi: 10.1002/syn.890020110.

Vijayan, V. and Verstreken, P. (2017) ‘Autophagy in the presynaptic compartment in health and disease’, *Journal of Cell Biology*. doi: 10.1083/jcb.201611113.

Wagh, D. A. *et al.* (2006) ‘Bruchpilot, a protein with homology to ELKS/CAST, is required for structural integrity and function of synaptic active zones in *Drosophila*’, *Neuron*, 49(6), pp. 833–844. doi: 10.1016/j.neuron.2006.02.008.

Wang, M. M. *et al.* (2019) ‘The relationship between autophagy and brain plasticity in neurological diseases’, *Frontiers in Cellular Neuroscience*, 13. doi: 10.3389/fncel.2019.00228.

Winkle, C. C. *et al.* (2016) ‘Beyond the cytoskeleton: The emerging role of organelles and membrane remodeling in the regulation of axon collateral branches’, *Developmental Neurobiology*. doi: 10.1002/dneu.22398.

Wu, M. and Zhang, P. (2020) ‘EGFR-mediated autophagy in tumourigenesis and therapeutic resistance’, *Cancer Letters*. Elsevier Ireland Ltd, pp. 207–216. doi: 10.1016/j.canlet.2019.10.030.

Xiong, W. *et al.* (2020) ‘Autophagy is Required for Remodeling in Postnatal Developing Ribbon Synapses of Cochlear Inner Hair Cells’, *Neuroscience*, 431, pp. 1–16. doi: 10.1016/J.NEUROSCIENCE.2020.01.032.

Xu, Y. and Quinn, C. C. (2016) ‘Transition between synaptic branch formation and synaptogenesis is regulated by the lin-4 microRNA’, *Developmental Biology*, 420(1), pp. 60–66. doi: 10.1016/j.ydbio.2016.10.010.

Zschätzsch, M. *et al.* (2014) ‘Regulation of branching dynamics by axon-intrinsic asymmetries in Tyrosine Kinase Receptor signaling’, *eLife*, 3. doi: 10.7554/elife.01699.

6. Manuscript 2

Brain connectivity inversely scales with developmental temperature in *Drosophila*

Ferdi Ridvan Kiral, **Suchetana B. Dutta**, Gerit Arne Linneweber, Selina Hilgert, Carolina Poppa, Carsten Duch, Max von Kleist, Bassem A. Hassan and P. Robin Hiesinger

Cell Reports, Volume 37, Issue 12, 110145 December 2021

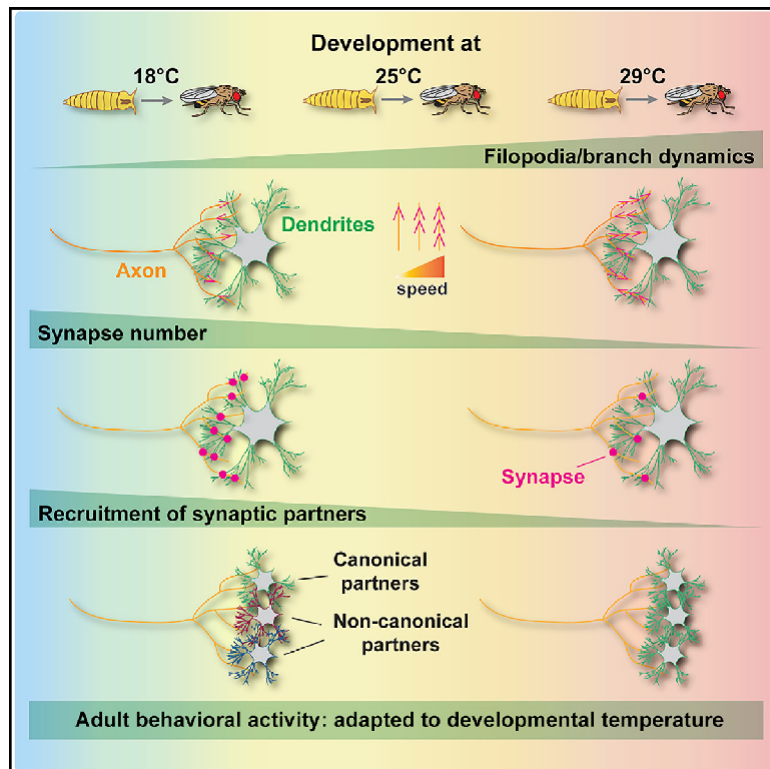
Contribution

I designed, performed and analyzed all experiments in this manuscript related to Dorsal Cluster Neurons (DCNs) under the supervision of Prof. Dr. P. Robin Hiesinger and Prof. Dr. Bassem Hassan. I contributed in writing the manuscript along with Ferdi Ridvan Kiral and Prof. Dr. P. Robin Hiesinger. The original article including the supplemental information is included on the following pages and available online at:

[DOI: 10.1016/j.celrep.2021.110145](https://doi.org/10.1016/j.celrep.2021.110145)

Brain connectivity inversely scales with developmental temperature in *Drosophila*

Graphical abstract



Authors

Ferdi Ridvan Kiral, Suchetana B. Dutta, Gerit Arne Linneweber, ..., Max von Kleist, Bassem A. Hassan, P. Robin Hiesinger

Correspondence

robin.hiesinger@fu-berlin.de

In brief

Different developmental temperatures lead to differently wired brains and behavioral adaptation to the temperature at which a fly developed. Kiral et al. propose that evolution has selected for a *Drosophila* genome that can develop functional, but non-identical, brains through scalable synapse formation based on relative availability of synaptic partners.

Highlights

- Developmental temperature affects synapse numbers and partner availability in flies
- Development at 18°C results in synaptic partnerships absent at 25°C
- The same non-canonical synapses form at 18°C and in the absence of a main partner at 25°C
- Adult behavioral activity is adapted for the temperature at which the fly developed



Kiral et al., 2021, Cell Reports 37, 110145
 December 21, 2021 © 2021 The Author(s).
<https://doi.org/10.1016/j.celrep.2021.110145>



Article

Brain connectivity inversely scales with developmental temperature in *Drosophila*Ferdi Ridvan Kiral,^{1,5} Suchetana B. Dutta,¹ Gerit Arne Linneweber,¹ Selina Hilgert,³ Caroline Poppa,¹ Carsten Duch,³ Max von Kleist,² Bassem A. Hassan,^{1,4} and P. Robin Hiesinger^{1,6,*}¹Division of Neurobiology, Institute for Biology, Freie Universität Berlin, 14195 Berlin, Germany²MFI Bioinformatics, Robert Koch-Institute, 13353 Berlin, Germany³Institute of Developmental Biology and Neurobiology (iDN), Hanns-Dieter-Hörsch-Weg 15, 55128 Mainz, Germany⁴Institut du Cerveau – Paris Brain Institute – ICM, Sorbonne Université, Inserm, CNRS, Hôpital Pitié-Salpêtrière, Paris, France ⁵Present address: Department of Genetics, Yale Stem Cell Center, Yale School of Medicine, New Haven, CT 06520, USA ⁶Lead contact*Correspondence: robin.hiesinger@fu-berlin.de<https://doi.org/10.1016/j.celrep.2021.110145>

SUMMARY

Variability of synapse numbers and partners despite identical genes reveals the limits of genetic determinism. Here, we use developmental temperature as a non-genetic perturbation to study variability of brain wiring and behavior in *Drosophila*. Unexpectedly, slower development at lower temperatures increases axo-dendritic branching, synapse numbers, and non-canonical synaptic partnerships of various neurons, while maintaining robust ratios of canonical synapses. Using R7 photoreceptors as a model, we show that changing the relative availability of synaptic partners using a DIP γ mutant that ablates R7's preferred partner leads to temperature-dependent recruitment of non-canonical partners to reach normal synapse numbers. Hence, R7 synaptic specificity is not absolute but based on the relative availability of postsynaptic partners and presynaptic control of synapse numbers. Behaviorally, movement precision is temperature robust, while movement activity is optimized for the developmentally encountered temperature. These findings suggest genetically encoded relative and scalable synapse formation to develop functional, but not identical, brains and behaviors.

INTRODUCTION

In genetically identical organisms, brain wiring is not only precise but also flexible, robust to perturbation, and variable within limits (Goodman, 1978; Hiesinger and Hassan, 2018; Linneweber et al., 2020). Non-genetic perturbation can therefore reveal the limits of genetic determinism when combined with a quantitative description of precision versus variability. A non-genetic perturbation that affects all developmental processes is temperature (Gilbert, 2012; Gillooly et al., 2002). However, the extent to which developmental temperature changes synapse-specific connectivity of neural circuits is largely unknown.

Animals have adopted one of two evolutionary strategies to ensure functional outcomes: either to precisely control the developmental temperature (e.g., mammals, bee hives) or to evolve a developmental process that is robust to a certain temperature range (e.g., fish, flies). *Drosophila melanogaster* develops functional brains at temperatures between ~15°C and ~29°C, albeit with a more than 2-fold difference of developmental tempo (Kohrs et al., 2021). Temperature strictly determines molecular kinetics apparent as Brownian motion. However, the extent to which subcellular dynamics, synapse formation, and precise neural circuit formation change as a consequence of these molecular kinetic changes is, to our knowledge, not known for any neuron inside a developing brain.

Increasing temperature increases the pace of development in ectotherms such as amphibians and arthropods (Hertwig, 1898; Kuntz and Eisen, 2014; Zuo et al., 2012). Many neuron-based processes are unaffected by different temperatures (within a certain range) at the level of development or function, for example, the precision of circadian clocks (Kidd et al., 2015) and other rhythmic circuits (Alonso and Marder, 2020; Kushinsky et al., 2019). On the other hand, developmental temperature can change outcomes, for example, sex determination in reptiles (Ferguson and Joanen, 1982; Gutzke and Crews, 1988). Already before 1920, studies in *Drosophila* revealed temperature dependencies of the development of fly legs (Hoge, 1915), wings (Roberts, 1918), and eye facet numbers (Seyster, 1919). More than 100 years later, the *Drosophila* connectome is being finalized on the basis of specimens that developed at 25°C (Bates et al., 2020; Li et al., 2020; Scheffer et al., 2020; Takemura et al., 2015). Information about how the connectome might differ after development at a different temperature is currently not available.

In this study, we quantitatively investigated the influence of developmental temperature on brain development from subcellular neuronal filopodial dynamics to synapse numbers, synaptic partnerships, neuronal branch complexity, and behavior. We show that all developmental parameters quantitatively depend on developmental temperature. Specifically, lower temperature leads to an increase in synapse numbers and partnerships based



on increased availability of axo-dendritic branches and filopodia. For R7 photoreceptor neurons, we show that this increased availability leads to synapses with the same non-canonical synaptic partners as ablation of R7's preferred postsynaptic partner. Synapse formation based on relative synaptic availability leads to stable ratios of majority synapses, while total synapse numbers scale inversely with developmental temperature. Multiparametric behavior measurements in a visual choice assay revealed that adult movement activity is highly dependent on, and optimized for, the temperature at which the flies developed. We propose that evolution has selected for a *Drosophila* genome that can develop functional, but non-identical, brains through scalable synapse formation based on relative availability of synaptic partners during development.

RESULTS

Drosophila pupal development, the time during which the adult brain is wired, is almost precisely twice as fast at 25°C compared with 18°C (2.04 times faster, 98 versus 201 h) (Kohrs et al., 2021). In theory, every molecular and cellular developmental process could be sped up by a factor of 2 at 25°C, which would result in identical outcomes after development at both temperatures (Figure 1A). Alternatively, development at 18°C and 25°C could in fact lead to different outcomes. To quantitatively test how developmental processes and outcomes scale with developmental temperature, we devised a set of assays ranging from subcellular dynamics to behavior (Figure 1A).

Subcellular dynamics and synapse formation of R7 photoreceptor neurons inversely scale with developmental temperature

R7 photoreceptors in the *Drosophila* visual system are a well-studied model for axon targeting and synapse formation in a columnar and layered brain region *in vivo* (Figure S1A) (Douthit et al., 2021; Hadjiconomou et al., 2011; Kolodkin and Hiesinger, 2017; Trush et al., 2019). To measure the temperature dependency of subcellular dynamics, we first performed live imaging of developing R7 axon terminals during synapse formation, for which we have previously described the underlying quantitative dynamics (Özel et al., 2015, 2019). First, we measured the temperature dependency of filopodial dynamics that are known to mediate synapse formation and partner choice (Figure 1B) (Kiral et al., 2020; Kolodkin and Hiesinger, 2017; Özel et al., 2019). At 18°C, filopodia were 1.39 times slower and exhibited 1.52 times longer lifetimes compared with 25°C (Figures 1C and 1D; Video S1; Table S1). These measurements reveal a temperature dependency compared with a theoretical complete robustness to temperature (factor of 1); however, these values are less than the increased speed of pupal development at 18°C or 25°C (factor of 2). Development at 29°C (at the upper end of tolerable fly developmental temperatures) further exacerbated this effect (Figures 1C and 1D; Video S1). The relative frequency of synaptogenic filopodia with longer lifetimes (marked by bulbous tips and increased stability) was increased in a similar range at lower temperatures (Figure 1E). Hence, subcellular dynamics that underlie the development of synaptic connectivity differ signifi-

cantly at different developmental temperatures, but not as much as overall pupal developmental tempo.

The kinetics of synaptogenic (bulbous) filopodia throughout development allow to quantitatively predict adult synapse numbers, as previously shown in a computational model of this process (Kiral et al., 2020; Özel et al., 2019). On the basis of 60 min live imaging data, we calculated that at 18°C, synaptogenic filopodia had a probability of 69% to live for at least 60 min, which reduced to 45% at 25°C and 23% at 29°C; synaptogenic filopodia lifetimes were 1.52 times higher at 18°C compared with 25°C (Figure 1F; Table S1). On the basis of these lifetime measurements, a Markov state model simulation predicts the progression of synapse formation throughout pupal development; the model accurately recapitulates progression of synaptogenic filopodia occurrences (Figure 1G) and predicts significantly different synapse numbers after development at the three different temperatures (Figure 1H; see [Mathematical modeling in STAR Methods](#)). To test these predictions, we measured synapse numbers immediately after pupal development at 18°C, 25°C, and 29°C using three independent methods.

First, we used the presynaptic release site marker BrpD3 probe (Fouquet et al., 2009), which revealed significantly increased numbers following development at lower temperature (Figures 1I–1L). Adult synapse numbers after development at the three different temperatures were in line with the model predictions (Figure 1L; Table S1).

Second, to count synaptic connections on the basis of synaptically connected postsynaptic partners of R7 neurons, we used a specific driver line that labels a subset of R7 neurons named yellow R7 (yR7) (reviewed in Rister et al., 2013) and the genetically encoded transsynaptic tracer technique *trans*-Tango (Talay et al., 2017). Adult connectivity on the basis of *trans*-Tango revealed a 1.26-fold increase in postsynaptically connected partners after development at 18°C compared with 25°C (Figures 2A–2D; Table S1). Remarkably, the *trans*-Tango labeling reproducibly identified several cell types after development at 18°C that are very rarely, or not at all, postsynaptically connected to yR7 photoreceptors according to available connectome data (Takemura et al., 2015). In particular, we found R7 synaptic connections to interneurons of the C2/C3 cell type (zero synapses in the connectome), Tm9 cells (zero synapses in the connectome), and Mi cell types including Mi1 and Mi4 (zero to two synapses in the connectome) (Figure 2A; Figures S1A and S1B). Notably, the electron microscopy-based connectome data are based on a specimen that developed at 25°C. Correspondingly, and consistent with the connectome data, these synaptic connections were not detected in *trans*-Tango experiments after development at 25°C or 29°C (Figures 2B–2D). These findings suggest increased synapse numbers after developmental at lower temperatures that can include synaptic partners excluded at higher developmental temperatures.

To control for the reported temperature dependency of the *trans*-Tango method (Talay et al., 2017), the newly hatched flies of all experimental groups were kept at 25°C for 1 week and treated identically for the *trans*-Tango labeling protocol. In addition, we tested the temperature dependency of the method during the first week of adulthood during which most

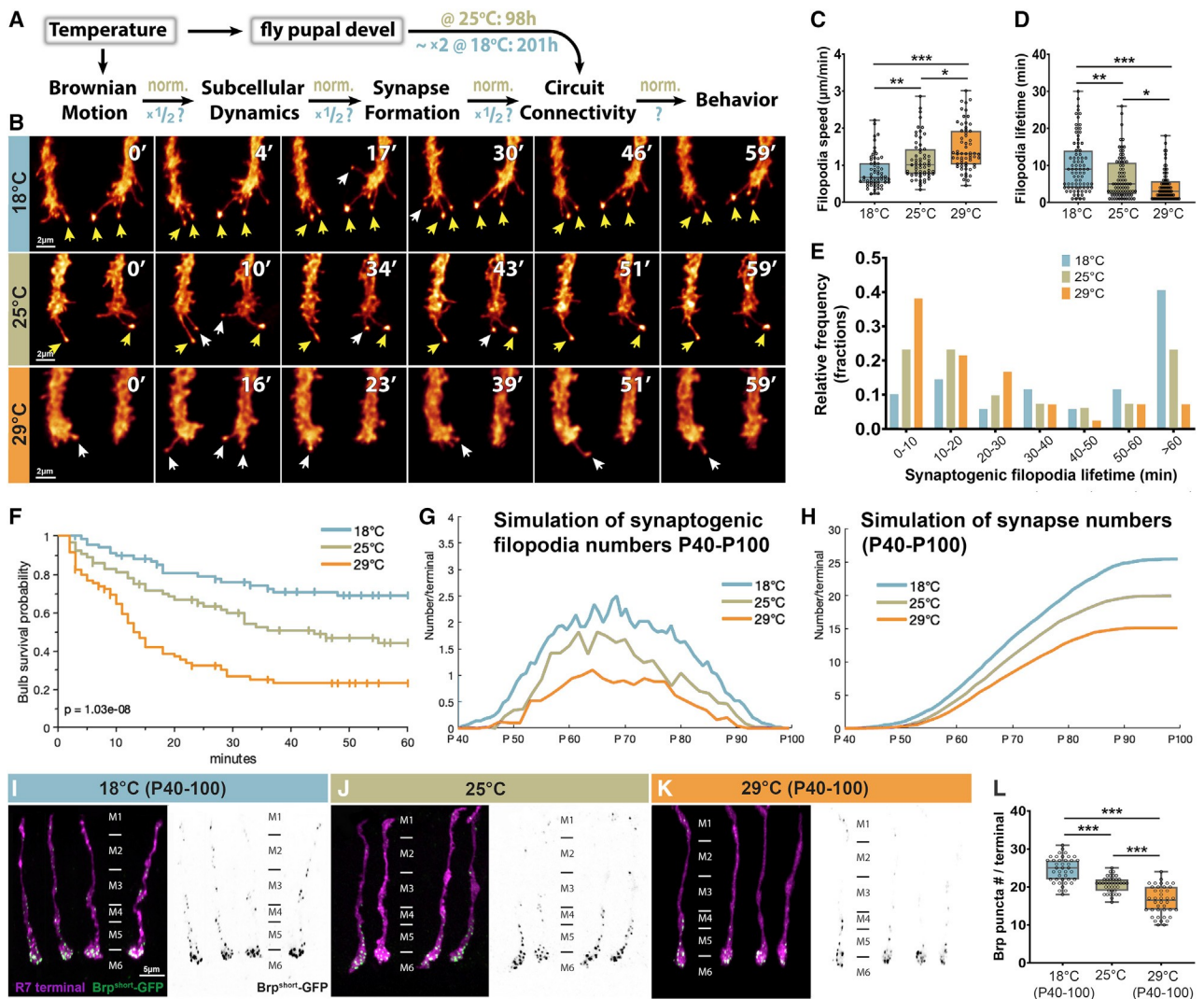


Figure 1. Temperature dependency of synapse formation in the R7 photoreceptor neuron

(A) Schematic of temperature effects during pupal developmental.

(B) Live imaging of filopodial dynamics during the time period of synapse formation (1 h with 1 min time lapse; yellow arrows, long-lived synaptogenic filopodia; white arrows, short-lived synaptogenic filopodia).

(C) Filopodial extension/retraction speeds are highly temperature dependent. n = 80 terminals (eight flies) per condition.

(D) Filopodial lifetimes are temperature dependent. n = 80 terminals (eight flies) per condition.

(E) The relative frequency of long-lived synaptogenic filopodia is temperature dependent. n = 23 terminals (eight flies) per condition.

(F–H) Computational modeling predicts how the measured filopodia dynamics affect synapse formation. (F) Calculation of synaptogenic filopodia survival probabilities on the basis of measured lifetimes. (G) Computational modeling of synapse development between P40 and P100 on the basis of synaptogenic filopodia dynamics. (H) Computational modeling of synapse number development between P40 and P100 on the basis of synaptogenic filopodia dynamics at different developmental temperatures.

(I–L) Synapse numbers on the basis of counts of the presynaptic active zone marker GFP-BrpD3 (Brp^{short}) are dependent on the developmental temperature between P40 and P100. n = 40 terminals (six flies) per condition.

Data were analyzed using the Kruskal-Wallis test and Dunn's post hoc test; *p < 0.0332, **p < 0.0021, and ***p < 0.0002.

the *trans*-Tango signal develops. In contrast to developmental temperature, 7 days at 18°C, 25°C, or 29°C during adulthood did not lead to differences in the number of labeled postsynaptic cells (Figure S2). Hence, both *trans*-Tango labeling and brpD3 labeling indicate a similar dependency of synapse numbers on developmental temperature. These synaptic connections remain stable for several days in the adult.

As a third method to validate changes of synapse numbers found in both BrpD3 active zone counts and *trans*-Tango experiments, we probed specific synaptic connections using the activity-dependent GRASP method (Macpherson et al., 2015). We first test synapse numbers between yR7 and its main postsynaptic partner neuron, the amacrine-like cell type Dm8 (Karuppururai et al., 2014; Menon et al., 2019). Consistent with the connectome

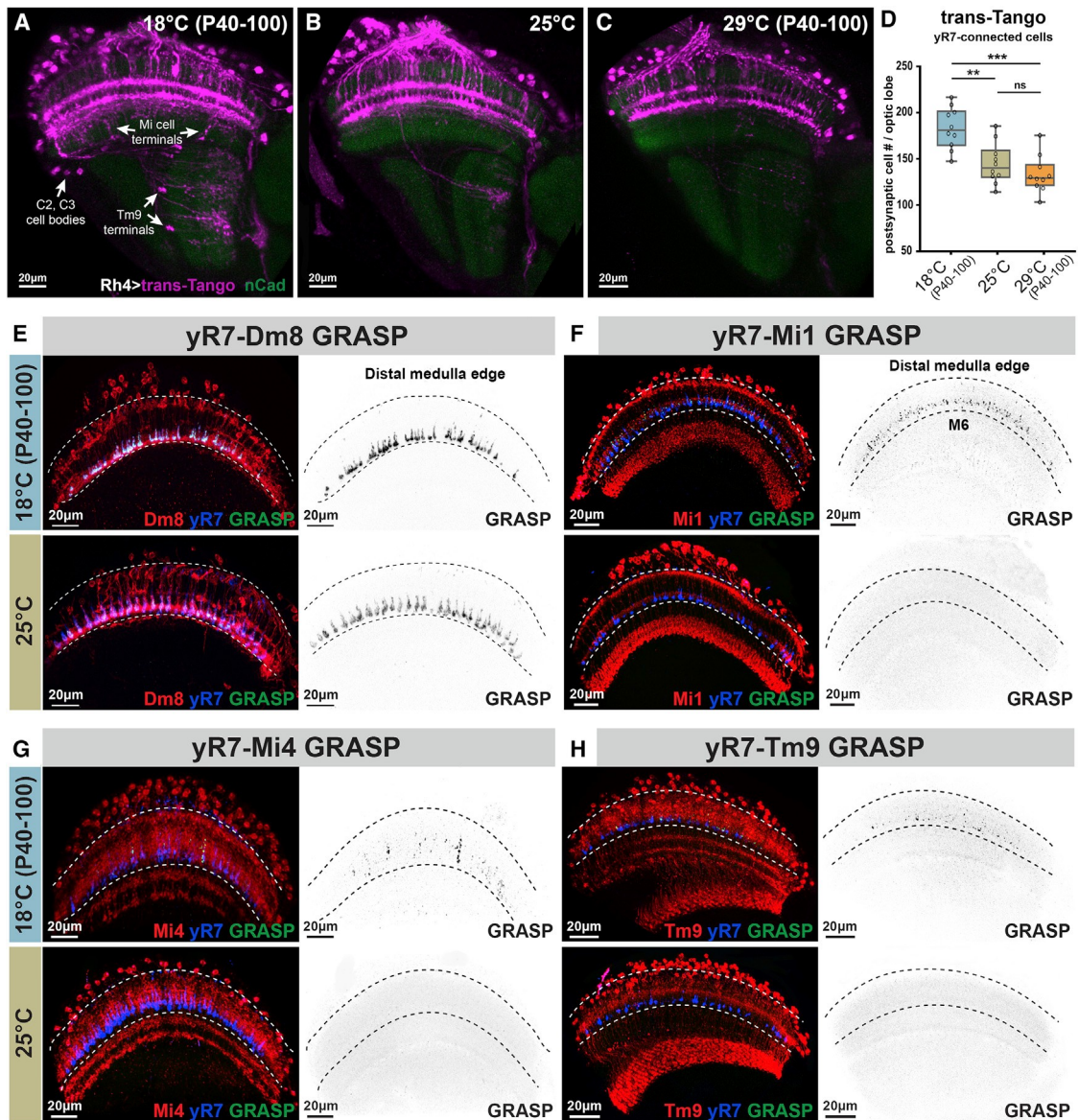


Figure 2. Synaptic connectivity scales with developmental temperature and includes additional, non-canonical synapses of yR7 photoreceptors at lower temperature

(A–C) Representative images of neurons (in magenta) that are postsynaptically connected to R7 neurons on the basis of the genetically encoded transsynaptic tracer method *trans-Tango* (Talay et al., 2017). See Figure S1A for identified cell types.

(D) Quantification of cell body counts of *trans-Tango*-labeled postsynaptic cells per optic lobe. $n = 10$ optic lobes (from ten flies) per condition.

(E–H) Validation of active synapses using the activity-dependent GRASP method (Macpherson et al., 2015) for the main postsynaptic partner Dm8 (E) and three identified postsynaptically connected neurons seen in (A) after development at 18°C that are not known to be synaptically connected on the basis of published connectome information. Blue, yR7; red, the potential postsynaptic partner; green, activity-dependent GRASP signal (reconstituted GFP). Black/white panels, single channel of the green GRASP signal. Data were analyzed using the Kruskal-Wallis test and Dunn’s post hoc test; * $p < 0.0332$, ** $p < 0.0021$, and *** $p < 0.0002$; ns, not significant.

data, activity-dependent GRASP produced a strong signal precisely and selectively in the region where yR7 and Dm8 are known to form synapses (Figures 2E and S3). The synaptic labeling was 1.24 times stronger after development at 18°C compared with development at 25°C (Figure S3C), in line with the increases in synapse numbers found using the presynaptic active zone marker (Figure 1L) and *trans-Tango* (Figure 2D). Finally, computational

modeling based on measured filopodial dynamics yields the same numbers. We conclude that R7 synapse numbers inversely scale with developmental temperature on the basis of four independent measurement methods.

Next, we validate the synaptic partnerships seen in transsynaptic labeling after development at 18°C (but not at higher developmental temperatures) using activity-dependent GRASP.

Specifically, we tested interneurons Mi1, Mi4, and Tm9, for which the connectome analyses of a specimen that developed at 25°C have so far identified very few or no synapses. These are, specifically, two R7-Mi1 synapses in 1 of 18 reconstructed Mi1s, one R7-Mi4 synapse in 1 out of 16 reconstructed Mi4s, and zero R7-Tm9 synapses in 11 reconstructed Tm9s (Takemura et al., 2015). We therefore refer to these synapses as “non-canonical” synapses. Consistent with the connectome data, we found no GRASP signal between yR7 and Mi1, Mi4, or Tm9 after brain development at 25°C (Figures 2F–2H). In contrast, brain development at 18°C leads to robust labeling of these non-canonical synapses in exactly the layers in which their axonal and dendritic processes are present (Figures 2F–2H). We conclude that development at 18°C leads to a significant increase of R7 synapses that includes both the main synaptic partner Dm8 as well as synaptic partners excluded during faster brain development at higher temperature.

We have previously shown that loss of autophagy in R7 photoreceptors leads to increased stability of synaptogenic filopodia and increased synapse formation with Dm8 as well as non-canonical postsynaptic partner neurons (Kiral et al., 2020). The observation that lower temperature alone is sufficient to increase synapse formation with both canonical and non-canonical partner neurons suggests a model whereby all possible partner neurons increase their availability similarly (i.e., synaptic availability scales inversely with developmental temperature). For non-canonical partner neurons, this model predicts no or almost no synapses after development at higher temperature, while canonical synapses decrease equally with increasing temperature, thereby maintaining relative synaptic ratios (Figure 3O). Hence, synapse formation based on relative availability can in theory confer robustness to developmental temperature without keeping synapse numbers constant.

Loss of yR7’s main postsynaptic partner neuron increases relative availability of the same non-canonical partners as development at lower temperature in wild-type

To test relative partner availability and its role in temperature-dependent scaling of synapse numbers, we devised an experi-

ment to change the availabilities of canonical and non-canonical postsynaptic partner neurons of yR7 photoreceptors. The yR7 subtype constitutes 65% of the total R7 population and specifically expresses the cell surface molecule Dpr11, while the second R7 subtype is Dpr11 negative. Correspondingly, the matching postsynaptic Dm8 partner neuron expresses the interacting partner molecule DIPg, while the non-matching Dm8 neurons are DIPg negative. Loss of this molecular interaction leads to cell death of the majority of DIPg(+)Dm8 neurons (Carrillo et al., 2015). Surprisingly, the synapse numbers in presynaptic yR7 terminals remain unaltered in a *dpr11* mutant despite the loss of DIPg(+)Dm8 neurons (Xu et al., 2018). If yR7s maintain their synapse numbers in the absence of their major synaptic partner, what other synaptic partner neurons do yR7 terminals recruit, and does their recruitment scale with different developmental temperatures similar to wild-type?

To answer these questions, we first analyzed synapses between yR7 and possible partner neurons in a DIPg mutant. We first validated the previously reported widespread loss of (about two-thirds of) Dm8 cells in this mutant (Figures S4A–S4C). Loss of DIPg(+)Dm8 cells is specific to columns containing the yR7 subtype and easily recognized by the loss of a Dm8 distal protrusion, also called “sprigs,” in such columns (Courgeon and Desplan, 2019; Menon et al., 2019); the sprigs mark an extended region of synaptic contacts between R7 and Dm8 cells (Figures S4D and S4E). Correspondingly, we find less activity-dependent GRASP signal between yR7 neurons and Dm8 cells in the region of the missing sprigs because of missing DIPg(+) Dm8 cells (Figures 3A–3C). Note that we used a Dm8 cell driver that expresses in both Dm8 subtypes, and in the absence of two-thirds of all DIPg(+)Dm8 cells, active synapses with DIPg(–)Dm8 cells and remaining DIPg(+)Dm8 cells are detectable. Indeed, the most proximal region of yR7 terminals exhibits levels of activity-dependent GRASP between yR7 and Dm8 that are indistinguishable from control even in the absence of the matched DIPg(+) Dm8 in the home column (Figures 3B and 3C). Dm8 neurons are amacrine-like interneurons that extend axo-dendritic branches across more than ten columns; consequently, a yR7

Figure 3. Loss of the postsynaptic partner neuron DIPg(+)Dm8 reveals synapse formation of yR7 neurons on the basis of relative availability

(A and B) Activity-dependent GRASP between yR7 and Dm8 neurons in a DIPg mutant lacking DIPg(+)Dm8 neurons and in a heterozygous control. (A¹ and B¹) Single-channel GRASP signal. (C) GRASP signal intensity along the yR7 terminals reveals a loss of signal in the absence of DIPg(+)Dm8 “sprigs” between M4 and M5 but no reduced intensity in the main synaptic layer M6. (D–F) Synapse numbers on the basis of counts of the presynaptic active zone marker GFP-BrpD3 are not significantly altered in the DIPg mutant. n = 40 terminals (8 flies) per condition. (G and H) Representative images of the postsynaptically connected neurons (magenta) to yR7 on the basis of the genetically encoded transsynaptic tracer method *trans*-Tango. Note that the same additional cell types are present in the DIPg mutant (H) as in wild-type after development at 18°C (Figure 2A). (I) The number of non-canonical postsynaptic partners in the DIPg mutant is dependent on the developmental temperature; the mutant relative connectivity scales with temperature similar to wild-type. n = 10 optic lobes (from 10 flies) per condition. (J–L) Validation of active synapses using the activity-dependent GRASP method (Macpherson et al., 2015) for three non-canonical postsynaptically connected neurons identified in (H) in a DIPg mutant lacking DIPg(+)Dm8 neurons and in a heterozygous control that developed at 25°C. Blue, yR7; red, the potential postsynaptic partner; green, activity-dependent GRASP signal (reconstituted GFP). Black/white panels, single channel of the green GRASP signal. (M) Mean signal intensities of activity-dependent GRASP between yR7 and canonical partners (Dm8, Dm9, and Dm11) in a DIPg mutant lacking DIPg(+)Dm8 neurons and in a heterozygous control. n = 70–80 terminals (10–12 flies) per condition. (N) Mean signal intensities of activity-dependent GRASP between yR7 and non-canonical partners (Mi1, Mi4, Tm9) in a DIPg mutant lacking DIPg(+)Dm8 neurons and in a heterozygous control. n = 70–80 (9–12 flies) terminals per condition. (O) A model based on GRASP and *trans*-Tango measurements that predicts no synapse formation between R7 and non-canonical partners (Mi1, Mi4, and Tm9) at higher developmental temperatures, while maintaining relative synaptic ratios of canonical partner neurons (Dm8, Dm9, and Dm11). Data were analyzed using the Kruskal-Wallis test and Dunn’s post hoc test; *p < 0.0332, **p < 0.0021, and ***p < 0.0002; ns, not significant.

axon terminus with a missing matched DIPg(+)Dm8 neuron is not prevented from forming synapses with processes from neighboring Dm8s despite their lack of the DIPg, suggesting that DIPg is not required for synapse formation between yR7 and Dm8 cells.

Because of the reduced number of synapses in the sprig region, the activity-dependent GRASP analysis between yR7 and Dm8s suggests an overall reduction of synapses between these two cell types (Figure 3C). However, our synapse counts based on the presynaptic marker BrpD3 indicate that yR7 synapse numbers in the DIPg mutant were not significantly altered (Figures 3D–3F), in agreement with previous synapse counts in the *dpr11* mutant yR7s (Xu et al., 2018). To identify other postsynaptic partners, we performed *trans*-Tango experiments in the DIPg mutant (at 25°C developmental temperature and using a +/DIPg heterozygote as control; Figures 3G and 3H). Remarkably, *trans*-Tango labeling in the DIPg mutant optic lobe after development at 25°C looked very similar to a wild-type optic lobe after development at 18°C, prominently including postsynaptically connected C2/3 cells, Tm9 cells, and Mi cells (compare Figures 3H and 2A). A cell-by-cell comparison revealed identical postsynaptically connected neurons for 18°C wild-type and 25°C DIPg mutant brains (Figures S1A–S1C).

Our transsynaptic tracing results suggest that loss of DIPg increases the relative availability of non-canonical partner neurons in a manner similar to lower developmental temperature in wild-type (i.e., by increasing the pool of possible postsynaptic partners). Although in wild-type the non-canonical synapses are effectively absent after development at 25°C or above, their overall increase in the DIPg mutant makes it possible to test for their relative frequency at different temperatures. We found that the number of transsynaptically labeled low-probability Mi1/4-yR7, C2/3-yR7, and Tm9-yR7 synaptic connections could be dialed down at 29°C and dialed up at 18°C, while maintaining their relative frequencies (Figure 3I; Figures S4F and S4G). These findings indicate robustness of relative frequency to different developmental temperatures without keeping total synapse numbers constant, similar to our observation for canonical synapses in wild-type (Figure 3O).

To validate the *trans*-Tango results, we performed activity-dependent GRASP experiments for the non-canonical pairings yR7-Mi1, yR7-Mi4, and yR7-Tm9 in control and DIPg mutants after development at 25°C. As in wild-type (Figures 2F–2H) and in the available connectome data, the +/DIPg heterozygote control exhibited no or very rare GRASP signals for these non-canonical synapses. In contrast, the non-canonical synapses were prominent in the DIPg mutant in the correct layer of their known axo-dendritic overlap and looked virtually indistinguishable from the wild-type GRASP signal after development at 18°C (Figures 3J–3L; compare Figures 2F–2H). Similarly, activity-dependent GRASP analyses of cell types that are known to be synaptically connected to yR7 (Dm9 and Dm11 cells) revealed similar increases of synaptic labeling in the DIPg mutant (Figures S5A–S5G; Table S2). These findings indicate that a loss or reduction of the number of DIPg(+) Dm8 cells creates a situation in which yR7 neurons recruit more synaptic partners from a pool of both canonical (Figure 3M) and non-canonical (Figure 3N) partners. The recruitment of these alternative synaptic partners appears to be specific to those that have

dendritic arborizations in the correct medulla layer, as Dm3 and Dm6 cells never form synapses with yR7 in control of the DIPg mutant (Figures S5H–S5K). Despite these shifts in synaptic partnerships, the final number of yR7 synapses is not significantly different from wild-type at the same developmental temperature (Figures 3F and 1L). These findings suggest a presynaptic mechanism for the determination of synapse numbers independent of the types of postsynaptic partners, consistent with the presynaptic serial synapse formation model for R7 (Özel et al., 2019) as well as previous observations for R1–R6 photoreceptors (Hiesinger et al., 2006). We conclude that the absence of Dm8 neurons increases the relative availability of other possible R7 partner neurons, in effect “filling vacant Dm8 slots” up to the number observed in wild-type for a given temperature.

In sum, our analyses of yR7 synapse formation as a function of developmental temperature and partner availability revealed that overall synapse numbers increase with lower temperatures, including low-probability synapses not observed at higher temperatures. By contrast, relative synaptic frequencies are robust to different developmental temperatures unless a type of synapses drop to zero at a higher temperature (Figure 3O).

Morphogenesis and synapse formation of branched interneurons in the brain depend on developmental temperature

To what extent is the temperature dependency of neuronal development and synapse formation a general phenomenon in the fly brain? To approach this question, we analyzed a series of neuron types that face diverse challenges during the establishments of synaptic partner contacts.

First, we analyzed photoreceptors R1–R6, which terminate in a different brain region from R7, the lamina; in contrast to R7, growth cones of R1–R6 need to undergo a lateral sorting process to form a functional visual map required for motion vision according to the principle of neural superposition (Agi et al., 2014; Hadjiconomou et al., 2011; Langen et al., 2015), and their functional output can be estimated on the basis of electroretinogram (ERG) recordings (Pak et al., 1969). Similar to our findings for R7, synapse numbers of adult R1–R6 increased by a factor of 1.15 on the basis of the presynaptic BrpD3 marker after development at 18°C compared with development at 25°C (Figure 4A; Figures S6A–S6D). Synaptic transmission (as measured by the ERG “on” transients) was significantly increased after development at 18°C compared with 25°C, consistent with increased numbers of synaptic connections (Figures 4B and 4C; Figures S6E and S6F). These findings indicate that the increased numbers of synapses after development at 18°C compared with 25°C are functional. In contrast, phototransduction (i.e., the ability of R1–R6 to convert a light stimulus into an electrical signal in the cell body, as measured by the ERG depolarization component) revealed no significant differences after development at different temperatures (Figures S6E and S6G). We conclude that although phototransduction is unaffected by variability of developmental temperatures, synapse numbers and neurotransmission are increased after development at a lower temperature.

Next, we analyzed Dm8 neurons, the main synaptic partner neuron of R7 photoreceptors, whose dynamic and competitively regulated branch development has recently been analyzed in

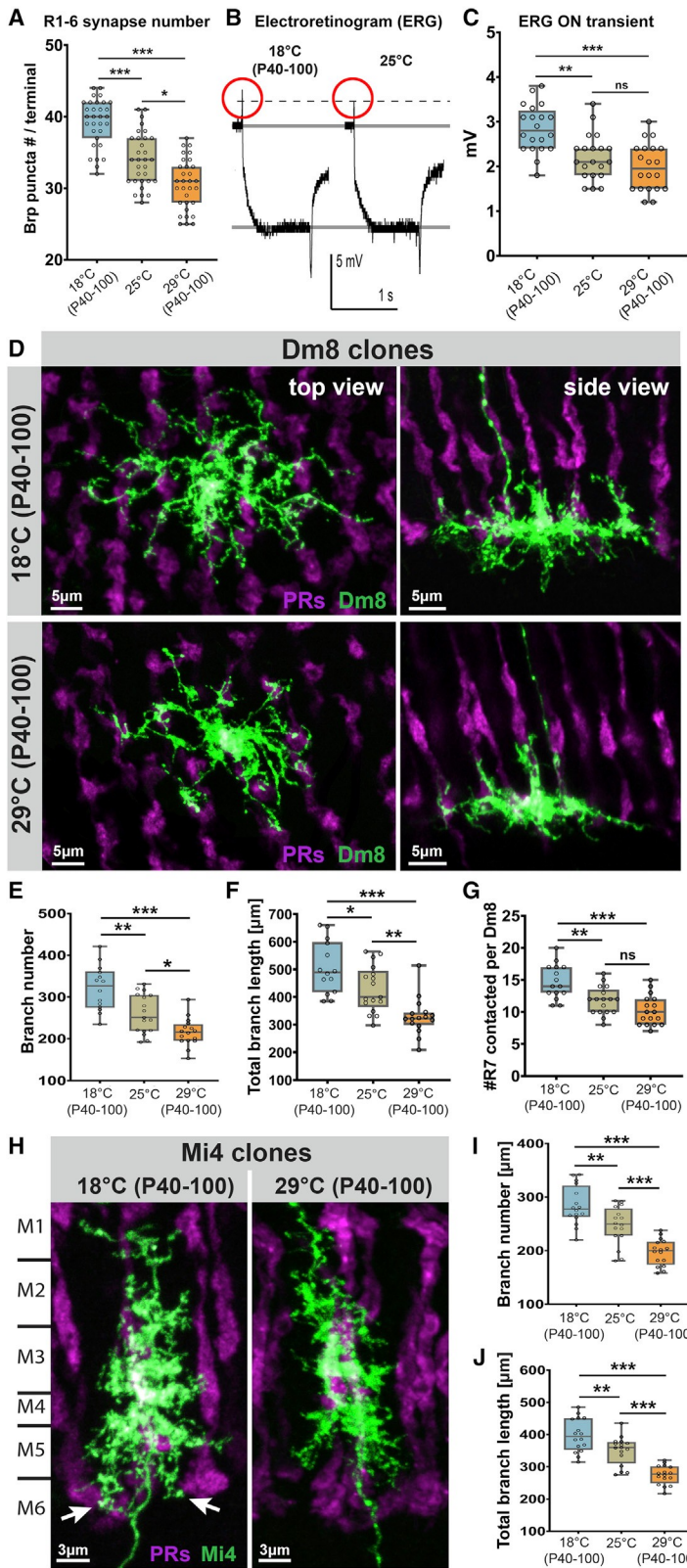


Figure 4. Neurotransmission of R1–R6 photoreceptors and branch morphology of Dm8 and Mi4 interneurons scale with developmental temperature

(A) R1–R6 photoreceptor synapse numbers on the basis of counts of the presynaptic active zone marker GFP-BrpD3 (Brp^{short}) depend on the developmental. $n = 30$ terminals (6 flies) per condition.

(B) Representative electroretinogram (ERG) traces recorded from wild-type (WT) fly eyes developed at different temperatures.

(C) Development at lower temperature increases neurotransmission of R1–R6 photoreceptors on the basis of ERG “on-transient” amplitudes. $n = 20$ flies per condition.

(D) Single-cell clone representative images of Dm8 neurons developed at low (18°C, P40–P100) and high (29°C, P40–P100) temperatures.

(E–G) Dm8 neurons exhibit increased branch numbers (E), total branch length (F), and numbers of R7 contact sites (G) after development at 18°C. $n = 14–17$ cells (6 flies) per condition.

(H) Single-cell clone representative images of Mi4 neurons developed at low (18°C, P40–P100) and high (29°C, P40–P100) temperatures. White arrows point to Mi4 branches invading M6 medulla layer after development at 18°C where R7s are synaptically most active.

(I and J) Mi4 interneurons (which are only connected to yR7 neurons after development at 18°C or in the absence of Dm8s) also exhibit increased branch numbers (I) and total branch lengths (J) after development at 18°C. $n = 16$ terminals (7 flies) per condition.

Data were analyzed using the Kruskal-Wallis test and Dunn’s post hoc test; * $p < 0.0332$, ** $p < 0.0021$, and *** $p < 0.0002$; ns, not significant.

detail (Luo et al., 2020). The overall morphology of Dm8 neurons (Figure 4D), including branch numbers (Figure 4E) and total branch lengths (Figure 4F) differed markedly depending on the developmental temperature. As Dm8 extends its branches across several medulla columns, the temperature dependency of its branch morphology leads to on average of 14 columns contacted by a single Dm8 after development at 18°C, 12 columns after development at 25°C, and 10 columns after development at 29°C (Figure 4G; Figures S6H–S6J). These findings correspond well with the temperature dependency of synapse numbers between yR7 and Dm8 (Figures 2E and S3C; Table S1). The observations further suggest that increased branching of the canonical R7 partner Dm8 increases its availability for synapse formation.

To test whether increased availability through increased branching also occurs for a non-canonical partner of R7 photoreceptors, we analyzed Mi4 neurons after development at different temperatures. Similar to Dm8 neurons, Mi4 neurons exhibited a comparable temperature dependency of both branch numbers and total branch lengths (Figures 4H–4J; Table S1). Taken together, these findings suggest that visual interneuron branching, photoreceptor filopodial dynamics, and synapse formation all scale with similar ratios with developmental temperature (Table S1).

Next, we analyzed the effect of developmental temperature on two other neuron types outside the *Drosophila* visual system. First, we searched the Fly Light split-Gal4 collection for sparsely labeled central nervous system neurons and chose descending neurons as candidates (Namiki et al., 2018). We selected DNp24 neurons (line SS00732) for quantification because of its distinct axonal arborizations and the strength of the Gal4 driver line (Figure S7A). The number of DNp24 branch terminals was significantly reduced after development at higher temperature (Figure S7B), while the overall area covered by branches was not significantly different (Figures S7C–S7F). These findings show that axonal branches can cover similar regions with variable numbers of branches.

Finally, we analyzed the effect of temperature on dendritic development of adult motoneurons. We selected motoneurons MN1–5 that innervate the dorsal longitudinal flight muscle (DLM). MN1–5 have dendrites of similar sizes that intermingle in the same space of the flight neuropil. We have previously characterized the dendritic architecture of MN5 in animals raised at 25°C throughout development (Vönhoff and Duch, 2010), as well as MN5's activity-dependent development on the basis of intra-neuronal competition (Ryglewski et al., 2017). Using the same intracellular filling technique as in the previous studies, we therefore analyzed MN5 dendritic branching structure after development at all three temperatures on the basis of geometric three-dimensional (3D) reconstructions (Evers et al., 2005), one for each temperature (Figures S8Ai–S8Ci). Developmental temperature only had no or very mild effects on the total number or the mean radius of dendritic branches (MDR; Figure S8D) or the mean length of dendritic branches (MDL) and total dendritic length (TDL) (Figure S8D). In contrast, the organization of dendritic branches within the tree was remarkably different: dendritic trees after development at 18°C contained increased branch numbers at higher orders (i.e., branches that formed on other

branches: up to 50 or 60 levels), whereas dendritic trees that developed at higher temperature contained increased branch numbers at lower orders and decreased branch numbers at high orders (Figure S8E). Given that low branch orders form earlier than high order branches, this indicates that increased temperature causes increased early branch formation but decreased late branch formation. We conclude that developmental temperature can have different effects on different neuron types that require type-specific investigation.

Dorsal cluster interneurons scale filopodial dynamics, branching, synapse numbers, and synaptic partnerships with developmental temperature

To analyze temperature-dependent developmental dynamics, branching, and synapse formation in a large interneuron that has been shown to directly affect behavior, we focused on contralaterally projecting interneurons called dorsal cluster neurons (DCNs). DCNs form highly distinctive branched axonal patterns in the contralateral brain hemisphere (Figure 5A); differences in these patterns predictively and quantitatively affect individual fly behavior (Linneweber et al., 2020). Similar to Dm8 and Mi4, we found that DCNs exhibited increased numbers of branches after development at 18°C compared with 25°C and 29°C (Figures 5B–5D). To observe the development of the different branching patterns, we established multiphoton live imaging of branching dynamics in the intact developing brain on the basis of our *ex vivo* imaging culture system (Özel et al., 2015). Time-lapse videos obtained during development at all three temperatures revealed a significant temperature dependency of extension and retraction speeds, similar to R7 axon terminals (Figures 5E–5G; Video S2; compare Figures 1B–1D and Video S1). Correspondingly, synapse numbers based on the BrpD3 presynaptic marker were increased after development at 18°C compared with 25°C and 29°C (Figures 5H–5J).

To validate the temperature-dependent scaling of synapse numbers and connectivity, we performed both *trans*-Tango and GRASP labeling of synaptic connections, similar to our analyses of R7 neurons. Transsynaptic tracing of postsynaptically connected cells with *trans*-Tango revealed a significant difference in the number of labeled postsynaptic cells after development at 18°C compared with 25°C, similar to our findings for R7 neurons (Figures 5K–5M). We identified several of the postsynaptically connected neurons on the basis of morphology, including Lamina widefield (Lawf) interneurons as well as at least two more rarely connected cell types (L cells and Lpi cells) that we observed only after development at 18°C, but not 25°C (Figures S7D and S7E). To validate the temperature dependency of active synapses for these interneurons, we performed activity-dependent GRASP experiments between DCNs and Lawf1 neurons. We observed activity-dependent GRASP labeling of DCN-Lawf1 synapses after development at 18°C and to a significantly lesser degree after development at 25°C and 29°C; in all cases, the GRASP signal was specific to the brain region where DCN-Lawf1 contacts are predicted (Figures 5N–5P). As with R7 photoreceptors, the temperature-dependent scaling of connectivity is supported by independent measurements of life dynamics and synapse numbers on the basis of three independent methods. We conclude that slower development at

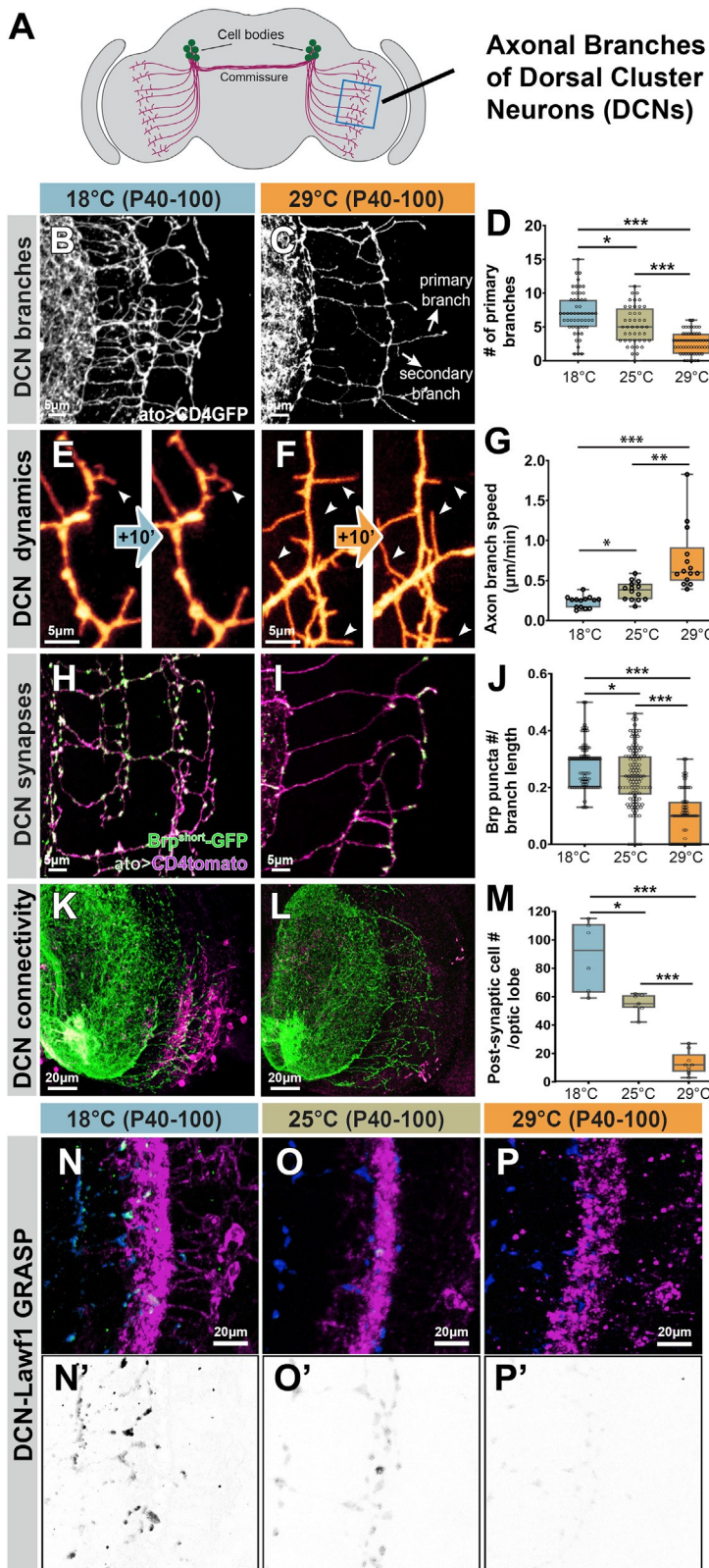


Figure 5. Branching dynamics, branch elaboration, syn-apse formation, and partnerships of dorsal cluster neurons scale with developmental temperature

(A) Schematic of dorsal cluster neurons (DCN) in the fly brain. (B–D) DCNs exhibit increased number of axonal branches after development at 18°C. n = 45–58 branches (five to seven flies) per condition.

(E–G) Axonal branch dynamics of DCNs are highly temperature dependent. n = 14 branches (four flies) per condition.

(H–J) Synapse numbers based on the presynaptic active zone marker GFP-BrpD3 reveals increased synapse formation of DCNs after development at 18°C. n = 90–120 branches (six flies) per condition.

(K–M) DCNs form more postsynaptic connections after development at 18°C on the basis of transsynaptic tracing method *trans-Tango*. n = 6–9 optic lobes (from six to nine individual flies) per condition.

(N–P) Activity-dependent GRASP between DCN and Lawf2. Note increased GRASP signal after development at 18°C.

Data were analyzed using the Kruskal-Wallis test and Dunn's posthoc test; *p < 0.0332, **p < 0.0021, and ***p < 0.0002.

lower temperature leads to decreased dynamics and increased branching and synapse formation with a larger pool of postsynaptic partners in DCNs, similar to our findings for R7 photoreceptors.

Movement activity is adapted to the temperature at which the fly developed, while movement precision is largely unaffected by developmental temperature

The developmental temperature-dependent differences of DCN branch morphologies are quantitatively similar to differences in DCNs that are known to significantly affect behavior in a visual choice assay (Linneweber et al., 2020). This assay, Buridan's paradigm, is a multiparametric single-fly behavioral paradigm that allows to quantitatively measure more than 25 different parameters related to fly movements in response to defined visual stimuli (black bars on two sides of an arena; Figure 6Y) (Colomb et al., 2012; Linneweber et al., 2020). The assay is sufficiently sensitive to measure specific behavioral differences as a consequence of different DCN morphologies (Linneweber et al., 2020). We assessed 25 behavioral parameters that include measures related to overall activity (e.g., walking speed, pause lengths, overall walking distance), measures for movement angles or location that are independent of visual cues (e.g., the amount of turns taken or the time spent at or away from the center of the arena), and measures directly related to movement angles or location relative to the visual cues (Table S3). We tested a *Janelia* wild-type strain used for recent connectome analyses (Takemura et al., 2015) following development between P40 and P100 at different temperatures.

First, we tested flies after development at 18°C, 25°C, or 29°C at a "behavioral temperature" of 25°C. Most parameters related to overall activity were significantly lower after development at 18°C compared with 25°C (Figure S10), including number of walks (1.59 times more; Figure 6G), the total distance traveled (1.51 times more; Figure 6H), and pause durations (1.54 times less; Figure 6I). In contrast, parameters associated with movement angles or location relative to the visual cues were not significantly altered, such as axis deviation (Figure 6J), angle deviation (Figure 6K), and horizon deviation (Figure 6L). Hence, parameters related to the precision of movement angles were largely unaffected by different developmental temperatures, while general activity levels scaled with developmental temperature in a range similar to neuronal branch morphologies and synapse numbers (Tables S1 and S3).

The observed increased adult activity levels after development at 25°C and 29°C might be the result of a brain wired for more behavioral activity at any behavioral temperature, or a brain adapted for that exact behavioral temperature. The latter idea of adaptation would predict that development at 18°C might lead to more activity at 18°C. To distinguish between these possibilities, we performed experiments at the behavioral temperatures 18°C and 29°C. Measures for overall activity at behavioral temperatures 18°C and 29°C changed largely in agreement with the adaptation hypothesis. For example, flies that had developed at 18°C exhibited more overall activity at the behavioral temperature 18°C than flies that had developed at 25°C or 29°C (Figures 6A–6C and 6S–6U). On the other hand, flies that had developed at higher temperatures exhibited selectively increased overall

activity at 25°C and 29°C (Figures 6S–6U). By contrast, similar to behavior at 25°C, most parameters associated with movement precision were not or only mildly affected (Figures 6D–6F, 6P–6R, and 6V–6X; Figures S11 and S12). We conclude that overall activity levels depend on developmental temperature in a manner that increases activity for the temperature at which the flies developed. These observations are consistent with evolutionary selection for functional flies, but not identical brains.

DISCUSSION

The genome contains information to grow network connectivity, not information that describes network connectivity. Selection occurs at the level of behavior, on the basis of developmental processes that are flexible enough to ensure robustness to variable environmental conditions (Hiesinger and Hassan, 2018). Many animals, including *Drosophila*, have evolved robustness of brain development to varying developmental temperatures. However, robustness does not need to ensure identical development or outcomes as long as the resulting connectivity is functional. In this study, we have shown that non-identical functional connectivity and adult behavior result from development at different temperatures. We propose that the underlying developmental processes do not specify synaptic connectivity in absolute terms but on the basis of scalable, relative availabilities of synaptic partners.

Temperature robustness through developmental synaptic scaling

We found temperature dependencies at every level from subcellular dynamics to synapse formation and circuit connectivity. However, the doubling of the developmental tempo at 25°C compared with 18°C is not accompanied by a doubling of the rate of synapse formation—or any other developmental parameter measured in our study. Instead, processes ranging from filopodial dynamics to branching and active zone formation were all only increased between ~1.2- and 1.8-fold (Table S1). Consequently, development in half the time with less than a doubling of synapse formation leads to fewer overall synapses at 25°C compared with 18°C. Synaptic ratios are robust to temperature if synapse numbers and types exhibit the same relative changes.

In brain function, synaptic scaling is well characterized as a means of homeostatic regulation of destabilizing variability (Turrigiano, 2012), with important consequences for learning and mental health (Kavalali and Monteggia, 2020; Turrigiano, 2017). Like its functional counterpart, developmental synaptic scaling may provide a basis for the maintenance of relative input strengths in neural circuits. Other mechanisms that have been shown to contribute to temperature robustness include ion channel degeneracy and regulation (Goaillard and Marder, 2021; O'Leary and Marder, 2016). However, we do not yet know how ion channel expression and regulation is affected by development at different temperatures. We speculate that developmental temperature may have differential effects on specific proteins such as ion channels, cytoskeletal proteins, and molecules of the transmitter release machinery, all of which contribute to circuit properties and ultimately behavior.

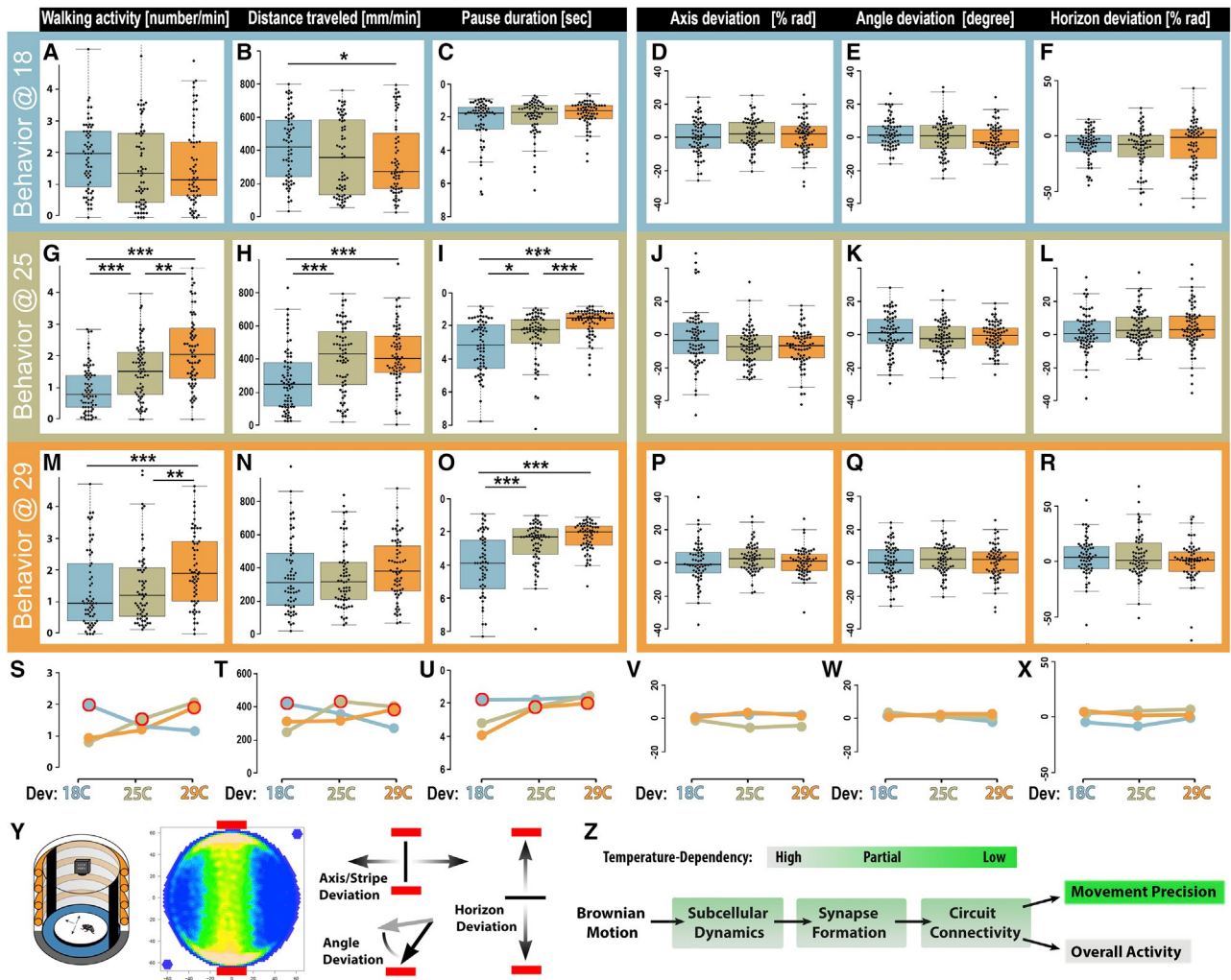


Figure 6. Developmental temperature affects overall movement activity but not movement precision

(A–R) Six of a total of 25 behavioral parameters analyzed for differences between adult behavior after development at 18°C, 25°C, or 29°C (colored boxplots) and the same three behavioral temperatures (colored borders). $n = 70$ flies per condition. Quantitative data in Table S3. Nine plots on the left: the three most significantly temperature-dependent behavioral parameters: walking activity (A, G, and M), distance traveled (B, H, and N), and pause duration (C, I, O). Nine plots on the right: three parameters that are largely unaffected by developmental temperature: axis deviation (D, J, and P), angle deviation (E, K, and Q), and horizon deviation (F, L, and R).

(S–X) Schematic plots based on the data in (A)–(R) showing the mean values for a behavioral temperature (indicated by graph color) in dependence of developmental temperature.

(Y) Buridan's paradigm (from left to right): experimental setup, heatmap of typical fly movement activity, illustrations of the parameters axis deviation, angle deviation, and horizon deviation.

(Z) Summary of temperature dependencies.

See Figures S10–S12 for all behaviors and STAR Methods for details on each parameter. Data were analyzed using the Kruskal-Wallis test and Dunn's post hoc test; * $p < 0.05$, ** $p < 0.01$, and *** $p < 0.001$.

Similar to a lower temperature, reduced metabolism decreases the pace of *Drosophila* development and has recently been shown to increase robustness by decreasing developmental errors (Cassidy et al., 2019). Although the mechanism of error suppression in this study is likely different from the temperature effects observed here, we note that scalable relative connectivity is also likely more robust at lower temperatures because the synaptic ratio of high-probability synapses is established by larger numbers.

A contribution of relative synaptic partner availability to synaptic connectivity

The genome encodes developmental programs that produce remarkably precise synaptic connectivity. Yet individual neurons across animal species, taken out of the context of these developmental programs, readily form “incorrect” synapses, including with themselves (Bekkers and Stevens, 1991; Clements et al., 2008; Harris et al., 2020; Hiesinger et al., 2006; Van der Loos and Glaser, 1972). Even during normal development some

degree of synaptic promiscuity is prevalent, for example, as a basis for subsequent pruning or fine-tuning (Agi et al., 2020; Hassan and Hiesinger, 2015; Lieberman et al., 2019; Shatz, 1996; Wilton et al., 2019). The notion of promiscuous synapse formation on the basis of relative partner availability is not at odds with precise outcomes. Instead, it offers the opportunity to explain precision in the context of developmental plasticity and robustness to perturbation. The limiting case of “total promiscuity” (i.e., the ability of any neuron to form synapses with any other neuron) is highly unlikely given known molecular interactions that specify or bias connections (de Wit and Ghosh, 2016; Dudanova and Klein, 2013; Sanes and Zipursky, 2020; Sädhof, 2018). At the other end of the spectrum, precise molecular key-and-lock mechanisms for all synapses represent the antithesis to promiscuous synapse formation: if the key does not fit the lock, a synapse should not form. This is equally unlikely, given the known ability, and often developmental necessity, to form synapses with variable partners.

Synapse formation requires proximity- and kinetics-based mechanisms involving locally restricted molecular machinery (Agi et al., 2020; Hoerding and Schmucker, 2021). In addition, molecular specificity or selectivity with a “hierarchy of preference” (Sanes and Zipursky, 2020) are principally consistent with developmental synaptic scaling, as more stable filopodia and branches will also increase, and thus scale, molecular recognition. However, such a molecular “hierarchy of preference” would have to include at least all the non-canonical synapses shown in this study for yR7 neurons and DCNs. To what extent molecular interactions play earlier developmental roles prior to synapse formation (Petrovic and Schmucker, 2015) and to what extent synapse formation could be promiscuous on the basis of specification through proximity and kinetics (Agi et al., 2020) remain a matter of debate (Hassan and Hiesinger, 2015; Hiesinger, 2021; Sanes and Zipursky, 2020).

Lower developmental temperature in wild-type flies increased numbers of synapses with both canonical and non-canonical partners, similar to previous observations in autophagy mutants (Kiral et al., 2020). Our findings suggest that temperature alone is sufficient to raise the availability of some synaptic partners above zero. Our distinction of canonical and non-canonical synapses is based solely on the probability to form synapses and their absence in EM connectome analyses on the basis of specimens that developed at 25°C (Scheffer et al., 2020; Takemura et al., 2015). The observation that the number of these non-canonical synapses is significantly increased after development at a lower but still physiological temperature opens the possibility that these synapses are functional and evolutionarily selected (or at least not selected against) parts of the connectome.

Genetically encoded brain wiring based on relative synaptic partner availability allows surprising variability among brains, even if genetically identical. Both stochastically encoded developmental processes (Linneweber et al., 2020) as well as environmental differences (this study) may contribute to such variability of genetically encoded brain wiring. Further support for this idea comes from recent comparative connectomics analyses in *C. elegans* demonstrating that more than 40% of all cell-cell connections are not conserved between isogenic worms (Witvliet et al., 2021).

Dpr11 and DIPg function prior to, but not during, synapse formation

Our findings are consistent with the reported role of the Dpr11/DIPg interaction for partner cell survival during a developmental process prior to synapse formation (Carrillo et al., 2015; Courgeon and Desplan, 2019; Menon et al., 2019). Loss of DIPg leads to loss of the majority of DIPg(+)Dm8 cells and, as we show here, a widening of the pool of possible partners for Dpr11-positive yR7 terminals during the later process of synapse formation. We conclude that in wild-type, the Dpr11/DIPg interaction-mediated survival of DIPg(+)Dm8 cells effectively reduces the pool of postsynaptic partners by placing the main postsynaptic partner in close proximity and thereby increasing its relative availability.

Contrary to previous interpretations, we show that the actual synapse formation process does not use Dpr11/DIPg interaction. Instead, yR7 axon terminals form a remarkably invariant number of synapses at a given temperature independent of the presence or absence of Dpr11 (Xu et al., 2018), DIPg, or the main postsynaptic partner neuron Dm8 (this study). In a DIPg mutant, yR7 axon terminals form synapses with non-matched Dm8s, plus other known synaptic partners based on the 25°C connectome, as well as available partners that are not, or very rarely, present in the 25°C connectome (Takemura et al., 2015). Remarkably, the additionally recruited synaptic partners are identical in a DIPg mutant after development at 25°C and wild-type after development at 18°C. Hence, at least the cell types that are shown here to be recruited as postsynaptic partners during development at 18°C or in the absence of DIPg(+) Dm8 cells are not prevented from synapse formation by molecular mismatch.

As both the number and the specificity of partnerships of yR7 synapses in the DIPg mutant scale with developmental temperatures similar to wild-type, we propose that synaptic specificity is a developmental outcome of a composite of relative contributors that include spatiotemporal availability, interaction kinetics, and interaction biases through molecular recognition between partner cells (Hiesinger, 2021). In this view, the removal or alteration of a single relative contributor (e.g., the spatiotemporal availability of the main postsynaptic partner cell) increases the relative contribution of other factors, including the availability of other cells and their likelihood to form synapses on the basis of interaction kinetics (Agi et al., 2020; Kiral et al., 2020).

Increased *trans*-Tango labeling after development at 18°C reflects an actual increase in synapse numbers

The transsynaptic labeling technique *trans*-Tango has been known since its inception to label significantly more postsynaptic target cells at 18°C compared with 25°C. This effect could be the result of a technique-specific artifact or reflect a real temperature effect on the brain (Talay et al., 2017). Our data provide evidence for the latter hypothesis. As shown in Figure S2, the development of *trans*-Tango labeling over 7 days in the adult is identical at all temperatures. Hence, *trans*-Tango labels more cells only if the 2 critical days of late pupal development occur at lower temperature, not if 7 further days during adulthood occur at a lower temperature. Furthermore, we found the increased number of *trans*-Tango-labeled cells to be quantitatively validated with GRASP, brpD3-labeled active zones as well as

transgenics-independent measures including branch extensions and, in the case of R1–R6, neurotransmission on the basis of ERG recordings (see [Table S1](#) for all parameters).

Developmental temperature adapts movement behavior for the same adult environmental temperature

Our description of behavioral differences in response to environmental changes during development is reminiscent of the often excruciatingly stringent developmental conditions required for fly behavioral assays. Our findings suggest that behavioral differences are a direct consequence of connectivity differences associated with different developmental temperatures. A direct relation of neuronal morphology and individual behavior was previously shown for DCN neurons ([Linneweber et al., 2020](#)). This study identified a relation of left/right DCN wiring asymmetry to the behavioral parameter “absolute stripe deviation,” which is more related to movement precision. Indeed, we found no significant differences for this parameter after development at 18°C or 25°C at the behavioral temperatures 18°C and 25°C. Yet “absolute stripe deviation” did show some temperature dependency after development at 29°C and at the behavioral temperature of 29°C, suggesting increased asymmetry after development at 29°C or an exacerbation of behavioral differences at 29°C.

Our findings show that adult wild-type flies that developed at a lower temperature have more elaborately branched interneurons, have more synapses with more varied synaptic partners, and exhibit most overall movement activity at the same low temperature at which they developed, but mostly lower levels of overall activity at higher behavioral temperatures. In contrast, adult flies that developed at a higher temperature during time period of synapse formation have fewer branched interneurons, have fewer synapses with fewer synaptic partners, and exhibit more overall movement activity at higher behavioral temperatures than at lower temperatures. These findings are consistent with a preference of adult flies ([Rajpurohit and Schmidt, 2016](#)) and worms ([Hedgecock and Russell, 1975](#)) for the temperature at which they developed, but how the underlying connectivity difference cause behavioral adaptation remains to be determined. In *Drosophila melanogaster*, as in other species, evolution likely has selected a genome that encodes different brain connectivity at different developmental temperature to increase behavioral fitness.

Limitations of the study

Key to our study is the validation of non-canonical synapses using multiple methods, including synaptic markers, transsynaptic tracing, and activity-dependent split-GFP (GRASP). Yet electrophysiological recordings of synaptically connected neuronal pairs remain the gold standard to validated synaptic connectivity. Here, we only provided extracellular recordings of photoreceptor neurons. Furthermore, electron microscopy, combined with stringent criteria for synapses, is the basis of connectomics. Further validation of our findings using both electrophysiological and electron microscopy methods is desirable.

We found behavioral adaptation of walking activity to the temperature at which the flies developed on the basis of a simple, multiparametric behavioral assay. It remains unclear to what extent this behavioral adaptation represents a fitness advantage.

Similarly, how different developmental temperatures bring about such adaptive brain wiring remains a mystery.

STAR+METHODS

Detailed methods are provided in the online version of this paper and include the following:

- d [KEY RESOURCES TABLE](#)
- d [RESOURCE AVAILABILITY](#)
 - B Lead contact
 - B Materials availability
 - B Data and code availability
- d [EXPERIMENTAL MODEL AND SUBJECT DETAILS](#)
 - B The following genotypes were used
- d [METHOD DETAILS](#)
 - B Immunohistochemistry and fixed imaging
 - B Brain culture and live imaging
 - B Trans-tango and activity-dependent GRASP
 - B Electretinogram (ERG) recordings
- d [QUANTIFICATION AND STATISTICAL ANALYSIS](#)
 - B Branch analysis (all neurons except adult motoneurons):
 - B Branch analysis of adult motoneurons
 - B Synapse number analysis:
 - B Filopodia/axon branch tracing
 - B Statistical analysis
 - B Bulbous life time estimation
 - B Buridan’s paradigm object orientation assay
 - B Measures of overall activity
 - B Measures of movement angles or location independent of visual cue
 - B Measures of angles or location relative to visual cue
 - B Mathematical modeling
 - B ‘Developmental time’ adjustment.
 - B Parameter estimation

SUPPLEMENTAL INFORMATION

Supplemental information can be found online at <https://doi.org/10.1016/j.celrep.2021.110145>.

ACKNOWLEDGMENTS

We would like to thank Emil Kind, Mathias Wernet, Claude Desplan, and all members of the Hiesinger, Wernet, and Hassan labs for their support and help-ful discussions. We thank Mathias Wernet, Claude Desplan, Michael Reiser, Stephan Sigrist, Gilad Barnea, Ian Meinertzhagen, the Janelia Research Institute, and the Bloomington *Drosophila* Stock Center for reagents. This work was supported by grants from the NIH (RO1EY018884) and the German Research Foundation (DFG; HI1886/5-1 and SFB186 TP02) to P.R.H. S.B.D. and B.A.H. were supported by an Einstein BIH Fellowship. C.D. was supported by the DFG (DU 331/12-1). M.v.K. acknowledges financial support from the German Ministry for Education and Science (BMBF) through grant 01KI2016 and from the DFG, provided through the excellence cluster Math+, project EF3-2.

AUTHOR CONTRIBUTIONS

Conceptualization, F.R.K. and P.R.H.; Methodology, F.R.K., S.B.D., S.H., C.P., G.A.L., and M.v.K.; Investigation, F.R.K., S.B.D., S.H., C.P., G.A.L., and

M.v.K.; Visualization, F.R.K., S.B.D., G.A.L., B.A.H., M.v.K., and P.R.H.; Funding Acquisition, B.A.H., M.v.K., and P.R.H.; Project Administration, P.R.H.; Supervision, P.R.H., B.A.H., C.D., and M.v.K.; Writing – Original Draft, F.R.K. and P.R.H.; Writing – Review & Editing, F.R.K., S.B.D., G.A.L., C.D., M.v.K., B.A.H., and P.R.H.

DECLARATION OF INTERESTS

The authors declare no competing interests. Received: May

29, 2021

Revised: October 4, 2021

Accepted: November 29, 2021

Published: December 21, 2021

REFERENCES

- Agi, E., Langen, M., Altschuler, S.J., Wu, L.F., Zimmermann, T., and Hiesinger, P.R. (2014). The evolution and development of neural superposition. *J. Neurogenet.* **28**, 216–232.
- Agi, E., Kulkarni, A., and Hiesinger, P.R. (2020). Neuronal strategies for meeting the right partner during brain wiring. *Curr. Opin. Neurobiol.* **63**, 1–8.
- Alonso, L.M., and Marder, E. (2020). Temperature compensation in a small rhythmic circuit. *eLife* **9**, e55470.
- Bates, A.S., Schlegel, P., Roberts, R.J.V., Drummond, N., Tamimi, I.F.M., Turnbull, R., Zhao, X., Marin, E.C., Popovici, P.D., Dhawan, S., et al. (2020). Complete connectomic reconstruction of olfactory projection neurons in the fly brain. *Curr. Biol.* **30**, 3183–3199.e6.
- Bekkers, J.M., and Stevens, C.F. (1991). Excitatory and inhibitory autaptic currents in isolated hippocampal neurons maintained in cell culture. *Proc. Natl. Acad. Sci. U S A* **88**, 7834–7838.
- Carrillo, R.A., Özkan, E., Menon, K.P., Nagarkar-Jaiswal, S., Lee, P.T., Jeon, M., Birnbaum, M.E., Bellen, H.J., Garcia, K.C., and Zinn, K. (2015). Control of synaptic connectivity by a network of *Drosophila* IgSF cell surface proteins. *Cell* **163**, 1770–1782.
- Cassidy, J.J., Bernasek, S.M., Bakker, R., Giri, R., Peláez, N., Eder, B., Bobrowska, A., Bagheri, N., Nunes Amaral, L.A., and Carthew, R.W. (2019). Repressive gene regulation synchronizes development with cellular metabolism. *Cell* **178**, 980–992.e17.
- Clements, J., Lu, Z., Gehring, W.J., Meinertzhagen, I.A., and Callaerts, P. (2008). Central projections of photoreceptor axons originating from ectopic eyes in *Drosophila*. *Proc. Natl. Acad. Sci. U S A* **105**, 8968–8973.
- Colomb, J., Reiter, L., Blaszkiewicz, J., Wessnitzer, J., and Brembs, B. (2012). Open source tracking and analysis of adult *Drosophila* locomotion in Buridan's paradigm with and without visual targets. *PLoS ONE* **7**, e42247.
- Courgeon, M., and Desplan, C. (2019). Coordination between stochastic and deterministic specification in the *Drosophila* visual system. *Science* **366**, eaay6727.
- Creed, J.H., Gerke, T.A., and Berglund, A.E. (2020). MatSurv: survival analysis and visualization in MATLAB. *J. Open Source Softw.* **5**, 1830.
- de Wit, J., and Ghosh, A. (2016). Specification of synaptic connectivity by cell surface interactions. *Nat. Rev. Neurosci.* **17**, 22–35.
- Douthit, J., Hairston, A., Lee, G., Morrison, C.A., Holguera, I., and Treisman, J.E. (2021). R7 photoreceptor axon targeting depends on the relative levels of *lost* and *found* expression in R7 and its synaptic partners. *eLife* **10**, e65895.
- Duch, C., Vonhoff, F., and Ryglewski, S. (2008). Dendrite elongation and dendritic branching are affected separately by different forms of intrinsic motor neuron excitability. *Journal of Neurophysiology* (**100**), 2525–2536.
- Dudanova, I., and Klein, R. (2013). Integration of guidance cues: parallel signaling and crosstalk. *Trends Neurosci.* **36**, 295–304.
- Evers, J.F., Schmitt, S., Sibila, M., and Duch, C. (2005). Progress in functional neuroanatomy: precise automatic geometric reconstruction of neuronal morphology from confocal image stacks. *J. Neurophysiol.* **93**, 2331–2342.
- Ferguson, M.W., and Joanen, T. (1982). Temperature of egg incubation determines sex in *Alligator mississippiensis*. *Nature* **296**, 850–853.
- Fouquet, W., Oswald, D., Wichmann, C., Mertel, S., Depner, H., Dyba, M., Halbermann, S., Kittel, R.J., Eimer, S., and Sigrist, S.J. (2009). Maturation of active zone assembly by *Drosophila* Bruchpilot. *J. Cell Biol.* **186**, 129–145.
- Gilbert, S.F. (2012). Ecological developmental biology: environmental signals for normal animal development. *Evol. Dev.* **14**, 20–28.
- Gillooly, J.F., Charnov, E.L., West, G.B., Savage, V.M., and Brown, J.H. (2002). Effects of size and temperature on developmental time. *Nature* **417**, 70–73.
- Goaillard, J.M., and Marder, E. (2021). Ion channel degeneracy, variability, and covariation in neuron and circuit resilience. *Annu. Rev. Neurosci.* **44**, 335–357.
- Goodman, C.S. (1978). Isogenic grasshoppers: genetic variability in the morphology of identified neurons. *J. Comp. Neurol.* **182**, 681–705.
- Gutzke, W.H., and Crews, D. (1988). Embryonic temperature determines adult sexuality in a reptile. *Nature* **332**, 832–834.
- Hadjieconomou, D., Timofeev, K., and Salecker, I. (2011). A step-by-step guide to visual circuit assembly in *Drosophila*. *Curr. Opin. Neurobiol.* **21**, 76–84.
- Harris, J.M., Wang, A.Y., Boulanger-Weill, J., Santoriello, C., Foianini, S., Lichtman, J.W., Zon, L.I., and Arlotta, P. (2020). Long-range optogenetic control of axon guidance overcomes developmental boundaries and defects. *Dev. Cell* **53**, 577–588.e7.
- Hassan, B.A., Bermingham, N.A., He, Y., Sun, Y., Jan, Y., Zoghbi, H.Y., and Bellen, H.J. (2000). *atonal* regulates neurite arborization but does not act as a proneural gene in the *Drosophila* brain. *Neuron* **25** (3), 549–561.
- Hassan, B.A., and Hiesinger, P.R. (2015). Beyond molecular codes: simple rules to wire complex brains. *Cell* **163**, 285–291.
- Hedgecock, E.M., and Russell, R.L. (1975). Normal and mutant thermotaxis in the nematode *Caenorhabditis elegans*. *Proc. Natl. Acad. Sci. U S A* **72**, 4061–4065.
- Hertwig, O. (1898). Über den Einfluss der Temperatur auf die Entwicklung von *Rana fusca* und *Rana esculenta*. *Archiv für Mikrosk. Anat.* **51**, 319–382.
- Hiesinger, P.R. (2021). Brain wiring with composite instructions. *BioEssays* **43**, e2000166.
- Hiesinger, P.R., and Hassan, B.A. (2018). The evolution of variability and robustness in neural development. *Trends Neurosci.* **41**, 577–586.
- Hiesinger, P.R., Zhai, R.G., Zhou, Y., Koh, T.W., Mehta, S.Q., Schulze, K.L., Cao, Y., Verstreken, P., Clandinin, T.R., Fischbach, K.F., et al. (2006). Activity-independent prespecification of synaptic partners in the visual map of *Drosophila*. *Curr. Biol.* **16**, 1835–1843.
- Hoerstering, A.K., and Schmucker, D. (2021). Axonal branch patterning and neuronal shape diversity: roles in developmental circuit assembly: Axonal branch patterning and neuronal shape diversity in developmental circuit assembly. *Curr. Opin. Neurobiol.* **66**, 158–165.
- Hoge, M.A. (1915). Influence of temperature on the expression of a mendelian character. *J. Exp. Zool.* **18**, 241–286.
- Karupudurai, T., Lin, T.Y., Ting, C.Y., Pursley, R., Melnattur, K.V., Diao, F., White, B.H., Macpherson, L.J., Gallio, M., Pohida, T., and Lee, C.H. (2014). A hardwired glutamatergic circuit pools and relays UV signals to mediate spectral preference in *Drosophila*. *Neuron* **81**, 603–615.
- Kavalali, E.T., and Monteggia, L.M. (2020). Targeting homeostatic synaptic plasticity for treatment of mood disorders. *Neuron* **106**, 715–726.
- Kidd, P.B., Young, M.W., and Siggia, E.D. (2015). Temperature compensation and temperature sensation in the circadian clock. *Proc. Natl. Acad. Sci. U S A* **112**, E6284–E6292.
- Kiral, F.R., Linneweber, G.A., Mathejczyk, T., Georgiev, S.V., Wernet, M.F., Hassan, B.A., von Kleist, M., and Hiesinger, P.R. (2020). Autophagy-dependent filopodial kinetics restrict synaptic partner choice during *Drosophila* brain wiring. *Nat. Commun.* **11**, 1325.

- Kohrs, F.E., Daumann, I.M., Pavlovic, B., Jin, E.J., Kiral, F.R., Lin, S.C., Port, F., Wolfenberger, H., Mathejczyk, T.F., Linneweber, G.A., et al. (2021). Systematic functional analysis of rab GTPases reveals limits of neuronal robustness to environmental challenges in flies. *eLife* **10**, e59594.
- Kolodkin, A.L., and Hiesinger, P.R. (2017). Wiring visual systems: common and divergent mechanisms and principles. *Curr. Opin. Neurobiol.* **42**, 128–135.
- Kuntz, S.G., and Eisen, M.B. (2014). *Drosophila* embryogenesis scales uniformly across temperature in developmentally diverse species. *PLoS Genet.* **10**, e1004293.
- Kushinsky, D., Morozova, E.O., and Marder, E. (2019). *In vivo* effects of temperature on the heart and pyloric rhythms in the crab *Cancer borealis*. *J. Exp. Biol.* **222**, jeb199190.
- Langen, M., Agi, E., Altschuler, D.J., Wu, L.F., Altschuler, S.J., and Hiesinger, P.R. (2015). The developmental rules of neural superposition in *Drosophila*. *Cell* **162**, 120–133.
- Langen, M., Koch, M., Yan, J., De Geest, N., Erfürth, M.L., Pfeiffer, B.D., Schmucker, D., Moreau, Y., and Hassan, B.A. (2013). Mutual inhibition among postmitotic neurons regulates robustness of brain wiring in *Drosophila*. *eLife* **2** (e00337).
- Li, F., Lindsey, J.W., Marin, E.C., Otto, N., Dreher, M., Dempsey, G., Stark, I., Bates, A.S., Pleijzier, M.W., Schlegel, P., et al. (2020). The connectome of the adult *Drosophila* mushroom body provides insights into function. *eLife* **9**, e62576.
- Lieberman, O.J., McGuirt, A.F., Tang, G., and Sulzer, D. (2019). Roles for neuronal and glial autophagy in synaptic pruning during development. *Neuro-biol. Dis.* **122**, 49–63.
- Linneweber, G.A., Andriatsilavo, M., Dutta, S.B., Bengochea, M., Hellbrügge, L., Liu, G., Ejsmont, R.K., Straw, A.D., Wernet, M., Hiesinger, P.R., and Hassan, B.A. (2020). A neurodevelopmental origin of behavioral individuality in the *Drosophila* visual system. *Science* **367**, 1112–1119.
- Luo, J., Ting, C.Y., Li, Y., McQueen, P., Lin, T.Y., Hsu, C.P., and Lee, C.H. (2020). Antagonistic regulation by insulin-like peptide and activin ensures the elaboration of appropriate dendritic field sizes of amacrine neurons. *eLife* **9**, e50568.
- Macpherson, L.J., Zaharieva, E.E., Kearney, P.J., Alpert, M.H., Lin, T.Y., Turan, Z., Lee, C.H., and Gallio, M. (2015). Dynamic labelling of neural connections in multiple colours by trans-synaptic fluorescence complementation. *Nat. Commun.* **6**, 10024.
- Menon, K.P., Kulkarni, V., Takemura, S.Y., Anaya, M., and Zinn, K. (2019). Interactions between Dpr11 and DIP-g control selection of amacrine neurons in *Drosophila* color vision circuits. *eLife* **8**, e48935.
- Namiki, S., Dickinson, M.H., Wong, A.M., Korff, W., and Card, G.M. (2018). The functional organization of descending sensory-motor pathways in *Drosophila*. *eLife* **7**, e34272.
- O’Leary, T., and Marder, E. (2016). Temperature-robust neural function from activity-dependent ion channel regulation. *Curr. Biol.* **26**, 2935–2941.
- Özel, M.N., Langen, M., Hassan, B.A., and Hiesinger, P.R. (2015). Filopodial dynamics and growth cone stabilization in *Drosophila* visual circuit development. *eLife* **4**, e10721.
- Özel, M.N., Kulkarni, A., Hasan, A., Brummer, J., Moldenhauer, M., Daumann, I.M., Wolfenberger, H., Dercksen, V.J., Kiral, F.R., Weiser, M., et al. (2019). Serial synapse formation through filopodial competition for synaptic seeding factors. *Dev. Cell* **50**, 447–461.e8.
- Pak, W.L., Grossfield, J., and White, N.V. (1969). Nonphototactic mutants in a study of vision of *Drosophila*. *Nature* **222**, 351–354.
- Petrovic, M., and Schmucker, D. (2015). Axonal wiring in neural development: target-independent mechanisms help to establish precision and complexity. *BioEssays* **37**, 996–1004.
- Rajpurohit, S., and Schmidt, P.S. (2016). Measuring thermal behavior in smaller insects: a case study in *Drosophila melanogaster* demonstrates effects of sex, geographic origin, and rearing temperature on adult behavior. *Fly (Austin)* **10**, 149–161.
- Rister, J., Desplan, C., and Vasilias, D. (2013). Establishing and maintaining gene expression patterns: insights from sensory receptor patterning. *Development* **140**, 493–503.
- Roberts, E. (1918). Fluctuation in a recessive mendelian character. *J. Exp. Zool.* **27**, 157–192.
- Ryglewski, S., Vonhoff, F., Scheckel, K., and Duch, C. (2017). Intra-neuronal competition for synaptic partners conserves the amount of dendritic building material. *Neuron* **93**, 632–645.e6.
- Sanes, J.R., and Zipursky, S.L. (2020). Synaptic specificity, recognition molecules, and assembly of neural circuits. *Cell* **181**, 536–556.
- Scheffer, L.K., Xu, C.S., Januszewski, M., Lu, Z., Takemura, S.Y., Hayworth, K.J., Huang, G.B., Shinomiya, K., Maitlin-Shepard, J., Berg, S., et al. (2020). A connectome and analysis of the adult *Drosophila* central brain. *eLife* **9**, e57443.
- Schmitt, S., Evers, J.F., Duch, C., Scholz, M., and Obermayer, K. (2004). New methods for the computer-assisted 3D reconstruction of neurons from confocal image stacks. *Neuroimage* **23**, 1283–1298.
- Seyster, E.W. (1919). Eye facet number as influenced by temperature in the bar-eyed mutant of *Drosophila*. *Biol. Bull.* **37**, 168–181.
- Shatz, C.J. (1996). Emergence of order in visual system development. *Proc. Natl. Acad. Sci. U S A* **93**, 602–608.
- Südhof, T.C. (2018). Towards an understanding of synapse formation. *Neuron* **100**, 276–293.
- Takemura, S.Y., Xu, C.S., Lu, Z., Rivlin, P.K., Parag, T., Olbris, D.J., Plaza, S., Zhao, T., Katz, W.T., Umayam, L., et al. (2015). Synaptic circuits and their variations within different columns in the visual system of *Drosophila*. *Proc. Natl. Acad. Sci. U S A* **112**, 13711–13716.
- Talay, M., Richman, E.B., Snell, N.J., Hartmann, G.G., Fisher, J.D., Sorkac, A., Santoyo, J.F., Chou-Freed, C., Nair, N., Johnson, M., et al. (2017). Transsynaptic mapping of second-order taste neurons in flies by *trans*-Tango. *Neuron* **96**, 783–795.e4.
- Trush, O., Liu, C., Han, X., Nakai, Y., Takayama, R., Murakawa, H., Carrillo, J.A., Takechi, H., Hakeda-Suzuki, S., Suzuki, T., and Sato, M. (2019). N-cadherin orchestrates self-organization of neurons within a columnar unit in the *Drosophila* medulla. *J. Neurosci.* **39**, 5861–5880.
- Turrigiano, G. (2012). Homeostatic synaptic plasticity: local and global mechanisms for stabilizing neuronal function. *Cold Spring Harb. Perspect. Biol.* **4**, a005736.
- Turrigiano, G.G. (2017). The dialectic of Hebb and homeostasis. *Philos. Trans. R. Soc. Lond. B Biol. Sci.* **372**, 20160258.
- Van der Loos, H., and Glaser, E.M. (1972). Autapses in neocortex cerebri: synapses between a pyramidal cell’s axon and its own dendrites. *Brain Res.* **48**, 355–360.
- Vonhoff, F., and Duch, C. (2010). Tiling among stereotyped dendritic branches in an identified *Drosophila* motoneuron. *J. Comp. Neurol.* **518**, 2169–2185.
- Wilton, D.K., Dissing-Olesen, L., and Stevens, B. (2019). Neuron-glia signaling in synapse elimination. *Annu. Rev. Neurosci.* **42**, 107–127.
- Witvliet, D., Mulcahy, B., Mitchell, J.K., Meirovitch, Y., Berger, D.R., Wu, Y., Liu, Y., Koh, W.X., Parvathala, R., Holmyard, D., et al. (2021). Connectomes across development reveal principles of brain maturation. *Nature* **596**, 257–261.
- Xu, S., Xiao, Q., Cosmanescu, F., Sergeeva, A.P., Yoo, J., Lin, Y., Katsamba, P.S., Ahlsen, G., Kaufman, J., Linaval, N.T., et al. (2018). Interactions between the Ig-superfamily proteins DIP-a and Dpr6/10 regulate assembly of neural circuits. *Neuron* **100**, 1369–1384.e6.
- Zuo, W., Moses, M.E., West, G.B., Hou, C., and Brown, J.H. (2012). A general model for effects of temperature on ectotherm ontogenetic growth and development. *Proc. Biol. Sci.* **279**, 1840–1846.

STAR+METHODS

KEY RESOURCES TABLE

REAGENT or RESOURCE	SOURCE	IDENTIFIER
Antibodies		
Rat anti-Cadherin, DN (extracellular domain)	DSHB	Cat# DN-Ex #8; RRID: AB 528121
Goat anti-GFP pAb	Abcam	Cat# ab6673; RRID: AB 305643
Rat anti-GFP mAb	BioLegend	Cat# 338002; RRID: AB 1279414
Rabbit anti-CD4	Atlas Antibodies	Cat# HPA004252; RRID: AB 1078466
Rabbit anti-dsRed	Takara Bio	Cat# 632496; RRID: AB 10013483
Donkey anti-goat Alexa Fluor 488	Jackson ImmunoResearch Labs	Cat# 705-545-147; RRID: AB 2336933
Donkey Anti-goat Cy5	Jackson ImmunoResearch Labs	Cat# 705-175-147; RRID: AB 2340415
Donkey Anti-rabbit Cy3	Jackson ImmunoResearch Labs	Cat# 711-165-152; RRID: AB 2307443
Donkey Anti-rat Cy5	Jackson ImmunoResearch Labs	Cat# 112-175-143; RRID: AB 2338263
Chemicals, peptides, and recombinant proteins		
Vectashield	Vector Laboratories	H-1000
PBS	GIBCO	70011-36
Formaldehyde	Merck KGaA	1.03999.1000
Triton X-100	Sigma-Aldrich	T8787
Schneider's <i>Drosophila</i> Medium [+] L-Glutamine	GIBCO	21720-024
Agarose, low gelling temperature	Sigma-Aldrich	A9045-10G
Human insulin recombinant zinc	GIBCO	12585014
Penicillin/Streptomycin	GIBCO	15140122
ES Cell FBS	GIBCO	16141-061
20-Hydroxyecdysone	Sigma-Aldrich	5289-74-7
SilGard and Silicone Elastomer Kit	Dow Corning	184
Sodium Chloride	Merck KGaA	1.06404.1000
Experimental models: Organisms/strains		
<i>Drosophila</i> : UAS-brpD3::GFP	Gift from S.Sigrist	N/A
<i>Drosophila</i> : UAS-myr::GFP,QUAS-mtdTomato(3xHA)	Bloomington <i>Drosophila</i> Stock Center	RRID: BDSC_77479
<i>Drosophila</i> : trans-Tango	Bloomington <i>Drosophila</i> Stock Center	RRID: BDSC_77123
<i>Drosophila</i> : DIPY ^{null}	Gift from C.Desplan	N/
<i>Drosophila</i> : Rh4-Gal4	Gift from M.Wernet	A
<i>Drosophila</i> : Rh4-LacZ	Gift from M.Wernet	N/
<i>Drosophila</i> : R48A07-p65ADZp(attP40), R79H02-ZpGdbd(attP2)	Gift from M.Reiser	A
<i>Drosophila</i> : Lawf1-Gal4	Gift from M.Reiser	N/A
<i>Drosophila</i> : ato-Gal4-14a	Hassan et al., 2000	https://doi.org/10.1016/S0896-6273(00)81059-4
<i>Drosophila</i> : ato-LexA	Langen et al., 2013	https://doi.org/10.7554/eLife.00337
<i>Drosophila</i> : UAS-nSyb-spGFP1-10,lexAop-CD4-spGFP	Bloomington <i>Drosophila</i> Stock Center	RRID: BDSC_64314
<i>Drosophila</i> : lexAop-nSyb-spGFP1-10,UAS-CD4-spGFP11	Bloomington <i>Drosophila</i> Stock Center	RRID: BDSC_64315
<i>Drosophila</i> : hsFLP	Bloomington <i>Drosophila</i> Stock Center	RRID: BDSC_8862
<i>Drosophila</i> : GMR-Gal4	Bloomington <i>Drosophila</i> Stock Center	RRID: BDSC_8121
<i>Drosophila</i> : GMR-Flp	Bloomington <i>Drosophila</i> Stock Center	RRID: BDSC_42735

(Continued on next page)

Continued

REAGENT or RESOURCE	SOURCE	IDENTIFIER
Drosophila: FRT82B, tub-Gal80	Bloomington Drosophila Stock Center	RRID: BDSC_5135
Drosophila: lexAop-mCD8::GFP	Bloomington Drosophila Stock Center	RRID: BDSC_32203
Drosophila: UAS-mCD4::tdGFP	Bloomington Drosophila Stock Center	RRID:BDSC_35836
Drosophila: UAS-mCD4::tdTomato	Bloomington Drosophila Stock Center	RRID:BDSC_35837
Drosophila: GMR49B06-LexA Drosophila:	Bloomington Drosophila Stock Center	RRID:BDSC_52707
GMR19F01-LexA Drosophila:	Bloomington Drosophila Stock Center	RRID:BDSC_52547
GMR25F10-LexA Drosophila:	Bloomington Drosophila Stock Center	RRID:BDSC_54603
GMR42H01-LexA Drosophila:	Bloomington Drosophila Stock Center	RRID:BDSC_54204
GMR20D11-LexA Drosophila:	Bloomington Drosophila Stock Center	RRID:BDSC_52565
GMR38H06-LexA Drosophila:	Bloomington Drosophila Stock Center	RRID:BDSC_52775
GMR11C05-LexA	Bloomington Drosophila Stock Center	RRID:BDSC_54608
Drosophila: ortC1-3-LexADBBD, ortC2B-dVP16AD	Gift from M.Wernet	N/A
Drosophila: GMR24F06-Gal4	Bloomington Drosophila Stock Center	RRID: BDSC_49087
Software and algorithms		
GraphPad Prism	GraphPad Software	RRID: SCR_002798
ImageJ	National Institutes of Health (NIH)	RRID: SCR_002285
IMARIS	Bitplane AG	RRID: SCR_007370
Leica Application Suite X	Leica Microsystems	RRID: SCR_013673
Clampfit	Axon Instruments	RRID: SCR_011323
Clampex	Axon Instruments	RRID: SCR_011323
Amira	FEL-Thermo Fisher Scientific	RRID: SCR_014305
Custom code	Zenodo	https://doi.org/10.5281/zenodo.5708543

RESOURCE AVAILABILITY

Lead contact

Further information and requests for resources and reagents should be directed to and will be fulfilled by the lead contact, P. Robin Hiesinger (robin.hiesinger@fu-berlin.de).

Materials availability

All reagents and resources generated in this study are available from the Lead Contact without restriction..

Data and code availability

All data generated in this study are available from the Lead Contact without restriction.

A publication release of original code has been generated and deposited on Zenodo and is publicly available under <https://doi.org/10.5281/zenodo.5708543>.

Any additional information required to reanalyze the data reported in this work paper is available from the Lead Contact upon request.

EXPERIMENTAL MODEL AND SUBJECT DETAILS

Flies were reared at 25°C on standard cornmeal/yeast diet unless stated otherwise. For developmental analyses white pre-pupae (P+0%) were collected and staged to pupal developmental stages shown on figures. The following *Drosophila* strains were either obtained from Bloomington *Drosophila* Stock Center (BDSC) or other groups: UAS-Brp-short-GFP (S.Sigrist); Trans-tango flies (G.Barnea); DIPg^{null} (C.Desplan); Rh4-Gal4, Rh4-LacZ (M.Wernet); R48A07-p65ADZp(attP40); R79H02-ZpGdbd(attP2) (Mi4-specific split Gal4 driver), Lawf1-Gal4 (M.Reiser); ato-Gal4-14a, ato-LexA, GRASP flies, hsflp, GMRflp, GMR-Gal4, GMR(FRT.stop)Gal4, FRT82B, GMR-Gal80, tub-Gal80, LexAop-CD8-GFP, UAS-CD4-tdGFP, UAS(FRT.stop)CD4-tdGFP, UAS-CD4-tdTomato, GMRmyr-tomato, GMR49B06-LexA (Mi4-specific driver), GMR19F01-LexA (Mi1-specific driver), GMR25F10-LexA (Tm9-specific driver), GMR42H01-LexA (Dm9-specific driver), GMR20D11-LexA (Dm3-specific driver), GMR38H06-LexA (Dm6-specific driver), GMR11C05-LexA (Dm11-specific driver), ortC1-3-LexADBBD, ortC2B-dVP16AD (Dm8-specific driver), GMR24F06-Gal4 (Dm8-specific

driver), R14F03-p65ADZp, R24C07-ZpGdbd (DNp24- specific split-Gal4 driver) (BDSC). Flies of both sexes were equally used in all experiments unless otherwise noted in the paper.

The following genotypes were used

Figures 1B–1E: GMRflp; GMR-Gal4, UAS-CD4tdGFP; FRT82B, tub-Gal80/FRT82B
Figures 1I–1L: GMRflp; GMR-Gal4, UAS-CD4tdTomato/UAS-Brp^{short}-GFP; FRT82B, tub-Gal80/FRT82B
Figures 2A–2D: UAS-myrGFP, QUAS-mtdTomato(3xHA); Rh4-Gal4/*trans*-Tango
Figure 2E: Rh4-Gal4, UAS-nsyb::splitGFP1-10, LexAop-splitGFP11/ ortC1-3-LexADBD, ortC2B-dVP16AD (Dm8-specific driver)
Figure 2F: Rh4-Gal4, UAS-nsyb::splitGFP1-10, LexAop-splitGFP11/GMR19F01-LexA (Mi1-specific driver)
Figure 2G: Rh4-Gal4, UAS-nsyb::splitGFP1-10, LexAop-splitGFP11/GMR49B06-LexA (Mi4-specific driver)
Figure 2H: Rh4-Gal4, UAS-nsyb::splitGFP1-10, LexAop-splitGFP11/GMR25F10-LexA (Tm9-specific driver)
Figures 3A and 3A¹: Rh4-Gal4, UAS-nsyb::splitGFP1-10, LexAop-splitGFP11/ortC1-3-LexADBD, ortC2B-dVP16AD (Dm8-specific driver); *DIPg*^{null/+}
Figures 3B and 3B¹: Rh4-Gal4, UAS-nsyb::splitGFP1-10, LexAop-splitGFP11/ortC1-3-LexADBD, ortC2B-dVP16AD (Dm8-specific driver); *DIPg*^{null/} *DIPg*^{null}
Figures 3D and 3D¹: Rh4-Gal4/ UAS-Brp^{short}-GFP; *DIPg*^{null/+}
Figures 3E and 3E¹: Rh4-Gal4/ UAS-Brp^{short}-GFP; *DIPg*^{null/} *DIPg*^{null}
Figure 3G: UAS-myrGFP, QUAS-mtdTomato(3xHA); Rh4-Gal4/*trans*-Tango; *DIPg*^{null/+}
Figure 3H: UAS-myrGFP, QUAS-mtdTomato(3xHA); Rh4-Gal4/*trans*-Tango; *DIPg*^{null/} *DIPg*^{null}
Figure 3J: Rh4-Gal4, UAS-nsyb::splitGFP1-10, LexAop-splitGFP11/ GMR19F01-LexA (Mi1-specific driver); *DIPg*^{null/+} and *DIPg*^{null/} *DIPg*^{null}
Figure 3K: Rh4-Gal4, UAS-nsyb::splitGFP1-10, LexAop-splitGFP11/GMR49B06-LexA (Mi4-specific driver); *DIPg*^{null/+} and *DIPg*^{null/} *DIPg*^{null}
Figure 3L: Rh4-Gal4, UAS-nsyb::splitGFP1-10, LexAop-splitGFP11/ GMR25F10-LexA (Tm9-specific driver); *DIPg*^{null/+} and *DIPg*^{null/} *DIPg*^{null}
Figure 4A: GMRflp; GMR-Gal4, UAS-CD4tdTomato/UAS-Brp^{short}-GFP; FRT82B, tub-Gal80/FRT82B
Figures 4B and 4C: Canton-S WT flies
Figures 4D–4G: hsf1p; UAS(FRT.stop)CD4tdGFP; GMR24F06-Gal4 (Dm8-specific driver)
Figures 4H–4J: hsf1p; UAS(FRT.stop)CD4tdGFP/ R48A07-p65ADZp(attP40); R79H02-ZpGdbd(attP2) (Mi4-specific split Gal4 driver)
Figures 5B–5G: ;UAS-CD4tdGFP/+;Ato-Gal4,UAS-CD4tdGFP/+
Figures 5H–5J: ;UAS-Brp^{short}-GFP/+;Ato-Gal4,UAS-CD4tdTomato/+
Figures 5K–5M: UAS-myrGFP, QUAS-mtdTomato(3xHA); *trans*-Tango/+;Ato-Gal4/+
Figures 5N–5P¹: ;LexAop-nsyb::splitGFP1-10, UAS-splitGFP11/R52H01AD;Ato-LexA/R19C10DBD (Lawf1 split Gal4)
Figure 6: Canton-S WT flies (used in (12) to perform EM connectome analysis of synaptic partners in the *Drosophila* visual system)
Figure S1B: UAS-myrGFP, QUAS-mtdTomato(3xHA); Rh4-Gal4/*trans*-Tango
Figure S1C: UAS-myrGFP, QUAS-mtdTomato(3xHA); Rh4-Gal4/*trans*-Tango; *DIPg*^{null/} *DIPg*^{null}
Figure S2: UAS-myrGFP, QUAS-mtdTomato(3xHA); Rh4-Gal4/*trans*-Tango
Figure S3: Rh4-Gal4, UAS-nsyb::splitGFP1-10, LexAop-splitGFP11/ ortC1-3-LexADBD, ortC2B-dVP16AD (Dm8-specific driver)
Figures S4A–S4C: ortC1-3-LexADBD, ortC2B-dVP16AD (Dm8-specific driver), LexAop-CD8GFP
Figures S4D and S4D¹: ortC1-3-LexADBD, ortC2B-dVP16AD (Dm8-specific driver), LexAop-CD8GFP/Rh4-LacZ; *DIPg*^{null/+}
Figures S4E and S4E¹: ortC1-3-LexADBD, ortC2B-dVP16AD (Dm8-specific driver), LexAop-CD8GFP/Rh4-LacZ; *DIPg*^{null/} *DIPg*^{null}
Figures S4F and S4G: UAS-myrGFP, QUAS-mtdTomato(3xHA); Rh4-Gal4/*trans*-Tango; *DIPg*^{null/} *DIPg*^{null}
Figures S5B and S5B¹: Rh4-Gal4, UAS-nsyb::splitGFP1-10, LexAop-splitGFP11/GMR42H01-LexA (Dm9-specific driver); *DIPg*^{null/+}
Figures S5C and S5C¹: Rh4-Gal4, UAS-nsyb::splitGFP1-10, LexAop-splitGFP11/GMR42H01-LexA (Dm9-specific driver); *DIPg*^{null/} *DIPg*^{null}
Figures S5E and S5E¹: Rh4-Gal4, UAS-nsyb::splitGFP1-10, LexAop-splitGFP11/GMR11C05-LexA (Dm11-specific driver); *DIPg*^{null/+}
Figures S5F and S5F¹: Rh4-Gal4, UAS-nsyb::splitGFP1-10, LexAop-splitGFP11/GMR11C05-LexA (Dm11-specific driver); *DIPg*^{null/} *DIPg*^{null}
Figures S5H and S5H¹: Rh4-Gal4, UAS-nsyb::splitGFP1-10, LexAop-splitGFP11/GMR20D11-LexA (Dm3-specific driver); *DIPg*^{null/+}
Figures S5I and S5I¹: Rh4-Gal4, UAS-nsyb::splitGFP1-10, LexAop-splitGFP11/GMR20D11-LexA (Dm3-specific driver); *DIPg*^{null/} *DIPg*^{null}
Figures S5J and S5J¹: Rh4-Gal4, UAS-nsyb::splitGFP1-10, LexAop-splitGFP11/ GMR38H06-LexA (Dm6-specific driver); *DIPg*^{null/+}

Figures S5K and S5K': Rh4-Gal4, UAS-nsyb::splitGFP1-10, LexAop-splitGFP11/ GMR38H06-LexA (Dm6-specific driver); *DIPg^{null}/DIPg^{null}*
Figures S6A–S6D: GMRflp; GMR-Gal4, UAS-CD4tdTomato/UAS-Brp^{short}-GFP; FRT82B, tub-Gal80/FRT82B
Figures S6E–S6G: Canton-S WT flies
Figures S6H–S6J: hsf1p; UAS(FRT.stop)CD4tdGFP; GMR24F06-Gal4 (Dm8-specific driver)
Figure S7: R14F03-p65ADZp, R24C07-ZpGdbd (DNp24-specific split-Gal4 driver); UAS-CD4tdGFP
Figure S8: GMR23H06-ADZ attP40/UAS-cd4-tdGFP; GMR30A07-DBD attP2/+
Figure S9: UAS-myrGFP, QUAS-mtdTomato(3xHA); *trans-Tango/+; Ato-Gal4/+*
Figures S10–S12: Canton-S WT flies

METHOD DETAILS

Immunohistochemistry and fixed imaging

Pupal and adult eye-brain complexes were dissected in cold Schneider's *Drosophila* medium and fixed in 4% paraformaldehyde (PFA) in PBS for 40 minutes. Tissues were washed in PBST (0.4% Triton-X) and mounted in Vectashield (Vector Laboratories, CA). Images were obtained with a Leica TCS SP8-X white laser confocal microscope with a 63X glycerol objective (NA = 1.3). The primary antibodies used in this study with given dilutions were as follows: rat monoclonal anti-nCadherin (1:100; Developmental Studies Hybridoma Bank); goat polyclonal anti-GFP (1:1000; Abcam); rat monoclonal anti-GFP (1:500; BioLegend); rabbit polyclonal anti-CD4 (1:600; Atlas Antibodies); rabbit polyclonal anti-DsRed (1:500; ClonTech). The secondary antibodies Alexa488, Cy3, Cy5 (Jackson ImmunoResearch Laboratories) were used in 1:500 dilution.

Brain culture and live imaging

For all *ex vivo* live imaging experiments an imaging window cut open removing posterior head cuticle partially. The resultant eye-brain complexes were mounted in 0.4% dialyzed low-melting agarose in a modified culture medium. Live imaging was performed using a Leica SP8 MP microscope with a 40X IRAPO water objective (NA = 1.1) with a Chameleon Ti:Sapphire laser and Optical Parametric Oscillator (Coherent). The excitation laser was set to 900 nm for single channel CD4-tdGFP imaging. Live imaging of R7 axon terminals at different temperatures was performed as follows: white pre-pupae (P+0%) were collected and staged to P+60% at 25°C. After eye-brain complexes were mounted in 0.4% dialyzed low-melting agarose in a modified culture medium, they were incubated 1 hour in imaging chamber at given temperatures on figures and scanned live for another hour with 1-min time resolution at the same incubation temperature. The same experimental flow and imaging settings were used for live imaging of Dorsal cluster neuron (DCN) axonal branches except that live imaging was performed at P+50%.

Trans-tango and activity-dependent GRASP

Trans-tango and GRASP experiments were performed with yellow R7-specific driver Rh4-Gal4 and DCN-specific *ato-Gal4-14a*. Trans-tango flies were raised at 25°C until P+40% and moved to 18°C or 29°C for temperature shift experiments. On the day of eclosion, flies were transferred back to 25°C and dissected after 1 week. The number of postsynaptic neurons was counted manually from their cell bodies using cell counter plugin in Fiji including all cell bodies with weak or strong labeling to reveal all potential connections. Since postsynaptic partner labeling by Trans-tango is age-dependent, in another set of experiments, 1-day old flies were dissected to reveal the identity of cell types strongly connected to DCNs. For activity-dependent GRASP experiments, the same experimental flow was followed as in Trans-tango temperature shift experiments. To activate UV-sensitive R7-photoreceptors, flies were transferred to UV-transparent Plexiglas vials on the day of eclosion and kept in a custom-made light box with UV light (25°C, 20-4 light-dark cycle) for 4 days. To activate DCNs, flies were transferred to 25°C incubator with 12-12 light-dark cycle for 5 days. Brains were dissected and stained with a polyclonal anti-GFP antibody to label R7 photoreceptors, monoclonal anti-GFP antibody to label GRASP signal, and polyclonal anti-CD4 antibody to label postsynaptic neurons.

Electroretinogram (ERG) recordings

Newly-hatched (0-day old) adult flies were collected and glued on slides using nontoxic school glue. Flies were exposed to alternating 1 s "on" 2 s "off" light stimulus provided by computer-controlled white LED system (MC1500; Schott). ERGs were recorded using Clampex (Axon Instruments) and quantified using Clampfit (Axon Instruments).

QUANTIFICATION AND STATISTICAL ANALYSIS

Branch analysis (all neurons except adult motoneurons):

All imaging data were analyzed and presented with Imaris 9.0.1 (Bitplane). Branches were detected automatically with the filament module using identical parameters for all experimental conditions (largest dendrite diameter: 3.0 mm, thinnest dendrite diameter: 0.2 mm). Inconsistencies in automatic detection were checked and corrected manually. The resultant values of branch numbers and lengths were taken and recorded directly from the statistics tab of the filament module. The peripheral area of the branch arborization was marked manually with the Surface function using the same mode for all experimental conditions (selection mode: isoclick)

and a consequent surface was generated for the entire branching area marked manually. The resultant values of surface area were taken and recorded directly from the statistics tab of the surface module. Graph generation and statistical analyses were done using GraphPad Prism 8.2.0

Branch analysis of adult motoneurons

For analysis of motoneuron dendritic structure *Drosophila melanogaster* were reared at 25°C, on a 12/12hrs light/dark cycle, in plastic vials on a cornmeal, glucose, yeast, agar diet (for 6 l: 725.69 g glucose, 343.06 g cornmeal, 66 g Agar and 181.38 g active dry yeast; after cooling to 70°C 76.25 mL Tegosept (10% in 100% ethanol) were added. Ascorbic acid was added (3.5 g) after cooling to 65°C. For all experiments male flies that express *cd4*-tdGFP in DLM flight motoneurons were used (genotype: *w*;GMR23H06-ADZ attP40/UAS-*cd4*-tdGFP;GMR30A07-DBD attP2/+). To test for effects of temperature on dendritic differentiation of DLM flight motoneurons, animals were raised at 25°C from egg to late third instar larva and transferred at the prepupal stage to either 18°C, or 29°C, or kept at 25°C. After adult eclosion, all animals were transferred to 25°C. For each temperature protocol in 5 male animals one MN was stained intracellularly at the second day of adult life. Adult DLM flight motoneurons were filled as previously described (Duch et al., 2008; Ryglewski et al., 2017). Confocal image stacks were acquired with a Leica TSC SP8 confocal laser scanning microscope with a 40x, 1.25 NA oil lens at a zoom of 3.5. Excitation wavelength was 561 nm (DPSS laser) and PMT detection between 570 and 600 nm. Voxel dimensions were 863 863 300 nm (x, y, z). Image stacks were imported into Amira software (AMIRA 4.1.1, FEI, Hills-boro, Oregon, US) and dendritic structure reconstructions were conducted with custom plug-ins as previously described (Schmitt et al., 2004; Evers et al., 2005). As metric parameters the number of dendritic branches, total dendritic length (TDL), the mean length of all dendritic branches (MDL), and the mean radius of all dendritic branches (MDR) were readout. For branch order analysis, the entire neurite from the cell body to the axon leaving the ventral nerve cord was defined as tree origin and thus branch order 0. All dendrites that directly branch off that neurite were first order branches, all dendrites branching off first order branches were second order branches and so on. The number of dendrites in each branch order was counted for each temperature condition.

Synapse number analysis:

All imaging data were analyzed and presented with Imaris 9.0.1 (Bitplane). For synapse number analysis, CD4-tomato channel was used to generate surfaces for individual R7 axon terminals and DCN axonal branches. Brp-positive puncta inside the surface were filtered using the masking function and were automatically detected with the spot detection module (spot diameter was set to 0.3 μm). Synapse numbers were taken and recorded directly from the statistics tab of the spot function. To obtain synapse density, the number of Brp-positive puncta inside individual DCN branch was divided by the respective branch length. Graph generation and statistical analyses were done using GraphPad Prism 8.2.0

Filopodia/axon branch tracing

Filopodia/axon branch tracing was performed using the filament module of Imaris 9.0.1 (BitPlane). Each filopodia/axon branch for all time points was segmented manually using “automatic placement” option to ensure the measurement of actual 3D length of each filopodia/axonal branch. Node was defined by the junction of axon shaft-branching point, from which filaments were created covering the entire length of the respective branch for all time points. “Length over time” data for all segmented filopodia/axon branches were recorded directly from the statistics tab of the filament module to calculate speed. Graph generation and statistical analyses were done using GraphPad Prism 8.2.0.

Statistical analysis

Statistical comparison of two groups was performed with non-parametric Kolmogorov-Smirnov test. Statistical comparison of more than two groups was performed with non-parametric Kruskal-Wallis test and corrected for multiple comparisons with Dunn's as a post hoc test. All significance values are denoted on the graphs and in their respective legends. Graph generation and statistical analyses were done using GraphPad Prism 8.2.0.

Bulbous life time estimation

We used the Kaplan-Meier estimator provided in MatSurv (Creed et al., 2020) to estimate the Bulbous tip survival probability depicted in Figure 1F.

Buridan's paradigm object orientation assay

Fly object orientation behavior was tested according to standard protocols in a Buridan arena (Colomb et al., 2012; Linneweber et al., 2020) using flies grown in a 12/12 h light–dark cycle. The arena consisted of a round platform of 117 mm in diameter, surrounded by a water-filled moat and placed inside a uniformly illuminated white cylinder. The assay was lid using four circular fluorescent tubes (Osram, L 40w, 640 C circular cool white) powered by an Osram Quicktronic QT-M 1 3 26–42. The fluorescent tubes were located outside of a diffuser (DeBanier, Belgium, 2090051, Kalk transparent, 180 g, white) positioned 147.5 mm from the arena center. The temperature on the platform was 25 °C and 30 mm-wide stripes of black cardboard were placed on opposing sides inside of the diffuser. The retinal size of the stripes depended on the position of the fly on the platform and ranged from 8.4° to 19.6° in width (11.7° in the center of the platform). Fly tracks were analyzed using CeTrAn (Colomb et al., 2012) and custom-written python code

(Linneweber et al., 2020). We evaluated 44 partially overlapping behavioral parameters and have picked 25 representative from these for detailed analysis as shown in Figure 6 and Figure S8 and Table S2. The behavioral parameters are the following (Colomb et al., 2012; Linneweber et al., 2020):

Measures of overall activity

1. Number of walks: The number of times a fly walks from one stripe to the other. The fly needs to be on both ends near the edgemoore than 80% of the platform radius.
2. Pause duration (s): Median duration of pauses in seconds
3. Distance traveled (mm/min): Total distance traveled per minute.
4. Relative time moving: ratio of moving versus not moving over the entire length of the fly track.
5. Activity time (s): Time active per minute in seconds
6. Speed (mm/s): Division of the distance traveled by time in mm/s. The reported value is the median speed of each fly. Move-ments exceeding 50mm/s are excluded in the median speed calculation.
7. Number of pauses: number of pauses per minute.
8. Activity bouts (s): Median duration of bouts of activity in seconds

Measures of movement angles or location independent of visual cue

9. Meandering (degrees/mm): Measurement of the tortuosity (twistedness) of the track, calculated as Turning Angle divided by the speed. Shown as median value in degrees/mm.
10. Turning angle (degrees): Median angle of all turns a fly does in the arena.
11. Centrophobism while moving: The arena is divided in an inner and outer ring of equal size. The ratio of time spend in the inner and outer ring is calculated. 1 signifies the fly has spent all its time in the outer part of the arena. —1 signifies the fly was at all times in the inner part of the arena. 0 would signify an equal distribution between inner and outer part of the arena:
Only parts of the track while the fly is moving count to the calculation.
12. Centrophobism while stationary: Only parts of the track while the fly is not moving count to the calculation.
13. Center deviation while moving: Deviation away from the center of the platform. Values given in percent of the radius. Only parts of the track while the fly is moving count to the calculation.
14. Center deviation while stationary: Only parts of the track while the fly is not moving count to the calculation.

Measures of angles or location relative to visual cue

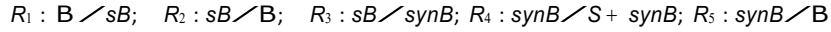
15. Absolute angle deviation: Deviation angle from the path a fly walks away from the direction of the closest stripe. Direction does not matter. Median of all deviations is reported in degrees.
16. Stripe deviation while moving: Deviation away from the idealized line through the middle of the stripe. Direction toward right or left does matter. Values given in percent of the radius
17. Stripe deviation while stationary: Deviation away from the idealized line through the middle of the stripe. Direction toward right or left does matter. Values given in percent of the radius.
18. Absolute stripe deviation while moving: Deviation away from the idealized line through the middle of the stripe. Direction toward right or left does not matter. Values given in percent of the radius.
19. Absolute stripe deviation while stationary: Deviation away from the idealized line through the middle of the stripe. Direction toward right or left does not matter. Values given in percent of the radius.
20. Angle deviation while stationary: Deviation away from the idealized line through the middle of the stripe. Direction toward right or left does not matter. Values given in percent of the radius.
21. Angle deviation while moving: Deviation angle from the path a fly walks away from the direction of the closest stripe. Direction does matter. Median of all deviations is reported in degrees.
22. Horizon deviation while moving: Deviation away from the idealized line perpendicular to the stripes. Direction toward top or bottom stripe does matter. Values given in percent of the radius.
23. Horizon deviation while stationary: Deviation away from the idealized line perpendicular to the stripes. Direction toward top or bottom stripe does matter. Values given in percent of the radius.
24. Absolute horizon deviation while moving: Deviation away from the idealized line perpendicular to the stripes. Direction toward top or bottom stripe does not matter. Values given in percent of the radius.
25. Absolute horizon deviation while stationary: Deviation away from the idealized line perpendicular to the stripes. Direction toward top or bottom stripe does not matter. Values given in percent of the radius.

The data was statistically analyzed using the Kruskal-Willis rank sum test and pairwise Wilcoxon rank sum test as a post hoc test using R. (The post hoc test was corrected with the Benjamini-Hochberg procedure to correct for multiple comparison.)

Mathematical modeling

We adapted the data-driven stochastic model from Özel et al., 2019 by omitting the filopodia compartment and estimating temperature-specific parameters from the live imaging data (bulbous life time, number of bulbous tips at P60). In brief, we modeled synapses (S), short-lived transient bulbous tips (sB) and stable synaptogenic bulbous tips (synB).

The model's reaction stoichiometries are determined by the following reaction scheme:



Reaction R_1 denotes the formation of a (transient) bulbous tip, while R_2 denotes its retraction. Reaction R_3 denotes the stabilization of a transient bulbous tip, a stable bulb forms a synapse with reaction R_4 , while the bulbous tip remains visible and R_5 denotes the retraction of a stable bulb. Note that in R_1 we only implicitly model filopodia as outlined below.

Similar to the published model in Özel et al., 2019, reaction rates/propensities of the stochastic model are given by

$$r_1 \delta t; B \rightarrow sB = r_1 \delta P60 \left(1 - \frac{f_1 \delta synB; B_{50}}{B_{50}} \right) \frac{f_{FB} \delta t; t}{f_{FB} \delta P60};$$

$$r_2 \delta sB \rightarrow B = c_2 sB;$$

$$r_3 \delta sB \rightarrow synB = c_3 sB;$$

$$r_4 \delta synB \rightarrow S + synB = c_4 synB;$$

$$r_5 \delta synB \rightarrow B = c_5 synB$$

where c_2, c_3, c_5 are reaction constants (estimated as outlined below). The feedback function $f_1 \delta synB; B_{50}$ models bulbous auto-inhibition due to limited resources and synaptic seeding factor competition as introduced before (Özel et al., 2019) and $r_1 \delta P60$ denotes the net rate of emergence of bulbous tips at developmental time P60. We do not consider the emergence of bulbous tips from filopodia as in previous work¹, but rather implicitly through the time-dependent function $f_{FB} \delta t$. The functions $f_{FB} \delta t$ and $f_{FB} \delta t; t_{1/2}$ model slow-scale dynamics of filopodia- and bulbous dynamics, with previously determined parameters (Özel et al., 2019):

$f_{FB} \delta t$ is a tanh function with

$$f_{FB} \delta t; t_{1/2} = \frac{1}{2} \left(1 + \tanh \frac{3}{t_{1/2}} (t - t_{1/2}) \right)$$

that models a time-dependent increase in the propensity to form bulbous tips with $t_{1/2} = 1000$ (min). The time-dependent function

$f_{FB} \delta t = \max_{i=0}^5 p_i t^i$ is a fifth-order polynome with coefficients $p_5 = -2.97 \times 10^{-14}$, $p_4 = 3.31 \times 10^{-13}$, $p_3 = -1.29 \times 10^{-9}$, $p_2 =$

2.06×10^{-6} , $p_1 = -1.45 \times 10^{-3}$ and $p_0 = 1$ that downregulates the generation of new filopodia at a slow timescale. Note, that t denotes the time in (min) after P40 (e.g., $t_{P40} = 0$ and $t_{P60} = 60 \times 20 \times \text{scaling factor}$), which is scaled according to the factors discussed in the section 'Developmental time adjustment' below. The model was simulated using the Gillespie algorithm as outlined in (Özel et al., 2019).

'Developmental time' adjustment.

At 25°C, the pupal developmental stages correspond to the number of hours passed since pupation. For example, 'P60' refers to the pupal development stage observed at 60 hours past pupation at 25°C. For the different temperatures the pupal development stages correspond to different durations past pupation. We measured that at 18°C, the pupal development stage P100 is achieved 200.88 hours after pupation. At 29°C it is achieved after 88.08 hours. Thus, for the different temperatures there are distinct factors that relate real time to pupal development stage as shown here:

temp	developmental time P0 to P100 [hours]	factor
18°C	200.88	2.05
25°C	98.16	1.00
29°C	88.08	0.90

We used these scaling factors to relate *real time* to *developmental time* in our model simulations

Parameter estimation

Using the methods explained below, we derived the parameters as shown below.

We first investigated the lifetimes of bulbous tips (Figure 1F) and fitted parameter c_2 and c_5 which relates to the retraction of short- and long-lived bulbous tips, as shown in Figure S13.

We then estimated the three parameters $r_1 \delta t = P60$; c_3 and B_{50} . To do so, we used the number distribution of short-lived and syn-aptogenic bulbous tips and set up the generator matrix

$$G_{[i,j];[i-1,j]} = i c_2; \quad G_{[i,j];[i,j-1]} = j c_5$$

$$G_{[i,j];[i+1,j]} = r_1 \delta P60 \rho_s f_1 \delta_j / B_{50}; \quad G_{[i,j];[i,j+1]} = j c_3$$

with diagonal elements such that the row sum equals 0. In the notation above, the tuple $[i, j]$ denotes the state where i short-lived bulbous tips sB and j synaptogenic bulbous tips $synB$ are present. The generator above has a reflecting boundary at sufficiently large N (maximum number of bulbous tips). Above, $r_3 \delta t$ is auto-inhibited by the number of stable bulbous tips through function f_1 . The stationary distribution of this model is derived by solving the eigenvalue problem

$$G^T v = v \lambda$$

and finding the eigenvector corresponding to eigenvalue $\lambda_0 = 0$. From this stationary distribution, we compute the marginal densities of sB and $synB$ (e.g., summing over all states where $i = 0, 1, \dots$ for sB) and fit them to the experimentally derived frequencies by minimizing the Kullback-Leibler divergence between the experimental and model-predicted distributions. Estimated parameters $r_1 \delta t = P60$; c_3 and B_{50} are shown in the following table:

	$r_1(P60)$	B_{50}	c_2	c_3	c_4	c_5
18°C	0.3056	0.1187	0.0706	0.0427	0.0033	0.006
25°C	0.0860	0.3505	0.0706	0.0207	0.0091	0.006
29°C	0.0569	0.1044	0.0706	0.0081	0.0200	0.006

Finally, c_4 was determined based on measured synapse numbers at P100.

Supplemental information

Brain connectivity inversely scales

with developmental temperature in *Drosophila*

Ferdi Ridvan Kiral, Suchetana B. Dutta, Gerit Arne Linneweber, Selina Hilgert, Caroline Poppa, Carsten Duch, Max von Kleist, Bassem A. Hassan, and P. Robin Hiesinger

Figure S1

A

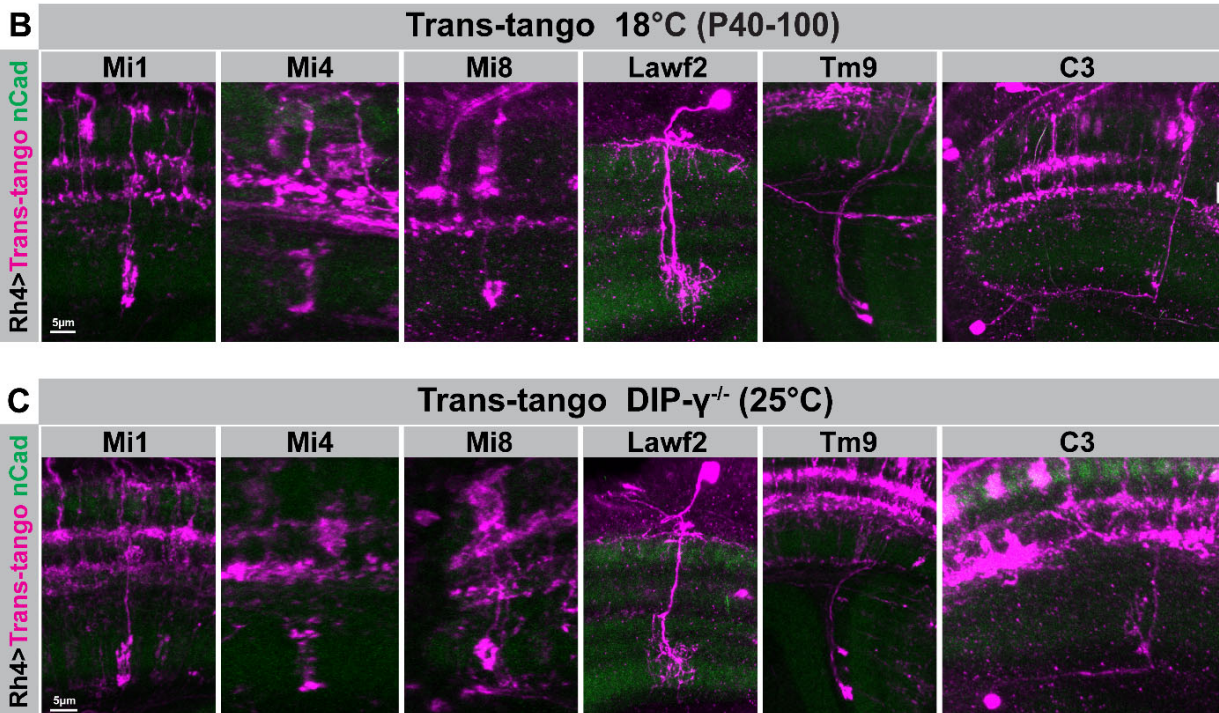
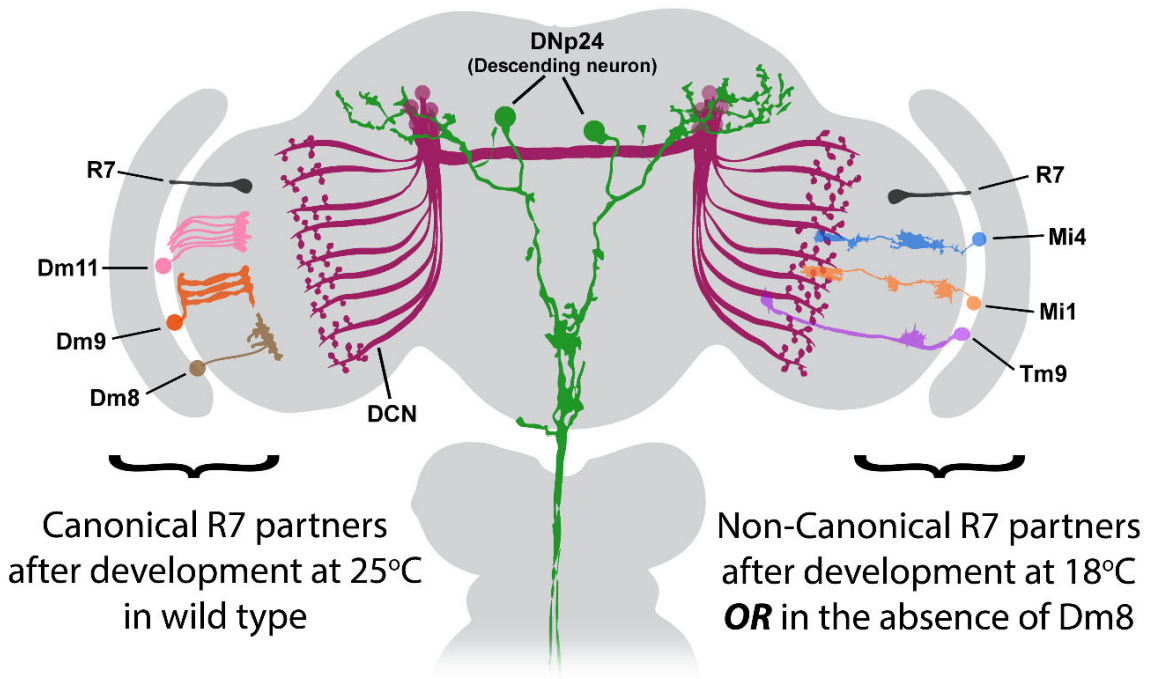


Figure S1. γ R7s connect to the same types of non-canonical postsynaptic partners in wild type after development at 18°C and in DIP γ mutants after development at 25°C. Related to Figures 2 and 3.

(A) Schematic of neurons investigated in this study. The left side depicts canonical R7 partnerneurons, the right side non-canonical R7 partners. (B-C) Representative images of neurons postsynaptically connected to γ R7 photoreceptors in wild-type brains after development at 18°C (B) and in DIP γ mutant brains after development at 25°C (C). Note that development at 18°C in wild type and at 25°C in the DIP γ mutant leads to non-canonical synaptic partnerships with the same type of neurons.

Figure S2

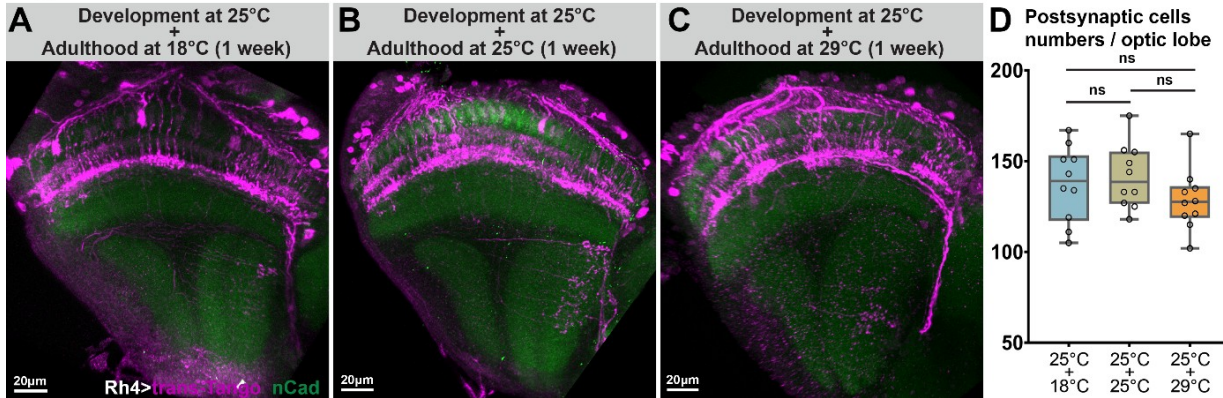


Figure S2. Alterations of temperature during the first week of life do not lead to differences in postsynaptically connected cell numbers. Related to Figure 2.

(A-C) Representative images of neurons postsynaptically connected to yR7 photoreceptors in brains developed at 25°C and then shift to either 18°C (A), kept at 25°C (B) or shift to 29°C (C) during the first week of adult life prior to a trans-Tango experiments. (D) The number of neurons connected to yR7 photoreceptors do not significantly change when developed at the same temperature (25°C) and exposed to different ‘functional’ temperatures during adulthood. n=10 optic lobes (from 10 individual flies) per condition. Data was analyzed with the Kruskal-Wallis test and Dunn’s as post-hoc test; ns=not significant.

Figure S3

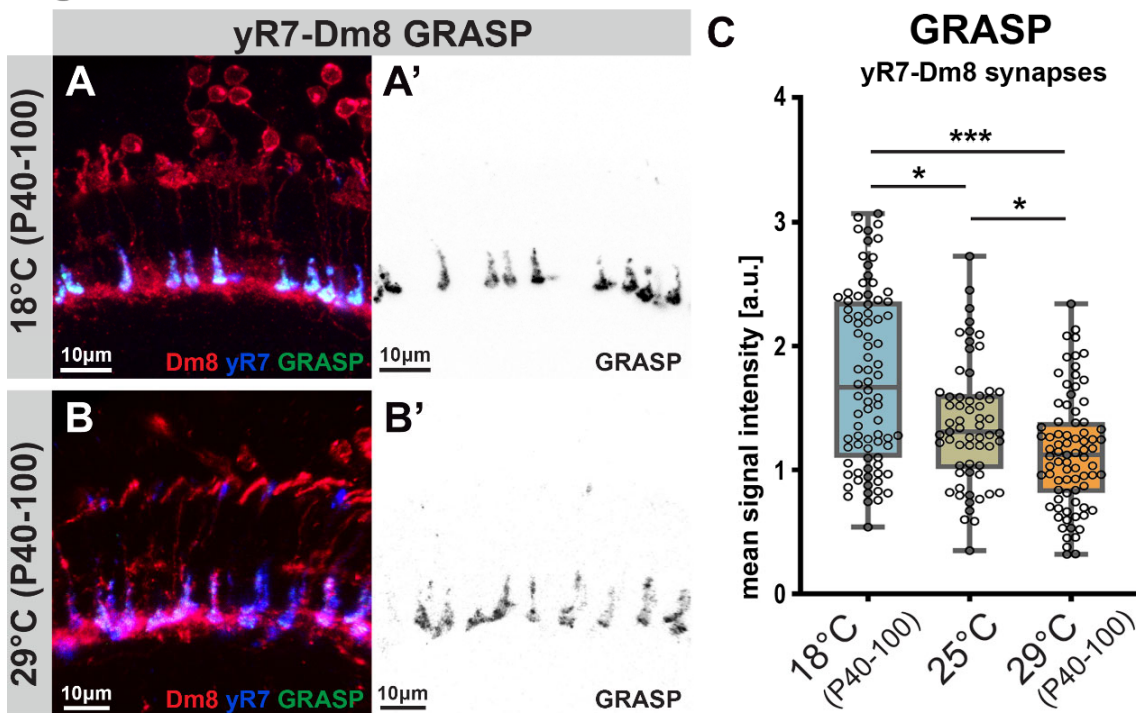


Figure S3. Activity-dependent GRASP labeling of yR7s and their main synaptic partner Dm8 scales with developmental temperature. Related to Figure 2.

(A-B') Representative images of activity-dependent GRASP between yR7s and Dm8 after development at 18°C (A-A') and after development at 29°C (B-B'). (C) Low developmental temperature scales with the GRASP signal between yR7s and their main synaptic partner Dm8. n=85 terminals, 13 flies per condition. Data was analyzed with the Kruskal-Wallis test and Dunn’s as post-hoc test; *p<0.0332, ***p<0.0002.

Figure S4

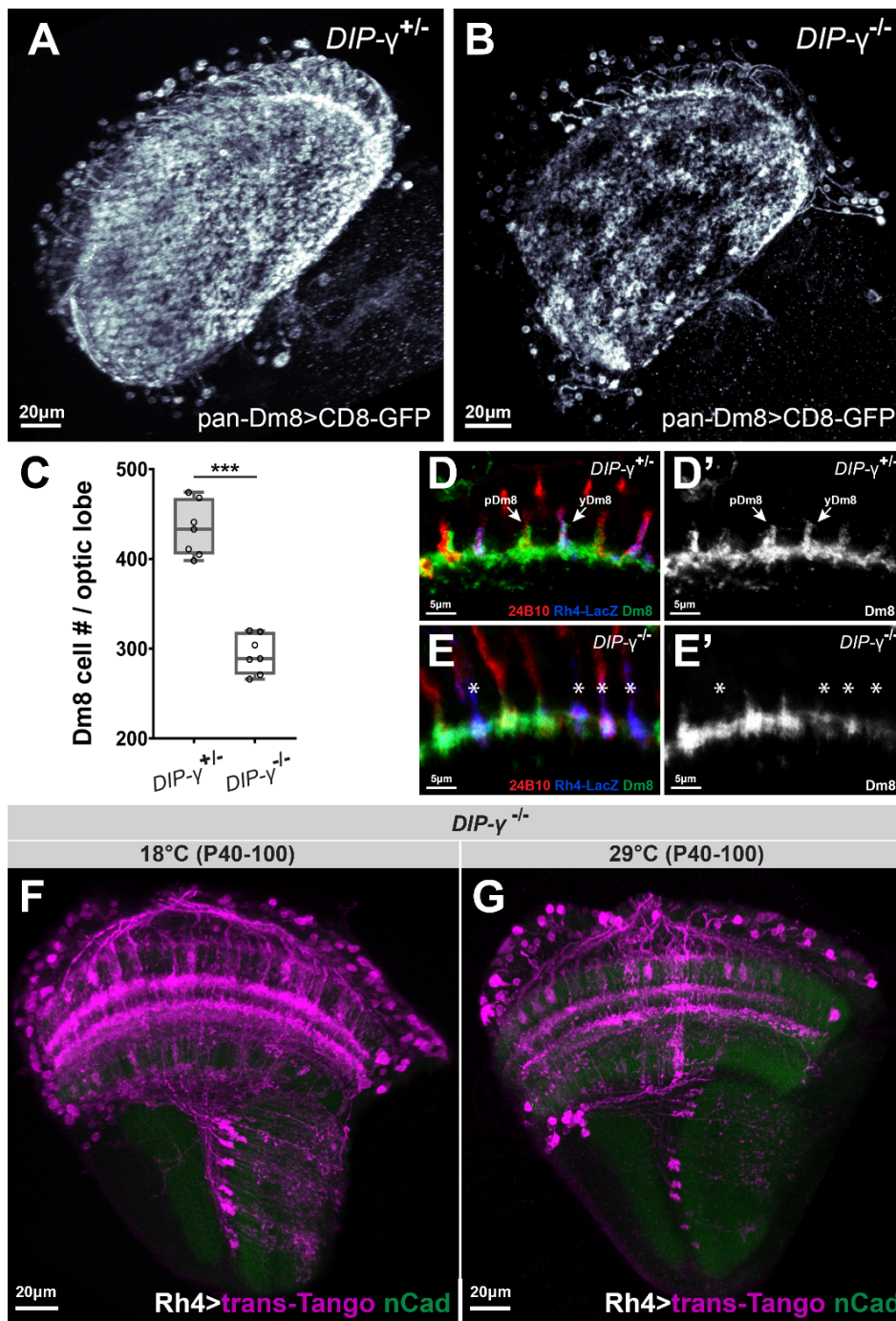


Figure S4. Loss of the majority of $DIP\gamma^+Dm8$ neurons leads to increased recruitment of non-canonical synapses of $yR7$ neurons. Related to Figure 3.

(A-C) $DIP\gamma$ loss-of-function leads to cell death of the majority of $DIP\gamma^+Dm8$ neurons. $n=7$ opticlobes (from 7 individual flies) per condition. (D-E) Surviving $DIP\gamma^+Dm8$ neurons lack distal membrane protrusions at medulla layers M4-M5. (F-G) Non-canonical partner neurons (Mi cells, C2/C3 cells, and Tm9) in $DIP\gamma$ mutant brains scale with developmental temperatures of 18°C (F) and 29°C (G), revealing an additive effect of low developmental temperature and main synaptic partner loss on partner availability. Data was analyzed with the Kolmogorov-Smirnov test; *** $p < 0.0002$.

Figure S5

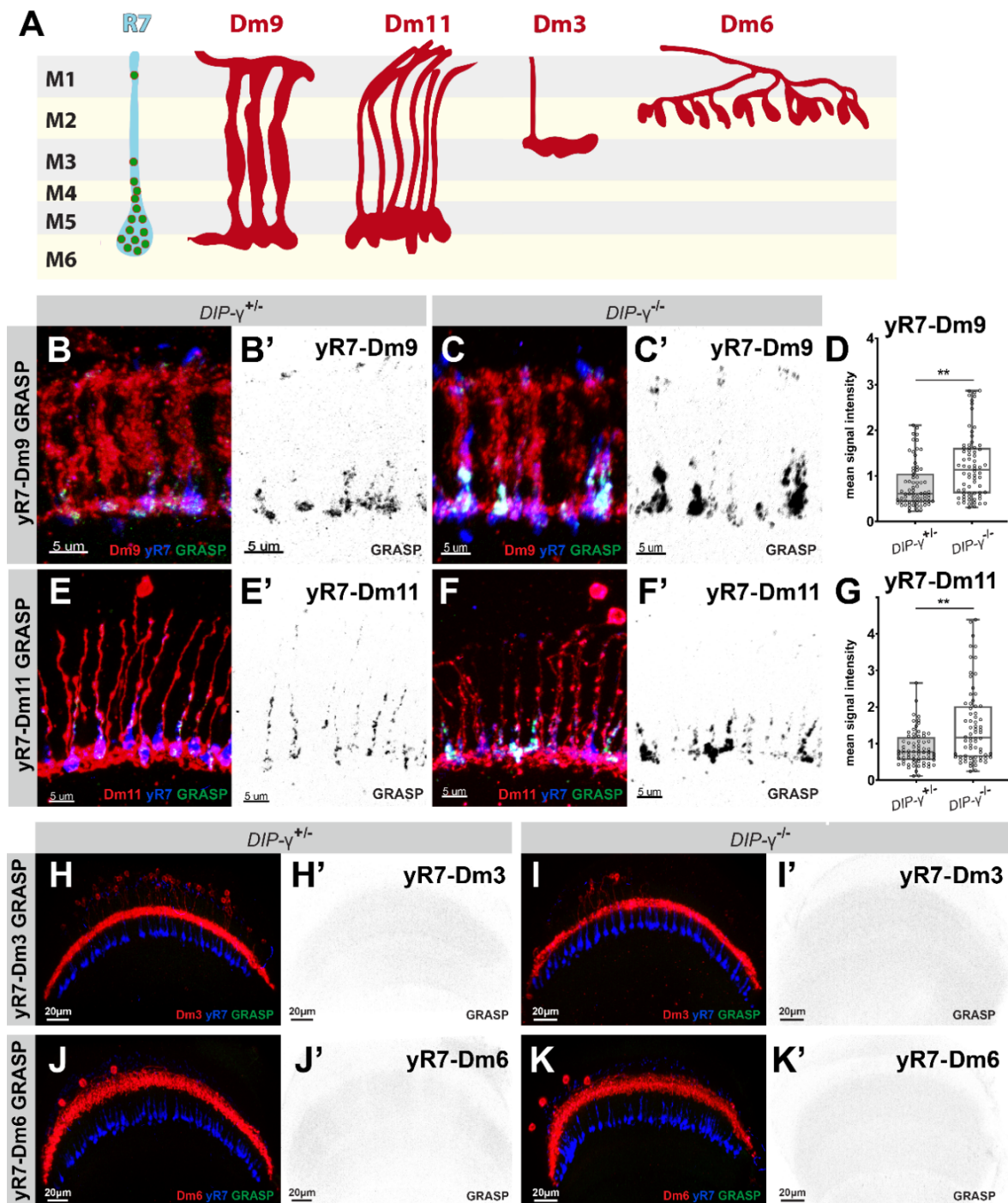


Figure S5. Loss of the majority of $DIP\gamma^+$ Dm8 neurons leads to increased activity-dependent GRASP signals of yR7 with canonical synaptic partners Dm9 and Dm11. Related to Figure 3.

(A) Schematic representations of Dm9, Dm11, Dm6, and Dm3 neurons with an R7 terminal through medulla layers M1-M6. Green dots demonstrate the distribution of active zones in R7 terminals based on the connectome data. (B-G) Activity-dependent GRASP between yR7s and Dm9 (B-D) and between yR7s and Dm11 (E-G) in control and $DIP\gamma$ mutant brains reveals stronger synaptic connections with the loss of main synaptic partner Dm8. $n=70-80$ terminals, 10-12 flies per condition. (H-K') Dm8 neuron loss in $DIP\gamma$ mutants does not lead to synapse formation with neurons (Dm3 and Dm6) that do not have dendritic branches in medulla layers. Data was analyzed with the Kolmogorov-Smirnov test; ** $p < 0.0021$.

Figure S6

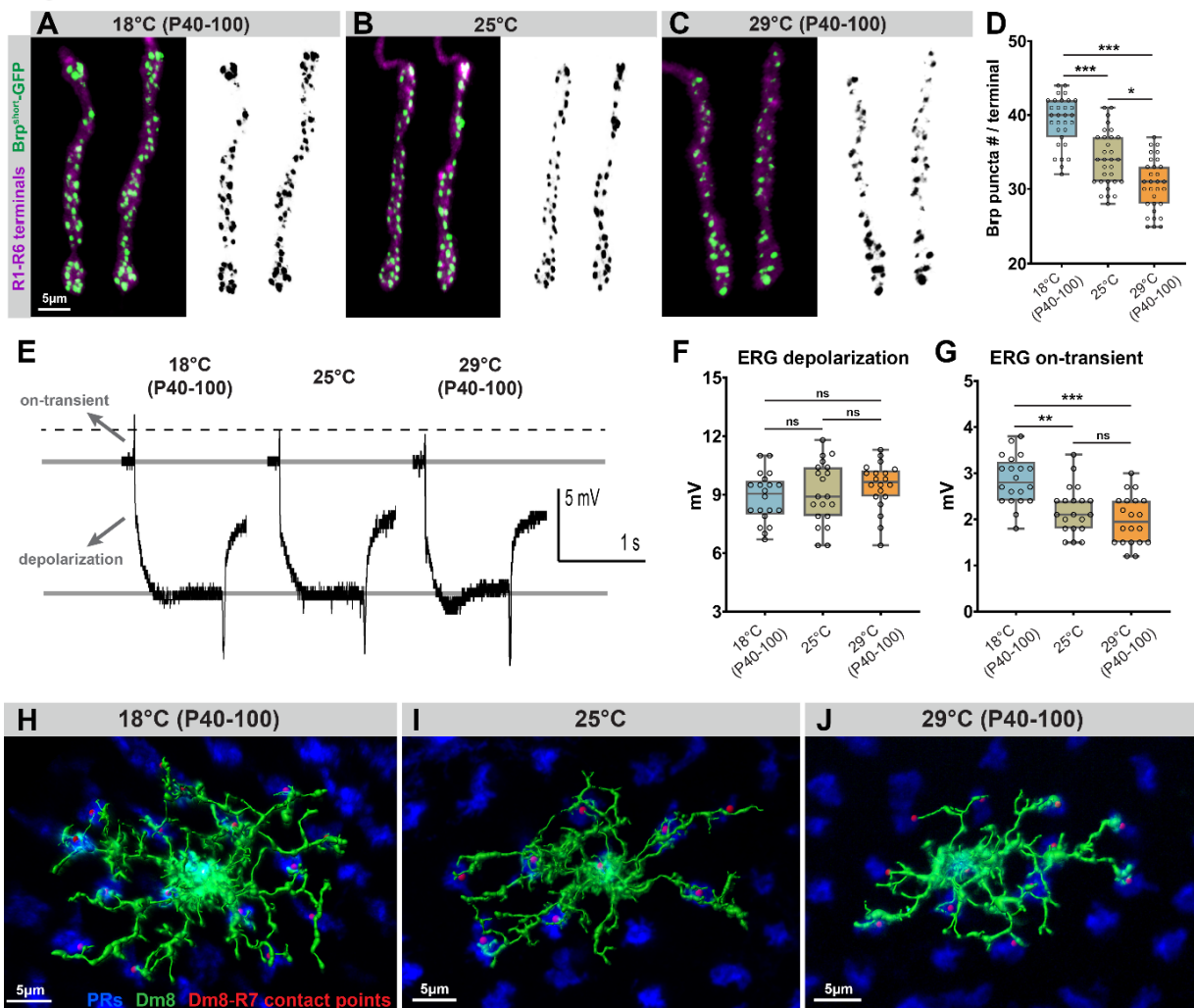


Figure S6. R1-R6 photoreceptor synapse number and neurotransmission as well as Dm8 arborizations scale with developmental temperature. Related to Figure 4.

(A-C) Representative images of R1-R6 photoreceptor axon terminals with GFP-BrpD3 (Brp^{short}) marked active zones developed at 18°C (A), 25°C (B), and 29°C (C). (D) The number of active zones per R1-R6 terminal at different developmental temperatures. n=30 terminals, 6 flies per condition. (E) Representative electroretinogram (ERG) traces recorded from fly eyes developed at 18°C, 25°C, and 29°C. (F) Developmental temperature does not affect phototransduction based on ERG 'depolarization' amplitudes. n=20 flies per condition. (G) Low developmental temperature increases neurotransmission of R1-R6 photoreceptors based on ERG 'on-transient' amplitudes. n=20 flies per condition. Data was analyzed with the Kruskal-Wallis test and Dunn's as post-hoc test; *p<0.0332, **p<0.0021, ***p<0.0002, ns=not significant. (H-J) Skeleton reconstructions of Dm8 cells developed at 18°C (A), 25°C (B), and 29°C (C).

Figure S7

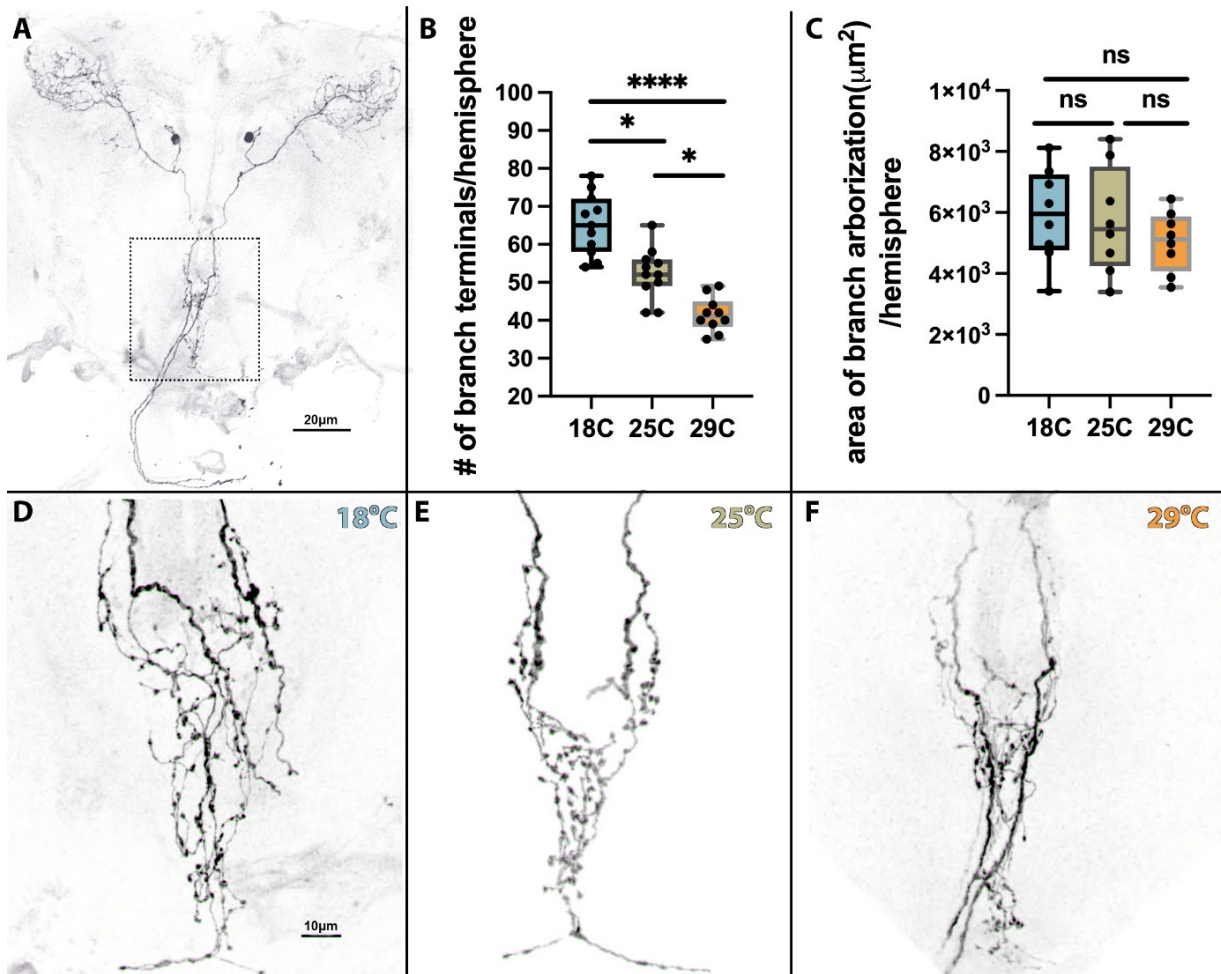


Figure S7. The descending neurons DNp24 exhibits temperature-dependent branch numbers, but temperature-independent areas of branch coverage. Related to Figure 4.

(A) Expression of the Janelie SS00732 split-Gal4 line. (B-C) quantification of axonal branches shown in the boxed region in (A). (D-F) representative pictures of the axonal branches after developmental at three different temperatures.

Figure S8

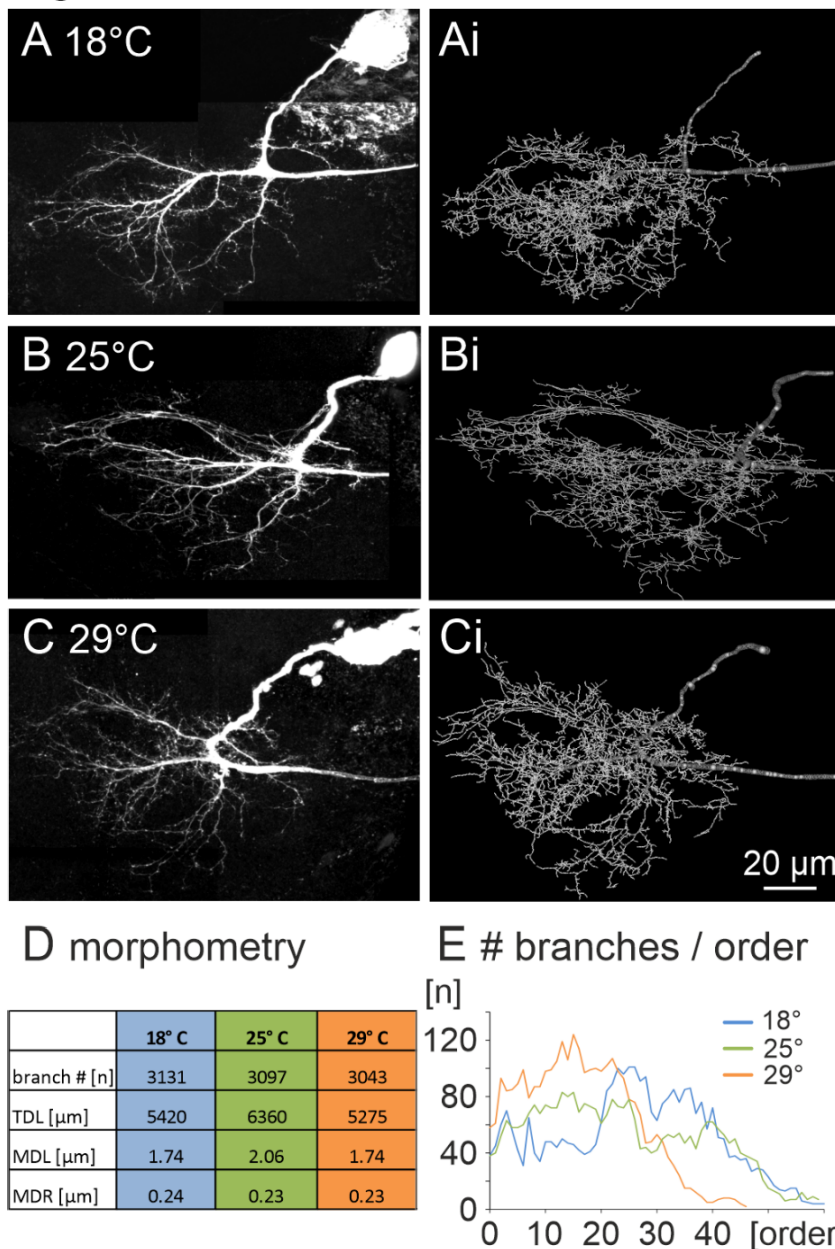


Figure S8. Developmental temperature does not affect motoneuron dendritic branch number but branch organization. Related to Figure 4.

(A-C) Maximum intensity projection views from confocal image stacks of representative adult DLM motoneurons filled intracellularly after pupal development at 18°C (A), 25°C (B), and 29°C (C). (Ai-Ci) 3D geometric reconstructions of the motoneuron dendrites shown in A-C.

(D). The number of branches, total dendritic length (TDL), the mean length of all dendritic branches in a reconstruction (MDL), and the mean radius of all dendritic branches (MDR) for 18°C (blue), 25°C (green), and 29°C (orange). (E) For each temperature the number of dendritic branches is plotted over the branch order in which these branches occur. The primary neurite connecting the soma and the axon was defined as tree origin, and thus branch order 0. Any dendrite branching off the origin is branch order 1, any dendrite branching off order n is defined as order n+1.

Figure S9

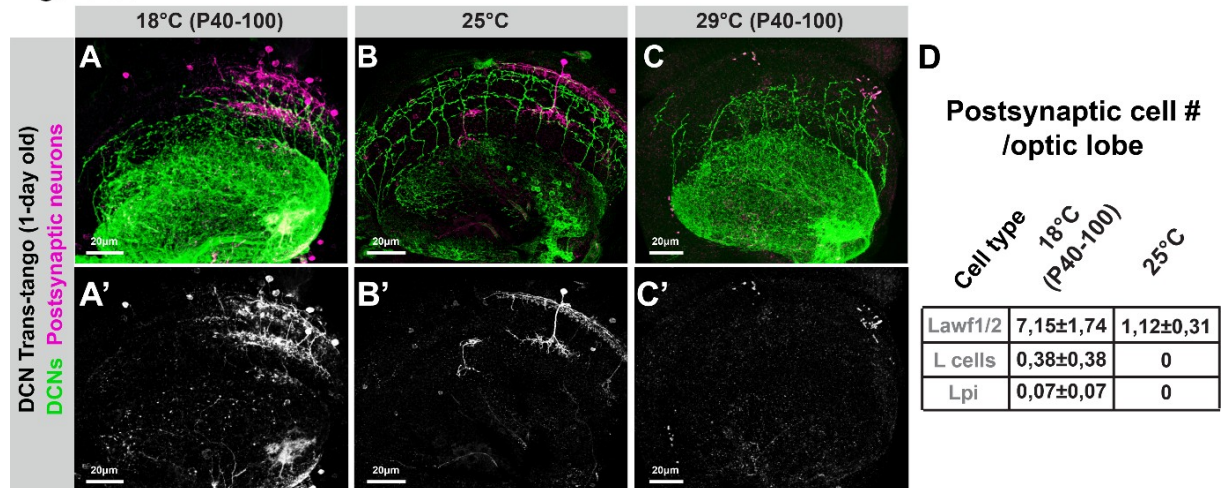


Figure S9. Branch elaboration and partner availability of DCNs scale with developmental temperature. Related to Figures 4 and 5.

(A-C) Low developmental temperature leads to more widespread labeling of neurons postsynaptically connected to DCNs. (D) rarely connected cell types (L cells and Lpi cells) were only observed when brains developed at 18°C. n=8 optic lobes (from 8 individual flies) per condition.

Supplementary Figure S10 - Behavioral Temperature 25°C

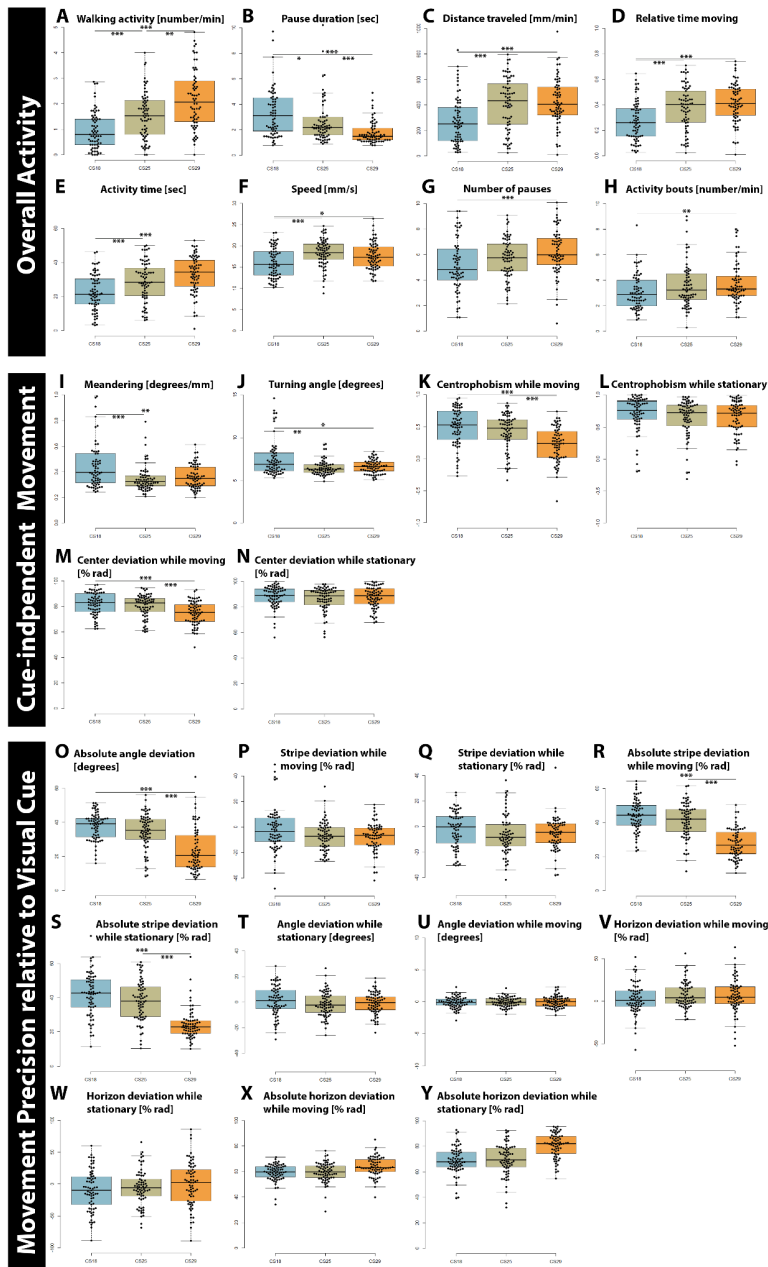


Figure S10. Analysis of 25 behavioral parameters in Buridan's paradigm at a behavioral temperature of 25°C. Related to Figure 6.

(A-H) Most parameters related to overall activity of flies in Buridan arena increase after development at high temperatures. (I-Y) Parameters related to cue-dependent and cue-independent movement precision are largely temperature-compensated. n=70 flies per condition. See Table S3 for quantifications.

Supplementary Figure S11 - Behavioral Temperature 18°C

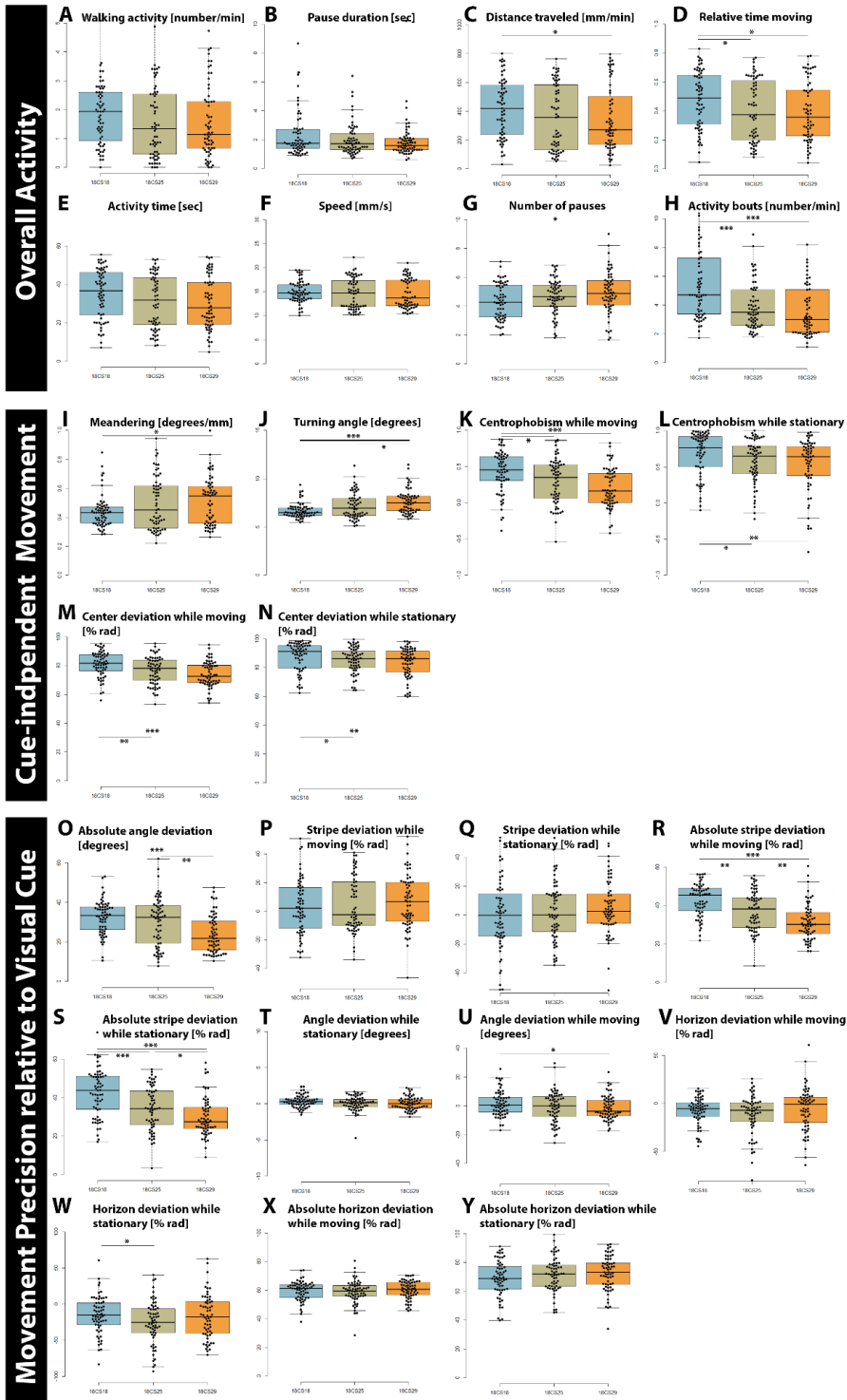


Figure S11. Analysis of 25 behavioral parameters in Buridan's paradigm at a behavioral temperature of 18°C. Related to Figure 6.

(A-H) Most parameters related to overall activity of flies in Buridan arena increase after development at high temperatures. (I-Y) Parameters related to cue-dependent and cue-independent movement precision are largely temperature-compensated. n=70 flies per condition.

Supplementary Figure S12 - Behavioral Temperature 29°C

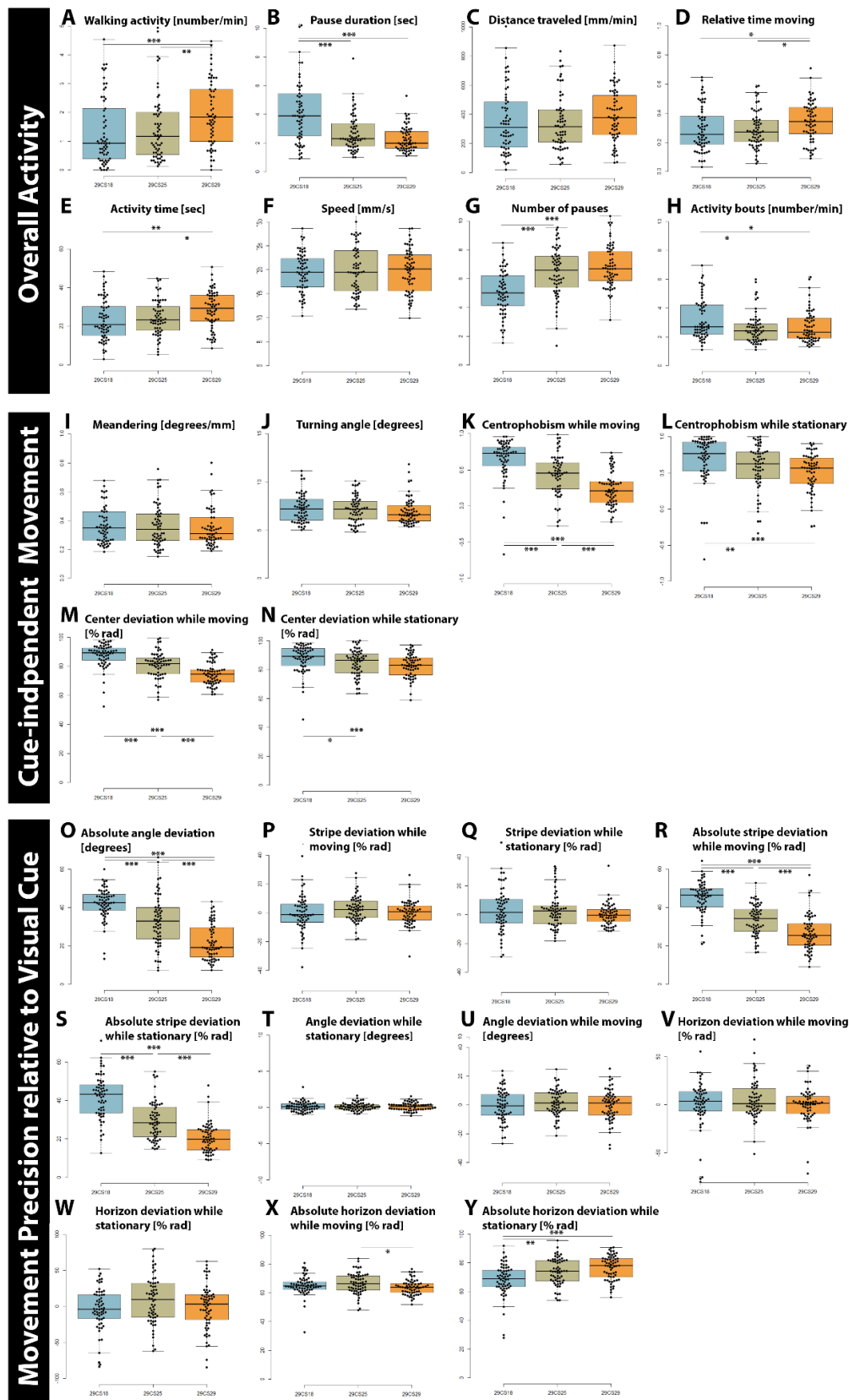


Figure S12. Analysis of 25 behavioral parameters in Buridan's paradigm at a behavioral temperature of 29°C. Related to Figure 6.

(A-H) Most parameters related to overall activity of flies in Buridan arena increase after development at high temperatures. (I-Y) Parameters related to cue-dependent and cue-independent movement precision are largely temperature-compensated. n=70 flies per condition.

Figure S13

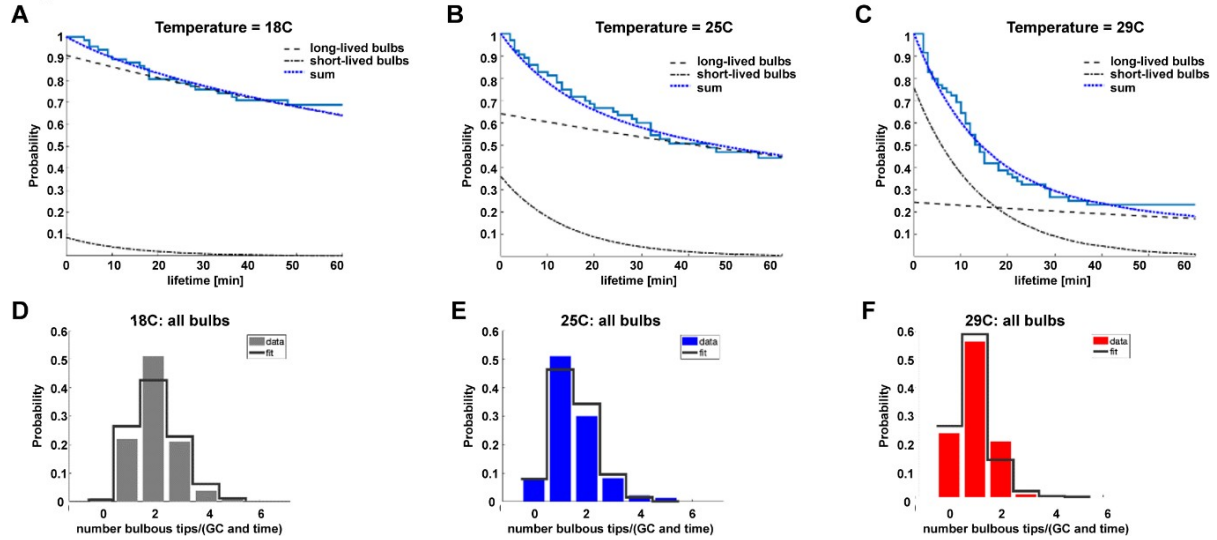


Figure S13. Quantitative analyses of R7 bulbous tips (synptogenic filopodia) lifetimes and numbers. Related to STAR Methods.

(A-C) Data derived (solid blue stairs) and fitted (continuous dotted blue line) bulbous lifetimekinetics. We assumed that the life time kinetics are resulting from the combined kinetics of short-lived and synptogenic bulbous tips (black dotted and dashed lines). Fitted parameters: $c_2 = 0.0706 \text{ min}^{-1}$; retraction rate of the synptogenic bulbous tips was estimated to be $c_5 = 0.006 \text{ min}^{-1}$ and the proportion of synptogenic bulbous tips was 0.92, 0.64 and 0.24 at 18, 25 and 29°C. (D-F) Data derived (bars) and fitted (solid line) numberdistribution for bulbous tips at developmental stage P60 for 18, 25 and 29°C.

	18	sem	25	sem	29	sem	25/18	29/18	29/25
R7 Filopodia speed (um/min)	0,827	0,058	1,155	0,072	1,472	0,079	1,396614	1,779927	1,274459
R7 Filopodia Lifetime (min)	10,088	0,807	6,638	0,627	4,3	0,429	1,519735	2,346047	1,543721
R7 BrpD3 active zones (#/terminal)	24,65	0,523	20,65	0,323	16,35	0,597	1,193705	1,507645	1,262997
R7 trans-Tango (# cell/optic lobe)	183,7	7,106	145,3	7,027	133,8	6,335	1,264281	1,372945	1,085949
R7-Dm8 GRASP (mean signal int.)	0,17	0,008	0,137	0,006	0,116	0,005	1,240876	1,465517	1,181034
R7-Dm9 GRASP (mean signal int.)	0,093	0,009	0,066	0,006	n/a	n/a	1,409091	n/a	n/a
R7-Dm11 GRASP (mean signal int.)	0,115	0,011543	0,079	0,003	n/a	n/a	1,455696	n/a	n/a
DCN Filopodia speed (um/min)	0,235738736	0,01946	0,372921847	0,031406	0,761213	0,105939	1,581929	3,229053	2,041213
DCN primary branch number	7,074074074	0,417336	5,227272727	0,40649	2,62069	0,209537	1,353301	2,699318	1,994617
DCN secondary branch number	3,676470588	0,54257	1,484848485	0,267191	0,489796	0,115911	2,47599	7,506127	3,031566
DCN BrpD3 active zones (#/terminal)	0,275	0,008	0,241	0,009	0,104	0,01	1,141079	2,644231	2,317308
DCN trans-Tango (# cells/optic lobe)	88,83	9,964	55	2,637	13	2,65	1,615091	6,833077	4,230769
DCN-Lawf1 GRASP (mean signal int.)	0,259354806	0,009516	0,173174065	0,00545	n/a	n/a	1,497654	n/a	n/a
R1-6 BrpD3 active zones (#/terminal)	39,223	0,595	34,097	0,668	30,548	0,637	1,150336	1,283979	1,116178
R1-6 ERG on transient (mV)	2,85	0,118433	2,205	0,114817	1,985	0,118383	1,292517	1,435768	1,110831
R1-6 ERG depolarization (mV)	8,855	0,283445	9,095	0,356996	9,46	0,273515	0,973612	0,936047	0,961416
Dm8 branch numbers	321,28	14,4	259,94	11,29	215,87	8,35	1,235978	1,488303	1,204151
Dm8 total branch length	505,5074801	25,38734	429,0747891	20,30404	328,7044	16,81363	1,178134	1,537878	1,305351
Dm8 overlap with #R7s	14,733333333	0,693278	11,76470588	0,525311	10,23529	0,565747	1,252333	1,439464	1,149425
Mi4 branch numbers	284,12	9,06	246,43	8,93	197	6,14	1,152944	1,442234	1,250914
Mi4 total branch length	397,4117872	12,90929	349,6517454	11,07318	274,7308	7,369114	1,136593	1,44655	1,272707

Table S1. Related to Figures 1, 2, 3, 4, and 5. Summary of quantitative analyses of temperature effects in wild type.

	<i>DIPy</i> control	sem	<i>DIPy</i> null	sem	<i>DIPy</i> null/control
R7-Dm8 GRASP (mean signal int.)	0,12866698	0,010655	0,074990253	0,007825	0,58282438
R7-Dm9 GRASP (mean signal int.)	0,07956988	0,005975	0,122924772	0,00872	1,544865632
R7-Dm11 GRASP (mean signal int.)	0,087511903	0,005743	0,147890694	0,012554	1,689949474
R7-Mi1 GRASP (mean signal int.)	0,008177834	0,000401	0,080416746	0,005984	9,833502068
R7-Mi4 GRASP (mean signal int.)	0,007972476	0,000409	0,045601459	0,003249	5,719861385
R7-Tm9 GRASP (mean signal int.)	0,006905958	0,000597	0,041563339	0,002742	6,018475543

Table S2. Related to Figure 3. Summary of quantitative analyses of temperature effects in *DIPy* mutants.

	25/18	29/18	29/25	
Walking activity	1,597938144	2,278350515	1,425806452	Temperature-Dependent
Pause duration	1,541818182	2,141414141	1,388888889	
Distance traveled	1,505164492	1,560668995	n.s.	
Relative time moving	1,407407407	1,518518519	n.s.	
Meandering	1,351351351	1,388888889	n.s.	
Activity time	1,311461067	1,46544182	n.s.	
Turning angle	1,178678679	1,193009119	n.s.	
Speed	1,143125	1,09875	n.s.	
Number of pauses	n.s. (p=0.053)	1,202312139	n.s. (p=0.06)	
Activity bouts	n.s.	1,179245283	n.s.	
Centrophobism while moving	n.s.	2,272727273	1,909090909	
Absolute stripe deviation while moving	n.s.	1,718685832	1,566735113	
Absolute stripe Deviation while stationary	n.s.	1,605501267	1,491132827	
Absolute angle Deviation	n.s.	1,595699831	1,452782462	
Absolute horizon deviation while stationary	n.s.	n.s.	1,154741379	
Absolute horizon deviation while moving	n.s.	n.s.	1,071260504	
Center deviation while moving	n.s.	n.s.	0,931900537	Temperature-Compensated
Stripe deviation while stationary	n.s. (p=0.051)	n.s.	n.s.	
Stripe deviation while moving	n.s. (p=0.057)	n.s.	n.s.	
Angle deviation while stationary	n.s.	n.s.	n.s. (p=0.054)	
Centrophobism while stationary	n.s.	n.s.	n.s.	
Horizon deviation while stationary	n.s.	n.s.	n.s.	
Center deviation while stationary	n.s.	n.s.	n.s.	
Angle deviation while moving	n.s.	n.s.	n.s.	
Horizon deviation while moving	n.s.	n.s.	n.s.	
overall activity				
movement angles or location independent of visual cue				
movement angles or location relative to visual cue				

Table S3. Related to Figure 6. Summary of quantitative analyses of behavioral parameters.

7. Manuscript 3

A neurodevelopmental origin of behavioral individuality in the *Drosophila* visual system

Gerit Arne Linneweber, Maheva Andriatsilavo, **Suchetana B. Dutta**, Mercedes Bengochea, Liz Hellbruegge, Guangda Liu, Radoslaw K. Ejsmont, Andrew D. Straw, Mathias Wernet, Peter Robin Hiesinger, Bassem A. Hassan

Science, Volume 367, Issue 6482, 1112-1119 March 2020

Contribution

I designed, performed, and analyzed experiments showing the stability of adult DCN branching pattern. I also contributed in DCN neural reconstruction for individual flies tested and painting fly eyes to perform behavioral tests for asymmetric visual input. The original article including the supplemental information is included on the following pages and available online at:

[DOI: 10.1126/science.aaw7182](https://doi.org/10.1126/science.aaw7182)

8. Manuscript 4

A GRASP based screening pipeline reveals new connectivity in the *Drosophila* visual system

Suchetana B. Dutta, Maheva Andriatsilavo, Bassem Hassan, Peter Robin Hiesinger and Gerit Arne Linneweber

The manuscript is in preparation

Contribution

I designed, performed and analyzed all experiments in this chapter along with Maheva Andriatsilavo and Gerit Linneweber under the supervision of Prof. Dr. P. Robin Hiesinger and Prof. Dr. Bassem Hassan. I contributed to writing the chapter along with Maheva Andriatsilavo and Gerit Linneweber.

Article

A GRASP based screening pipeline reveals new connectivity in the *Drosophila* visual system

Suchetana B. Dutta^{1,#}, Maheva Andriatsilavo^{1,2,#}, Bassem A. Hassan², Peter Robin Hiesinger¹ and Gerit Arne Linneweber^{1,#,*}

¹Division of Neurobiology, Institute for Biology, Freie Universität Berlin, 14195 Berlin, Germany.

²Institut du Cerveau et de la Moelle Épineière (ICM) - Hôpital Pitié-Salpêtrière, Sorbonne Université, Inserm, CNRS, Paris, France.

Equal contribution

*Correspondence to: gerit.linneweber@fu-berlin.de

ABSTRACT:

Mapping neuronal circuits is a key step in understanding brain function. Abnormal neuronal circuit formation is causal to several neurodevelopmental or psychiatric disorders. Light-microscopic and high-throughput techniques have emerged in the last decade facilitating synaptic partner tracing. The GFP Reconstitution Across Synaptic Partners technique (GRASP) is a key light-microscopic method to confirm neuronal connections and in its more modern versions active synapses. Its commonly used protocol lacks the methodological nuance of being able to visualize both pre- and postsynaptic partners along with reconstituted synaptic GFP. In this study, we have modified the standard GRASP protocol and have taken advantage of polyclonal GFP antibody properties to recognise presynaptically targeted splitGFP1-10. By combining both mono- and polyclonal GFP antibodies along with the detection of the membrane marker CD4, we were able to simultaneously visualize pre- and postsynaptic components of a particular circuit. This method not only works with activity dependent GRASP but is robust enough to be adapted to other CD4-GRASP-like methods and perform high-throughput screens. As a proof of concept, through a GRASP screen we could identify partners of the T4/5 motion detection neurons in the *Drosophila* visual system. Hence, we show the adaptability of our approach to high-throughput screening systems for synaptic partner search in neurobiology.

INTRODUCTION:

The precision of neuronal wiring is of crucial importance, as imperfect neuronal connections or malformations of neuronal circuit underlie various neuropsychiatric (Andrews et al., 2017) or neuro-developmental (Di Martino et al., 2014). Thus, studying synaptic specificity at a cellular level is crucial for our understanding of circuit formation. Electron microscopy and electrophysiology are powerful and important techniques to visualize synapses and to analyze their synaptic release properties. But both techniques are labor intensive and require significant investments of time and only reflect the circuit of few individuals. For example, the original ultrastructural analysis of the roughly 7000 synapses of *C.elegans* took almost a decade (White et al., 1986). Till now, the availability of whole brain connectome is limited to few organisms; including the nematode *C. elegans* (Cook et al., 2019; White et al., 1986), the *Drosophila melanogaster* larvae nervous system (Schneider-Mizell et al., 2016) and incomplete parts of the adult connectome (Scheffer et al., 2020; Takemura et al., 2013; Zheng et al., 2018)), or the tunicate *Ciona intestinalis* tadpole larvae brain (Ryan et al., 2016). Although these hallmark ultrastructural studies are extremely important to establish the connectome in several model species; they do not provide comparative high throughput analysis or subsequent functional analysis. These follow up analysis can to this date only be performed by light microscopy.

Over the last decades, light microscopic techniques have become essential to study synaptic connectivity in a high throughput comparative manner. For instance, trans-synaptic labelling anterograde and retrograde labeling techniques of neuron targets are efficient tools to trace pre- and post-synaptic neurons (Li et al., 2019) (Cachero et al., 2020; Talay et al., 2017). It nevertheless does not provide further tools to functional study of the identified circuit and can be biased toward the most frequent partners, which might not accurately represent active partners or synaptic strength. Genetically encoded tools have also been developed to specifically label synapses using fluorescent synaptic proteins like VAMP::GFP (Nonet, 1999) or by trans-synaptic complementation using a split-GFP version like in GFP Reconstitution Across Synaptic Partners (GRASP) technique (Feinberg et al., 2008; Kim et al., 2012). While the GRASP techniques depend on the availability of cell specific drivers, they can mark proximal partners or functional synapses in the case of the Activity-dependent GRASP (nSyb-GRASP) (Macpherson et al., 2015). Nevertheless, the signal strength might not be directly proportional to the strength of synaptic connectivity. Highly active connections that are weakly connected will produce a strong GRASP signal.

To ameliorate the technical challenges of the different GRASPs techniques and to improve their versatility, we have used the labeling specificity of monoclonal GFP and polyclonal GFP antibodies to split-GFP components to our advantage (Gordon and Scott, 2009) and combined these with a staining of the membrane marker CD4 (Macpherson et al., 2015). The GRASP technique consists of two split-GFP genetic components; spGFP1-10 fragment fused to either neurexin or neuronal synaptobrevin (nSyb) and thus localizes to the pre-synaptic sites and GFP11 is fused to CD4 membrane protein and label the post-synaptic neuron (Feinberg et al., 2008). First, we have found that the monoclonal GFP antibody labels specifically reconstituted GFP (GRASP signal) and hence detect only synaptic sites or regions of close neural contact as reported in the original studies (Feinberg et al., 2008; Gordon and Scott, 2009), the polyclonal GFP antibody is not specific and additionally binds to the spGFP1-10 fragment. Hence, by using antibodies against polyclonal GFP, monoclonal GFP and CD4 we could label pre-synaptic sites (spGFP1-10), synapses (reconstituted GFP) and post synaptic neuron

respectively. We have validated this method in different known neuronal synaptic pairs of the fly brain using both the original CD4-GRASP and the activity dependent nSyb-GRASP. Upon successful labeling of pre and post synapse along with marking functional synapses, we extended our method to screen for proximity partners of the motion detection T4/T5 neurons in the fly visual system. Using the proximity dependent CD4-GRASP we found that out of 26 selected neurons based on their projection pattern, we validated 5 neuronal populations to be in close contact with T4/T5 neurons. This study not only overcome the challenges of nSyb-GRASP but also can be implemented for high throughput genetic screens for connectome analysis.

METHODS:

Key resource table

Fly husbandry

Flies were maintained on standard cornmeal molasses food at 25°C and a 12 hour light/dark cycle unless otherwise mentioned. The following flies were used in the study:

Original GRASP Experiments:

UAS-CD4-spGFP1-10, LexAop-CD4-spGFP11(Feinberg et al., 2008)

Activity GRASP experiments

UAS-nSyb-spGFP1-10, LexAop-CD4-spGFP11, LexAop-nSyb-spGFP1-10 and UAS-CD4-spGFP11 (Macpherson et al., 2015).

Trans-tango

UAS-myr::GFP, QUAS-mtdTomato(3xHA)and trans-Tango (Talay et al., 2017)

Immunohistochemistry and Imaging

Adult brain dissections were performed in ice-cold PBS and brains were fixed with 4% PFA (v/w) in PBS for 20 - 30 minutes at room temperature. After 3 washes in PBS the brains were washed with PBS-T [PBS with 0.5% (v/v) Triton X-100 (Sigma Aldrich, # X100)]. Fixed brains were first blocked for 30 minutes and afterwards incubated with primary antibody containing 10% Normal Horse Serum in 0.5% PBS-T overnight at 4C. Following three washes with PBS-T, brains were incubated with secondary antibody solution containing 10% Normal Horse Serum in 0.5% PBS-T overnight. After 3 times 15 minutes washes with PBS-T they were washed with PBS and they were finally mounted in Vectashield H-1000 (Vector Laboratory, Burlingame, CA) anti-fade mounting medium for confocal microscopy. The primary antibodies used in this study were, Anti-HA Rat (1:250), AntiCD4 Rabbit (Sigma HPA004252, 1:500), Anti-dsRed Rabbit (1:500), Anti-FLAG Chicken (1:1000), Anti-GFP mAb Rat (1:500), Anti-GFP mAb mouse 3E6 (Life Technology A11120 1:200), Anti-GFP pAb Rabbit(1:1000), Anti-GFP pAb Goat (ab6673, 1:1000), Anti-HTH (dN-19) Goat (1:50), V5 Epitope Tag Antibody Dylight 549 Conjugated Rabbit (1:1000). Secondary antibodies were diluted at 1:500 and were as follows: Anti-chicken Cy5 Donkey, Anti-goat Alexa Fluor 488 Donkey, Anti-goat Cy5 Donkey (1:500) Jackson Immuno Research, Anti-Rabbit Cy3 Donkey, Anti-Mouse Alexa Fluor 594 Donkey, Anti-Mouse Cy5 Donkey, Anti-Rabbit Alexa Fluor 488 Donkey, Anti-Rat Alexa Fluor 488 Donkey. For confocal imaging a Leica SP8 confocal microscope equipped with a white light laser and two HyD detectors was used. Image stacks were acquired in resolution of 1024x1024x0.5 mm with a 63x lens.

Activity GRASP

Flies were grown in a 25°C, 12h-12h light/dark cycle incubator. Dissection & staining occurred as described above. Brains were stained with polyclonal GFP (anti GFP goat pAB) and monoclonal GFP (anti-GFP rat mAB) antibody to visualize postsynaptic cells and GRASP signal, respectively. Post-synaptic cells were visualized by staining with CD4 antibody

Trans-Tango

Flies for trans-Tango experiment were either kept in 18C or 25C, in 12h light/dark cycle incubator and dissected when they were either 3, or 15 days old (depending on the experiment).

RESULTS:

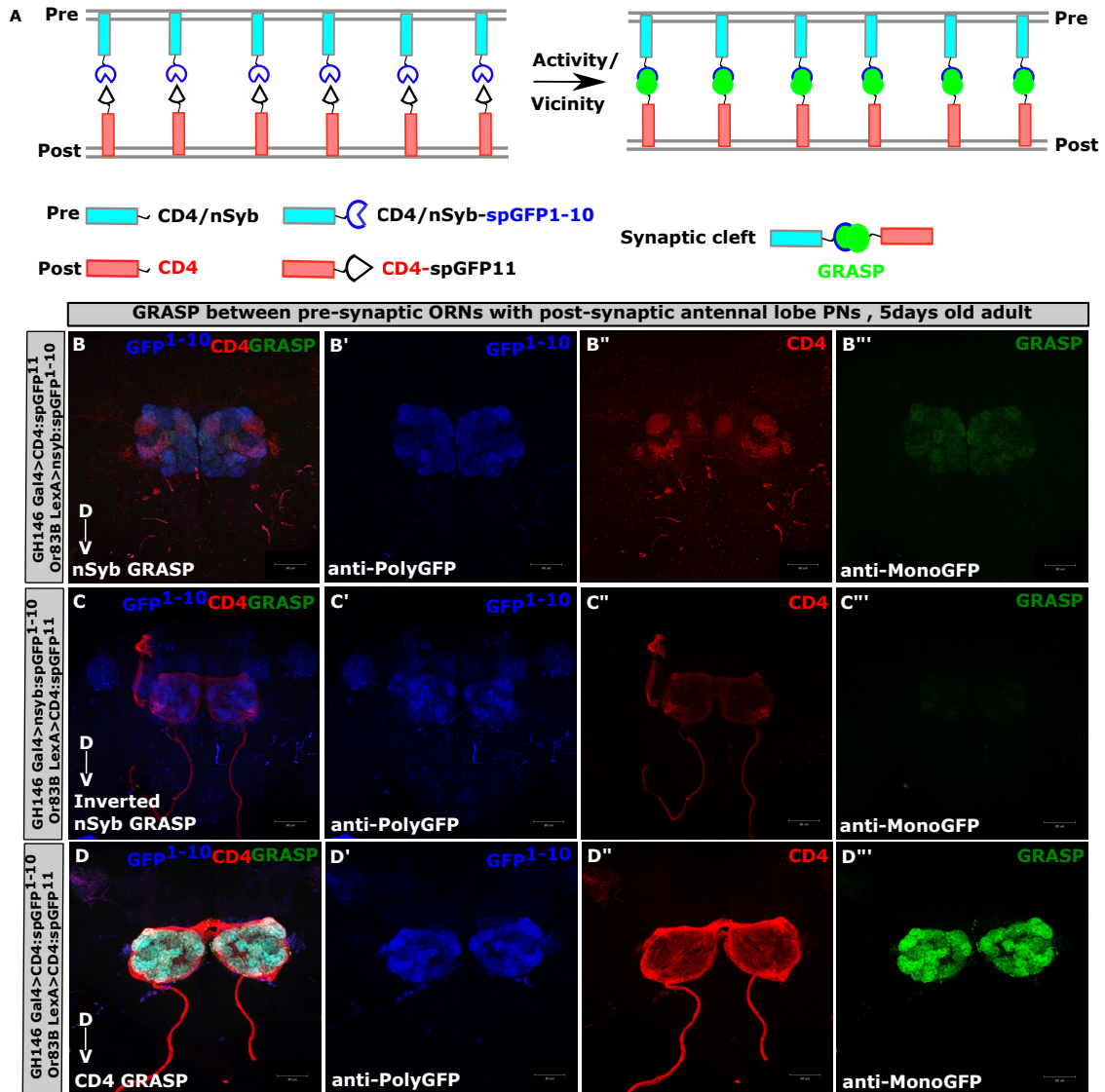


Fig.1: Validation of synaptic connection between presynaptic Olfactory receptor neurons (ORNs) with the post-synaptic antennal lobe Projection neurons (PNs) using nsyb-GRASP and CD4-GRASP

(A) Schematic representation of activity dependent nSyb-GRASP.

(B-B'') nSyb-GRASP used to validate ORN(pre)-PN(post) circuitry. nSyb-spGFP1-10 fragment were expressed in pre-synaptic ORNs (blue, B') driven by Or83b-LexA and CD4-spGFP11 in post-synaptic antennal lobe PNs driven by GH146-Gal4 (red, B''). In the canonical direction a clear GRASP signal is visible (green, B'''). The flies in this and the following experiments were 5 days old.

(C-C'') nSyb-GRASP expressed in inverted orientation of the ORN-PN circuitry. The presynaptic nSyb-spGFP1-10 fragment is expressed in the post-synaptic PNs (blue, C'). The CD4-spGFP11 fragment is expressed in pre-synaptic ORNs (red, C''). No or weak GRASP signal was detected (C''').

(D-D'') The proximity dependent CD4-GRASP shows different expression strength of the drivers and a better signal to noise ratio. The polyclonal antibody (blue) detects the spGFP1-10 fragment in ORNs (blue, D'). The CD4 antibody detects CD4 in both pre ORNs and postsynaptic PNs. The signal (red, D'') is dominated by the ORNs. The monoclonal GFP detects the strong GRASP signal (green, D''').

Scale bars represents 60 μ m.

In CD4-GRASP or neurexin-based GRASP (Feinberg et al., 2008; Gordon and Scott, 2009), GFP reconstitution happens when cells are in close contact to each other, whereas in activity-dependent nSyb-GRASP, the GFP reconstitution depends on neuronal activity (Macpherson et al., 2015). In all these GRASP constructs the spGFP1-10 fragment is either tethered to a CD4 membrane protein or nSyb and spGFP11 fragment is tethered to CD4. Depending on the type of GRASP, reconstituted GRASP signal can be seen when partners come in close contact (CD4-GRASP) or are synaptically active (nSyb-GRASP) (Fig.1 A). We used a combination of polyclonal and monoclonal GFP antibodies, which recognize the spGFP1-10 and GRASP signal, respectively, along with CD4 staining to additionally visualize the overall neuronal structure expressing the spGFP11 fragment (Feinberg et al., 2008).

To test our strategy, we first focused on the olfactory system, a well-established circuit of olfactory information processing present in several insect species (Galizia and Rössler, 2010). In the antennal lobe of the *Drosophila* central brain olfactory receptor neurons (ORNs) project their axons to the projection neurons (PNs) and form synaptic contact (ORN-PN connection) (Gordon and Scott, 2009). Therefore we expressed the syb:spGFP1-10 fragment in ORNs [GH146-Gal4] pre-synaptic sites and the CD4:spGFP11 fragment in PNs [OR83B-LexA] post-synaptic sites (Fig.1 B). The activity-dependent GRASP signal (green) (Fig.1 B''') could be observed revealing the functional synaptic contacts between the two neuronal populations. The combination of both polyclonal GFP and CD4 antibodies additionally revealed the overall structure of the pre-synaptic sites in ORNs (blue) (Fig.1 B') and post-synaptic PNs (red) (Fig.1 B'').

To test the specificity of the monoclonal GFP antibody for the GRASP reconstituted GFP, we expressed the syb:spGFP1-10 fragment in the antennal lobe PNs and CD4:spGFP11 in ORNs (Fig.1 C). While both the PNs pre-synaptic terminals labeled by polyclonal GFP (blue) (Fig.1 C') and the ORNs labelled by CD4 staining (red) (Fig.1 C'') could be observed, they were no monoclonal GFP labeled GRASP signal (green) (Fig.1 C'''). Hence, the monoclonal GFP only binds to reconstituted GFP, whereas polyclonal GFP is not sensitive to GFP reconstitution and binds also to spGFP1-10 fragment alone. Interestingly, our staining method could also apply to the *Drosophila* CD4-GRASP (Gordon and Scott, 2009), where GRASP signal can be seen in the case of close proximity between the ORNs and antennal lobe PNs (Fig.1 D). We could recapitulate our activity GRASP data by using the polyclonal GFP to visualize the spGFP1-10 fragment (blue) in ORNs (Fig.1 D'), CD4 staining for visualizing the antennal lobe PNs (red) (Fig.1 D'') and monoclonal GFP for GRASP (green) (Fig.1 D'''). We noted that the signal to noise ratio is much better for the CD4-GRASP in comparison to the activity GRASP.

To further validate the robustness of our activity-GRASP staining strategy across several neuronal connections, we focused on the connections from projection neuron (PNs) to the Kenyon cells (KCs) in the mushroom body calyx [35B12] (PN-MB connection) (Li et al., 2013). By expressing the syb:spGFP1-10 fragment in the PNs pre-synaptic sites and the CD4:spGFP11 fragment in mushroom body neurons (PNs post-synaptic partners) (Fig.2 A), we could see the activity-dependent GRASP signal (green) (Fig.2 A''') along with pre-synaptic sites in PNs (blue) (Fig.2 A') and post-synaptic MB neurons (red) (Fig.2 A''). Furthermore, by expressing the syb:spGFP1-10 fragment in the PN post-synaptic partners (MB) and the CD4:spGFP11 fragment in PNs pre-synaptic sites (Fig.2 B-B'''), we could validate the specificity of the monoclonal GFP antibody for the GRASP signal (Fig.2 B''), and validate our

strategy for the visualization of both the mushroom body post-synaptic structure labeled by polyclonal GFP (blue)(Fig.2 B') and the PNs pre-synaptic terminals labelled by CD4 staining (red) (Fig.2 B''). As previously, the proximity-dependent CD4 GRASP (Fig.2 C-C'') could recapitulate our finding by using the polyclonal GFP to visualize the spGFP1-10 fragment (blue) in PNs(Fig.2 C'), CD4 staining for visualizing the antennal lobe MB neurons(red) (Fig.2 C') and monoclonal GFP for GRASP (green) (Fig.2 C''). In that case, the proximity GRASP signal reflects the close contact between the PNs and MB neurons.

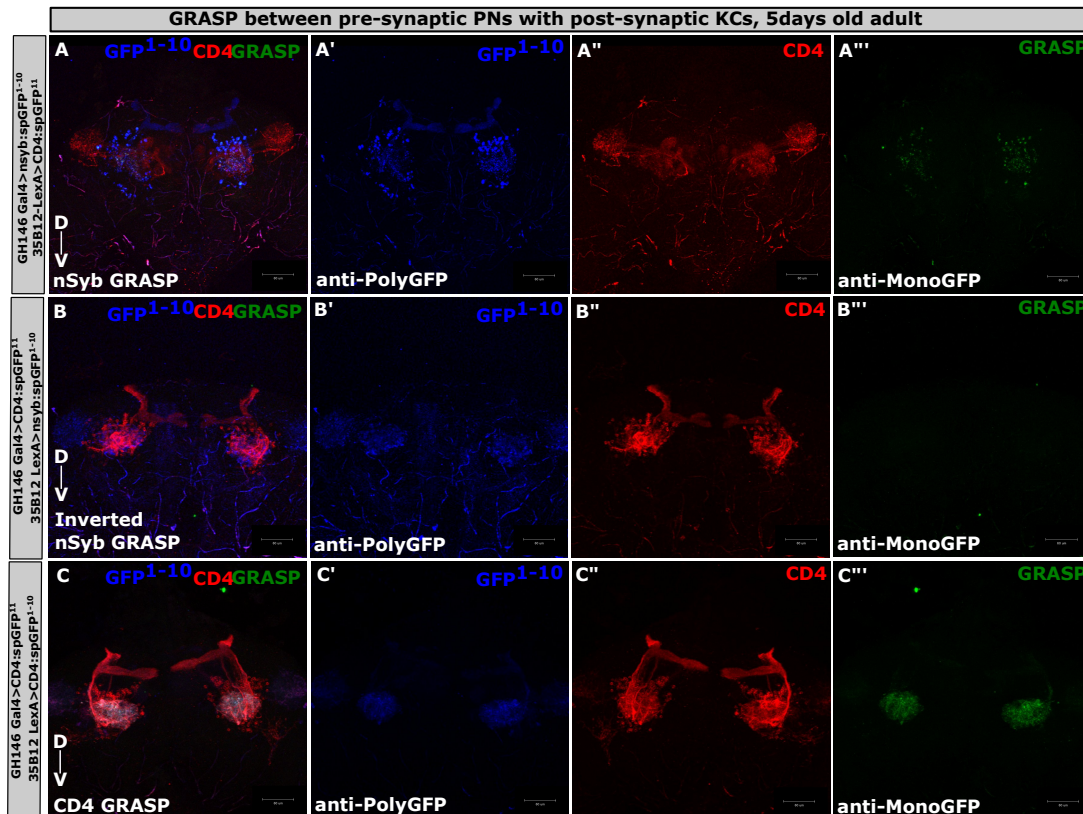


Fig.2: Validation of synaptic connection between presynaptic PNs with post-synaptic Kenyon cells (KCs) in mushroom body calyx PNs using nsyb-GRASP and CD4-GRASP

(A-A'') nSyb-GRASP used to validate PN(pre)-KC(post) circuitry. nSyb-spGFP1-10 fragment expressed in pre-synaptic PNs (blue, A') driven by GH146-Gal4 and CD4-spGFP11 in post-synaptic KCs (red, A'') driven by 35B12-LexA shows activity dependent GRASP signal (green, A''').

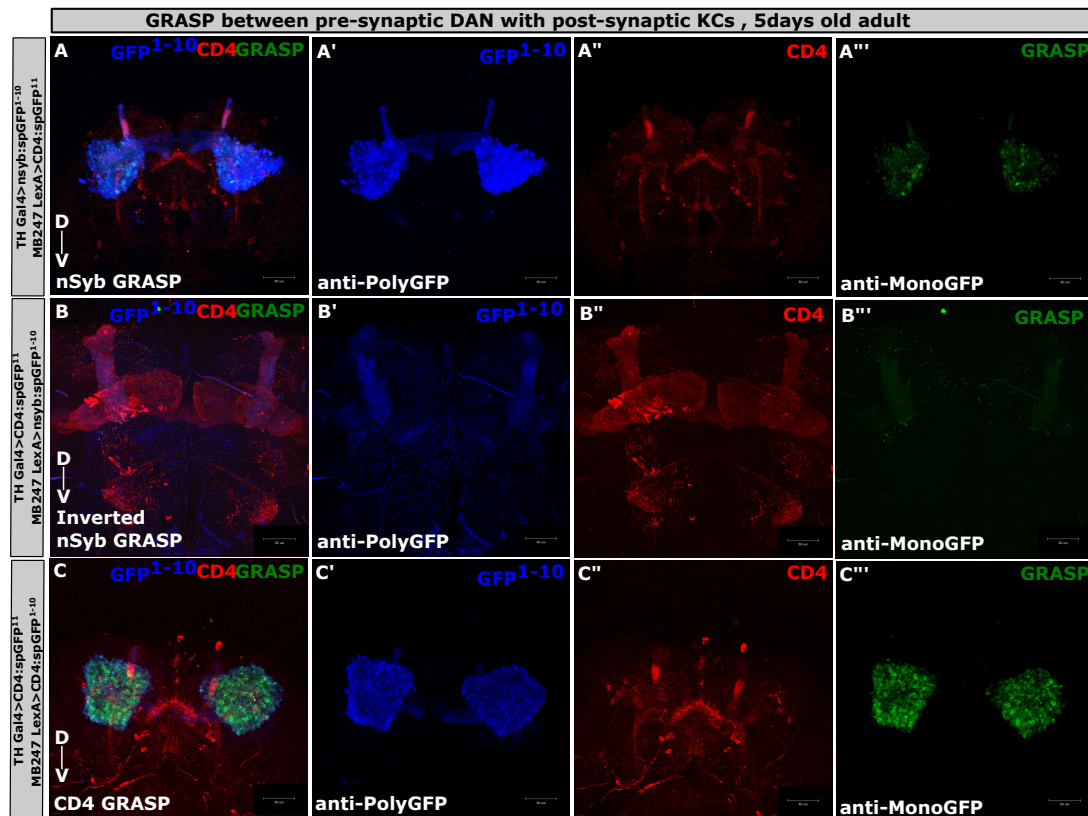
(B-B'') nSyb-GRASP expressed in inverted orientation of the PN-KC circuitry. The presynaptic nSyb-spGFP1-10 fragment expressing in post-synaptic MB neurons (blue, B') and CD4-spGFP11 in pre-synaptic projection neurons (red) shows no detectable GRASP signal (B''').

(C-C'') Proximity dependent traditional CD4-GRASP shows GRASP signal (green, C'') CD4-spGFP1-10 fragment is expressed in ORNs (blue, C') and CD4-spGFP11 expressed in mushroom body PNs (red, C'').

Scale bars represents 60µm.

We further checked the neuronal connection between mushroom body neurons and dopamine neurons, which synapses onto each other (Takemura et al., 2017) and forms a positive feedback loop by forming axo-axonic reciprocal synapses which is critical for olfactory learning (Cervantes-Sandoval et al., 2017). We used TH-Gal4 as a dopaminergic neuron (DAN) driver (Friggi-Grelin et al., 2003) and MB247-LexA for driving the mushroom body Kenyon cell (KC) (Pitman et al., 2011). We checked at mushroom body calyx region where major types of

Kenyon cells project their dendrites (Li et al., 2020). We could confirm that DAN neurons are presynaptic and in close proximity to MB-KCs in the calyx region and post-synaptic to KCs in alpha lobe of mushroom body using both activity dependent GRASP (Fig.3 A/A'''-B/B''') and CD4 GRASP signal respectively (Fig.3 C-C''').



DAN-Kenyon cell (KC) feedback circuitry using nsyb-GRASP and CD4-GRASP

(A-A''') nSyb-GRASP used to validate DAN (pre)- KC (post) circuitry in MB calyx. nSyb-spGFP1-10 fragment expressed in pre-synaptic DAN (blue, A') driven by TH-Gal4 and CD4-spGFP11 in post-synaptic KCs (red, A'') driven by MB247-LexA shows activity dependent GRASP signal (green, A''').

(B-B''') nSyb-GRASP used to validate KC (pre)-DAN (post) circuitry in MB alpha lobe. nSyb-spGFP1-10 fragment expressing in post-synaptic DAN (blue, B') and CD4-spGFP11 in pre-synaptic MB neurons (red, B'') shows weak GRASP signal (B''').

(C-C''') Traditional CD4 GRASP shows GRASP signal (green, C''') upon expressing CD4-spGFP1-10 fragment is expressed in DAN (blue, C') and CD4-spGFP11 expressed in KC (red, C'').

Scale bar represents 60µm.

By expressing the syb:spGFP1-10 fragment in the DAN pre-synaptic sites and the CD4:spGFP11 fragment in KC neurons post-synaptic sites (Fig.3 A), we could see the activity-dependent GRASP signal (green) (Fig.3 A''') in the MB calyx along with pre-synaptic sites (blue)(Fig.3 A') and post-synaptic neurons (red) (Fig.3 A''). This confirms that DANs are presynaptic to KCs in the MB calyx. Further, on expressing the syb:spGFP1-10 fragment in the pre-synaptic sites of KC and the CD4:spGFP11 fragment in the post-synaptic compartment of DAN (Fig. 3B) showed weak GRASP signal in the deeper alpha lobes of mushroom body (Fig. 3B''') with no signal in the calyx region. This in turn confirmed the feedback circuitry of DAN-KCs in different MB lobes and showed the robustness of our staining protocol. We could

see the KC pre-synaptic terminals labelled by polyclonal GFP (blue) (Fig.3 A') and the DAN labeled by CD4 staining (red) (Fig.3 B'')

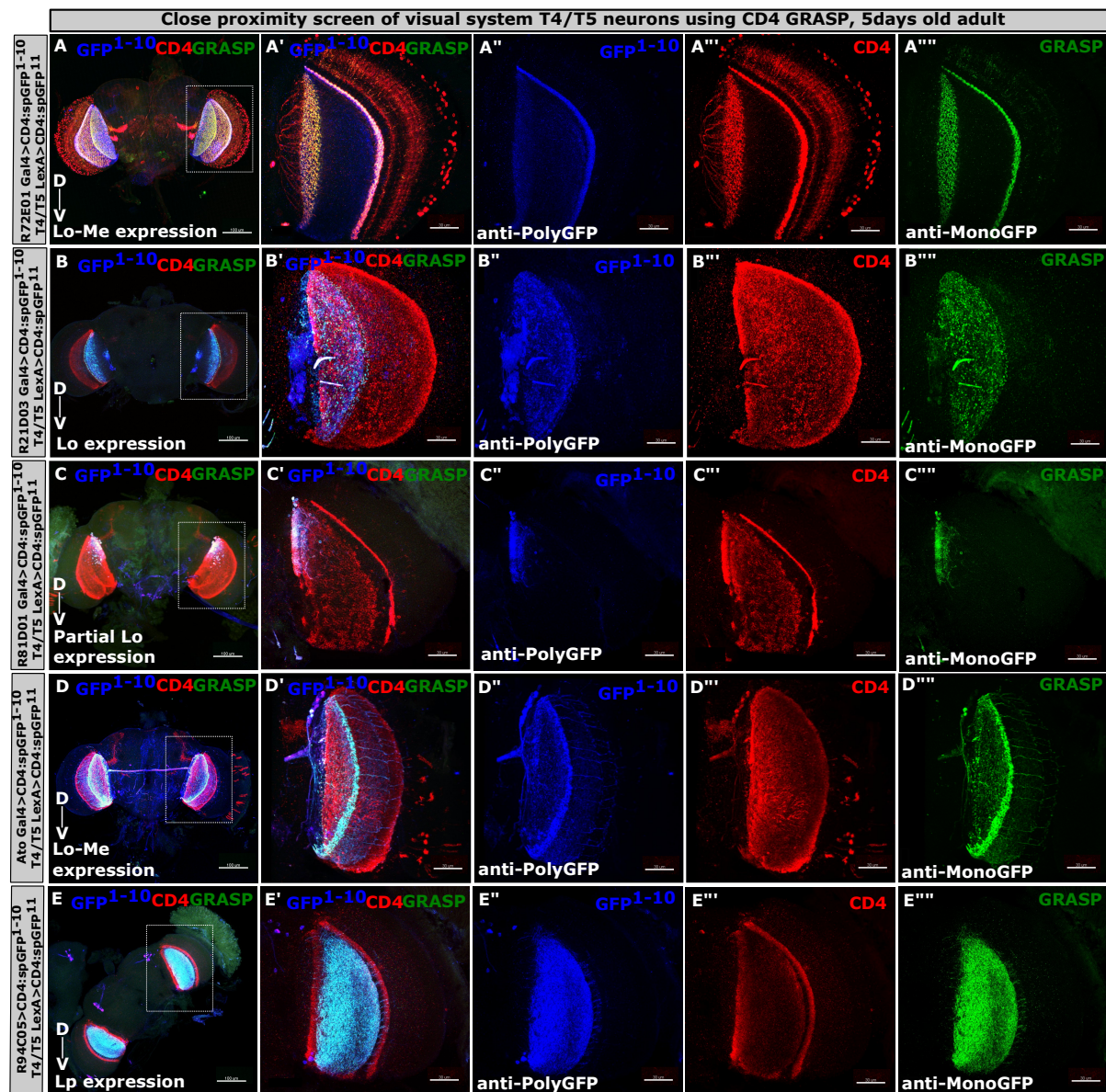


Fig.4: Screen for close proximity partners of T4/T5 neurons

Screen for close proximity partners of T4/T5 neurons of visual system using proximity dependent CD4 GRASP expressing pre-synaptic CD4-spGFP1-10 fragment in T4/T5 neurons (blue) and CD4-spGFP11 fragment on potential post-synaptic targets (red); showing GRASP signal (green) only if they are potential partners. Potential post-synaptic partners (red) projecting in (A-A''') cell bodies in medulla and neurites in lobula (red), (B-B''') cell bodies in central brain with neurites in lobula, (C-C''') cell bodies in lobula, (D-D''') cell bodies in central brain with neurites in lobula and medulla, (E-E''') neurites in lobula plate, of pre-synaptic T4/T5 neurons (blue) showing positive GRASP signal (green).

Scalebars represent 30 μ m except in (A,B,C,D,E) where they represent 100 μ m.

To this end, we have shown that our staining protocol works in both activity-dependent syb GRASP and proximity-dependent CD4-GRASP in different neuronal connections in the fly

olfactory system. To further test the usability of our staining protocol, we wanted to test if CD4-GRASP can be used for screening post-synaptic partners. We chose T4/T5 neurons as our neurons of interest, the direction-sensitive interneurons of motion vision pathway. T4/T5 neurons have their cell bodies between the Lobula-plate and Medulla and projects their dendrites either in the proximal Medulla (Me10) or distal Lobula (Lo1) respectively. First we used the anterograde trans-synaptic neuron tracing method, *trans*-Tango to detect the entire projection pattern of T4/T5 neurons in adults (Fig.4 Video1). Based on the expression pattern from *Trans*-Tango, we selected a list of probable post-synaptic partners based on their expression profile published in Janelia (Table 1) and shortlisted 26 neuronal types (Table 2) with varied expression in lobula, lobula plate and medulla. We showed that T4/T5 neurons are in close proximity with different syb-types of neurons with expression throughout the brain: projecting in lobula-medulla (Fig.4 A), lobula specific expression (Fig.4 B), partial expression in lobula (Fig.4 C), commissural inter-neurons projecting in lobula and medulla (Fig.4 D) and lobula plate specific projection (Fig.4 E). All of the target neurons showed GRASP signal in proximity dependent CD4 GRASP, with T4/T5 neurons being labeled by polyclonal GFP and post-synaptic neurons with CD4 staining (Fig.4 A/A'''-E/E'''). In conclusion, we could adapt our technique to perform a wide range of screen for unknown partners in the fly visual system.

Discussion:

We have refined the technical implications of a widely used synaptic labeling tool GRASP (Feinberg et al., 2008), by our staining strategy. GRASP contains split-GFP fragments on pre (spGFP1-10) and post-synaptic sites(spGFP11), which reconstitutes GFP upon coming in close contact. In non-activity-dependent GRASP, split GFPs are fused to transmembrane protein CD4 or cell-adhesion molecule neurexin, hence GFP reconstitution in these cases correlates with neuronal proximity (Feinberg et al., 2008). Whereas activity-dependent nSyb-GRASP relies on neurotransmission and therefore is a more reliable method for marking active synapses (Macpherson et al., 2015). For long, the connectome field had to weigh out the balance between ultrastructural analysis with EM and light-microscopy-based neuronal tracing and validation of synaptic contact. While one is more time-consuming, labor-intensive, and less high-throughput, the other is less sensitive with a higher possibility of false positives.

We have shown in this study a time-efficient method to modify the read-out of the well-established GRASP tool and use it for proper screening of close proximity and/or synaptic partners. We have utilized the less specificity of polyclonal GFP antibodies in recognizing only the reconstituted GFP in our favor and used it as a marker of presynaptic sites. On top of that, we have used the CD4 staining to mark the post-synaptic site and monoclonal GFP, which is specific to reconstituted GFP as mentioned in the original studies (Feinberg et al., 2008; Macpherson et al., 2015). Our staining method works in both the original CD4-GRASP and nSyb-GRASP, showing its broad application. We have also used the nSyb-GRASP in wrong direction (spGFP1-10 in post-synaptic side and spGFP11 on pre-synaptic site) as a negative control. It didn't result in any significant GRASP signal (in comparative experiments) which suggests the sensitivity of the labeling method, but we could label the spGFP1-10 fragment irrespective of the directionality which suggests the robustness of the staining method. We have used our staining method in 3 different known neuronal circuitries to demonstrate the robustness of our method. And could also adapt the technique in CD4-GRASP to use it for screening post-synaptic targets of the motion vision circuit of fruit fly, T4/T5 neurons. Our study highlights the importance of using the mono GFP+poly GFP+CD4 staining method. We can visualize the pre-synaptic and post-synaptic neuron bearing the GRASP signal. Also this method can be applied in all forms of GRASP techniques like CD4-GRASP (Gordon and Scott, 2009), nSyb-GRASP (Macpherson et al., 2015) or t-GRASP (Shearin et al., 2018).

We know that the major caveat of our technique is its bias towards known/pre-existing neuronal drivers to use for GRASP technique which limits the screening process. To have an unbiased activity dependent screen, it will be advantageous to develop a hybrid technique of Trans Tango and activity GRASP; activity-dependent Trans-Tango, where we can trace the potential post-synaptic partners only those that connect via functional synapses and is also sensitive to the strength and frequency of synapses formed. Here, with this staining approach, we have progressed one step towards that goal, although much remains to be addressed. Still, we believe our protocol will help in future generation of connectome studies which can be adapted in several models.

Supplemental information:

Supplementary video 1:

Trans-Tango based post-synaptic expression pattern of T4/T5 neurons of 15days old adult raised at 18C.

Supplementary table 1:

List of all close proximity partners of T4/T5 neurons tested

References:

- Andrews, D.S., Avino, T.A., Gudbrandsen, M., Daly, E., Marquand, A., Murphy, C.M., Lai, M.C., Lombardo, M.V., Ruigrok, A.N., Williams, S.C., *et al.* (2017). In Vivo Evidence of Reduced Integrity of the Gray-White Matter Boundary in Autism Spectrum Disorder. *Cereb Cortex* 27, 877-887.
- Bräcker, Lasse B., Siju, K.P., Varela, N., Aso, Y., Zhang, M., Hein, I., Vasconcelos, Maria L., and Grunwald Kadow, Ilona C. (2013). Essential Role of the Mushroom Body in Context-Dependent CO₂ Avoidance in *Drosophila*. *Current Biology* 23, 1228-1234.
- Cachero, S., Gkantia, M., Bates, A.S., Frechter, S., Blackie, L., McCarthy, A., Sutcliffe, B., Strano, A., Aso, Y., and Jefferis, G. (2020). BACTrace, a tool for retrograde tracing of neuronal circuits in *Drosophila*. *Nat Methods* 17, 1254-1261.
- Cook, S.J., Jarrell, T.A., Brittin, C.A., Wang, Y., Bloniarz, A.E., Yakovlev, M.A., Nguyen, K.C.Q., Tang, L.T., Bayer, E.A., Duerr, J.S., *et al.* (2019). Whole-animal connectomes of both *Caenorhabditis elegans* sexes. *Nature* 571, 63-71.
- Di Martino, A., Fair, D.A., Kelly, C., Satterthwaite, T.D., Castellanos, F.X., Thomason, M.E., Craddock, R.C., Luna, B., Leventhal, B.L., Zuo, X.N., *et al.* (2014). Unraveling the miswired connectome: a developmental perspective. *Neuron* 83, 1335-1353.
- Feinberg, E.H., Vanhoven, M.K., Bendesky, A., Wang, G., Fetter, R.D., Shen, K., and Bargmann, C.I. (2008). GFP Reconstitution Across Synaptic Partners (GRASP) defines cell contacts and synapses in living nervous systems. *Neuron* 57, 353-363.
- Friggi-Grelin, F., Coulom, H., Meller, M., Gomez, D., Hirsh, J., and Birman, S. (2003). Targeted gene expression in *Drosophila* dopaminergic cells using regulatory sequences from tyrosine hydroxylase. *Journal of Neurobiology* 54, 618-627.
- Galizia, C.G., and Rössler, W. (2010). Parallel Olfactory Systems in Insects: Anatomy and Function. *Annual Review of Entomology* 55, 399-420.
- Gordon, M.D., and Scott, K. (2009). Motor Control in a *Drosophila* Taste Circuit. *Neuron* 61, 373-384.
- Henderson, M.X., Cornblath, E.J., Darwich, A., Zhang, B., Brown, H., Gathagan, R.J., Sandler, R.M., Bassett, D.S., Trojanowski, J.Q., and Lee, V.M.Y. (2019). Spread of α -synuclein pathology through the brain connectome is modulated by selective vulnerability and predicted by network analysis. *Nature Neuroscience* 22, 1248-1257.
- Kim, J., Zhao, T., Petralia, R.S., Yu, Y., Peng, H., Myers, E., and Magee, J.C. (2012). mGRASP enables mapping mammalian synaptic connectivity with light microscopy. *Nature Methods* 9, 96-102.
- Lai, S.-L., and Lee, T. (2006). Genetic mosaic with dual binary transcriptional systems in *Drosophila*. *Nature Neuroscience* 9, 703-709.
- Levitt, J.J., Nestor, P.G., Kubicki, M., Lyall, A.E., Zhang, F., Riklin-Raviv, T., LJ, O.D., McCarley, R.W., Shenton, M.E., and Rathi, Y. (2020). Miswiring of Frontostriatal Projections in Schizophrenia. *Schizophr Bull* 46, 990-998.
- Li, H., Li, Y., Lei, Z., Wang, K., and Guo, A. (2013). Transformation of odor selectivity from projection neurons to single mushroom body neurons mapped with dual-color calcium imaging. *Proceedings of the National Academy of Sciences* 110, 12084-12089.
- Li, J., Liu, T., Dong, Y., Kondoh, K., and Lu, Z. (2019). Trans-synaptic Neural Circuit-Tracing with Neurotropic Viruses. *Neurosci Bull* 35, 909-920.

Macpherson, L.J., Zaharieva, E.E., Kearney, P.J., Alpert, M.H., Lin, T.Y., Turan, Z., Lee, C.H., and Gallio, M. (2015). Dynamic labelling of neural connections in multiple colours by trans-synaptic fluorescence complementation. *Nat Commun* 6, 10024.

Nonet, M.L. (1999). Visualization of synaptic specializations in live *C. elegans* with synaptic vesicle protein-GFP fusions. *J Neurosci Methods* 89, 33-40.

Pitman, J.L., Huetteroth, W., Burke, C.J., Krashes, M.J., Lai, S.L., Lee, T., and Waddell, S. (2011). A pair of inhibitory neurons are required to sustain labile memory in the *Drosophila* mushroom body. *Curr Biol* 21, 855-861.

Ryan, K., Lu, Z., and Meinertzhagen, I.A. (2016). The CNS connectome of a tadpole larva of *Ciona intestinalis* (L.) highlights sidedness in the brain of a chordate sibling. *Elife* 5.

Scheffer, L.K., Xu, C.S., Januszewski, M., Lu, Z., Takemura, S.Y., Hayworth, K.J., Huang, G.B., Shinomiya, K., Maitlin-Shepard, J., Berg, S., *et al.* (2020). A connectome and analysis of the adult *Drosophila* central brain. *Elife* 9.

Schneider-Mizell, C.M., Gerhard, S., Longair, M., Kazimiers, T., Li, F., Zwart, M.F., Champion, A., Midgley, F.M., Fetter, R.D., Saalfeld, S., *et al.* (2016). Quantitative neuroanatomy for connectomics in *Drosophila*. *eLife* 5, e12059.

Shah, A., Lenka, A., Saini, J., Wagle, S., Naduthota, R.M., Yadav, R., Pal, P.K., and Ingalthalikar, M. (2017). Altered Brain Wiring in Parkinson's Disease: A Structural Connectome-Based Analysis. *Brain Connect* 7, 347-356.

Shearin, H.K., Quinn, C.D., Mackin, R.D., Macdonald, I.S., and Stowers, R.S. (2018). t-GRASP, a targeted GRASP for assessing neuronal connectivity. *J Neurosci Methods* 306, 94-102.

Stocker, R.F., Heimbeck, G., Gendre, N., and de Belle, J.S. (1997). Neuroblast ablation in *Drosophila* P[GAL4] lines reveals origins of olfactory interneurons. *J Neurobiol* 32, 443-456.

Takemura, S.Y., Bharioke, A., Lu, Z., Nern, A., Vitaladevuni, S., Rivlin, P.K., Katz, W.T., Olbris, D.J., Plaza, S.M., Winston, P., *et al.* (2013). A visual motion detection circuit suggested by *Drosophila* connectomics. *Nature* 500, 175-181.

Talay, M., Richman, E.B., Snell, N.J., Hartmann, G.G., Fisher, J.D., Sorkac, A., Santoyo, J.F., Chou-Freed, C., Nair, N., Johnson, M., *et al.* (2017). Transsynaptic Mapping of Second-Order Taste Neurons in Flies by trans-Tango. *Neuron* 96, 783-795 e784.

White, J.G., Southgate, E., Thomson, J.N., and Brenner, S. (1986). The structure of the nervous system of the nematode *Caenorhabditis elegans*. *Philos Trans R Soc Lond B Biol Sci* 314, 1-340.

Zheng, Z., Lauritzen, J.S., Perlman, E., Robinson, C.G., Nichols, M., Milkie, D., Torrens, O., Price, J., Fisher, C.B., Sharifi, N., *et al.* (2018). A Complete Electron Microscopy Volume of the Brain of Adult *Drosophila melanogaster*. *Cell* 174, 730-743 e722.

9. General Discussion

The aim of my doctoral work has been on contributing to answer long-lasting and challenging questions in neurobiology like “How are synaptogenesis and axon branching tightly coupled and regulated during development at a molecular level in order to form circuit patterns for robust behavioral outcomes?” Following such co-regulated processes once synaptic partners form, I asked “Are neurons genetically programmed to form specific synaptic contacts or rather is it an outcome of repetitive developmental algorithms? How promiscuous is the process of synapse formation?” To address these questions, I have used Dorsal Cluster Neurons (DCNs) of the *Drosophila* visual system, which is one of the most variable interneurons in the fly brain and has been shown to be responsible for object fixation behavior. It is a good model system to study non-genetic stochastic developmental processes such as axonal branching and synapse formation. Previous studies have shown that development of synapse specific neuronal wiring is a very complex process involving spatio-temporal regulation of several sub-cellular processes which underlies behavioral robustness. In the final steps of neuronal circuit connectivity, stochastically exploring axonal filopodia are stabilized through the formation of synaptic contacts with post-synaptic partners. This necessitates an intimate spatial and temporal coordination of filopodial dynamics, synaptic seeding and maintenance through poorly understood molecular mechanisms. How and when such complex coordination is achieved and its impact on adult brain function is also very poorly understood. Also, once such mechanistic coordination is achieved, when and what kind of cell intrinsic or extrinsic cues decouple all the processes is not well known. The goal is to form stereotypical yet variable adult brain wiring patterns which are robust to perturbations. To challenge the genetic determinism of brain circuit assembly, I have used temperature as a non-genetic and non-biased tool to perturb all developmental processes. This addresses developmental robustness at different levels like synapse formation, neuronal circuit assembly and finally in behavior. In the following sections, the results obtained during my doctoral work will be discussed in relation to previously published studies.

9.1 Spatial and temporal regulation of signaling receptor molecules in synaptogenesis and axon branching

Synapse formation and axon branching are spatio-temporally regulated processes during brain development which is crucial for robust brain wiring. Several observations upon live imaging of the two processes suggests that synapse formation and axon branching positively reinforce each other, the synaptotropic growth. Since the brain develops in a wave of complex instructions, it is crucial to play the right molecular card at an appropriately timed entry point. Because de-regulation of either branch or synapse formation during development manifests several neurodevelopmental and psychiatric disorders. Although previous studies have shown tight coupling of axon branching and synaptogenesis, only some revealed possible molecular mechanisms. For example, interaction between synaptic adhesion molecule Syg1/Syg2 assemble local F-actin network which links the two parallel processes in time and space (Chia et al., 2014). Again, protein tyrosine kinases like FAK regulates axon branching by modulating interactions with RhoGTPases and consequently synapse formation in vertebrate(Rico et al., 2004). Complex organisms have evolved sophisticated molecular networks where a single molecule can potentially participate in multiple pathways by its precise spatial and temporal regulation as happens during T-cell activation (Garcia & Ismail, 2020). It is completely unknown whether similar efficient and effective regulation might couple synapse formation to axon branching.

I have addressed this question in my first study (Chapter 1) by using a temperature sensitive Gal80 to repress Gal4 activity, thus blocking EGFR DN specifically in DCNs in distinct developmental time windows; before and after synaptogenesis. My data from temporal inactivation strongly suggests that EGFR activity has a dual role during brain development; an early role in consolidating axon branching and a later role in protecting late AZ material from endo-lysosomal degradation in DCNs. Lack of proper establishment of DCN branches and synapse affects its wiring pattern, as synapse loss also translates to loss of postsynaptic partner. This in turn makes an individual highly active in visual object fixation assays. My data also shows that DCNs, upon not being able to form stable synapses in EGFR DN, re-initiates the synaptotropic feedback loop by

forming more exploratory secondary branches. This also phenocopies Brp RNAi phenotype in developing and adult DCNs in terms of increased exploration by forming secondary branches which made me hypothesize that these branches are exploring their postsynaptic territory for searching available partners. It has been shown before that the activity of EGFR itself and random recycling of the same in axon terminals is crucial for proper DCN branch refinement. Hence when DCNs lack EGFR activity, this local asymmetry in vesicle recycling is hampered, leading to an over branching phenotype in adults. But my study shows that this increase in overall branching is a cumulative effect of two step or dual regulation of EGFR on branching and synapse formation in separate developmental time windows as discussed above. On top of this temporal requirement of EGFR, the spatial distribution of the molecule itself correlates with branch stability and synapse formation. I have shown that random, asymmetric distribution of EGFR itself in the local axon branches correlates strongly to the stability of a branch. Higher proportions of EGFR being recycled in stable ones compared to transient/unstable branches. Following the asymmetric recruitment of EGFR in the branches, late AZ protein Bruchpilot (Brp) selectively accumulates only in stable branches and eventually juxtapose with EGFR in adult branches. This suggests that presence of EGFR itself in a branch signals active recruitment of synaptic material thus facilitating synapse formation which in turn stabilizes that branch. My first study also shows that DCN axons exhibit parts of synaptotropic growth in separate branch compartments; first, putative synapses stabilize primary branches followed by synapse directed/mediated further secondary branch formation.

My study identified a novel role of EGFR in establishing proper brain wiring for robust behavioral output, but what remains downstream of EGFR that signals both axon branching and synapse formation remains unanswered. One possible effector might be actin cytoskeleton. Previous work already showed that lack of EGFR activity in DCNs leads to de-regulated actin polymerization and inhibited branch dynamics (Zschätzsch et al., 2014). My data suggests that axon branching is a highly dynamic process, with both stable and transient ones extending and retracting. I made an unpublished observation that stable branches tend to be more dynamic compared to transient ones during the pruning process. Several studies have confirmed that actin network is key to synapse formation and

maintenance in both vertebrates and invertebrates (Nelson et al., 2013). EGFR and its ligand Gurken has been shown to be involved in synaptic target selection in *Drosophila* neuromuscular system (Naylor & Diantonio, 2012). Hence, it is my hypothesis that EGFR is the main regulator acting spatiotemporally upstream of actin cytoskeleton which links axon branching to synapse formation in DCNs.

9.2 Suppression of local synaptic protein degradation via autophagy as a homeostatic mechanism for proper neuronal assembly:

Macro-autophagy (Autophagy) is one the key cellular homeostatic mechanisms for maintaining neuronal health and longevity where defective proteins and organelles are targeted for degradation. Recent studies suggest its direct effect on neurotransmission, synaptic plasticity, circuit development and maintenance (Filippone et al., 2022; Kallergi et al., 2022; Kuijpers et al., 2021). Synapse formation in mammalian brain involves active synapse elimination and refinement which plays an important role in normal brain development (Hashimoto & Kano, 2013; Yasuda et al., 2021). This is an important process in adolescent human brain maturation and sensory critical periods (Huttenlocher PR, 1984; Selemon, 2013). It has been shown that autophagy is required for dendritic spine pruning in mice, which is disrupted in individuals with ASD and that upregulation of autophagy could rescue back synaptic and behavioral deficits (Tang et al., 2014). Recently, autophagy has been shown to be regulating synapse formation and affecting neuronal partner choice in photoreceptors of *Drosophila* (Kiral et al., 2020). The complexity of long distance neuronal cyto-architecture necessitates local protein synthesis and degradation since several physiological processes like synaptic transmission or plasticity are fast cellular events.

So far, there has been speculation about the importance of local synaptic protein degradation in the axon terminals and homeostatic regulation of autophagic activity in brain development. I have addressed this question in my first study (Chapter 1) by performing colocalizing studies of endogenous expression of Rab7 (late endosomal marker), Atg8 (autophagosomal marker)

and Spinster (lysosomal marker) with Bruchpilot (marked by BrpD3) in adult DCN presynaptic branches. I observed a few instances of colocalization of autophagy markers with BrpD3 in wild type controls which strongly suggests that basal level of autophagic degradation is required for brain homeostasis. Even when I downregulated autophagy by using Rab7 RNAi and Atg6 RNAi, I did not see any significant effect on synapse density per axon which again suggests an intrinsic limit of synapse formation per branch. Maybe this happens due to mere space constraint in axon terminals and that brain development is highly robust to certain perturbations within a certain threshold. But when I expressed EGFR DN in the DCNs specifically, I observed massive reduction of synapse density and the BrpD3 GFP puncta tend to accumulate in bigger volumes. Further live-imaging data in EGFR DN DCN branch terminals revealed decrease of stable BrpD3-GFP puncta with lifetime more than 2 hours compared to control during synaptogenesis. This suggests lack of EGFR activity affects the stability of Brp marked synapses in DCN branches. Colocalization analysis with several autophagic markers revealed that a significant proportion of these BrpD3 puncta tend to closely associate with Rab7/Atg8/Spinster in adult branches and cell bodies. And this association tends to increase at a time when I start seeing reduction of synapses in the branches upon lack of EGFR activity. Further, downregulation of autophagy with Rab7 RNAi and Atg6 RNAi in EGFR DN background could rescue back the loss of synapse phenotype, along with increased secondary branching defect associated with synapse loss. Taken together, I conclude that in DCNs EGFR activity inhibits autophagy to keep within a basal threshold. This helps to maintain synaptic material from getting degraded, thus ensuring proper brain wiring. Additionally, I also used the degradation probe (mCherry-pHlourin) tagged with general membrane protein myr and BrpD3 to validate synaptic degradation locally at axon branches. In addition to our colocalization data, lack of EGFR activity increased both myr and BrpD3 mCherry intensity compared to pHlourin intensity in the branches, strongly suggesting their presence in degradative acidic compartments. Whereas in constitutively active form of EGFR, there is over-branching defect owing to dys-regulated actin dynamics, but no Brp marked synapse loss followed by loss of post-synaptic partners. This shows that EGFR signaling acts as an instructive signal for synapse maintenance by suppressing autophagy.

My study identified increased local synaptic protein degradation in the pre-synaptic terminals when EGFR activity is hampered. While retrograde transport of machinery for cellular protein degradation might still coexist, my study shows the possibility of local autophagic degradation at the synapses. Since DCNs are commissural interneurons covering long distances, simultaneous protein degradation in the cell bodies as well as axon terminals might make it time and energy efficient. It will be interesting to perform comparative studies in long range vs short range neurons in terms of local protein degradation, also to investigate the redundancy of the two modes of degradation in a particular neuronal subtype.

9.3 Brain wiring as a functional output of time

Till today, brain patterning is widely viewed as a hardly wired process, where a particular neuron makes specific sets of connections owing to processes like axon guidance, where local or distal instructive cues match and pair pre-decided neuronal connections like a key-and-lock mechanism. Over the years some examples of such instructive cues like several cell adhesion molecules or attractive/repulsive molecular gradients have been shown to influence precise axon growth for specific target preference (Dent et al., 2004; Menon et al., 2019; Serafini et al., 1996). Such deterministic processes leave little room for flexible changes in response to altered environmental effects and would never be positively selected in evolution. According to another school of thought, brain wiring is more like a set of simple, repetitive rules where each step defines its successive step where all these instructive molecules are a part of the rule (Hassan & Hiesinger, 2015). For example, neurons readily form synapses with non-canonical partners or even with itself (autapses) under altered circumstances which wouldn't be possible in synapse specific brain wiring (Van Der Loos Hendrik & Glaser Edmund M., 1972). Previous work from our lab demonstrated that photoreceptors show altered post synaptic choice with changed filopodial dynamics (Kiral et al., 2020).

From this I hypothesized that following neuronal birth and migration, neurites follow a simple logic that is to grow based and interact with others in an unbiased manner via stochastic filopodial dynamics. Neuronal pairs innervating

common target regions simultaneously exhibit more filopodial interactions with each other, finally forming synaptic connections. What we define as correct post synaptic partners simply the winners in a game of time in each developmental context. To test this hypothesis, one needs to alter developmental time or context by manipulating the kinetics of neuronal growth across the brain or relative to its neighbors respectively. Our expectation will be to end up having a completely different yet functional brain wiring diagram.

To test this hypothesis in Chapter 2, I altered (decreased/increased) developmental temperature as it is known to change (increase/decrease) developmental speed, specifically during synaptogenesis in *Drosophila* optic lobe and asked how it affects final adult brain wiring and behavior. I looked at how different neuronal populations like DCNs and other projection neurons of sensory pathway scales with change in temperature to form a robust and functional brain. Since entropy is directly proportional to temperature, higher temperature makes every cellular processes faster throughout the brain and vice versa, thus changing the developmental time. In coherence with my hypothesis, all the tested neuronal subtypes showed increased filopodial dynamics at elevated temperature, less time interacting with their neighbors resulting in less synapses formed. While decreased developmental temperature restricted their filopodial dynamics allowing them to interact more with the neighbors, thus forming more and sometimes even non canonical synapses. This study shows that neuronal partners are not solely genetically determined, but rather it is a combinatorial effect of stochastic developmental processes like filopodial kinetics and trans-synaptic interactions occurring at specific developmental time. That means, there is no single perfect brain wiring diagram, rather neuronal processes adapt to different environmental cues to form selectable and heritable brain wiring diagrams optimized for robust behavioral outputs.

10. Outlook and future directions

The goal of this doctoral study was to identify possible regulatory mechanisms coupling axon branching and synaptogenesis, which is at the heart of the synaptotropic hypothesis. The first work successfully led to the discovery of the dual role of branch localized EGFR in a temporally restricted fashion. This regulates axon branch consolidation in the early phase by directly affecting actin cytoskeleton whereas the same activity protects specific synaptic proteins from getting degraded via autophagy. I have shown that optimum level of EGFR activity is required in the DCN branches for adequate synapse formation. It leads to variable post-synaptic partner choice with differential affinities which finally results in robust behavioral activity. Both loss and gain of EGFR activity results in over-branching defects in adults. Only EGFR LOF results in synaptic protein loss along with losing the weakly connected synaptic partners. This changes the M-DCN wiring pattern which increases overall fly activity. There are several studies suggesting the role of post-synaptic signaling in forming proper pre-synaptic arborizations possibly by stabilizing synapses without any direct live evidence (Regehr et al., 2009; Tao & Poo, 2001). An unpublished observation I made during this study was DCN axon branch dynamics (ext./retr.) follows a similar and overlapping trend as branch pruning; more dynamic before synapse formation which gradually reduces over time as one would expect from synapse mediated branch stabilization. When I knocked down late AZ protein Bruchpilot which is crucial for functional synapse formation, I observed highly dynamic axon branches during synaptogenesis phase. This strongly suggests that lack of synapse formation re-initiates the feedback loop. I hypothesize that the branches start to explore more of their post-synaptic territory to form possible synaptic contacts. This idea can be tested by live-imaging DCNs with their post-synaptic partners, which was not known until my doctoral study.

Following this observation, it will be interesting to address the following questions: Do DCNs see/interact with their future canonical partners prior to non-canonical ones? Are there any biases of DCN axon branch dynamics or overlap of neurite arborization during synaptogenesis towards the strong vs weakly connected partners? If yes, what happens if one kills the strongly connected partners or inhibit their filopodial dynamics locally? Will DCNs change

their order or preference of target selection? Is there any correlation between pre and post synaptic interaction to stabilization of synaptic proteins or vice versa? In other words, does trans-synaptic interaction stabilize synapses in pre-synaptic branches which in turn ends the synaptotropic growth phase. This might help us better understand the rate limiting factor of synaptotropic growth, which needs to end at a certain timepoint to build a precise neuronal circuitry. These questions will help us further understand whether neuronal circuit assembly is solely “genetically determined” or rather a result of composite instructions. It will also give us some insight into the cellular mechanisms of neuronal strategies for post-synaptic partner recognition for robust circuit formation. This will have huge implications in understanding brain development and the underlying disease causalities of several neurodevelopmental and psychiatric disorders.

My observation on temperature dependent scaling effect on filopodial dynamics, axon branching, synapse formation and post-synaptic target choice in DCNs along with other visual system neurons of the fly brain shows how an environmental perturbation can wire the fly brain in an optimum way to make it functionally robust. The intriguing point is flies that develop at a certain temperature, perform functional behavior best at that temperature which is like selective evolutionary force. Although I mainly focused on visual system neurons, some unpublished data strongly suggests that some projection neurons of the olfactory system or sensory-motor pathway did not show such similar temperature dependent branching effects. It made me hypothesize that not all neurons show equal degree of robustness to perturbations and might indeed be hardly wired in terms of neuronal patterning owing to its behavioral significance. It would be interesting to follow up and test this at different cellular and functional levels; filopodial dynamics, synapse formation, neuronal circuit formation or behavior - do they compensate for changed developmental temperature? If they do, then to what extent and at which cellular level? Based on my study, our hypothesis will be that neurons scale up/down proportionately and inversely to temperature shifts at different cellular levels. If not, then it will mean that different brain regions are not equally susceptible to environmental changes, and it might be caused by the necessity to conserve certain behavioral outputs in response to varied perturbations. Also, it will be interesting to

challenge neuronal homeostasis in different sets of populations independent of temperature and look at behavioral robustness as an outcome. For example, by modulating autophagy level or changing internal state like hormonal levels. Addressing these questions will intensify our understanding of brain development and how different brain regions cope up distinctly, with the goal to build a functional brain. One can extrapolate similar studies to vertebrate systems to understand the robustness of human brain development.

11. References

- Abram, P. K., Boivin, G., Moiroux, J., & Brodeur, J. (2017). Behavioural effects of temperature on ectothermic animals: unifying thermal physiology and behavioural plasticity. *Biological Reviews*, 92(4), 1859–1876. <https://doi.org/10.1111/brv.12312>
- Agi, E., Kulkarni, A., & Hiesinger, P. R. (2020). Neuronal strategies for meeting the right partner during brain wiring. In *Current Opinion in Neurobiology* (Vol. 63, pp. 1–8). Elsevier Ltd. <https://doi.org/10.1016/j.conb.2020.01.002>
- Alvarez-Castelao, B., & Schuman, E. M. (2015). The regulation of synaptic protein turnover. In *Journal of Biological Chemistry* (Vol. 290, Issue 48, pp. 28623–28630). American Society for Biochemistry and Molecular Biology Inc. <https://doi.org/10.1074/jbc.R115.657130>
- Angilletta, M. J., Steury, T. D., & Sears, M. W. (2004). *Temperature, Growth Rate, and Body Size in Ectotherms: Fitting Pieces of a Life-History Puzzle 1* (Vol. 44). <https://academic.oup.com/icb/article/44/6/498/610205>
- Arnsten, A. F. T., Paspalas, C. D., Gamo, N. J., Yang, Y., & Wang, M. (2010). Dynamic network connectivity: A new form of neuroplasticity. *Trends in Cognitive Sciences*, 14(8), 365–375. <https://doi.org/10.1016/j.tics.2010.05.003>
- Baas, P. W., Deitch, J. S., Black, M. M., & Banker, G. A. (1988). Polarity orientation of microtubules in hippocampal neurons: Uniformity in the axon and nonuniformity in the dendrite. In *Proc. Natl. Acad. Sci. USA* (Vol. 85).
- Bagri, A., Cheng, H.-J., Yaron, A., Pleasure, S. J., & Tessier-Lavigne, M. (2003). Stereotyped Pruning of Long Hippocampal Axon Branches Triggered by Retraction Inducers of the Semaphorin Family of the target regions to which it initially projected. Within each region, further branch formation (terminal arborization) and retraction then shapes the final pattern of synaptic contacts. At the same time, naturally occurring neuronal cell death culls many of these neurons, estab. In *Cell* (Vol. 113).
- Berger-Müller, S., Sugie, A., Takahashi, F., Tavosanis, G., Hakeda-Suzuki, S., & Suzuki, T. (2013). Assessing the role of cell-surface molecules in central synaptogenesis in the Drosophila visual system. *PLoS ONE*, 8(12). <https://doi.org/10.1371/journal.pone.0083732>
- Berke, B., Wittnam, J., McNeill, E., Van Vactor, D. L., & Keshishian, H. (2013). Retrograde BMP signaling at the synapse: A permissive signal for synapse maturation and activity-dependent plasticity. *Journal of Neuroscience*, 33(45), 17937–17950. <https://doi.org/10.1523/JNEUROSCI.6075-11.2013>
- Bingol, B., & Schuman, E. M. (2005). Synaptic protein degradation by the ubiquitin proteasome system. In *Current Opinion in Neurobiology* (Vol. 15, Issue 5, pp. 536–541). <https://doi.org/10.1016/j.conb.2005.08.016>
- Boecker, C. A., & Holzbaur, E. L. (2019). Vesicular degradation pathways in neurons: at the crossroads of autophagy and endo-lysosomal degradation. In *Current Opinion in Neurobiology* (Vol. 57, pp. 94–101). Elsevier Ltd. <https://doi.org/10.1016/j.conb.2019.01.005>
- Boyle, M., Nighorn, A., & Thomas, J. B. (2006). *Drosophila Eph receptor guides specific axon branches of mushroom body neurons*.
- Braithwaite, S. P., Stock, J. B., Lombroso, P. J., & Nairn, A. C. (2012). Protein phosphatases and Alzheimer's Disease. In *Progress in Molecular Biology and Translational Science* (Vol. 106, pp. 343–379). Elsevier B.V. <https://doi.org/10.1016/B978-0-12-396456-4.00012-2>
- Braun, S. M. G., & Jessberger, S. (2014). Adult neurogenesis: Mechanisms and functional

- significance. *Development (Cambridge)*, 141(10), 1983–1986. <https://doi.org/10.1242/dev.104596>
- Bright, N. A., Davis, L. J., & Luzio, J. P. (2016). Endolysosomes Are the Principal Intracellular Sites of Acid Hydrolase Activity. *Current Biology*, 26(17), 2233–2245. <https://doi.org/10.1016/j.cub.2016.06.046>
- Budnik, V., Zhong, Y., & Wu, C.-F. (1990). Morphological Plasticity of Motor Axons in *Drosophila* Mutants with Altered Excitability. In *The Journal of Neuroscience* (Issue 11).
- Chan, C. C., Scoggin, S., Wang, D., Cherry, S., Dembo, T., Greenberg, B., Jin, E. J., Kuey, C., Lopez, A., Mehta, S. Q., Perkins, T. J., Brankatschk, M., Rothenfluh, A., Buszczak, M., & Hiesinger, P. R. (2011). Systematic discovery of Rab GTPases with synaptic functions in *Drosophila*. *Current Biology*, 21(20), 1704–1715. <https://doi.org/10.1016/j.cub.2011.08.058>
- Chédotal, A. (2019). Roles of axon guidance molecules in neuronal wiring in the developing spinal cord. In *Nature Reviews Neuroscience* (Vol. 20, Issue 7, pp. 380–396). Nature Publishing Group. <https://doi.org/10.1038/s41583-019-0168-7>
- Chédotal, A., & Richards, L. J. (2010). Wiring the brain: The biology of neuronal guidance. *Cold Spring Harbor Perspectives in Biology*, 2(6). <https://doi.org/10.1101/cshperspect.a001917>
- Cheng, P. L., & Poo, M. M. (2012). Early events in axon/dendrite polarization. In *Annual Review of Neuroscience* (Vol. 35, pp. 181–201). <https://doi.org/10.1146/annurev-neuro-061010-113618>
- Cherra Iii, S. J., & Chu, C. T. (n.d.). Autophagy in neuroprotection and neurodegeneration: A question of balance. 2008. <https://doi.org/10.2217/14796708.3.3.309>
- Chia, P. H., Chen, B., Li, P., Rosen, M. K., & Shen, K. (2014a). Local F-actin network links synapse formation and axon branching. *Cell*, 156(1–2). <https://doi.org/10.1016/j.cell.2013.12.009>
- Chia, P. H., Chen, B., Li, P., Rosen, M. K., & Shen, K. (2014b). Local F-actin network links synapse formation and axon branching. *Cell*, 156(1–2), 208–220. <https://doi.org/10.1016/j.cell.2013.12.009>
- Choe, K.-M., Prakash, S., Bright, A., & Clandinin, T. R. (2006). *Liprin-is required for photoreceptor target selection in Drosophila*. www.pnas.org/cgi/doi/10.1073/pnas.0601185103
- Christos Samakovliss†, ‡, Nir Hacohen†, Gerard Manning†, David C. Sutherland, Karen Guillemin and Mark A. Krasnow*. (1996). Development of the *Drosophila* tracheal system occurs by a series of morphologically distinct but genetically coupled branching events. *Development*, 122, 1395–1407.
- Ciechanover, A., & Schwartz, A. L. (1998). *The ubiquitin-proteasome pathway: The complexity and myriad functions of proteins death* (Vol. 95). www.pnas.org.
- Clark, S. G., Graybeal, L. L., Bhattacharjee, S., Thomas, C., Bhattacharya, S., & Cox, D. N. (2018). Basal autophagy is required for promoting dendritic terminal branching in *drosophila* sensory neurons. *PLoS ONE*, 13(11). <https://doi.org/10.1371/journal.pone.0206743>
- Cohen-Cory, S., & Fraser, S. E. (1995). *Effects of brain-derived neurotrophic factor on optic axon branching and remodelling in vivo*.
- Constance, W. D., Mukherjee, A., Fisher, Y. E., Pop, S., Blanc, E., Toyama, Y., & Williams, D. W. (2018). Neurexin and neuroligin-based adhesion complexes drive axonal arborisation growth independent of synaptic activity. *ELife*, 7. <https://doi.org/10.7554/eLife.31659>
- Cornejo, F., Cortés, B. I., Findlay, G. M., & Cancino, G. I. (2021). LAR Receptor Tyrosine

- Phosphatase Family in Healthy and Diseased Brain. In *Frontiers in Cell and Developmental Biology* (Vol. 9). Frontiers Media S.A. <https://doi.org/10.3389/fcell.2021.659951>
- Courchet, J., Lewis, T. L., Lee, S., Courchet, V., Liou, D. Y., Aizawa, S., & Polleux, F. (2013). Terminal axon branching is regulated by the LKB1-NUAK1 kinase pathway via presynaptic mitochondrial capture. *Cell*, *153*(7), 1510. <https://doi.org/10.1016/j.cell.2013.05.021>
- Courgeon, M., & Desplan, C. (2019). Coordination between stochastic and deterministic specification in the *Drosophila* visual system. *Science*, *366*(6463). <https://doi.org/10.1126/science.aay6727>
- Coyle, I. P., Koh, Y.-H., Lee, W.-C. M., Slind, J., Fergestad, T., Littleton, J. T., & Ganetzky, B. (2004). Nervous Wreck, an SH3 Adaptor Protein that Interacts with Wsp, Regulates Synaptic Growth in *Drosophila* active in the GTP bound form and inactive in the GDP bound form. Rho signaling is modulated by GTPase activating proteins (GAPs) that acceler. In *Neuron* (Vol. 41). <http://www.neuron.org/cgi/content/full/>
- Dahmen, D., Layer, M., Deutz, L., Dąbrowska, P. A., Voges, N., Von Papen, M., Brochier, T., Riehle, A., Diesmann, M., Grün, S., & Helias, M. (2022). Global organization of neuronal activity only requires unstructured local connectivity. *ELife*, *11*. <https://doi.org/10.7554/eLife.68422>
- Dailey, M. E., & Smith, S. J. (1996). *The Dynamics of Dendritic Structure in Developing Hippocampal Slices*.
- Deglincerti, A., Liu, Y., Colak, D., Hengst, U., Xu, G., & Jaffrey, S. R. (2015). Coupled local translation and degradation regulate growth cone collapse. *Nature Communications*, *6*. <https://doi.org/10.1038/ncomms7888>
- Dent, E. W., Barnes, A. M., Tang, F., & Kalil, K. (2004). Netrin-1 and Semaphorin 3A Promote or Inhibit Cortical Axon Branching, Respectively, by Reorganization of the Cytoskeleton. *Journal of Neuroscience*, *24*(12), 3002–3012. <https://doi.org/10.1523/JNEUROSCI.4963-03.2004>
- Dent, E. W., & Kalil, K. (2001). *Axon Branching Requires Interactions between Dynamic Microtubules and Actin Filaments*. <http://kalil.anatomy.wisc.edu>.
- Donato, A., Kagias, K., Zhang, Y., & Hilliard, M. A. (2019). Neuronal sub-compartmentalization: a strategy to optimize neuronal function. *Biological Reviews*, *94*(3), 1023–1037. <https://doi.org/10.1111/brv.12487>
- Eberwine, J., Miyashiro, K., Kacharina, J. E., & Job, C. (2001). *Local translation of classes of mRNAs that are targeted to neuronal dendrites*. www.pnas.org/cgi/doi/10.1073/pnas.121146698
- Faust, T. E., Gunner, G., & Schafer, D. P. (2021). Mechanisms governing activity-dependent synaptic pruning in the developing mammalian CNS. In *Nature Reviews Neuroscience* (Vol. 22, Issue 11, pp. 657–673). Nature Research. <https://doi.org/10.1038/s41583-021-00507-y>
- Feinberg, I. (1982). *SCHIZOPHRENIA: CAUSED BY A FAULT IN PROGRAMMED SYNAPTIC ELIMINATION DURING ADOLESCENCE?* (Vol. 17, Issue 4).
- Fiala, J. C., Feinberg, M., Popov, V., & Harris, K. M. (1998). *Synaptogenesis Via Dendritic Filopodia in Developing Hippocampal Area CA1*.
- Fiederling, F., Weschenfelder, M., Fritz, M., Von Philipsborn, A., Bastmeyer, M., & Weth, F. (2017). *Ephrin-A/EphA specific co-adaptation as a novel mechanism in topographic axon guidance*. <https://doi.org/10.7554/eLife.25533.001>
- Filippone, A., Esposito, E., Mannino, D., Lyssenko, N., & Praticò, D. (2022). The contribution of altered neuronal autophagy to neurodegeneration. In *Pharmacology and Therapeutics*

- (Vol. 238). Elsevier Inc. <https://doi.org/10.1016/j.pharmthera.2022.108178>
- Fischbach, K. F., & Dittrich, A. P. M. (1989). The optic lobe of *Drosophila melanogaster*. I. A Golgi analysis of wild-type structure. *Cell and Tissue Research*, 258(3), 441–475. <https://doi.org/10.1007/BF00218858>
- Fraguas, S., Barberán, S., & Cebrià, F. (2011). EGFR signaling regulates cell proliferation, differentiation and morphogenesis during planarian regeneration and homeostasis. *Developmental Biology*, 354(1), 87–101. <https://doi.org/10.1016/j.ydbio.2011.03.023>
- Frampton, J. P., Guo, C., & Pierchala, B. A. (2012). Expression of axonal protein degradation machinery in sympathetic neurons is regulated by nerve growth factor. *Journal of Neuroscience Research*, 90(8), 1533–1546. <https://doi.org/10.1002/jnr.23041>
- G.M.Innocenti. (1981). *Growth and Reshaping of Axons in the Establishment of Visual Callosal Connections*.
- Gallo, G., & Letourneau, P. C. (2004). Regulation of Growth Cone Actin Filaments by Guidance Cues. In *Journal of Neurobiology* (Vol. 58, Issue 1, pp. 92–102). <https://doi.org/10.1002/neu.10282>
- García-Alonso, L., Romani, S., & Jiménez, F. (2000). The EGF and FGF Receptors Mediate Neuroglial Function to Control Growth Cone Decisions during Sensory Axon Guidance in *Drosophila*. In *Neuron* (Vol. 28).
- Garcia, E., & Ismail, S. (2020). Spatiotemporal regulation of signaling: Focus on T cell activation and the immunological synapse. In *International Journal of Molecular Sciences* (Vol. 21, Issue 9). MDPI AG. <https://doi.org/10.3390/ijms21093283>
- Gentile, J. E., Carrizales, M. G., & Koleske, A. J. (2022). Control of Synapse Structure and Function by Actin and Its Regulators. In *Cells* (Vol. 11, Issue 4). MDPI. <https://doi.org/10.3390/cells11040603>
- Georgieff, M. K., Ramel, S. E., & Cusick, S. E. (2018). Nutritional influences on brain development. In *Acta Paediatrica, International Journal of Paediatrics* (Vol. 107, Issue 8, pp. 1310–1321). Blackwell Publishing Ltd. <https://doi.org/10.1111/apa.14287>
- Gibson, D. A., & Ma, L. (2011). Developmental regulation of axon branching in the vertebrate nervous system. In *Development* (Vol. 138, Issue 2). <https://doi.org/10.1242/dev.046441>
- Glock, C., Heumüller, M., & Schuman, E. M. (2017). mRNA transport & local translation in neurons. In *Current Opinion in Neurobiology* (Vol. 45, pp. 169–177). Elsevier Ltd. <https://doi.org/10.1016/j.conb.2017.05.005>
- Gomperts, S. N., Rao, A., Craig, A. M., Malenka, R. C., & Nicoll, R. A. (1998). Postsynaptically Silent Synapses in Single Neuron Cultures neighboring synapses can spill over and activate receptors at synapses that have not, themselves, released glutamate. Since the affinity of glutamate for NMDARs. In *Neuron* (Vol. 21).
- Goo, M. S., Sancho, L., Slepak, N., Boassa, D., Deerinck, T. J., Ellisman, M. H., Bloodgood, B. L., & Patrick, G. N. (2017). Activity-dependent trafficking of lysosomes in dendrites and dendritic spines. *Journal of Cell Biology*, 216(8), 2499–2513. <https://doi.org/10.1083/jcb.201704068>
- Granseth, B., Fukushima, Y., Sugo, N., Lagnado, L., & Yamamoto, N. (2013). Regulation of thalamocortical axon branching by BDNF and synaptic vesicle cycling. *Frontiers in Neural Circuits*, 7(DEC). <https://doi.org/10.3389/fncir.2013.00202>
- Gumy, L. F., Tan, C. L., & Fawcett, J. W. (2010). The role of local protein synthesis and degradation in axon regeneration. In *Experimental Neurology* (Vol. 223, Issue 1, pp. 28–37). <https://doi.org/10.1016/j.expneurol.2009.06.004>
- Hakim, V., Cohen, L. D., Zuchman, R., Ziv, T., & Ziv, N. E. (2016). The effects of proteasomal

- inhibition on synaptic proteostasis. *The EMBO Journal*, 35(20), 2238–2262. <https://doi.org/10.15252/embj.201593594>
- Hashimoto, K., & Kano, M. (2013). Synapse elimination in the developing cerebellum. In *Cellular and Molecular Life Sciences* (Vol. 70, Issue 24, pp. 4667–4680). <https://doi.org/10.1007/s00018-013-1405-2>
- Hassan, B. A., & Hiesinger, P. R. (2015). Beyond Molecular Codes: Simple Rules to Wire Complex Brains. *Cell*, 163(2). <https://doi.org/10.1016/j.cell.2015.09.031>
- Hassan Bassem A. (2000). *atonal Regulates Neurite Arborization but Does Not Act as a Proneural Gene in the Drosophila Brain*.
- He, H., Kise, Y., Izadifar, A., Urwyler, O., Ayaz, D., Parthasarthy, A., Yan, B., Erfurth, M. L., Dascenco, D., & Schmucker, D. (2014). Cell-intrinsic requirement of Dscam1 isoform diversity for axon collateral formation. *Science*, 344(6188), 1182–1186. <https://doi.org/10.1126/science.1251852>
- Hernandez, D., Torres, C. A., Setlik, W., Cebrián, C., Mosharov, E. V., Tang, G., Cheng, H. C., Kholodilov, N., Yarygina, O., Burke, R. E., Gershon, M., & Sulzer, D. (2012). Regulation of Presynaptic Neurotransmission by Macroautophagy. *Neuron*, 74(2), 277–284. <https://doi.org/10.1016/j.neuron.2012.02.020>
- Hiesinger, P. R. (2021). The Self-Assembling Brain. In *How Neural Networks Grow Smarter*. Princeton University Press. <https://doi.org/doi:10.1515/9780691215518>
- Hobson, B. D., Kong, L., Angelo, M. F., Lieberman, O. J., Mosharov, E. V., Herzog, E., Sulzer, D., & Sims, P. A. (2022). Subcellular and regional localization of mRNA translation in midbrain dopamine neurons. *Cell Reports*, 38(2). <https://doi.org/10.1016/j.celrep.2021.110208>
- Hofman, M. A. (2014). Evolution of the human brain: When bigger is better. *Frontiers in Neuroanatomy*, 8(MAR). <https://doi.org/10.3389/fnana.2014.00015>
- Holguera, I., & Desplan, C. (2018). *Neuronal specification in space and time*. <http://science.sciencemag.org/>
- Holland, S. J., Pelesl, E., Pawson, T., & Schlessinger, J. (1998). Cell-contact-dependent signalling in axon growth and guidance: Eph receptor tyrosine kinases and receptor protein tyrosine phosphatase 13. In *Current Opinion in Neurobiology* (Vol. 8). <http://biomednet.com/elecref/O959438800800117>
- Horton, A. C., & Ehlers, M. D. (2003). Review Neuronal Polarity and Trafficking How are membrane constituents trafficked through such The establishment of subcellular domains with distinct 2 Department of Cell Biology molecular components and functional properties is a fun. In *Neuron* (Vol. 40).
- Huttenlocher PR. (1984). Synapse elimination and plasticity in developing human cerebral cortex. *Am J Ment Defic.*, 88(5), 488–496.
- Jeibmann, A., & Paulus, W. (2009). *Drosophila melanogaster* as a model organism of brain diseases. In *International Journal of Molecular Sciences* (Vol. 10, Issue 2, pp. 407–440). <https://doi.org/10.3390/ijms10020407>
- Jin, E. J., Kiral, F. R., & Hiesinger, P. R. (2018). The where, what, and when of membrane protein degradation in neurons. In *Developmental Neurobiology* (Vol. 78, Issue 3, pp. 283–297). John Wiley and Sons Inc. <https://doi.org/10.1002/dneu.22534>
- Kallergi, E., Daskalaki, A. D., Kolaxi, A., Camus, C., Ioannou, E., Mercaldo, V., Haberkant, P., Stein, F., Sidiropoulou, K., Dalezios, Y., Savitski, M. M., Bagni, C., Choquet, D., Hossy, E., & Nikolettoulou, V. (2022). Dendritic autophagy degrades postsynaptic proteins and is required for long-term synaptic depression in mice. *Nature Communications*, 13(1).

- <https://doi.org/10.1038/s41467-022-28301-z>
- Kase, Y., Kase, Y., Shimazaki, T., & Okano, H. (2020). Current understanding of adult neurogenesis in the mammalian brain: How does adult neurogenesis decrease with age? In *Inflammation and Regeneration* (Vol. 40, Issue 1). BioMed Central Ltd. <https://doi.org/10.1186/s41232-020-00122-x>
- Kawamura, Y., Nakayama, H., Hashimoto, K., Sakimura, K., Kitamura, K., & Kano, M. (2013). Spike timing-dependent selective strengthening of single climbing fibre inputs to Purkinje cells during cerebellar development. *Nature Communications*, 4. <https://doi.org/10.1038/ncomms3732>
- Keeble, T. R., Halford, M. M., Seaman, C., Kee, N., Macheda, M., Anderson, R. B., Stacker, S. A., & Cooper, H. M. (2006). The Wnt receptor Ryk is required for Wnt5a-mediated axon guidance on the contralateral side of the corpus callosum. *Journal of Neuroscience*, 26(21), 5840–5848. <https://doi.org/10.1523/JNEUROSCI.1175-06.2006>
- Kent, D. (1960). *A Study of the Structure of the Area Postrema with Golgi Methods*.
- Ketschek, A., Jones, S., Spillane, M., Korobova, F., Svitkina, T., & Gallo, G. (2015). Nerve growth factor promotes reorganization of the axonal microtubule array at sites of axon collateral branching. *Developmental Neurobiology*, 75(12), 1441–1461. <https://doi.org/10.1002/dneu.22294>
- Keunen, K., Van Elburg, R. M., Van Bel, F., & Benders, M. J. N. L. (2015). Impact of nutrition on brain development and its neuroprotective implications following preterm birth. In *Pediatric Research* (Vol. 77, pp. 148–155). Nature Publishing Group. <https://doi.org/10.1038/pr.2014.171>
- Khan, R., Kulasiri, D., & Samarasinghe, S. (2021). Functional repertoire of protein kinases and phosphatases in synaptic plasticity and associated neurological disorders. In *Neural Regeneration Research* (Vol. 16, Issue 6, pp. 1150–1157). Wolters Kluwer Medknow Publications. <https://doi.org/10.4103/1673-5374.300331>
- Kidd, T., Bland, K. S., & Goodman, C. S. (1999). Slit Is the Midline Repellent for the Robo Receptor in Drosophila together, these results suggest that Comm regulates Robo function by either controlling Robo levels or Robo signaling. Further analysis revealed that Comm controls Robo expression; increasing Comm leads to a reduction Department of Molecular and Cell Biology of Robo protein. In *Cell* (Vol. 96).
- Kim, H. J., Cho, M. H., Shim, W. H., Kim, J. K., Jeon, E. Y., Kim, D. H., & Yoon, S. Y. (2017). Deficient autophagy in microglia impairs synaptic pruning and causes social behavioral defects. *Molecular Psychiatry*, 22(11), 1576–1584. <https://doi.org/10.1038/mp.2016.103>
- Kim, J. H., Wang, X., Coolon, R., & Ye, B. (2013). Dscam expression levels determine presynaptic arbor sizes in drosophila sensory neurons. *Neuron*, 78(5), 827–838. <https://doi.org/10.1016/j.neuron.2013.05.020>
- Kim, M., Baek, M., & Kim, D. J. (2017). Protein Tyrosine Signaling and its Potential Therapeutic Implications in Carcinogenesis. *Current Pharmaceutical Design*, 23(29). <https://doi.org/10.2174/1381612823666170616082125>
- Kiral, F. R., Dutta, S. B., Linneweber, G. A., Hilgert, S., Poppa, C., Duch, C., von Kleist, M., Hassan, B. A., & Hiesinger, P. R. (2021). Brain connectivity inversely scales with developmental temperature in Drosophila. *Cell Reports*, 37(12), 110145. <https://doi.org/10.1016/j.celrep.2021.110145>
- Kiral, F. R., Linneweber, G. A., Mathejczyk, T., Georgiev, S. V., Wernet, M. F., Hassan, B. A., von Kleist, M., & Hiesinger, P. R. (2020). Autophagy-dependent filopodial kinetics restrict

- synaptic partner choice during *Drosophila* brain wiring. *Nature Communications*, 11(1). <https://doi.org/10.1038/s41467-020-14781-4>
- Koh, Y. H. (2018). Heat Stroke with Status Epilepticus Secondary to Posterior Reversible Encephalopathy Syndrome (PRES). *Case Reports in Critical Care*, 2018, 1–4. <https://doi.org/10.1155/2018/3597474>
- Kuijpers, M., Kochlamazashvili, G., Stumpf, A., Puchkov, D., Swaminathan, A., Lucht, M. T., Krause, E., Maritzen, T., Schmitz, D., & Haucke, V. (2021). Neuronal Autophagy Regulates Presynaptic Neurotransmission by Controlling the Axonal Endoplasmic Reticulum. *Neuron*, 109(2), 299–313.e9. <https://doi.org/10.1016/j.neuron.2020.10.005>
- Kulkarni, A., Ertekin, D., Lee, C.-H., & Hummel, T. (2016). Birth order dependent growth cone segregation determines synaptic layer identity in the *Drosophila* visual system. <https://doi.org/10.7554/eLife.13715.001>
- Langen, M., Koch, M., Yan, J., De Geest, N., Erfurth, M. L., Pfeiffer, B. D., Schmucker, D., Moreau, Y., & Hassan, B. A. (2013). Mutual inhibition among postmitotic neurons regulates robustness of brain wiring in *Drosophila*. *ELife*, 2013(2). <https://doi.org/10.7554/eLife.00337>
- Lee, H. K. (2006). Synaptic plasticity and phosphorylation. In *Pharmacology and Therapeutics* (Vol. 112, Issue 3, pp. 810–832). <https://doi.org/10.1016/j.pharmthera.2006.06.003>
- Lee, L. T. H., & Godenschwege, T. A. (2015). Structure-function analyses of tyrosine phosphatase PTP69D in giant fiber synapse formation of *Drosophila*. *Molecular and Cellular Neuroscience*, 64, 24–31. <https://doi.org/10.1016/j.mcn.2014.11.002>
- Lewis, T. L., Kwon, S. K., Lee, A., Shaw, R., & Polleux, F. (2018). MFF-dependent mitochondrial fission regulates presynaptic release and axon branching by limiting axonal mitochondria size. *Nature Communications*, 9(1). <https://doi.org/10.1038/s41467-018-07416-2>
- Liang, Y. T. (2019). Emerging concepts and functions of autophagy as a regulator of synaptic components and plasticity. In *Cells* (Vol. 8, Issue 1). MDPI. <https://doi.org/10.3390/cells8010034>
- Linda, K., Lewerissa, E. I., Verboven, A. H. A., Gabriele, M., Frega, M., Klein Gunnewiek, T. M., Devilee, L., Ulferts, E., Hommersom, M., Oudakker, A., Schoenmaker, C., van Bokhoven, H., Schubert, D., Testa, G., Koolen, D. A., de Vries, B. B. A., & Nadif Kasri, N. (2022). Imbalanced autophagy causes synaptic deficits in a human model for neurodevelopmental disorders. *Autophagy*, 18(2), 423–442. <https://doi.org/10.1080/15548627.2021.1936777>
- Linneweber, G. A., Andriatsilavo, M., Dutta, S. B., Bengochea, M., Hellbruegge, L., Liu, G., Ejsmont, R. K., Straw, A. D., Wernet, M., Hiesinger, P. R., & Hassan, B. A. (2020). A neurodevelopmental origin of behavioral individuality in the *Drosophila* visual system. *Science*, 367(6482). <https://doi.org/10.1126/science.aaz4547>
- Liu, Y., Shi, J., Lu, C. C., Wang, Z. B., Lyuksyutova, A. I., Song, X., & Zou, Y. (2005). Ryk-mediated Wnt repulsion regulates posterior-directed growth of corticospinal tract. *Nature Neuroscience*, 8(9), 1151–1159. <https://doi.org/10.1038/nn1520>
- Lom, B., & Cohen-Cory, S. (1999). Brain-Derived Neurotrophic Factor Differentially Regulates Retinal Ganglion Cell Dendritic and Axonal Arborization In Vivo.
- Ludwig, D., & Cable, R. M. (1933). THE EFFECT OF ALTERNATING TEMPERATURES ON THE PUPAL DEVELOPMENT OF *DROSOPHILA MELANOGASTER MEIGEN* (One figure): Vol. VI (Issue 4). <http://www.journals.uchicago.edu/t-and-c>
- Luo, L., & O’Leary, D. D. M. (2005). Axon retraction and degeneration in development and disease. In *Annual Review of Neuroscience* (Vol. 28, pp. 127–156).

<https://doi.org/10.1146/annurev.neuro.28.061604.135632>

- Luo, Y., Raible, D., & Raper, J. A. (1993). Collapsin: A Protein in Brain That Induces the Collapse and Paralysis of Neuronal Growth Cones. In *Cell* (Vol. 75).
- MacGillavry, H. D., Song, Y., Raghavachari, S., & Blanpied, T. A. (2013). Nanoscale scaffolding domains within the postsynaptic density concentrate synaptic ampa receptors. *Neuron*, 78(4), 615–622. <https://doi.org/10.1016/j.neuron.2013.03.009>
- Malin, J., & Desplan, C. (2021). Neural specification, targeting, and circuit formation during visual system assembly. *Proceedings of the National Academy of Sciences of the United States of America*, 118(28). <https://doi.org/10.1073/pnas.2101823118>
- McNeill, E. M., Thompson, C., Berke, B., Chou, V. T., Rusch, J., Duckworth, A., Deproto, J., Taylor, A., Gates, J., Gertler, F., Keshishian, H., & Van Vactor, D. (2020). Drosophila enabled promotes synapse morphogenesis and regulates active zone form and function. *Neural Development*, 15(1). <https://doi.org/10.1186/s13064-020-00141-x>
- Menon, K. P., Kulkarni, V., Shin-Ya, T., Anaya, M., & Zinn, K. (2019). Interactions between dpr11 and dip-y control election of amacrine neurons in drosophila color vision circuits. *ELife*, 8. <https://doi.org/10.7554/eLife.48935>
- Meyer, M. P., & Smith, S. J. (2006). Evidence from in vivo imaging that synaptogenesis guides the growth and branching of axonal arbors by two distinct mechanisms. *Journal of Neuroscience*, 26(13). <https://doi.org/10.1523/JNEUROSCI.0223-06.2006>
- Ming, G. li, & Song, H. (2011). Adult Neurogenesis in the Mammalian Brain: Significant Answers and Significant Questions. In *Neuron* (Vol. 70, Issue 4, pp. 687–702). <https://doi.org/10.1016/j.neuron.2011.05.001>
- Mirzoyan, Z., Sollazzo, M., Allocca, M., Valenza, A. M., Grifoni, D., & Bellosta, P. (2019). Drosophila melanogaster: A model organism to study cancer. In *Frontiers in Genetics* (Vol. 10). Frontiers Media S.A. <https://doi.org/10.3389/fgene.2019.00051>
- Morante, J., & Desplan, C. (2008). *The color vision circuit in the medulla of Drosophila*.
- Naylor, S. A., & Diantonio, A. (2012). EGFR signaling modulates synaptic connectivity via Gurken. *Developmental Neurobiology*, 72(9), 1229–1242. <https://doi.org/10.1002/dneu.20992>
- Neben, C. L., Lo, M., Jura, N., & Klein, O. D. (2019). Feedback regulation of RTK signaling in development. In *Developmental Biology* (Vol. 447, Issue 1, pp. 71–89). Elsevier Inc. <https://doi.org/10.1016/j.ydbio.2017.10.017>
- Nelson, J. C., Stavoe, A. K. H., & Colón-Ramos, D. A. (2013). The actin cytoskeleton in presynaptic assembly. In *Cell Adhesion and Migration* (Vol. 7, Issue 4, pp. 379–387). Taylor and Francis Inc. <https://doi.org/10.4161/cam.24803>
- O’leary, D. D. M., & Koester, S. E. (1993). Development of Projection Neuron Types, Axon Pathways, and Patterned Connections of the Mammalian Cortex Review. In *Neuron* (Vol. 10). CopyrightO 1993 by Cell Press.
- Osterhout, J. A., El-Danaf, R. N., Nguyen, P. L., & Huberman, A. D. (2014). Birthdate and outgrowth timing predict cellular mechanisms of axon target matching in the developing visual pathway. *Cell Reports*, 8(4), 1006–1017. <https://doi.org/10.1016/j.celrep.2014.06.063>
- Özel, M Neset, Kulkarni, A., Hasan, A., Brummer, J., Moldenhauer, M., Daumann, I. M., Wolfenberg, H., Dercksen, V. J., Kiral, F. R., Weiser, M., Prohaska, S., von Kleist, M., & Hiesinger, P. R. (2019). Serial Synapse Formation through Filopodial Competition for Synaptic Seeding Factors. *Developmental Cell*, 50(4), 447-461.e8. <https://doi.org/10.1016/j.devcel.2019.06.014>

- Özel, Mehmet Neset, Langen, M., Hassan, B. A., & Hiesinger, P. R. (2015). Filopodial dynamics and growth cone stabilization in *Drosophila* visual circuit development. *ELife*, 4(OCTOBER2015). <https://doi.org/10.7554/eLife.10721>
- Pacheco, A., & Gallo, G. (2016). Actin filament-microtubule interactions in axon initiation and branching. In *Brain Research Bulletin* (Vol. 126, pp. 300–310). Elsevier Inc. <https://doi.org/10.1016/j.brainresbull.2016.07.013>
- Paolicelli, R. C., Bolasco, G., Pagani, F., Maggi, L., Scianni, M., Panzanelli, P., Giustetto, M., Ferreira, T. A., Guiducci, E., Dumas, L., Ragozzino, D., & Gross, C. T. (2011). Synaptic pruning by microglia is necessary for normal brain development. *Science*, 333(6048), 1456–1458. <https://doi.org/10.1126/science.1202529>
- Pende, M., Becker, K., Wanis, M., Saghafi, S., Kaur, R., Hahn, C., Pende, N., Foroughipour, M., Hummel, T., & Dodt, H. U. (2018). High-resolution ultramicroscopy of the developing and adult nervous system in optically cleared *Drosophila melanogaster*. *Nature Communications*, 9(1). <https://doi.org/10.1038/s41467-018-07192-z>
- Phillips, P. K., & Heath, J. E. (1995). DEPENDENCY OF SURFACE TEMPERATURE REGULATION ON BODY SIZE IN TERRESTRIAL MAMMALS. In *J. therm. Biol* (Vol. 20, Issue 3).
- Powchik, P., Davidson, M., Haroutunian, V., Gabriel, S. M., Purohit, D. P., Perl, D. P., Harvey, P. D., & Davis, K. L. (1998). Postmortem studies in schizophrenia. *Schizophrenia Bulletin*, 24(3). <https://doi.org/10.1093/oxfordjournals.schbul.a033330>
- Powsner, L. (1935). *THE EFFECTS OF TEMPERATURE ON THE DURATIONS OF THE DEVELOPMENTAL STAGES OF DROSOPHILA MELANOGASTER*'.
- Rajgor, D., Welle, T. M., & Smith, K. R. (2021). The Coordination of Local Translation, Membranous Organelle Trafficking, and Synaptic Plasticity in Neurons. In *Frontiers in Cell and Developmental Biology* (Vol. 9). Frontiers Media S.A. <https://doi.org/10.3389/fcell.2021.711446>
- Ramos, B. P., Birnbaum, S. G., Lindenmayer, I., Newton, S. S., Duman, R. S., & Arnsten, A. F. T. (2003). Dysregulation of Protein Kinase A Signaling in the Aged Prefrontal Cortex: New Strategy for Treating Age-Related Cognitive Decline functions dependent on the amygdala and posterior cor-tices (Barros et al PKA activity can also be increased through the sys-temic administration of agents that inhibit phosphodies. In *Neuron* (Vol. 40). Schafe and LeDoux.
- Raper Jonathan A. (2000). Semaphorins and their receptors in vertebrates and invertebrates. *Current Opinion in Neurobiology* , 88–94.
- Ray, S. K. (2020). Modulation of autophagy for neuroprotection and functional recovery in traumatic spinal cord injury. In *Neural Regeneration Research* (Vol. 15, Issue 9, pp. 1601–1612). Wolters Kluwer Medknow Publications. <https://doi.org/10.4103/1673-5374.276322>
- Regehr, W. G., Carey, M. R., & Best, A. R. (2009). Activity-Dependent Regulation of Synapses by Retrograde Messengers. In *Neuron* (Vol. 63, Issue 2, pp. 154–170). <https://doi.org/10.1016/j.neuron.2009.06.021>
- Reiter, L. T., Potocki, L., Chien, S., Gribskov, M., & Bier, E. (2001). A systematic analysis of human disease-associated gene sequences in *Drosophila melanogaster*. *Genome Research*, 11(6), 1114–1125. <https://doi.org/10.1101/gr.169101>
- Rico, B., Beggs, H. E., Schahin-Reed, D., Kimes, N., Schmidt, A., & Reichardt, L. F. (2004). Control of axonal branching and synapse formation by focal adhesion kinase. *Nature Neuroscience*, 7(10). <https://doi.org/10.1038/nn1317>
- Ruffolo, R. R., Eisenbarth, G. S., Thompson, J. M., & Nirenberg, M. (1978). *Synapse turnover:*

- A mechanism for acquiring synaptic specificity (retina/muscle cell/neurons/development/cell culture) (Vol. 75, Issue 5).
- Sakai, J. (2020). How synaptic pruning shapes neural wiring during development and, possibly, in disease. *Proceedings of the National Academy of Sciences of the United States of America*, 117(28), 16096–16099. <https://doi.org/10.1073/pnas.2010281117>
- Sanes, J. R., & Zipursky, S. L. (2020). Synaptic Specificity, Recognition Molecules, and Assembly of Neural Circuits. In *Cell* (Vol. 181, Issue 3, pp. 536–556). Cell Press. <https://doi.org/10.1016/j.cell.2020.04.008>
- Schmitt, A. M., Shi, J., Wolf, A. M., Lu, C. C., King, L. A., & Zou, Y. (2006). Wnt-Ryk signalling mediates medial-lateral retinotectal topographic mapping. *Nature*, 439(7072), 31–37. <https://doi.org/10.1038/nature04334>
- Schnaitmann, C., Haikala, V., Abraham, E., Oberhauser, V., Thestrup, T., Griesbeck, O., & Reiff, D. F. (2018). Color Processing in the Early Visual System of *Drosophila*. *Cell*, 172(1–2), 318–330.e18. <https://doi.org/10.1016/j.cell.2017.12.018>
- Scholl, C., Rule, M. E., & Hennig, M. H. (2021). The information theory of developmental pruning: Optimizing global network architectures using local synaptic rules. *PLoS Computational Biology*, 17(10). <https://doi.org/10.1371/journal.pcbi.1009458>
- Selemon, L. D. (2013). A role for synaptic plasticity in the adolescent development of executive function. In *Translational psychiatry* (Vol. 3). <https://doi.org/10.1038/tp.2013.7>
- Serafini, T., Colamarino, S. A., David Leonardo, E., Wang, H., Beddington, R., Skarnes, W. C., & Tessier-Lavigne, M. (1996). Netrin-1 Is Required for Commissural Axon Guidance in the Developing Vertebrate Nervous System. In *Cell* (Vol. 87).
- Shah, A., Lenka, A., Saini, J., Wagle, S., Naduthota, R. M., Yadav, R., Pal, P. K., & Ingalthalikar, M. (2017). Altered Brain Wiring in Parkinson’s Disease: A Structural Connectome-Based Analysis. *Brain Connectivity*, 7(6). <https://doi.org/10.1089/brain.2017.0506>
- Shatz, C. J., & Kirkwood, P. A. (1984). *PRENATAL DEVELOPMENT OF FUNCTIONAL CONNECTIONS IN THE CAT’S RETINOGENICULATE PATHWAY* (Vol. 4, Issue 5).
- Shirasaki, R., & Pfaff, S. L. (2002). Transcriptional codes and the control of neuronal identity. In *Annual Review of Neuroscience* (Vol. 25, pp. 251–281). <https://doi.org/10.1146/annurev.neuro.25.112701.142916>
- Song, J. K., Giniger, E., & Desai, C. J. (2008). *The Receptor protein tyrosine phosphatase PTP69D antagonizes Abl tyrosine kinase to guide axons in Drosophila*.
- Song, J., Wu, L., Chen, Z., Kohanski, R. A., & Pick, L. (2003). Axons Guided by Insulin Receptor in *Drosophila* Visual System. In *Source: Science, New Series* (Vol. 300, Issue 5618).
- Soykan, T., Haucke, V., & Kuijpers, M. (2021). Mechanism of synaptic protein turnover and its regulation by neuronal activity. In *Current Opinion in Neurobiology* (Vol. 69, pp. 76–83). Elsevier Ltd. <https://doi.org/10.1016/j.conb.2021.02.006>
- Spear, L. P. (2013). Adolescent neurodevelopment. In *Journal of Adolescent Health* (Vol. 52, Issue 2 SUPPL.2). <https://doi.org/10.1016/j.jadohealth.2012.05.006>
- Sperry, R. W. (1963). *CHEMOAFFINITY IN THE ORDERLY GROWTH OF NERVE FIBER PATTERNS AND CONNECTIONS**. <https://www.pnas.org>
- Srahna, M., Leyssen, M., Ching, M. C., Fradkin, L. G., Noordermeer, J. N., & Hassan, B. A. (2006). A signaling network for patterning of neuronal connectivity in the *Drosophila* brain. *PLoS Biology*, 4(11), 2076–2090. <https://doi.org/10.1371/journal.pbio.0040348>
- Stavoe, A. K. H., & Holzbaur, E. L. F. (2019). Autophagy in neurons. In *Annual Review of Cell and Developmental Biology* (Vol. 35). <https://doi.org/10.1146/annurev-cellbio-100818->

- Steward, O., & Worley, P. (2002). Local synthesis of proteins at synaptic sites on dendrites: Role in synaptic plasticity and memory consolidation? In *Neurobiology of Learning and Memory* (Vol. 78, Issue 3, pp. 508–527). Academic Press Inc. <https://doi.org/10.1006/nlme.2002.4102>
- Tang, G., Gudsruk, K., Kuo, S. H., Cotrina, M. L., Rosoklija, G., Sosunov, A., Sonders, M. S., Kanter, E., Castagna, C., Yamamoto, A., Yue, Z., Arancio, O., Peterson, B. S., Champagne, F., Dwork, A. J., Goldman, J., & Sulzer, D. (2014). Loss of mTOR-Dependent Macroautophagy Causes Autistic-like Synaptic Pruning Deficits. *Neuron*, 83(5), 1131–1143. <https://doi.org/10.1016/j.neuron.2014.07.040>
- Tao, H. W., & Poo, M.-M. (2001). *Retrograde signaling at central synapses*. <https://www.pnas.org>
- Taoufik, E., Kouroupi, G., Zygogianni, O., & Matsas, R. (2018). Synaptic dysfunction in neurodegenerative and neurodevelopmental diseases: An overview of induced pluripotent stem-cell-based disease models. In *Open Biology* (Vol. 8, Issue 9). Royal Society Publishing. <https://doi.org/10.1098/rsob.180138>
- Tasic, B., Nabholz, C. E., Baldwin, K. K., Kim, Y., Rueckert, E. H., Ribich, S. A., Cramer, P., Wu, Q., Axel, R., & Maniatis, T. (2002). Promoter Choice Determines Splice Site Selection in Protocadherin and Pre-mRNA Splicing retina. Retinal ganglion, amacrine, and bipolar cells with distinct laminar positions are further subdivided by their function and morphology to reveal more than 50 distinct neuronal subtypes (Masland, 2001). The diversity of neurons is mirrored by extensive di. In *Molecular Cell* (Vol. 10).
- Thompson, J. M., Eisenbarth, G. S., Ruffolo, R. R., & Nirenberg, M. (1983). SYNAPSE SELECTION BASED ON DIFFERENCES IN SYNAPSE TURNOVER. In *hr. J. Devl. Neuroscience* (Vol. 1, Issue 1).
- Tolwinski, N. S. (2017). Introduction: Drosophila-A model system for developmental biology. In *Journal of Developmental Biology* (Vol. 5, Issue 3). MDPI Multidisciplinary Digital Publishing Institute. <https://doi.org/10.3390/jdb5030009>
- Van Der Loos Hendrik, & Glaser Edmund M. (1972). *Autapses in neocortex cerebri: synapses between a pyramidal cell's axon and its own dendrites*.
- Vaughn, J. E., Barber, R. P., & Sims, T. J. (1988). Dendritic development and preferential growth into synaptogenic fields: A quantitative study of Golgi-impregnated spinal motor neurons. *Synapse*, 2(1). <https://doi.org/10.1002/syn.890020110>
- Vaughn, J. E., Henrikson, C. K., & Grieshaber, J. A. (1974). A quantitative study of synapses on motor neuron dendritic growth cones in developing mouse spinal cord. *Journal of Cell Biology*, 60(3). <https://doi.org/10.1083/jcb.60.3.664>
- Waites, C. L., Leal-Ortiz, S. A., Andlauer, T. F. M., Sigrist, S. J., & Garner, C. C. (2011). Piccolo regulates the dynamic assembly of presynaptic F-actin. *Journal of Neuroscience*, 31(40), 14250–14263. <https://doi.org/10.1523/JNEUROSCI.1835-11.2011>
- Wang, C.-C., Tsai, M.-K., Chen, I.-H., Hsu, Y.-D., Hsueh, C.-W., & Shiang, J.-C. (2008). NEUROLOGICAL MANIFESTATIONS IN A PATIENT OF HEAT STROKE-CASE REPORT AND LITERATURE REVIEW. In *Taiwan Crit. Care Med* (Vol. 9).
- Wit, C., Hiesinger, P. R. (2022). Neuronal filopodia: From stochastic dynamics to robustness of brain morphogenesis. *Semin. Cell Dev. Biol.* <https://doi.org/10.1016/j.semcdb.2022.03.038>
- Wojtowicz, W. M., Flanagan, J. J., Millard, S. S., Zipursky, S. L., & Clemens, J. C. (2004). Alternative splicing of Drosophila Dscam generates axon guidance receptors that exhibit

- isoform-specific homophilic binding. *Cell*, 118(5), 619–633.
<https://doi.org/10.1016/j.cell.2004.08.021>
- Yao, Y., Wu, Y., Yin, C., Ozawa, R., Aigaki, T., Wouda, R. R., Noordermeer, J. N., Fradkin, L. G., & Hing, H. (2007). Antagonistic roles of Wnt5 and the Drl receptor in patterning the Drosophila antennal lobe. *Nature Neuroscience*, 10(11), 1423–1432.
<https://doi.org/10.1038/nn1993>
- Yasuda, M., Nagappan-Chettiar, S., Johnson-Venkatesh, E. M., & Umemori, H. (2021). An activity-dependent determinant of synapse elimination in the mammalian brain. *Neuron*, 109(8), 1333–1349.e6. <https://doi.org/10.1016/j.neuron.2021.03.006>
- Zheng, J. Q., Wan, J.-J., & Poo, M.-M. (1996). Essential Role of Filopodia in Chemotropic Turning of Nerve Growth Cone Induced by a Glutamate Gradient. In *The Journal of Neuroscience* (Vol. 76, Issue 3).
- Zhu, K., Xu, Y., Liu, J., Xu, Q., & Ye, H. (2011). Down syndrome cell adhesion molecule and its functions in neural development. In *Neuroscience Bulletin* (Vol. 27, Issue 1, pp. 45–52). <https://doi.org/10.1007/s12264-011-1045-1>
- Zhu, Y. (2013). The Drosophila visual system: From neural circuits to behavior. In *Cell Adhesion and Migration* (Vol. 7, Issue 4, pp. 333–344). Taylor and Francis Inc. <https://doi.org/10.4161/cam.25521>
- Zschätzsch, M., Oliva, C., Langen, M., De Geest, N., Özel, M. N., Williamson, W. R., Lemon, W. C., Soldano, A., Munck, S., Hiesinger, P. R., Sanchez-Soriano, N., & Hassan, B. A. (2014). Regulation of branching dynamics by axon-intrinsic asymmetries in Tyrosine Kinase Receptor signaling. *ELife*, 3. <https://doi.org/10.7554/elife.01699>

12. Appendix

12.1 Dedication & Acknowledgement

I am dedicating this thesis to my maternal grandmother whose love for me knew no bounds, and who taught me the value of hard work, patience, and perseverance. I will never forget you.

This incredible journey wouldn't have begun without the encouragement and constant support of my family. I am highly indebted to them for making it possible to have my own little dream and provide me with the courage to chase it. I am grateful to my PhD supervisors for their incredible support and guidance all along. They have nurtured me all these years and turned me into a more confident scientist. This endeavor would not have been possible without my friends who never failed to cheer me up and make me feel at home with all their love and support. Last but not the least, words cannot express my gratitude to my partner who relentlessly tried to show me the light at the end of the tunnel during my most difficult times, with a smile on his face. I love you all.

12.2 List of publications from the doctoral work

A neurodevelopmental origin of behavioral individuality in the *Drosophila* visual system

Linneweber GA, Andriatsilavo M, **Dutta SB**, Bengochea M, Hellbruegge L, Liu G, Ejsmont RK, Straw AD, Wernet M, Hiesinger PR, Hassan BA. *Science*. 2020 Mar 6;367(6482):1112-1119.

The *Drosophila* amyloid precursor protein homologue mediates neuronal survival and neuroglial interactions

Kessissoglou IA, Langui D, Hasan A, Maral M, **Dutta SB**, Hiesinger PR, Hassan BA. *PLoS Biol*. 2020 Dec 8;18(12):e3000703. doi: [10.1371/journal.pbio.3000703](https://doi.org/10.1371/journal.pbio.3000703). eCollection 2020 Dec. PMID: [33290404](https://pubmed.ncbi.nlm.nih.gov/33290404/)

Brain connectivity inversely scales with developmental temperature in *Drosophila*

Kiral FR, **Dutta SB**, Linneweber GA, Hilgert S, Poppa C, Duch C, von Kleist M, Hassan BA, Hiesinger PR. *Cell Rep*. 2021 Dec 21;37(12):110145. doi: [10.1016/j.celrep.2021.110145](https://doi.org/10.1016/j.celrep.2021.110145). PMID: [34936868](https://pubmed.ncbi.nlm.nih.gov/34936868/)

A critical developmental interval of coupling axon branching to synaptic degradation during neural circuit formation

Suchetana B. Dutta, Gerit Arne Linneweber, Maheva Andriatsilavo, Peter Robin Hiesinger, Bassem A Hassan
doi: [10.1101/2022.04.06.486606](https://doi.org/10.1101/2022.04.06.486606)

Probabilistic axon targeting dynamics lead to individualized brain wiring

Maheva Andriatsilavo, Alexandre Dumoulin, **Suchetana Bias Dutta**, Esther Stoeckli, P. Robin Hiesinger, Bassem A. Hassan
doi: [10.1101/2022.08.26.505432](https://doi.org/10.1101/2022.08.26.505432)

List of manuscripts in preparation from the doctoral work:

A GRASP based screening pipeline reveals new connectivity in the *Drosophila* visual system

Suchetana B. Dutta 1,# , Maheva Adriatsilavo 1,2,# , Bassem A. Hassan 2 , Peter Robin Hiesinger 1 and Gerit Arne Linneweber 1,#,*

The connectivity of LC14, one of the most variable neurons in the fly visual system

Gerit Arne Linneweber*, Forian Freitag, Edda Kunze, Deborah Hollaender, Muhammad Ali Haidar, Samra Hamidovic, Veronica Lukynova, **Suchetana B. Dutta**, Laia Pons, Emil Kind, Mathias Wernet, Michael Riser, Eugenia Chiappe, Bassem Hassan and Ronny Rosner